UNIVERSIDADE DA BEIRA INTERIOR

Ciências

Desenvolvimento de novos biomateriais para aplicação na área de engenharia de tecidos

Tiago Ruivo Correia

Tese para obtenção do Grau de Doutor em

Bioquímica

(3º ciclo de estudos)

Orientador: Professor Doutor Ilídio Joaquim Sobreira Correia

Coorientadora: Doutora Paula Cristina Nunes Ferreira Calvinho

Covilhã, janeiro de 2017

Dedicatory

To my parents for their belief and support.

To Rita, the least of my problems.

Acknowledgments

First of all, I would like to thank my supervisor, Professor Doutor Ilídio Correia for his scientific support, availability and friendship. I am also grateful to him for the professional person that I became. It has been a difficult path to overrun, thanks for all the advices and guidance.

I am also thankful to Doutora Paula Calvinho for her scientific support and tireless motivation. It has been a privilege to work with you.

I would also like to acknowledge Universidade da Beira Interior, particularly Health Sciences Research Center, for the opportunity to develop this study in its facilities.

I would also like to thank to Dr. Ana Gomes and Catarina Ferreira for their contribution in data understanding and analysis.

Moreover, I would like to express my gratitude to all my team and closest friends, specially to Sónia and Maximiano for all the confession moments and tireless help. You have been my "brothers in arms".

I am also grateful to my family, specially, my parents for all their love, presence, patience, and support.

Last but not least, I would like to thank to one of the persons that I most care about, Rita, thanks for your complicity, friendship and love. It has been a wonderful relationship.

List of Publications

Publications published in Peer-Reviewed International Scientific Journals included in the thesis

I. Fradique, R.G., **Correia, T.R.**, Miguel, S. P., de Sá, K.D., Figueira, D.R., Mendonça, A.G., Correia, I.J., (2016) "Production of new 3D scaffolds for bone tissue regeneration by rapid prototyping", Journal of Materials Science: Materials in Medicine, Vol. 27(4), pp. 1-14, (http://dx.doi.org/10.1007%2Fs10856-016-5681-x).

II. **Correia, T.R.**, Figueira, D.R., de Sá, K.D., Miguel S.P., Fradique, R.G., Mendonça, A.G., Correia, I.J., (2016) "3D printed scaffolds with bactericidal activity aimed for bone tissue regeneration", International Journal of Biological Macromolecules, (http://dx.doi.org/10.1016/j.ijbiomac.2016.06.004).

III. **Correia, T.R.**, Ferreira, P., Vaz, R., Alves, P., Figueiredo, M.M., Correia, I.J., Coimbra, P., (2016) "Development of UV cross-linked gelatin coated electrospun poly(caprolactone) fibrous scaffolds for tissue engineering", International Journal of Biological Macromolecules, (http://dx.doi.org/10.1016/j.ijbiomac.2016.05.045).

Papers not included in the thesis

I. **Correia, T.R.**, Antunes, B.P., Castilho, P.H., Nunes, J.C., Amorim, M.T.P., Escobar, I. C., Queiroz, J.A., Correia, I.J., Morão, A.M. (2013) "A bi-layer electrospun nanofiber membrane for plasmid DNA recovery from fermentation broths", Separation and Purification Technology, Vol. 112, pp. 20–25, (http://dx.doi.org/10.1016/j.seppur.2013.03.049).

II. Ferreira, P., Carvalho, A., **Correia, T.R.**, Antunes, B.P., Correia, I.J., Alves, P. (2013) "Functionalization of polydimethylsiloxane membranes to be used in the production of voice prosthesis", Science and Technology of Advanced Materials, Vol. 14(5), (DOI: 10.1088/1468-6996/14/5/055006).

III. Fonseca, A.C. Coelho, J. F.J., Valente, J. F.A., **Correia, T. R.**, Correia, I.J., Gil, M. H., Simões, P. N. (2013) "Poly(ester amide)s based on (L)-lactic acid oligomers and alpha-amino acids: influence of the alpha-amino acid side chain in the poly(ester amide)s properties", Journal of Biomaterials Science Polymer Edition, Vol. 24(12), pp. 1391-409, (DOI:10.1080/09205063.2012.762293).

IV. Alves, P., Cardoso, R., **Correia, T.R.**, Antunes, B.P., Correia, I.J., Ferreira, P. (2014) "Surface modification of polyurethane films by plasma and ultraviolet light to improve haemocompatibility for artificial heart valves", Colloids and Surfaces B Biointerfaces, Vol. 113, pp. 25-32 (DOI: 10.1016/j.colsurfb.2013.08.039).

V. Araújo, M., Viveiros, R., **Correia, T.R.**, Correia, I.J., Bonifácio, V.D.B., Casimiro, T., Aguiar-Ricardo, A. (2014) "Natural melanin: A potential pH-responsive drug release device", International Journal of Pharmaceutics, Vol. 469, pp. 140-145, (DOI: 10.1016/j.ijpharm.2014.04.051).

VI. Carreira A.S., Ferreira P., Ribeiro M.P., **Correia T.R.**, Coutinho P., Correia I.J., Gil M.H. (2014) "New drug-eluting lenses to be applied as bandages after keratoprosthesis implantation", International Journal of Pharmaceutics, Vol. 477 (1-2), pp. 218-226, (DOI: 10.1016/j.ijpharm.2014.10.037).

VII. Castilho P.H., **Correia T.R.**, Amorim M.T.P., Escobar I.C., Queiroz J.A., Correia I.J., Morão A.M. (2015) "Modification of microfiltration membranes by hydrogel impregnation for pDNA purification", Journal of Applied Polymer Science, Vol. 132(21): pp. 41610 (DOI: 10.1002/app.41610).

VIII. Serra, I.R., Fradique, R., Vallejo M.C.S., **Correia T.R.**, Miguel, S.P., Correia I.J., (2015) "Production and characterization of chitosan/gelatin/ß-TCP scaffolds for improved bone tissue regeneration", Materials Science and Engineering: C, Vol. 55, pp. 592–604, (DOI:10.1016/j.msec.2015.05.072).

IX. Santos, J.M.C., Marques, D.S., Alves, P., **Correia, T.R.**, Correia, I.J., Baptista, C.M.S.G., Ferreira, P., (2015) "Synthesis, functionalization and characterization of UV-curable lactic acid based oligomers to be used as surgical adhesives", Reactive and Functional Polymers, Vol.94, pp. 43–54, (DOI:10.1016/j.reactfunctpolym.2015.07.003).

X. Marques, D.S., Santos, J.M.C., Ferreira, P., **Correia, T.R.**, Correia, I. J., Gil, M. H., Baptista, C. M. S.G., (2015), "Photocurable Bioadhesive Based on Lactic Acid", Materials Science and Engineering: C, Vol.58; pp. 601-609, (DOI:10.1016/j.msec.2015.09.009).

XI. Marques, D.S., Santos, J.M.C., Ferreira, P., **Correia, T.R.**, Correia, I. J., Gil, M. H., Baptista, C. M. S.G., (2015), "Functionalization and photocuring of a L-lactic acid macromer for biomedical applications", International Journal of Polymeric Materials, Vol.65, pp. 497-507, (DOI: 10.1080/00914037.2015.1129962).

XII. de Sá, K.D., Figueira, D.R., Miguel S.P., **Correia, T.R.**, Silva, A.P., Correia, I.J., (2016) "3D scaffolds coated with nanofibers displaying bactericidal activity for bone tissue applications", International Journal of Polymeric Materials, *in press*, (DOI: 10.1080/00914037.2016.1236338).

Resumo

O envelhecimento da população tem provocado um aumento do número de lesões ósseas e de doenças cardiovasculares que afetam a população mundial. As lesões ósseas têm uma maior incidência na população mais idosa que apresenta uma menor densidade óssea. Por outro lado, esta população está também predisposta a doenças cardiovasculares que ocorrem devido a quadros clínicos como a calcificação dos vasos sanguíneos, o aparecimento de arteriosclerose e o aumento de radicais livres na corrente sanguínea. Atualmente, as terapias disponíveis para o tratamento deste tipo de patologias têm uma eficácia limitada. Em meio clínico os tratamentos preferencialmente usados consistem em autoenxertos devido à aceitação pelo hospedeiro. No entanto, devido à baixa disponibilidade deste tipo de enxertos, os investigadores da área de Engenharia de Tecidos têm procurado desenvolver biomateriais para aplicação nas diversas áreas da Medicina Regenerativa. Neste contexto, estruturas temporárias tridimensionais (3D) denominadas de *scaffolds* têm sido estudados com o intuito de serem utilizados como soluções terapêuticas para o tratamento do tecido ósseo, de forma a promover a reparação deste tecido, conferindo-lhe características físicas e biológicas essenciais ao seu correto funcionamento. Da mesma forma, no tratamento de doenças vasculares tem-se recorrido a soluções que se baseiam em redes nanofibrosas ocas com arquitetura semelhante à de um vaso sanguíneo. Na presente tese foram efetuados diferentes estudos que tinham como objetivo a produção de biomateriais para posterior aplicação na área da regeneração óssea e do tecido vascular. As estruturas 3D produzidas foram caracterizadas recorrendo a testes físico-químicos e biológicos. Os resultados obtidos revelaram que os biomateriais aqui produzidos possuem propriedades adequadas para a sua futura aplicação na Medicina Regenerativa.

Palavras-chave

Doenças cardiovasculares, Biomateriais, Lesões ósseas, *Scaffolds.*

Resumo Alargado

A procura de uma melhor qualidade de vida é uma das principais preocupações atuais da sociedade atual. Na área da Medicina Regenerativa, novas abordagens terapêuticas estão a ser estudadas com o intuito de restaurar a integridade de tecidos ou órgãos que tenham sido danificados e, consequentemente, promover uma maior longevidade do Ser Humano. Os diferentes tecidos que constituem o corpo humano desempenham funções importantes, que incluem suporte, termorregulação, proteção e transporte de nutrientes. O osso é uma estrutura complexa, que está envolvido na locomoção e assegura o suporte do esqueleto, a produção de células sanguíneas e o armazenamento de minerais. Por outro lado, o sistema vascular (coração e os vasos sanguíneos) exibe um papel crucial no nosso organismo, uma vez que, garantem o correto aporte sanguíneo às diferentes partes do corpo humano. O envelhecimento é uma preocupação real que afeta milhões de pessoas em todo mundo e que leva ao enfraquecimento do tecido ósseo, tornando-o mais vulnerável a fraturas. Os mecanismos responsáveis pela formação e reabsorção óssea começam por falhar e consequentemente a integridade estrutural do osso é corrompida. Outros fatores de origem genética, ambiental e patológica estão também envolvidos no enfraquecimento do osso. Além disso, as infeções no local do implante após cirurgia são também uma preocupação. Os autoenxertos são atualmente o tratamento *standard* utilizado na clínica, no entanto, também apresentam desvantagens tais como uma disponibilidade limitada. Os allo e xenoenxertos têm sido evitados devido às desvantagens que apresentam, tal como a rejeição imune ou a transmissão de doenças. Por outro lado, as doenças cardiovasculares são a principal causa de mortalidade em todo o mundo. A maioria da população idosa apresenta condições patológicas que envolvem a calcificação de vasos sanguíneos, aterosclerose e ainda o aumento do número de radicais livres na corrente sanguínea, que contribuem para o desenvolvimento de doenças cardiovasculares. A falta de exercício físico regular associado à falta de bons hábitos alimentares pode contribuir para o desenvolvimento destas patologias. De forma a melhorar os tratamentos disponíveis, a engenharia de tecidos e a medicina regenerativa têm procurado desenvolver novas abordagens terapêuticas, que reúnem os princípios de biologia e da engenharia para reparar, regenerar ou substituir um tecido ou órgão danificado. Para tal, têm sido produzidas estruturas tridimensionais, conhecido como andaimes, que têm a capacidade de reproduzir as propriedades estruturais, mecânicas e biológicas de tecidos nativos. Estas estruturas biomiméticas devem ser caracterizadas a fim de cumprir todos os requisitos exigidos pelas entidades reguladoras. Neste projeto foram ainda estudados novos substitutos ósseos com propriedades antimicrobianas para aplicação na regeneração óssea, bem como o desenvolvimento de redes à base de nanofibras com destino à sua utilização como implantes vasculares.

Palavras-chave

Doenças cardiovasculares, Envelhecimento, Implantes vasculares, Lesões ósseas, Propriedades antimicrobianas, substitutos ósseos.

Abstract

The search for a better quality of life and a higher longevity is one of the main concerns of nowadays worldwide society. In the area of Regenerative Medicine, new therapeutic approaches are currently being studied to restore the integrity of damage tissues or organs of the human body and consequently expand the life time of Human Beings. All biological tissues present in our body play important functions ranging from support and thermoregulation to protection and nutrient transport. Bone is a complex structure that is involved in the locomotion and assures functions such as the support of body skeleton, homeostasis of blood cells production, and minerals storage. On the other hand, the vascular system also displays a crucial role on our organism, involving the heart and blood vessels, structures that assure the maintenance of blood flow. Ageing is a real concern that affects millions of people worldwide that leads to the weakness of bone tissue, turning it more vulnerable to fractures. The mechanisms responsible for bone formation and resorption start to fail and consequently bone structural integrity is compromised. Additionally, genetic, environmental and pathological factors also contribute to the limited mechanical properties of bones. Moreover, infections at the implantation site after surgical procedures are also a concern. Autografts are currently the gold standard used in the clinic, however, they have several handicaps such as the tissue limited source. Allo and xenografts have been avoided due to disadvantages as immune rejection or disease transmission. On the other hand, cardiovascular diseases are the leading cause of mortality all over the world. The older population presents in some cases calcification of the blood vessels, atherosclerosis and an increased number of free radicals on the blood flow that can trigger cardiovascular diseases. The lack of regular exercise associated with irregular eating habits can contribute to the development of such diseases. To overcome those scenarios, Tissue Engineering and Regenerative Medicine (TERM) have been studying new therapeutic approaches, by assembling the principles of biology and engineering sciences to repair, regenerate or replace a damaged tissue or organ. TERM studies rely on the development of three dimensional (3D) structures, known as scaffolds, that are able to mimic the structural, mechanical and biological properties of the native tissue. These biomimetic structures must be fully characterized in order to fulfil all the requirements demanded by the regulatory agencies. In this work, the development of bone substitutes with antimicrobial properties have been studied as well as the development of electrospun nanofibers aimed to be used as vascular grafts.

Keywords

Ageing, Antimicrobial properties, Bone substitutes, Electrospun, Scaffolds, Vascular grafts.

Table of Contents

List of Figures

List of Tables

List of Acronyms

ß-TCP	Beta-tricalcium phosphate
AgNPs	Silver nanoparticles
ANOVA	One-way analysis of variance
ARS	Alizarin red staining
ASTM	American Society for Testing and Materials
ATR-FTIR	Attenuated total reflectance – Fourier transform infrared spectroscopy
BMU	Bone morphogenic unit
BTE	Bone tissue engineering
CABG	Coronary artery bypass grafting
CAD	Computer aided design
CAM	Computer aided manufacturing
CEC	Rabbit corneal endothelial cells
CHD	Coronary heart disease
CLF	Chloroform
CLSM	Confocal laser scanning microscopy
CPC	Calcium phosphate cement
Cs	Compressive Strength
CT	Computer tomography
CVD	Cardiovascular diseases
DD	Degrees of deacetylation
DLS	Dynamic light scattering
DMF	Dimethylformamide
DS	Degree of substitution
EC	Endothelial cell
ECM	Extracellular matrix
EDS	Energy dispersive spectroscopy
EGF	Epidermal growth factor
ESB	European Society for Biomaterials
FDA	Food and Drug Administration
FDM	Fused deposition modelling
FGF	Fibroblast growth factor
GA	Glycolic acid
GelMA	Gelatin methacrylate
GRAS	Generally-regarded-as-safe
HAp	Hydroxyapatite
Hb	Haemoglobin released by haemolysis
HCA	Hydroxycarbonate apatite

HI	Haemolytic index
hOB	Human osteoblast cells
ISO	International Standard Organization
LA	Lactic acid
MIC	Minimum inhibitory concentration
MRI	Magnetic resonance imaging
MSC	Mesenchymal stem cell
MTS	3-(4,5-dimethylthiazol-2-yl)-5-(3-carboxymethoxyphenyl)-2-(4-sulfophenyl)-2H tetrazolium reagent, inner salt
MTT	3-(4,5-dimethylthiazol-2-yl)-2,5-diphenyltetrazolium bromide
NGF	Nerve Growth Factor
PBS	Phosphate buffer saline solution
PCL	Poly ε-caprolactone
PDB	Paget's disease of bone
PE	Polyethylene
PED	Precision extrusion deposition
PEG	Polyethylene glycol
PEGA	Polyethylene glycol acrylate
PEGDA	Polyethylene glycol diacrylate
PEO	Polyethylene oxide
PET	Polyethylene terephthalate
PGA	Poly glycolic acid
PLA	Poly (lactic acid)
PLGA	Poly (lactic-co-glycolic acid)
PMS	Phenazine methosulfate reagent solution
PTFE	Polytetrafluoroethylene
PU	Polyurethane
RGD	Arginine-glycine–asparagine
RP	Rapid prototyping
RT	Room temperature
SA	Sodium alginate
SBF	Simulated body fluid
SEM	Scanning electron microscopy
SLS	Selective laser sintering
TCP	Tricalcium phosphate
TE	Tissue engineering
TEM	Transmission electron microscopy
TERM	Tissue engineering and regenerative medicine
TEVG	Tissue engineering vascular graft

TPU	Thermoplastic polyurethane
UV	Ultraviolet radiation
VTE	Vascular tissue engineering
YM	Young modulus

Thesis structure

The present thesis comprises 5 chapters.

The first chapter presents the basic concepts of Tissue Engineering field as well as the biomaterials and techniques used for the production of new therapeutic approaches that are currently being developed for bone tissue and vascular tissue regeneration. The second chapter describes the "Production of new 3D scaffolds for bone tissue regeneration by rapid prototyping", where the use of this technology allowed the production of 3D scaffolds with highly controlled structure and orientation, based on computer-aided design models or medical data. To accomplish that, tricalcium phosphate (TCP) and sodium alginate (SA) were mixed using specific ratios of each material. Then, the obtained mixture was extruded based on a Computer Aided Design/Computer Aided Manufacturing (CAD/CAM) model, design in SolidWorks, and subsequently printed using a Fab@Home equipment. Subsequently, the physicochemical, mechanical and biological properties of the obtained 3D structures were characterized. The third chapter reports "3D printed scaffolds with bactericidal activity aimed for bone tissue regeneration". The 3D scaffolds described in this chapter were produced by rapid prototyping (RP) and subsequently functionalized with an antibacterial agent. To do that, TCP/SA scaffolds were produced as reported in chapter 2 and functionalized with silver nanoparticles (AgNPs) using two different incorporation methods. The TCP/SA scaffolds were obtained by using different ratios of TCP and SA materials. AgNPs were incorporated in the 3D scaffolds by direct incorporation of AgNPs solution in the composite mixture of TCP/SA, before the printing step, and by a physical adsorption of AgNPs solution to the scaffolds. Then, the mechanical, biological and bactericidal performance of the 3D scaffolds were evaluated. In the fourth chapter it is presented the "Development of UV cross-linked gelatin coated electrospun poly(caprolactone) fibrous scaffolds for tissue engineering". The electrospinning technique was used to produce fibrous matrices that were aimed to be used as vascular grafts. To attain such objective, electrospun polycaprolactone (PCL) fibrous mats were coated with different hydrogel formulations based on photocrosslinkable gelatin (GelMA), poly (ethylene glycol) acrylate (PEGA) and poly(ethylene glycol) diacrylate (PEGDA) that were photocrosslinked under UV irradiation by using Irgacure® 2959 (by BASF) as the photoinitiator. Then the properties of the 3D constructs were characterized and the results revealed that, the physicochemical properties of GelMA, associated with its remarkable biological features (excellent biocompatibility, non-immunogenicity and an outstanding capacity to promote cell adhesion and growth) make this material a very promising candidate for tissue engineering applications. Furthermore, the addition of PEGA and PEGDA macromeres aimed to improve the mechanical properties and slowdown the enzymatic degradation of the resultant material. Finally, the fifth chapter encloses the conclusions that were taken based on the gathered results and also presents future perspectives of work.

Thesis Aims

The main goal of this PhD work plan was the development and characterization of new biomaterials for tissue engineering applications. Up to date, there are a lot of structures capable of restoring soft and hard tissue. However, just a few of them are produced in a reproducible form and even a more limited number is able to avoid bacterial contamination when they are implanted at the injured site. To accomplish the production and characterization of biomaterials aimed for tissue engineering applications, the work plan comprised the following tasks:

Bone tissue regeneration:

- Optimization of scaffolds design for improving their mechanical properties of the final structures;

- Incorporation of antimicrobial agents within scaffolds structure to confer them bactericidal activity;

- Physicochemical characterization of the different scaffolds;

- Evaluation of the biological performance of the scaffolds through *in vitro* assays.

Vascular grafts:

- Production of biodegradable nanofibers that can mimic the mechanical properties of the native tissues while avoiding the thrombus formation;

- Modification of biomaterials' surface for improving cell adhesion and proliferation, when they are seeded in contact with these materials;

- Characterization of physicochemical and biological properties of the produced meshes.

Development of new biomaterials for tissue engineering applications

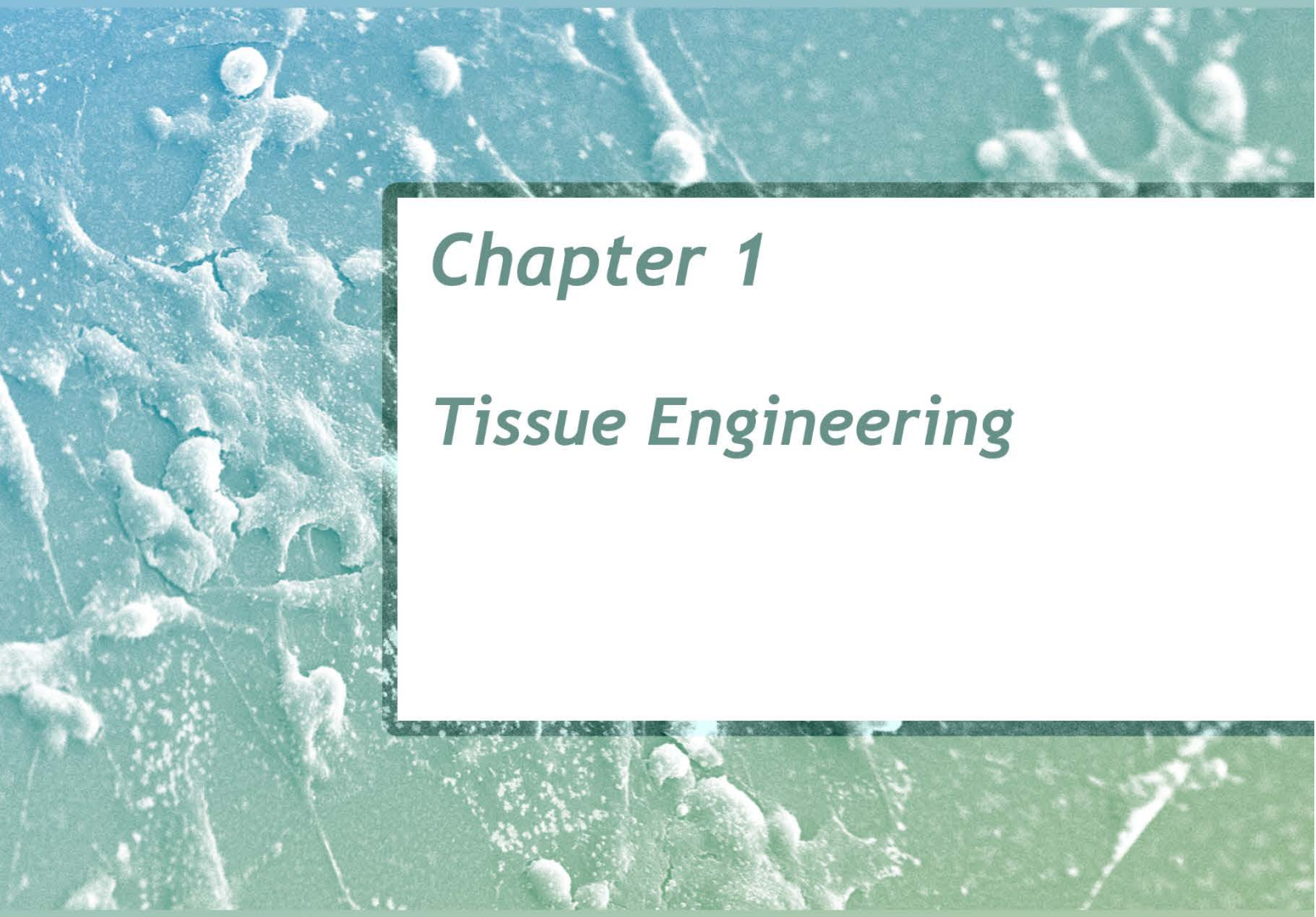

Chapter 1

Tissue Engineering

Correia, T.R

1. Tissue Engineering

Since antiquity, Human Beings have been seeking for a higher longevity with an improved quality of life. Nowadays, the ageing of the worldwide population triggered the necessity of replacing and repairing soft and hard tissues (Figure 1.1).

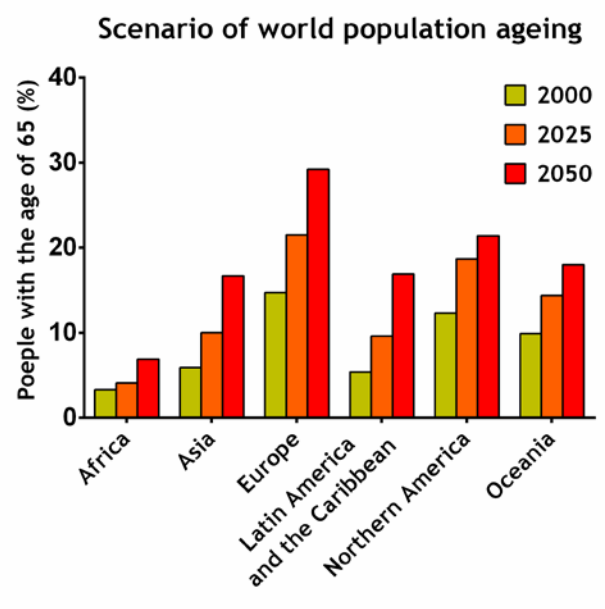

Figure 1.1 Illustration of the scenario of the world population over the age of 65 at year 2050 (1).

Tissue Engineering (TE), is a field of science that combines the knowledge from medicine, biology, materials science and engineering in order to develop a solution that is able to create, repair or even improve the function of a damaged tissue (2). Researchers from this area have been studying and developing therapeutic alternatives to repair and restore the functions of the different tissues of the body. Human body tissues can be organized based on the function that each of them must fulfil.

Bone and ligament/tendon are classified into mechano-sensitive tissues since they are responsible for the structural integrity of the body and also for its flexibility. Contrarily to skin, these tissues are exposed to mechanical forces that result from daily activities like walking or exercising. Besides, these tissues must possess high elasticity in order to absorb or diminish abrupt mechanical changes associated with locomotion. When these tissues are critically damaged, 3D constructs (3-6) are the most common solutions used in TE. However, bone tissue requires higher mechanical strength, whereas ligament/tendon demand for a higher elastic modulus.

Bone Tissue Engineering (BTE) is a field of Regenerative Medicine that is focused on the development of new therapies to overcome the drawbacks associated with bone diseases and fractures (7). To date, many studies have been performed in order to produce 3D structures

that can act as a support for the healing of bone tissue. Thus, permanent and temporary implants have been developed and some of them are, nowadays, used in the clinic. However, the majority of permanent implants induce morbidity at the implantation site and require multiple surgeries (8). Alternatively, temporary structures, also known as scaffolds, are currently being investigated. They can be produced with different types of materials: polymers (including natural and synthetic), ceramics, metals and composites (9-15). Furthermore, the application of such materials in BTE should fulfil essential requirements like osteoinductivity, (be able to recruit progenitor cells, allow their differentiation into osteoblasts; osteoconductivity, i.e., for promoting the bone growth and endorse the ingrowth of the surrounding tissue) and osseointegration, in order to allow its interaction in the surrounding bone (16).

Blood vessels, the organic conducts that are subjected to fluidic shear stress and cyclic expansion/contraction due to cardiac contractions, are considered shear stress-sensitive tissues (17). These structures display different functions such as the filtration in the kidney, gas exchange in the lungs, and extensive branching for coronary circulation (18). The shear stress property presented by blood vessels, is essential for intrinsic cellular tasks, that include proliferation, elongation and protein secretion, in order to avoid irregular tissue stresses and strains that induce changes on the biochemical homeostasis, leading to vascular remodelling and possible dysfunction (19). Moreover, the rigidity as well as the topographic features have also an important role since different pressures are found in arteries or veins. When abnormal situations occur, such as irregular pressures or the blockage of blood vessel, demand for therapeutic solutions that have include so far autologous grafts combined with host cells (20), or more recently the production of nanofibrous meshes (21, 22) that are able to reproduce the structure of the native blood vessel.

TE can also give an important contribute for the treatment of cardiovascular diseases which are one of the leading causes of mortality of the contemporary society (23). In the past twenty years, due to the increasing number of vascular diseases (including blood vessels obstruction and the need of vascularization of some tissues) that affects humans have triggered the development of new materials (24). Herein, reproducible methodologies were used to develop materials that can be used for the production of vascular grafts that are able to avoid thrombus formation.

1.1. Biomaterials

The term biomaterial was used for the first time in 1976, during a Conference of the European Society for Biomaterials (ESB) to describe “a nonviable material that was used in the production of a medical device, intended to interact with biological systems”. Currently and due to the intensive research performed in the fields of biomaterials and tissue engineering,

the definition given by ESB has evolved to a "material intended to interact with biological systems to evaluate, treat, augment or replace any tissue, organ or function of the body" (25).

During the last 60 years, biomaterials research comprised four generations of materials that display an increasing degree of complexity and that have the ability to interact with the biological tissues of the human body. Biomaterials of the first generation were selected and developed in order to match the physical properties of the damaged tissue with a minimal toxic response from the host. However, the first generation of biomaterials was not intended for medical applications. Instead, these materials were used in chemistry, food, transport and energy industries. Despite the efforts made to increase their purity degree in order to be used as a medical device, these materials were not successful, displaying toxicity issues and inability to interact with the host (26). Such lack of interaction with the biological systems gave them the designation of "inert materials" (27). This class of materials was mainly composed by metals, where stainless steel, titanium (Ti), chromium-cobalt and Ti alloys were the ones that are still in use.

Between 1980 and 1990, the second generation of biomaterials arose with the purpose to overcome the handicaps presented by the first generation of biomaterials (27). These materials were developed to interact with the biological environment, by eliciting a biological response while they were degraded as the new tissue is formed. Nowadays, they are known as bioactive materials and some of them are still in use, like calcium phosphates, polylactides, polyglycolides, polycaprolactones and trimethylcarbonates (28, 29). Despite the improvements made on these materials, their use is still limited by the capacity of the organism to tolerate them.

The third generation of biomaterials arose between the 1990s and 2000s, due to the demand for developing materials that contain features and properties that are able to be adapted to the organism, i.e., being not only bioactive but also resorbable (30). These type of materials, known as "biocompatible nanocomposites", were characterized by their ability to stimulate the regeneration of a tissue at a molecular level in a process that involved genes activation. Moreover, they were able to reproduce some of the structures found in the biological systems, due to chemical functionalizations performed on their structure (27, 31). Bioactive glass and porous foams as well as composites are examples of this class of biomaterials, which are still currently available in the market (32). Although these materials were able to mimic the structure and composition of the native biological tissues, they could not reproduce specific functions triggered by internal/external stimulus.

Finally, the fourth generation of biomaterials, also known as biomimetic or smart biomaterials, emerged in 2010 and revolutionized the area of biomaterials (30). This class of biomaterials has been characterized by its ability to trigger cellular and tissue functions in response to internal or external stimuli such as pH, temperature, ionic strength, and magnetism (33). Currently, the modification of materials surface properties has become an effective approach, where features like roughness, topography and chemistry have a crucial role on promoting cell responses like attachment, migration, proliferation as well as differentiation.

Furthermore, the porosity, pore size, surface area to volume ratio and pore interconnectivity contribute for tissue in-growth, vascularization and nutrient supply (34-36). In order to perform the material functionalizations' mentioned above, new rapid prototyping (RP) techniques such as 3D bioplotting and inkjet printing are being used. Thus, this new generation of biomaterials involves a wide range of suitable hybrids and composites, which can be produced in the form of 3D scaffolds, hydrogels and nanoparticles that have been functionalized with cells, antibacterial drugs, growth factors, peptides and genes in order to mimic as much as possible the native features found in the host tissue (33).

1.2. Bone Tissue

Bone is a highly regulated tissue that plays several functions in the organism. Bone confers protection to vital organs, such as brain, spinal cord and the heart. Moreover, bone is also involved in the storage of mineral compounds, like phosphorus and calcium. It also controls the haematopoiesis process, assuring blood cells production' in bone marrow (42). Furthermore, it has also self-healing capacity, i.e., it can regenerate by itself from non-critical lesions.

1.2.1. Bone composition

Macroscopically, human bone is typically composed of cortical bone, trabecular bone, periosteum, endosteum and articular cartilage (27). Trabecular or cancellous bone is considered as fresh and soft tissue that fills the interior of bone. It displays a large surface area, that allows a greater cellular exchange and a porosity level between 50-90%, which is highly distinct from the one displayed by cortical bone tissue. The metabolic activity of this tissue is very high and this tissue is constantly under remodelling (34). On the other hand, cortical bone is a rigid and denser tissue that can be found in the outer layers of bone. Cortical bone is a compact tissue that has few gaps or spaces (it presents a porosity range between 2-15%). It comprises a major structural subunit, the osteon, which is the central component of the Haversian system. The osteon is an irregular, branching and anastomosing cylinder composed of a centrally placed neurovascular canal surrounded by cell permeated layers of bone matrix (35). Its architecture, gives it a crucial role on the protection of the organs of the body.

Bone can also be classified as either lamellar or non-lamellar. Such classification is based on collagen fibers arrangement. Lamellar bone can be found in all mature bones, where collagen fibers display a parallel alignment while the non-lamellar has a random distribution of the collagen fibers and it is only present in the fetus, childhood or healing fractures.

At a microscopic level, bone is composed by 30% of organic (mainly collagen type I) and 70% of inorganic matrix (37). The collagen matrix controls the bone toughness while the mineral phase is responsible for bone stiffness. In addition, the proportion of organic and inorganic matrix can suffer variations with ageing. The organic matrix is mainly composed by extracellular matrix (ECM) and bone cells namely, osteocytes, osteoblasts and osteoclasts. The ECM offers not only the structural support required for cellular constituents but also a suitable milieu that contains the biomechanical signals essential for tissue morphogenesis, differentiation and homeostasis (38). Apart from collagen, the ECM is also composed by different classes of noncollagenous proteins, like, proteoglycans, adhesive glycoproteins, bone specific proteins, growth factors and cytokines (39).

Proteoglycans are made of glycosaminoglycan (GAG) chains (e.g. hyaluronan, chondroitin sulfate) which are connected to a specific protein core. GAGs are anionic polysaccharides of linear chain, composed by the repetition of disaccharide units. The negative charge of GAG chains enables the uptake of water and divalent cations by proteoglycans, which consequently confers highly hydrated filling spaces where fibrous proteins are embedded (40).

Adhesive glycoproteins include fibronectin, osteonectin, osteopontin, vitronectin and sialoproteins. These proteins are involved in the interaction between ECM and bone cells. These proteins are recognized by transmembrane protein receptors called integrins (41). Fibronectin is a dimeric protein that has a crucial role in cell attachment and migration, acting as "biological glue". Each fibronectin subunit contains three types of repeats I, II, and III. Type I repeat is composed of 40 amino acids in length and contains disulphide bonds. The type II regions comprise 60 amino acids and have also disulphide bonds. The type III repeat is formed by 90 amino acids long (42). Additionally, it has binding sites to other fibronectin dimers, collagen, heparin, and other cell surface receptors. Osteonectin is known to act as a glue between the collagen and hydroxyapatite crystals. Osteopontin mediates the attachment of cells to the bone matrix. Vitronectin is abundantly found in blood serum, extracellular matrix and bone. It promotes cell adhesion and spreading by binding to a specific integrin, the alpha-V beta-3. It is also involved in haemostasis process since it is a constituent of platelets. Sioaloproteins I and II are also glycoproteins that have an important role on the mediation of cell attachment and that are able to induce calcium phosphate formation during the mineralization process.

Bone specific proteins are a set of specific proteins that have an important role on the regulation of specific bone tasks. For example, osteocalcin, that belongs to this class of proteins, is responsible for collecting the calcium from blood circulation as well as for recruiting and stimulating osteoclasts in bone remodelling (43).

Growth factors and cytokines (interleukins) are involved in the regulation of specific cellular pathways. Bone morphogenic proteins (BMPs), are a group of proteins that belong to the Transforming Growth Factor beta superfamily (44). A total of twenty BMPs are known and some of them play important functions in bone tissue. Among them, BMP-2 and BMP-7 are

involved in osteoblast differentiation, BMP-3 has been reported to induce bone formation and BMP-6 has a key role in joint integrity by controlling iron homeostasis (43, 45, 46).

The inorganic component of bone comprises 50 to 70% of the dry weight of bone and it is mainly composed by hydroxyapatite (HAp), which is a calcium orthophosphate ($Ca_{10}(PO_4)_6(OH)_2$) containing water and other ions like strontium, zinc and carbonate (47) (41). This component of the bone provides mechanical resistance to this tissue.

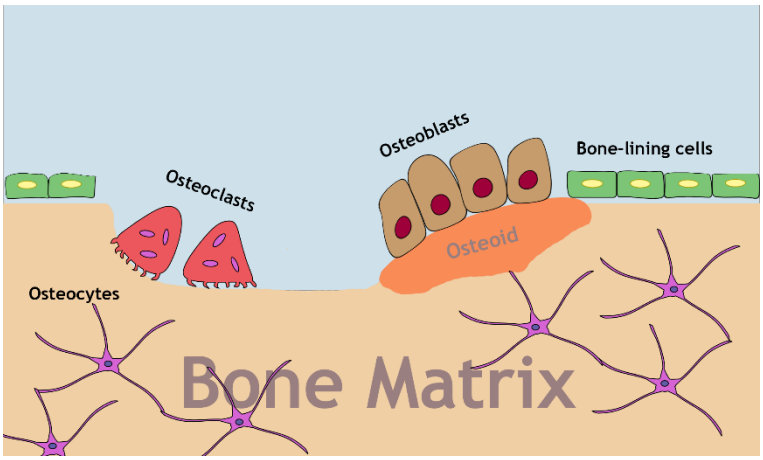

Figure 1.2 Representation of basic multicellular units involved in bone remodelling: osteocytes, osteoblasts, osteoclasts and bone-lining cells (adapt from (48)).

Different cell types are involved in bone formation and remodelling (see Figure 1.2 for further details).

Osteoblasts are polarized cells that present a nucleus on the surrounding area and are usually deposited along the interface that is adjacent to bone formation such as the periosteum (external surface) and bone marrow (internal surface). They are also composed of specific organelles, namely the ample endoplasmic reticulum, a higher number of ribosomes, a Golgi complex and a mitochondria (49). Osteoblasts are specialized mesenchymal cells that are responsible for the production of bone tissue. These cells produce collagen type I and other ECM proteins such as fibronectin, osteocalcin, osteonectin, sialoprotein and vitronectin (50). The produced collagen matrix is mineralized with hydroxyapatite crystals in order to originate bone tissue.

Osteocytes are bone cells obtained by osteoblasts maturation, i.e., osteoblasts become surrounded by osteoid or demineralized bone matrix and originate osteocytes. These cells represent 90% of the population of bone cells found in a mature human skeleton (51) and are commonly located between the bone gaps. Morphologically, osteocytes show a stellate shape, with a reduced endoplasmic reticulum, a mitochondria and a single nucleus, that allows these cells to maintain constant the mineral concentration of the bone matrix, namely, calcium and phosphorus (52).

Osteoclasts are transient multinucleated cells derived from hemopoietic cells of the monocyte/macrophage lineage, that are involved in bone resorption (53). These cells can be found at the surface of bone and at sites of old, injured, or unneeded bone. Structurally, they present a high number of mitochondria around the nucleus, a rough endoplasmic reticulum and a developed Golgi complex. Additionally, they are also composed by vesicles, vacuoles and lysosomes. Such organelles are crucial for osteoclasts be able to perform other tasks like energy generation, protein synthesis and lysosomal enzymes production (41).

1.2.2. Bone formation

Bone formation or osteogenesis is a process that starts in the third month of fetal life and lasts until the late adolescence. There are two major paths used for bone formation, known as intramembranous and endochondral.

Intramembranous ossification

Intramembranous bone formation occurs by direct ossification of mesenchymal tissue into bone. Such event is primarily responsible for the formation of skull bones. It is initiated around the eighth week of gestation in humans (52). This process takes place on a pre-existing fibrous layer of connective tissue (54). There, mesenchymal cells derived from neural crest migrate, proliferate and condense into compact nodules where the new bone tissue will be formed. Then, the cells located at the new tissue formation site differentiate into osteoprogenitor cells, that subsequently originate osteoblasts. These osteoblasts begin to produce the new bone matrix that binds calcium salts for assuring the mineralization of the matrix. Consequently, the osteoblasts that remain in bone matrix become differentiated into osteocytes. The accumulation of matrix occurs between the embryonic blood vessels, resulting on a network of trabecules. Moreover, by appositional growth, i.e., by adding tissue to the bone surface, spicules are formed and placed in the cortex layers of the ossification region. These structures are then surrounded by mesenchymal cells that originate the periosteum. After that, trabecules migrate to a deeper zone of the periosteum, creating a woven bone collar that is replaced by lamellar bone as it matures. The new spongy bone remains in the internal structure of the bone, where its vascular tissue represents the red marrow (52).

Endochondral ossification

Endochondral bone formation begins with a cartilaginous intermediate which is formed and replaced by embryonic bone. In particular, endochondral ossification starts by recruiting mesenchymal stem cells to the site where the new bone will grow (Figure 1.3). Such process is characteristic of long bones formation'. Initially, mesenchymal cells are differentiated into chondroblasts and are stimulated by fibroblastic growth factors and BMPs to produce collagen type II.

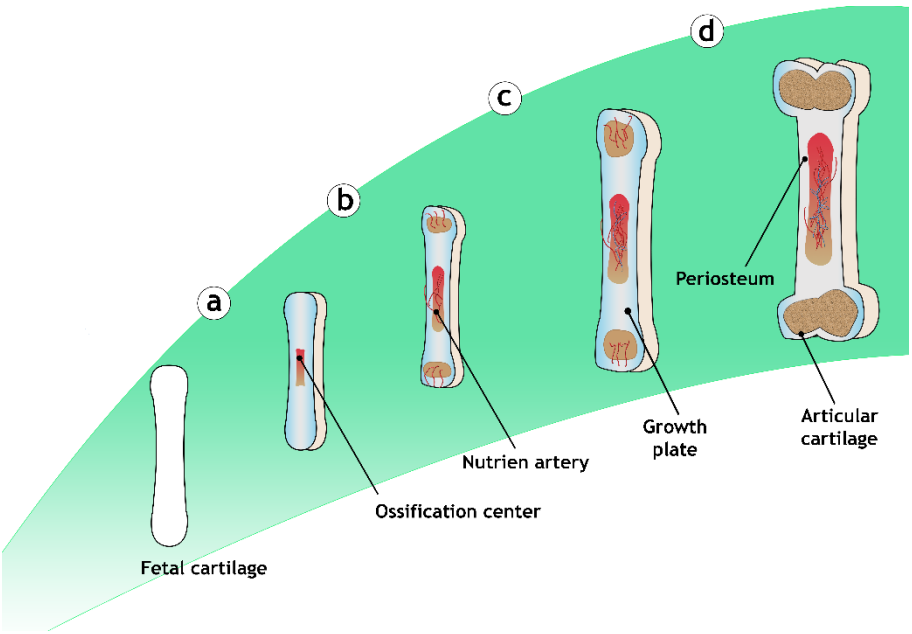

Figure 1.3 Representation of endochondral ossification process. It starts with the formation of a fetal cartilage. Subsequently, a set of specific events that include mineralization and angiogenesis will take place within the cartilage intermediate. Lastly, the mature structure of bone is assured through the replacement of cartilage by bone.

Furthermore, chondroblasts are also involved in the production of hyaline cartilage (Figure 1.3a). This fetal cartilage is obtained by interstitial and appositional growth, i.e., the new tissue is formed within the matrix midpoint and in the surface of the cartilage, respectively. Subsequently, the cells of the mid region of cartilage tissue begin to produce bone-forming cells or osteoblasts. The tissue located around cartilage, the perichondrium, originates the periosteum where an osteogenic layer is deposited by osteoblasts. This new bone establishes a cuff around the cartilage model located at the diaphysis portion of the bone. After that, blood vessels invade the cartilage and the new osteoblasts produce the primary ossification centre (Figure 1.3b). Then, a modular cavity is formed and secondary ossification centers emerge form in the bone epiphyses' (Figure 1.3c). After the

ossification of epiphyses, the hyaline cartilage remains in the epiphyseal plates and articular cartilages (Figure 1.3d) (52, 55).

1.2.3. Bone remodelling

Bone remodelling is a lifetime regulated mechanism that assures the repair and replacement of the old bone by the new one (56). Bone remodelling duration is dependent on the bone type. The remodelling of cancellous bone lasts about 200 days while the cortical bone remodelling occurs during 120 days (54, 56). As reported by Frost, bone remodelling is carried out by basic multicellular units (BMUs), in a process where osteoclasts, osteoblasts and osteocytes are involved (57). The first phase comprises a remodelling cycle and involves the recruitment of osteoclast precursors that differentiate into mature osteoclasts, that are involved in bone resorption. Subsequently, a reversal phase takes place, where the osteoclasts activity is ended with these cells becoming apoptotic. At the same time, osteoblasts are recruited and begin to differentiate into mature osteoblasts in order to produce the new bone matrix, leading to bone formation. The bone formation process takes more time than bone resorption, since it involves bone mineralisation and osteoblasts differentiation, making the last stage the longest of bone remodelling (54).

1.2.4. Bone diseases

The aging of worldwide population has associated an increased incidence of bone lesions. Various factors can influence bone homeostasis, like dietary intake of calcium and protein, serum vitamin D concentrations and weight-bearing physical activity, may lead to the formation of fragile bones or to the development of a bone disease (58, 59). Food habits are determinant for bone health since the ingestion of micronutrients (calcium, phosphorous, folate, vitamin A, B_{12}, B_6, C, D, K) and macronutrients (carbohydrates, proteins, fats) are highly associated the development of fractures due to malnutrition, a clinical situation that has been frequently observed, particularly in elderly people (60). Furthermore, in elderly population the bone formation is overcame by bone resorption (61). Nevertheless, recent studies have already reported that ions and organic compounds, like zinc and soybean (present in fruit and vegetables), are capable of stimulating osteoblastic bone formation and to inhibit osteoclast activity (62, 63). The lack of food habits in association with a sedentary life, can contribute for the development of skeletal disorders that cause chronic pain, having a high impact in population quality of life. Osteoporosis, Paget's disease and osteoarthritis are examples of diseases that affect the worldwide population (64). Currently, only few therapeutic approaches have been reported to diminish bone pain, and thus there is a huge demand for new therapeutic approaches.

Osteoporosis

Osteoporosis is a widespread musculoskeletal disease that is responsible for more than 1.5 million of fractures that occur annually (65). Several osteoporosis epidemiological studies have reported that approximately one-half of the fractures occur in individuals with nonosteoporotic bone mineral density, with higher incidence in men (around 70%) (66). On the other hand, osteoporotic fractures usually occur in older population and have a higher incidence in women than in men (50% and 20%, respectively). These type of fractures are a real concern, especially if it´s a hip fracture, since they increase the risk of death after the fracture has occurred until a period up to 10 years due to conditions like late comorbidities, functional decline, mental function or socioeconomic status (67, 68). Women due to menopause phenomenon are characterized by a disturbance in bone remodelling process since bone resorption exceeds bone formation (69).

Paget's disease

Paget's disease of bone (PDB) is the second most frequent skeletal disorder. It was described for the first time by Sir James Paget, who reported a condition of *Osteitis deformans* (70). This random disease, targets the axial skeleton, specifically the pelvis (67%), spine (39%), femur (33%), tibia (19%), and skull (25%) (69). Paget's has the highest incidence in England and has been spread to the rest of Europe and other countries. There are no reports of this disease prevalence in Africans and is considered rare in Scandinavian countries and Asia (70). PDB is characterized by being an asymptomatic disease, since patients show few symptoms, although they suffer bone pain, deformity, fracture, and deafness (47). It can be diagnostic through a conventional radiograph, by magnetic resonance imaging or computer tomography. Some indicators such as high levels of alkaline phosphatase and vitamin D deficiency may indicate a PBD status (53).

To treat such illness, bisphosphonates have been used to reduce bone pain, however they did not succeed (54).

Furthermore, different efforts have been made to understand the genetic factors that trigger PDB, although they are not completely known (71). It is believed that PDB illness is determined by mutations on genes that regulate osteoclast function. Not withstand, environmental factors such as diet, toxins and infections may also play a key role in the development of this disease (72). Moreover, PDB incidence has been reported to increase with age, being more common in men than in women (73).

Osteoarthritis

Another bone disease that also affects the population is osteoarthritis. It is believed that by the year of 2020, osteoarthritis will be the fourth leading cause of disability Worldwide (74). The

incidence of this illness is higher in women than men (69). Due to the irreversible condition, this disorder increases indefinitely with age. It is estimated that 9.6% of men and 18.0% of women, above the age of 60, have symptomatic osteoarthritis (73). Globally, osteoarthritis is more prevalent in Europe and United States of America (USA) than in other continents (69).

Osteoarthritis has been described as a degenerative joint disease, where an irregular remodelling of joint tissues occurs due to the presence of inflammatory mediators within the affected joint (75). Furthermore, the condition is characterized by joint pain, tenderness, mobility limitations, crepitus, occasional effusion, and different degrees of local inflammation. It can appear in any joint but commonly affects the hip, knee and the joints of hand, foot and spine. Osteoarthritis disease has been reported to be associated with several risk factors like obesity, trauma, ageing, sex, genetics, race/ethnicity and diet (76, 77). Currently, the treatments used in the clinic for osteoarthritis involve analgesia and surgical intervention. However, clinicians are focused on the control of the risk factors, specially, obesity. They believed that overweight or obese people should be encouraged to participate in aerobic exercise programmes such as walking, bike riding or swimming (77).

The pathological conditions presented before that may result on a critical fracture, commonly, require a clinical solution to promote patient's treatment. Thus, the initial approach that clinicians usually follow is the application of grafts for limited sized bone fractures.

1.2.5. Bone grafts

Since the antiquity, bone grafts have been proposed as a viable option to treat bone fractures. They can be classified into autograft, allograft, and xenograft (Figure 1.4). Every year, approximately 1 million of bone allografts are used in the clinic. Among the different grafts, autografts remain the gold standard used in clinic due to their significant osteoinductive and osteoconductive properties (78).

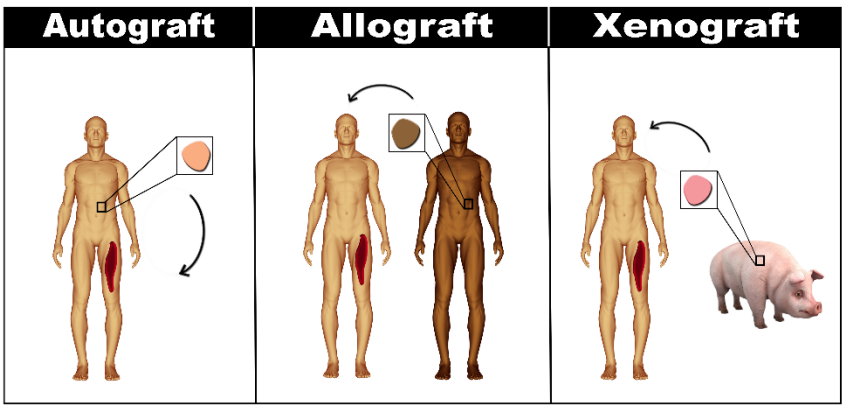

Figure 1.4 Schematic representation of the different types of grafts used in BTE.

Autografts

Autografts can be defined as the portion of tissue collected and reimplanted into the same individual. These type of implants are the preferred by the clinicians due to the absence of immune reactions from the host to the presence of the graft as well as the maintenance of cell viability and the occurrence of neovascularization. The autografting procedure usually uses the iliac crest as donor site, but other options can be taken into account such as the proximal tibial, distal radius, and femur (79). However, this type of implants has as handicaps donor site morbidity and limited tissue availability, that can consequently trigger significant issues such as fracture, pelvic instability, hematoma formation, infection and nerve palsies (80-82).

Allografts

Bone allografts are harvested tissue that is obtained from human cadaveric donors. Similarly to autografts, these implants possess properties such as osteoinduction and osteoconduction. This type of grafts is nowadays used for the treatment of large bone defects that must be fulfilled (47). Moreover, it is frequently applied in spinal fusion surgery, anterior cervical corpectomy and fusion, and anterior lumbar fusion (83). Allografting transplantations, including surfaces and ligaments, have been reported as suitable for 70% of the patients (84). However, allografts may trigger the occurrence of infections caused by bacteria, fungal or virus contamination (85, 86).

Xenografts

Ultimately, as a last resort, xenografts are used for patients who demand large amounts of tissue transplantation. This class of grafts are usually obtained from animals and they may be involved in virus transmission, infection, toxicity, immunogenicity and host rejection occur (87).

Due to these limitations of the different grafts, researchers have been looking for new therapeutic alternatives for bone regeneration replacement. Initially, titanium implants were frequently used on bone fractures due to features like mechanical strength and resistance to corrosion that were compatible with bone physical requirements (88). However, after surgery, these implants displayed limited interaction with the host tissue leading to the formation of a fibrous soft tissue capsule around themselves. This fibrous capsule avoids the implant fixation and consequently result on clinical failure (89). Moreover, titanium has poor shear strength, making it inappropriate for bone screws and plates. Furthermore, Ti alloys display a high coefficient of friction that can lead to the formation of wear debris resulting in inflammatory

reaction causing pain and loosening of implants due to osteolysis (88). To overcome those handicaps, the research work performed in BTE area is centred on the development of new bone substitutes with high potential to be used as medical devices. These new bone substitutes can be produced in the form of paste, powder or compact and have their origin from the combination of materials such as natural and synthetic polymers, ceramics, metals and composite materials.

1.2.6. Bone tissue Engineering

1.2.6.1. 3D scaffolds

In the last years, a huge effort has been done in order to develop an ideal structure that can be used for bone tissue regeneration. These 3D structures, also known as scaffolds, have been produced with different architectures according to the bone defect that is aimed to be treated (90). These scaffolds are conceived to provide enough mechanical support while allowing cell adhesion and proliferation as well as to deliver bioactive molecules (91). For BTE applications, an ideal scaffold must fulfil the following set of specific features:

- **Biocompatibility**

Biocompatibility was defined by Williams in 1987 as the capacity of a material to trigger an adequate response after its implantation in the host (92). The biocompatibility of biomaterials is an essential feature that any material aimed for TE must fulfil in order to provide beneficial effects, such as the stimulation of specific cell differentiation, enhance an appropriate vascularization and avoid toxic effects that could be associated with the by-products resulting from materials degradation (25, 93-95). Moreover, issues like thrombosis, which involves blood coagulation and adhesion of blood platelets to biomaterial's surface, and the fibrous tissue encapsulation of biomaterials implanted in soft tissues, are also biocompatibility concerns that must be avoided (96).

- **Biodegradability**

Scaffolds can be design according to the pretended biomedical application in order to act as permanent (e.g. titanium alloys) or temporary (eg. biodegradable polymers) implants. The temporary structures are currently the most investigated solutions since they can present different degradation rates, allowing the development of a new tissue. To accomplish that, the rate of a scaffold degradation must match the rate of new tissue formation (25, 95). Moreover, scaffold's degradation is also dependent on the local of implantation and patient age.

- **Mechanical properties**

3D structures aimed for bone regeneration must provide an adequate mechanical support that fulfil the demands of the site where they are implanted (25). Specifically, in the case of bone tissue, the mechanical properties of scaffolds must be compatible with those presented by the native bone (97). Trabecular bone displays a Young Modulus (YM) and a compressive strength (Cs) that range from 0.1 to 2 GPa and from 2-20 MPa, respectively, whereas the cortical bone displays a YM between 15-20 GPa and a Cs between 100-200 MPa (98).

- **Appropriate architecture**

Despite presenting mechanical properties that must be similar to that of native bone tissue, a scaffold must also possess an appropriate shape and size that enables the filling of bone defect and allows the exchange of gases and nutrients as well as cell adhesion and proliferation (25). Furthermore, the pore size of the scaffold (200–600 μm) is a key factor that determines the capacity of cells ingrowth (97, 99).

- **Osteoconductivity**

Osteoconductivity is defined as the ability of a scaffold to support the attachment of bone cells such as osteoblasts or osteoprogenitors cells and provide a suitable interconnected structure that is compatible with cell migration and angiogenesis processes to occur (98).

- **Osteoinductivity**

Osteoinductivity can be described as the ability of a scaffold to promote cell differentiation of the osteoprogenitor cells into osteoblasts (100). Such feature has a huge importance, since an increased number of osteoblast cells will trigger the bone formation process and consequently improve the regeneration of bone tissue.

- **Osseointegrative**

To be integrated in the pre-existing bone, the new structure must possess adequate properties, i.e., the material used on implant production should be bioinert or bioactive and present surface features like hydrophilicity, roughness, adequate design and geometry, where porosity and appropriate shapes allow the growth of the new bone tissue; adequate mechanical properties where the scaffold must support the formation of the bone tissue compatible with the force and load of the tissue to be repaired (101). The osseointegration mechanisms involve an initial interlocking between bone and the implanted body, followed by biological fixation through continuous bone apposition and remodelling toward the implant (102).

- **Suitability of the manufacturing method**

The methodology used for scaffold production must be fast, reproducible, cost effective, and also be scalable (103). Moreover, the manufacturing method depends on specific rules that turn it on a suitable procedure for scaffolds' production. The governmental agencies that certify these medical devices are the Food and Drug Administration (FDA) in United states and the CE in Europe. Although in US a premarket notification or 510k clearance of the product is required before being approved by FDA, in European countries a CE mark is a demand before it can be commercial available. In order to be used in clinical milieu, scaffolds must fulfil different standards established by the International Standards Organization (ISO) (100). The ISO 10993 establishes the requisites for a material to be considered biocompatible. This ISO comprises the guidelines for *in vitro* evaluation of the scaffolds. After that, the ISO 12485 defines the parameters for scaffolds´ quality management, where the sterilization step using radiation follows the guidelines of ISO 10337 and the microbiological assays are regulated by ISO 11737. Subsequently, they are labelled, packed and the expiration date is attributed (ISO 11607). At the last stage, clinical trials have to fulfil the Current Good Manufacturing Practices (cGMP). These cGMP are performed under controlled conditions in order to assure the quality and purity of the scaffolds during fabrication. Finally, clinical trials procedure has to follow a pre-defined protocol to test the safety and effectiveness of the biomedical device in humans (104, 105).

1.2.6.2. Materials used for scaffolds production

So far, different materials have been used for bone scaffolds production, including natural and synthetic polymers, ceramics, metals as well as composites. However, they all present advantages and limitations, as can be observed in Table 1.1.

Table 1.1 Advantages and disadvantages of the different materials used for scaffolds production (adapted from (95)).

Material type	Examples	Advantages	Disadvantages
Natural polymers	Chitosan, collagen, gelatin, sodium alginate, hyaluronic acid, carrageenan	Biocompatibility Biodegradability Cell binding epitopes	Hard processing Weak mechanical properties
Synthetic polymers	Poly ε-caprolactone (PCL), poly (lactid acid) (PLA), poly (lactic-co-glycolic acid) (PLGA), poly (methyl methacrylate) (PMMA)	Availability Biocompatibility Easy to modify and process Low Cost	Reduced cell attachment The by-products resulting from their degradation can interfere with the healing process
Ceramics	Tricalcium phosphates (TCPs), HAp	Biocompatibility Osteoconductive	Brittle and prone to fracture
Metals	Ti, cobalt alloys	Fracture resistance Mechanical strength	Do not allow tissue growth Immunogenicity Toxic degradation products
Composites	Alginate/TCP scaffolds Gelatin/PCL scaffolds PCL/HAp scaffolds	Specific composition Structural specific design	Complex process Prone to degradation Weak mechanical strength

Natural polymers have been widely used due to their biocompatibility, biodegradability and structural similarity with bone organic matrix. Among them, polysaccharides like chitosan, alginate and carrageenan, proteins such as collagen, gelatin and silk fibroin, and glycosaminoglycans as chondroitin sulphate and hyaluronic acid have been used for the production of scaffolds (106).

1.2.6.2.1. Natural Polymers

Alginate

Alginate is an anionic polysaccharide that presents a linear copolymer chain composed of blockwise structures of (1,4)-linked ß-D-mannuronic acid (M) and α-L-guluronic acid (G)

residues (Figure 1.5a) (107). Alginate presents an excellent biocompatibility, low toxicity, non-immunogenicity, low cost, and simple gelation behaviour in the presence of divalent cations such as Ca^{2+}, Mg^{2+}, Ba^{2+}, and Sr^{2+} allow its use for hydrogels, sponges, beads and fibers production and also enables its application in several areas of Tissue Engineering and Regenerative Medicine (TERM), namely skin (108), cartilage (109), bone (107, 110), liver (111) and cardiac tissue (107, 112). Additionally, alginate is non-degradable in physiological conditions since the enzyme alginase is not present in the organism. However, when alginate is crosslinked, it can be dissolved through a process involving a loss of divalent ions into the surrounding media (113). Furthermore, alginate is also able to mimic bone organic matrix providing a suitable milieu for cells adhesion and proliferation (5, 114). So far, the use of alginate has been reported in several structures for bone applications. Luo and colleagues have incorporated a peptide into a 3D porous alginate scaffold for improving *in vitro* bioactivity and osteogenesis process. Valente *et al.* in a recent study used sodium alginate to produce scaffolds aimed for BTE applications (107). In their study, microparticle and microfiber alginate scaffolds were produced using a particle aggregation technique. Their results demonstrated that alginate scaffolds had suitable mechanical and morphological properties that were compatible with cell adhesion and proliferation. In another study performed by Quinlan and his team alginate and PLGA microparticles were produced, using spray-drying and emulsion techniques, that were aimed to be used as carriers for performing a controlled delivery of recombinant bone morphogenic protein 2 (rhBMP-2) (115). They noticed that these scaffolds, were capable of performing a sustained release of rhBMP-2 that enhanced *in vitro* the osteogenesis process. Moshaverinia *et al.* produced alginate microspheres loaded with murine anti-BMP2 monoclonal antibodies and human bone marrow mesenchymal stem cells (hBMMSCs). Their results showed that it was possible to encapsulate stem cells while promoting their differentiation into bone cells by using inductive signals that are provided by the anti-BMP2 monoclonal antibodies (116).

Chitosan

Chitosan is a natural cationic polymer known for its versatility and it is obtained through the alkaline deacetylation of chitin, that is found on the exoskeleton of the crustaceans such as shrimp, crab and lobster (117). This polysaccharide is composed by glucosamine and N-acetyl glucosamine units linked by ß(1-4) glycosidic bonds (118) (Figure 1.5c). It can present a degree of deacetylation (DD) ranging from 50-95%. The DD of chitosan has been reported to strongly influence properties such as charge density (number of available amines for binding), solubility, crystallinity, and degradation rate (119). Furthermore, chitosan can be enzymatically degraded through lysozyme and chitosanase, being its degradation rate controlled by variables like temperature, ionic strength, and pH (113). Chitosan is also characterized by being bioactive, biodegradable, bioadhesive, hemostatic and displaying antimicrobial activity, properties that, in association with its low cost and high availability, make this polymer a highly promising biomaterial for the area of TE (117, 120). In BTE context, chitosan has become an attractive

material to produce scaffolds due to its ability to support osteoblast attachment and proliferation as well as the formation of mineralized bone matrix *in vitro* (121). Many studies have reported that scaffolds containing chitosan in its composition are osteoconductive (122-124). Furthermore, due to its easy processing it allows the production of 3D scaffolds with different pore structures and it can be combined with a large variety of materials, including ceramics and other polymers. The combination of chitosan with other materials allow the maintanance of features like mechanical strength and osteogenic character. Jin *et al.* reported the production of HAp/chitosan–alginate scaffolds that were able to provide a strong positive effect on bone formation when they were implanted *in vivo* (124). Fan *et al.* described the successful regeneration of a rat critical-sized mandibular defect by using 3D apatite-coated chitosan/chondroitin sulfate scaffolds supplemented with adipose-derived stem cells and BMP-2 (125). Serra and collaborators reported in a recent study the production of porous scaffolds composed of chitosan, gelatin and beta tricalcium phosphate (ß-TCP). Their results demonstrated that scaffolds were able to promote bone regeneration while avoiding biofilm formation (126).

Gelatin

Gelatin is a natural and cheap biopolymer that is obtained from the hydrolysis of collagen (Figure 1.5b). It is mainly composed by three aminoacids, glycine, proline and 4-hydroxyproline residues (127). Two types of gelatin can be obtained, depending on the pre-treatment procedure used, i.e., the acidic pre-treatment origins type A, where the amide groups are not modified while the alkaline pre-treatment originates gelatin type B, where the amide groups of asparagine and glutamine are hydrolyzed into carboxyl groups (128).

So far, this polymer has been widely used in the production of pharmaceuticals, cosmetics and food products since it is considered as a generally-regarded-as-safe (GRAS) material by FDA (129). Clinically, gelatin has been applied as a plasma expander or in the form of sponge (Gelfoam) (128). In TERM, the increasing interest on this biomaterial relies on its biological properties such as biocompatibility and biodegradability (12, 126, 130, 131). Moreover, it also presents low antigenicity, physicochemical stability as well as specific binding domains, known as arginine-glycine–asparagine (RGD) sequences. Such binding sites are crucial for cellular adhesion to occur (126). Lui and coworkers reported the production of nanofibrous gelatin/apatite scaffolds that mimic the natural bone ECM. Their study revealed that these structures were potential candidates for the intended application and when compared to a commercial gelatin foam, showed a much higher surface area and mechanical strength (12). A recent study performed by Yamamoto *et al.* described the combination of bone marrow cells with the BMP-2-releasing gelatin/ß-TCP sponge as a promising approach to induce bone regeneration at segmental bone defects (132).

Hyaluronic acid

Hyaluronic acid (HA) is a negatively charged and highly hydrated glycosaminoglycan that is present in all vertebrates, specifically in different extracellular tissues (91, 133). It comprises alternating disaccharide units of α-1,4-D-glucuronic acid and ß-1,3-N-acetyl-D-glucosamine (Figure 1.5d). In TE, hydrogel scaffolds produced with HA display different features including the capacity to enhance cell proliferation, wound healing, intracellular signalling and anti-inflammatory activity (91, 134). Moreover, due to its biocompatibility and structural composition, HA hydrogels have been widely used in several biomedical applications such as cell and molecule delivery or tumour models (91, 135). Kim and collaborators produced acrylated HA based scaffolds loaded with BMP-2 and hMSCs for bone regeneration (136). The obtained results showed that HA-1based hydrogel promoted bone formation through the delivery of hMSCs and BMP-2 that revealed a synergic effect during the regeneration process. Jhan *et al.* reported the production of a thermosensitive injectable hydrogel composed of doxorubicin and HA for the local treatment of cancer diseases (137). Their results demonstrated the ability of this hydrogel as a potential and novel injectable formulation to deliver doxorubicin to locally treat tumours and metastatic cancer cells. However, scaffolds produced with HA still display some limitations, such as water solubility, rapid resorption and short residence time in the tissue (138). In BTE, a study performed by Bae and collaborators described the production of a photocurable HA-hydrogel loaded with simvastatin. Their results showed that these scaffolds were able to promote higher levels of osteogenic differentiation of adipose tissue-derived stem cells (133). Moreover, in a recent study performed by Qian *et al.*, HA hydrogels having a triple degradation behavior were synthesized in order to mimic bone ECM. The obtained results revealed that the HA hydrogels were biocompatible and allowed the attachment and proliferation of osteoblast-like MC3T3-E1 cells (139).

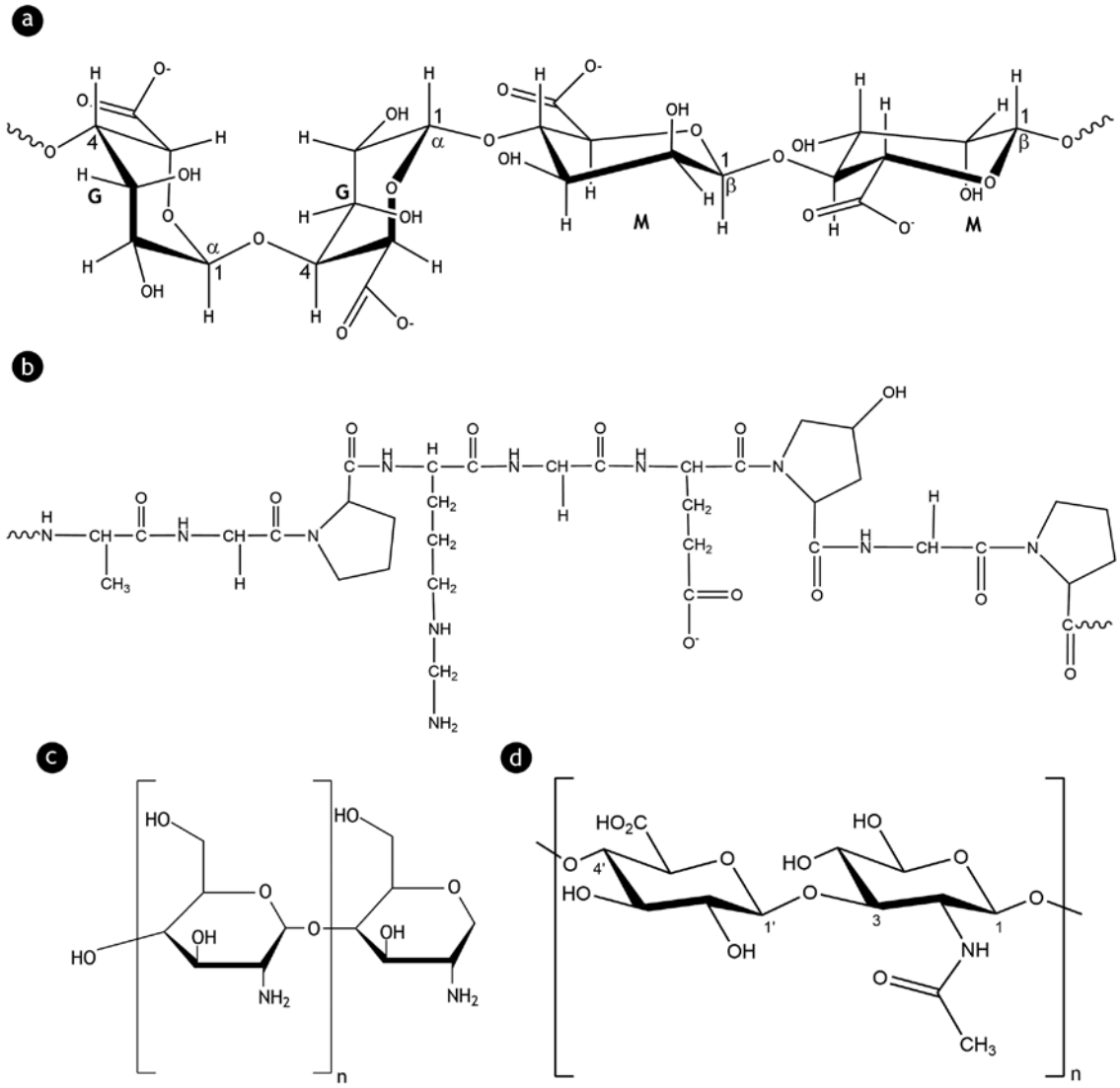

Figure 1.5 Representation of the chemical structure of the natural polymers: a) alginate, b) gelatin, c) chitosan, d) hyaluronic acid.

1.2.6.3. Ceramics

Calcium Phosphate Ceramics

Calcium phosphate ceramics (CPCs) are a remarkable class of materials that have been used for bone repair and regeneration for more than 20 years (140, 141). They have become very attractive to the area of BTE due to their unlimited availability, bioactivity, biocompatibility, hydrophilicity, osteoconductivity, osteoinductivity and structural similarity with the native bone inorganic components (140, 142). Moreover, their appropriate plasticity allows them to act as bone fillers (143). These materials have gain a huge interest due to their ability to promote *in vivo* bone growth and also recruit cells that are involved in its formation

(144). However, CPCs do not display a patterned biological behaviour when they are applied *in vivo*. Thus, their ability to enable osteoblastic differentiation may be dependent on their physical and chemical properties. Among them, surface charge and chemical arrangement may influence osteoblastic differentiation through cell-ECM interactions. On the other hand, roughness is responsible for inducing cell differentiation by creating an ideal environment for cell adhesion to occur. Commonly, the most used CPCs in BTE are HAp, tricalcium phosphates (TCPs), amorphous calcium phosphates and biphasic calcium phosphates (145).

Hydroxyapatite

HAp is one of the most used ceramics for bone regeneration, due to its similarity with bone mineral phase, that is composed by platelike nanosized crystals of HAp (146, 147). Among the monophasic CPCs, it is the most stable and less soluble. It has a Ks around $2.9x10^{-58}$ over a pH range of ≈3.5 to ≈9.7, i.e., the ions that result from HAp dissolution in an aqueous medium, have a high tendency to bind between each other again (145). Due to its low solubility, HAp remains for long periods in the body (148). Despite its similarity with the bone inorganic matrix, the commercial HAp is expensive when compared with other CPCs, which is a huge limitation for its application in scaffolds' production. Moreover, this ceramic also presents a high brittleness that limits its application in load-bearing sites, however there are some studies where HAp have revealed an unusual potential to be used in load-bearing applications. Deville and co-workers produced porous hydroxyapatite scaffolds by freeze drying. Their results showed that hydroxyapatite-based materials might be considered as potential candidates for load-bearing applications due to the high compressive strength (15). Furthermore, the combination of HAp with natural and synthetic polymers have emerged as a possible solution to address the mechanical weakness and brittleness of this ceramic (147, 149). Karadzic *et al.* performed a comparative study where porous HAp, HAp/PLGA, HAp/alginate and HAp ethylene vinylacetate / ethylene vinylversatate scaffolds were produced in order to evaluate their capacity to promote the differentiation of isolated dental pulp stem cells. The obtained results showed that all the formulations had the ability to enhance cell differentiation (150).

Beta Tricalcium Phosphate

ß-TCP is also a widely used ceramic in the area of BTE due to its properties like biodegradability, biocompatibility and osteoconductivity. Moreover, it's low price and degradation rate, which is 10 times higher than that of HAp, triggered its application in BTE (151). In addition, this ceramic has displayed suitable biodegradability when implanted *in vivo* while HAp presents almost no degradation (103, 152). Furthermore, ß-TCP scaffolds also present mechanical strength that is compatible with that of bone native tissue (7). Santos and

co-workers produced ß-TCP scaffolds using computer tomography data. The obtained results showed that these scaffolds were able to promote a good interaction with cells (153). However, ß-TCP scaffolds enclose some limitations, namely, the relative brittleness and poor resistance to fatigue (110). To overcome such drawbacks, this ceramic has been combined with other materials such as biopolymers. Arahira *et al.* produced collagen/ß-TCP composite scaffolds. The introduction of ß-TCP powder into the porous collagen matrix enhanced the mechanical and biological properties of the produced scaffolds (154). In another study PLGA/ ß-TCP scaffolds were functionalized with RGD sequences to improve the bone regeneration process (155). The addition of RGD peptide motifs to the composite scaffolds increased cell adhesion and proliferation as well as the osteogenic differentiation of bone mesenchymal stem cells.

Bioactive glass

Bioactive glass is known for inducing a specific biological response (156, 157). When implanted within a host, it allows the formation of hydroxycarbonate apatite (HCA) layers that establish a strong linkage with hard and soft tissues (158). It is described that the bone bonding to HCA might occur through a process that involves protein absorption, collagen fibrils incorporation, attachment of bone progenitor cells, cell differentiation and bone ECM production. The osteogenesis process is triggered by the dissolution of the components of glass, namely, soluble silica and calcium ions, that stimulate the osteogenic cells to produce bone matrix (32). However, not all the materials that are able to produce HCA layers *in vitro* can assure a direct binding *in vivo*. As an example, a ceramic like ß-TCP has been described as having an osteoinductive potential when implanted *in vivo,* although it was unable to form a HCA layer *in vitro*.

Currently, there are several types of bioactive glass that comprise the conventional silicates, such as Bioglass 45S5, borate-based and phosphate-based glasses. The bioactive glass commonly investigated for biomedical applications is 45S5. This silicate glass is composed of a 3D SiO_2 network. Its bioactive character is attributed to its composition, specifically to its low SiO_2, high Na_2O and CaO content, as well as high CaO/P_2O_5 ratio. Recently other glasses, such as borate glass, have been reported to be also bioactive (159). Due to their chemical weakness, this type of bioactive glasses degrades faster and become an HAp-like material, when compared to silicate 45S5 or 13-93 glass. These type of bioglasses have been displaying the ability to support cell proliferation and differentiation *in vitro*, to allow tissue infiltration in vivo and to act as a substrate for drug release in the treatment of bone infection. Another type of bioglass are the phosphate glasses (160, 161), which are composed by a P_2O_5 network which contains CaO and Na_2O on its composition. Phosphate glasses display a chemical affinity to bone since their ions are presented in the mineral phase of bone. Furthermore, they have demonstrated

to be potential candidates to be used as resorbable materials for clinical applications due to their solubility, which can be modulated by changing phosphate glasses composition (157).

In BTE, bioactive glass particles display a better performance than bioceramics particles. Indeed, the usual protocol used to produce bioactive glass scaffolds is to form glass particles into a structure with the desired properties. To do that, a glass must be melted to obtain the particles. Following, the model where the glass particles are introduced must be sintered so that the particles become bond between each other, giving place to a 3D porous network. Methods like sol-gel and recently electrospinning have been used to prepare bioactive glass scaffolds. However, these scaffolds still show some disadvantages as high brittleness, low mechanical strength and fracture toughness (158, 162), that limits their implantation at load bearing sites. To address such handicaps bioactive glasses have been combined with polymers (163, 164). Luo and colleagues have described a composite material consisting of mesoporous bioactive glass (MBG) and alginate pastes to produce scaffolds using 3D plotting (165). This study revealed that 3D-plotted MBG/alginate scaffolds present adequate processability, apatite-mineralization ability and cell recruiting capacity. In a recent study, Mouriño *et al.* coated AISI 316L stainless steel implants with bioglass particles and silver nanoparticles in order to confer bactericidal activity to these scaffolds (166). These scaffolds showed antibacterial activity against *Staphyloccocus aureus* up to 10 days and were able to support the growth of MG-63 osteoblast-like cells up to 7 days. However, the characterization of the cytotoxic character of these 3D structures upon the release of silver nanoparticles, revealed that the concentration of silver nanoparticles used was toxic for MG-63 osteoblast-like cells.

1.2.6.4. Composite materials

The demand for the development of new bone substitutes that are capable of fulfilling all the requirements of bone tissue has triggered several studies where metals, ceramics and polymers have been used to overcome the limitations of the scaffolds currently available. Metal implants, despite their mechanic properties, cannot promote any interaction with the native tissue, i.e., they are bioinert. In alternative, ceramic implants present a high bioactivity but at the same time they display weak mechanical properties.

Thus, the idea of combining different materials in order to obtain scaffolds with a set of specific properties has been pursued through the production of composite materials. These materials are composed by two phases, the matrix and the dispersed phase. Usually, the dispersed phase acts as a support of the matrix phase, thus providing resistance, stiffness and osteoconductivity, mimicking the role of natural minerals present in bone (100). The matrix phase is responsible for reproducing the biological interactions found in the bone native ECM, i.e., it is involved in the recruitment and internalization of cells that are responsible for the formation of new tissue while the composite materials are degraded. Due to these properties

these materials have triggered the interest of different scientists to overcome the limitations presented by other materials.

1.2.6.5. Commercial available scaffolds that are currently used in BTE

The huge demand for therapeutic tools that can be used in the clinic to treat orthopaedic lesions has triggered the production of several bone substitutes that are currently produced by different companies. Such therapeutic approaches include scaffolds, powders, pastes and putty. In table 1.2 are presented some examples of bone substitutes that have been approved by FDA and that are currently available in the market (100, 167). Although, the majority of them still display several handicaps like poor vascularization, weak mechanical integrity and long term infection.

Table 1.2 Examples of scaffolds that are approved by the FDA and that are currently used in the clinic for bone regeneration (adapted from (100)).

Company	Product	Composition	Applications
Biomet Spine	Biomet Microfixation HTR®-PMI	PMMA coated with hydroxyethyl-methacrylate, impregnated with calcium phosphate	Cranial applications
Integra Orthobiologics	Integra Mozaik™	80% high purity TCP and 20% high purity type-1 collagen	Injectable putty
Medtronic Sofamor Danek Wyeth Pharmaceuticals	Infuse® Bone Graft (marketed as InductOS in Europe)	rhBMP-2 with collagen sponge	For fusion or spinal cage
Styker Biotech	OP-1™ Implant	Recombinant osteogenic protein 1 (or BMP-7) and bovine bone collagen	Recalcitrant long bone non-unions
Zimmer	Collagraft® Bone Graft Substitute	HAp, TCP, bovine collagen in strips	Bone void filler for extremities, spine and pelvis

1.2.6.6. Techniques used for scaffolds manufacture

The methodology used for scaffolds production affects the properties displayed by the 3D constructs. The methods used so far for scaffolds manufacture are divided in conventional (Solvent casting, gas forming, phase separation and freeze-drying) and rapid-prototyping (RP) (fused deposition modelling, selective laser sintering and stereolithography) techniques.

Conventional techniques allow the custom production of scaffolds as they are usually handcraft. However, these procedures display some limitations like the use of toxic solvents that can have nefast effect for cells and can also affect the mechanical properties and morphological features like pore shapes and distribution, avoid interconnection between the pores of the produced structure as well as the production of models with shape constrains. The overall result is the fabrication of different structures with different properties despite using the same raw materials (168, 169). On the other hand, RP procedures are currently the ones that triggered the interest of researchers, especially due to their reproducibility and accuracy (110). These techniques allow the production of 3D structures with appropriate mechanical properties using CAD/CAM software. Also, scaffolds with the precise shape and size of bone defects can be produced by combining and integrating RP techniques with imaging techniques like Computer Tomography (CT) data, that allow the production of personalized therapeutic solutions (3, 170).

Conventional techniques

Solvent casting/particulate-leaching

Solvent casting has been widely used for the production of scaffolds aimed for bone tissue applications (171-173). This technique is based on the dissolution of a polymer in an organic solvent followed by a casting step into a mould. Similarly, composite scaffolds have been fabricated through this technique by mixing a polymer with a ceramic material (172). Zhu *et al.* produced highly porous scaffolds with a porosity of up to 93%, where pores displayed sizes with a diameter up to 500 μm, using this technique (174). To do that, usually a porous agent (salt or sugar) is added to the polymeric solution. Subsequently, the solvent is evaporated through air, vacuum or freeze-drying and the remaining salt particles are dissolved in water, creating pores within the structure (Figure 1.6). The benefits of using this procedure are the simplicity and low cost associated with this fabrication technique. However, the retention of toxic solvent can induce denaturation of any biomolecule and shapes constrictions are the major drawbacks of scaffolds produced through this technique.

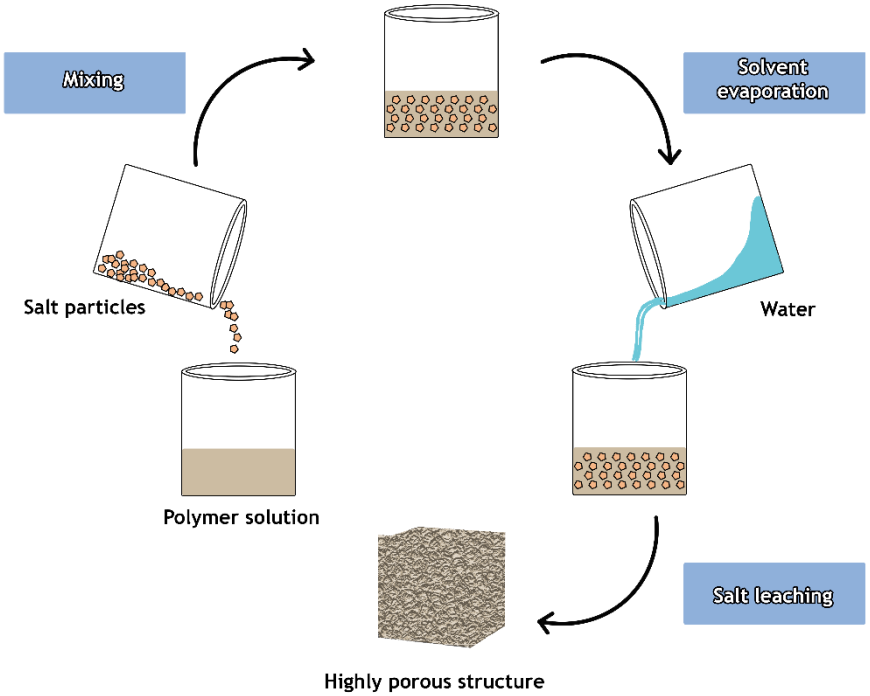

Figure 1.6 Schematic representation of the solvent casting/particle leaching technique used for scaffold production.

Gas foaming

Despite its wide application on the industrial field to produce foams, gas foaming has also been used for scaffolds production (10, 175-177). The production of a scaffold using this technique involves the use of a gas, such as nitrogen, fluoroform or carbon dioxide that is introduced on a melted polymer and then highly pressurized in order to obtain a porous scaffold (Figure 1.7). The pores formed within the structure, usually present a diameter range comprehended between 500 and 2000 µm. This technique is quite advantageous in comparison to casting/particle leaching method since it does not involve the use of organic solvents (178). However, during the process, the structure, to be produced, may present largely unconnected pores as well as a compact surface, which can avoid cellular adhesion, migration and proliferation, which is a major drawback of the 3D structures produced through this method (179). Almirall *et al.* have described the production of highly porous scaffolds using gas foaming and their results showed that the majority of the pores within the structures were not interconnected (180). Such fact highlights the limited applications of these scaffolds for bone tissue applications.

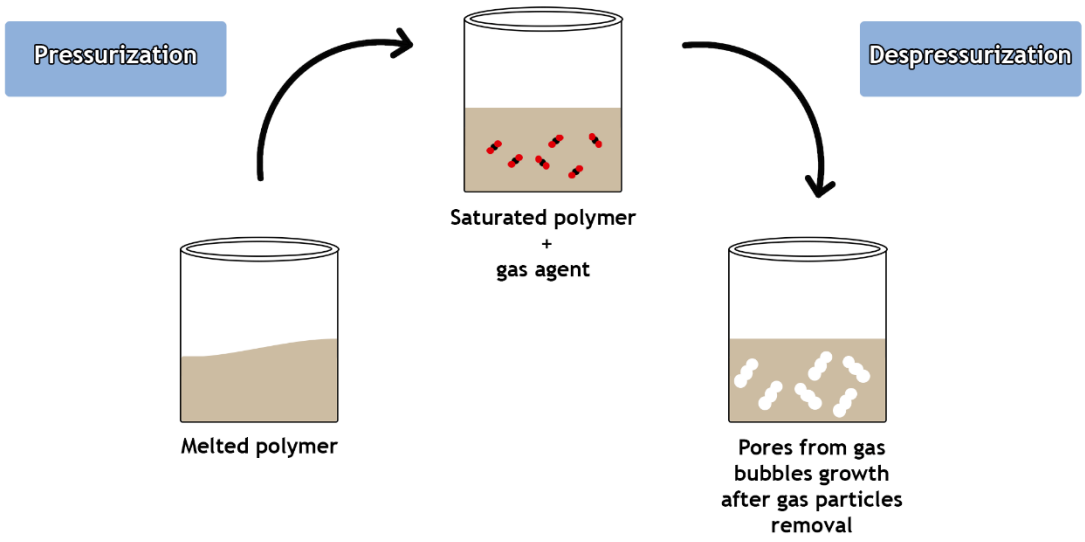

Figure 1.7 Representation of the protocol used for the production of scaffolds by gas foaming.

Phase separation

Phase separation is a procedure that involves the quenching of a polymer solution until it gets on a liquid-liquid phase separation (Figure 1.8), i.e., a polymer-rich phase and a polymer-poor phase are obtained. The polymer-poor phase is crystallized and removed, while the polymer rich phase originates a highly porous polymeric matrix. The structural features of the obtained scaffolds are dependent on polymer concentration, quenching temperature, and quenching rate (174). The temperature and quenching rate are known to affect solvent crystallization in such a way that at low temperatures a large amount of small crystals are formed, and consequently scaffolds with small pores are obtained (181). On the other hand, at high temperatures, larger crystals and pores are formed within the structure. The low temperature at which this method can be performed, enables the incorporation of bioactive molecules in scaffolds' structure (179). Yet, the pore size of the scaffolds produced with this technique usually does not overcome the 200 µm of diameter, limiting 3D structures applicability on tissue engineering applications. To address such issue, phase separation technique has been combined with particulate leaching (182, 183).

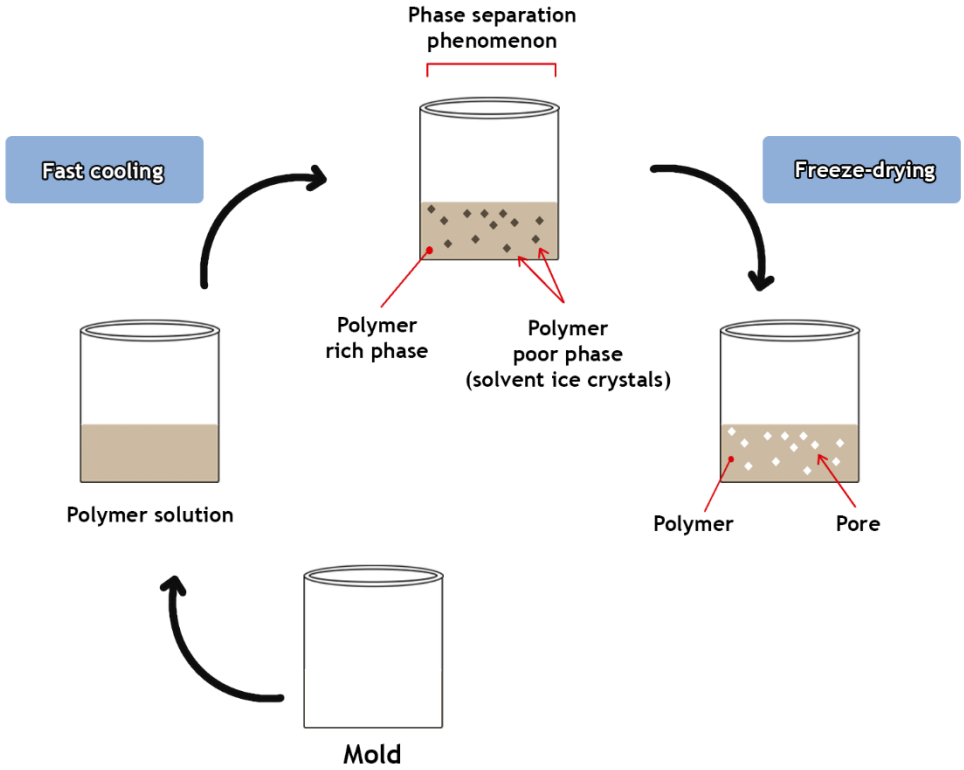

Figure 1.8 Schematic representation of the method used for producing scaffolds through phase separation technology.

Freeze-drying

Freeze-drying has been widely described in literature for the production of porous materials aimed for tissue engineering purposes (126, 184, 185). Such technique is commonly known as lyophilisation and it is able to avoid the use of organic solvents while providing materials with a high degree of purity. Briefly, the freezing stage involves the cooling of solution down to a certain temperature (usually -80°, -110°) at which all materials become frozen and the solvent forms ice crystals, forcing the aggregation of material molecules into the interstitial spaces. In a second phase, the solvent is removed through the downgrade of the pressure, which becomes lower than the equilibrium vapor pressure of the frozen solvent. At the end, the residual solvent is sublimated and a dry material with an interconnected porous microstructure is obtained (Figure 1.9). Variables like material concentration, freezing temperature or viscosity can influence the pore size of the final structure. The scaffolds produced through freezing-drying method can be used for different applications such as bone or skin regeneration (126) (186).

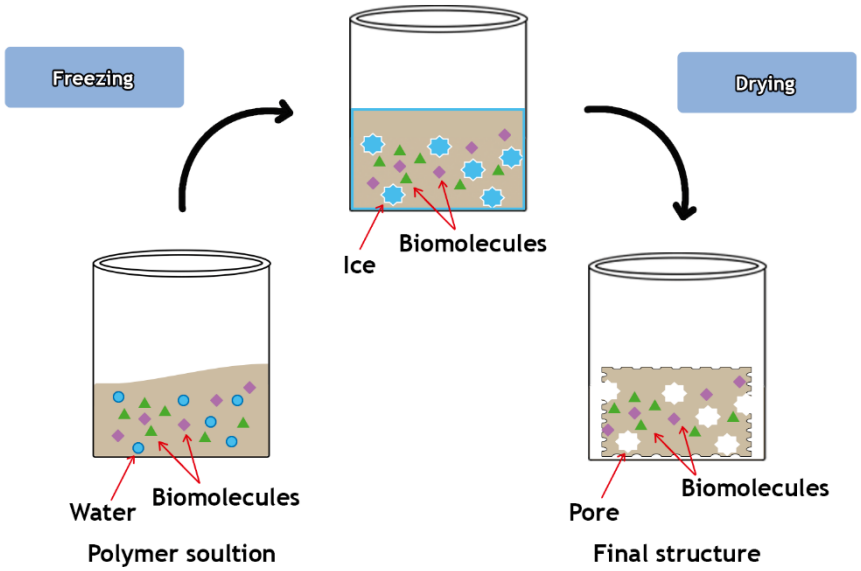

Figure 1.9 Representation of the procedure used to produce scaffolds through freeze-drying.

Rapid prototyping techniques

The group of methodologies that are able to be used to produce a physical model directly from CAD raw data is known as RP. This technique involves the assembly of the 3D scaffold. As a result, the production of customized scaffolds can be obtained by using magnetic resonance imaging (MRI) or CT data (187). Some of the RP techniques used for scaffolds production are described in the following topics.

Stereolithography

Stereolithography is one of the most primordial RP techniques. It is based on a ultraviolet (UV) light beam that is able to polymerize a UV curable photopolymer resin in a layer-by-layer process, resulting in the production of a 3D solid model (188). This fabrication method is fast and allows the production of scaffolds with different shapes. The resolution of the printed layers is controlled by the laser elevator and size. However, the final curing step may compromise the final resolution of the 3D model in such way that a shrinking event may occur. In addition, from all the materials described to be used in this procedure, just a few can be applied in biomedical area (168).

Fused deposition modelling

Fused deposition modelling (FDM) is a RP method, where a filament of a suitable material is used and melted inside a heated liquefier until it is extruded through a nozzle. In this procedure, it is crucial to control the environmental temperature in order to maintain sufficient fusion energy between each layer. Moreover, the deposition path and parameters for every layer depends on the material used, the processing conditions and the type of application. Several studies have shown the suitability of FDM to produce functional scaffolds for BTE applications. Chen *et al.* produced porous PCL scaffolds prepared by FDM containing biomolecules, namely filamentous hyaluronic acid and fibrillar collagen, for bone regeneration (189). Yao *et al.* reported the successful fabrication of 3D porous PCL-HAp scaffold using FDM for chondrogenic regeneration (190). Melocchi *et al.* also developed a 3D printed capsule by FDM for oral pulsatile drug release (191). However, this technology has a main drawback the type of material that can be used. Natural polymers cannot be used since the operating temperature of the system is too high to allow the incorporation of bioactive molecules and the filaments used to produce the structures does not present microporosity, a crucial factor for cellular attachment. To address such handicaps, different alternatives to FDM process including the 3D fiber-deposition technique (192), precision extruding deposition (PED) (193) and precise extrusion manufacturing (PEM) (194) have been implemented.

3D fiber deposition is a procedure where polymers are melted to produce scaffolds. It is based on a deposition system that includes a heating jacket around the container where the polymer is placed. To extrude the molten polymer from the nozzle, a pressurized gas is used. In addition, a movable X-Y-Z arm is used to selectivity orientate the melted polymer (195). Recently, Yilgor *et al.* reported the production of different PCL scaffolds containing BMP-2 and BMP-7 aimed to regenerate bone defects in a rat pelvis model, by using a 3D fiber deposition technique. The study revealed that an interconnecting pore geometry allows an enhanced healing of bone defects, an effect that can be potentiated by supplying growth factors (196).

On the other hand, PED consists on a screw extruder that allows the processing of polymer pellets to enable a controlled deposition of a melt filament (195). Shor *et al.* produced osteoblast-seeded PCL scaffolds using PED that were able to enhance the *in vivo* bone formation in nude mice (193).

PEM technique comprises the layer-by-layer production of physical objects based on a 3D CAD model. Briefly, the thermoplastic material is inserted into the extrusion sprayer that can move in X-Y directions. The sprayer extrudes the filament of the material to a platform that moves in Z direction. The sprayer and platform movements are controlled by a computer, where the CAD model is introduced to be printed (194).

Selective laser sintering

During the last decade, selective laser sintering (SLS) has been used to fabricate porous scaffolds (197-199). Biopolymers and blends of polymeric ceramic materials have been used to produce bioactive scaffolds. This technique usually comprises a roller or a sweeping blade that is used to spread a layer of powder on a platform, where a computer-controlled laser beam will scan the powder (197). In addition, two methods of SLS can be considered: direct and indirect. The direct method relies on feeding the SLS machine with a material powder without a binder. In the indirect method, a binder is mixed with the material powder to help in the fabrication process. To consolidate the layers, a low melting point polymer is frequently used to act as a binder to fuse the powder particles in order to a form a single solid layer (199). The use of SLS technique to synthetize scaffolds displays many benefits such as the creation of biphasic geometries, the incorporation of multiple materials, the absence of organic solvent and, contrarily to FDM, it does not need a filament. In addition, it is a fast process that has been considered suitable for the production of scaffolds for TE (197, 198). In contrast, the high costs associated with this method as well as the production settings such as high shrink rate and the lack of structural details remain its main drawbacks (200).

3D Bioplotting

Bioplotting is a 3D printing technique that triggered the interest in TE and biofabrication areas. This powder-based freeform fabrication method involves a regular ink-jet print-head, where binders are printed onto lose powders in a powder bed. This technique is able to produce scaffolds by deposition of a highly viscous biomaterial which is extruded through a fine nozzle using compressed air. In addition, biological components as well as living cells can be added to the plotting process due to the fact that this method takes place under mild conditions (6). The 3D plotting has been successfully performed using several types of materials like PCL (11, 201), bioactive glass (165), calcium phosphate (6) and also composites (110). However, some of them demand the use of heat or organic solvents in order to be processed. Such fact limits scaffolds' functionalization with bioactive molecules and living cells. To overcome those handicaps, researchers have been focusing on viscous material solutions that are able to provide the required mechanical properties and the suitable milieu for biological events, without the need of heat or toxic solvent to be processed. Inzana and co-workers reported the production of composite calcium phosphate and collagen scaffolds for bone regeneration using 3D printing. Their results showed that the incorporation of collagen via inkjet enhanced the material properties of 3D printed calcium phosphate scaffolds (202). Luo and colleagues produced biphasic calcium phosphate–alginate scaffolds by 3D plotting, and the obtained results demonstrated that these scaffold were able to provide suitable mechanical properties while

allowing cell adhesion and proliferation (203). Moreover, the mild preparation conditions allowed bovine serum albumin (BSA) protein loading into alginate and CPC pastes prior to the plotting step.

1.2.6.7. Functionalization of 3D scaffolds to improve its performance on bone tissue regeneration

The advances made on the biomedical field has triggered the development of new materials with higher efficiency to address the limitations of those currently available in the market. In BTE, bulk materials do not fulfil the requirements of some musculoskeletal diseases and disorders affecting the human beings. Associated to that and despite the sterilization and aseptic techniques used to implant these materials in bone, they are not able to avoid bacteria or fungi contamination, leading to inflammation and host tissue necrosis (204). In literature, it is reported that biomaterial-associated infections have become so common that it is estimated that at least 50% of all infections that occur in hospital are related with materials implantation (205). In order to overcome these limitations new strategies are currently being adopted to confer better properties to materials (Figure 1.10). To accomplish such objectives materials are being functionalized with biocompatible films, nanoparticles, bioactive molecules such as drugs and antibacterial agents (206).

In BTE, biocompatible films have been used as coatings in order to enhance cell adhesion, roughness, porosity, hydrophilic character, elastic modulus, among others, that have a key role in the biological processes occurring in living tissues. Thien *et al.* produced chitosan/HAp electropsun nanofibers aimed for bone tissue applications and they demonstrated that chitosan/HAp films were able to improve not only cell adhesion process but also the osteoconductivity properties of the film (207). Recently, Cardoso *et al.* fabricated thin films composed of PCL, oleic acid (OA) and HAp for BTE. Their results revealed that the addition of OA and HAp to PCL matrix affected the roughness, wettability, and mechanical properties of the films. The HAp reduced the material's surface contact angle and consequently the hydrophilicity of the film increased. Moreover, the elastic modulus of the film increased when the OA was dispersed within the HAp. Overall, the PCL/OA/HAp films were able to stimulate cell attachment, without causing any adverse effects on the tissue formation, resulting on an improved bone regeneration (208).

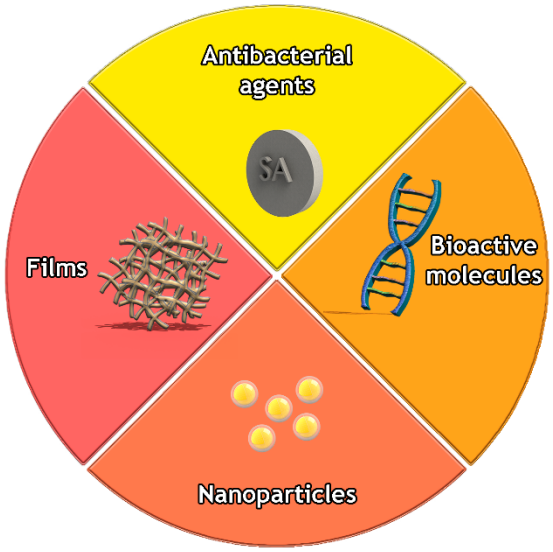

Figure 1.10 Illustration of the different functionalization strategies (antibacterial agents, biocompatible films, bioactive molecules and nanoparticles) used to enhance 3D scaffolds properties.

On the other hand, nanoparticles have been applied to deliver in a controlled manner specific biomolecules such as BMPs or ECM components, to act as antimicrobial agents or as a mechanical support element. Saravanan and co-workers investigated the synthesis of keratin nanoparticles through glutaraldehyde crosslinking that were further combined with a chitosan matrix for BTE. The obtained 3D structures displayed a porous structure compatible with cell penetration and nutrients diffusion. The addition of keratin nanoparticles to chitosan matrix enhanced the protein adsorption ability resulting in an improved cell–matrix interaction (209). In other study, Hickey and his team combined magnesium oxide (MgO) nanoparticles with poly (L-lactic acid) (PLLA) and HAp nanoparticle–PLLA composites for orthopaedic applications. Their results demonstrated that MgO nanoparticles can improve the adhesion and proliferation of bone cells on HA–PLLA nanocomposites while they do not affect the mechanical properties of the composites required for bone applications. Furthermore, MgO nanocomposites degradation products did not elicit any toxic effect on cells, triggering the proliferation of osteoblasts (210). Marsich *et al.* produced Alginate/HAp nanocomposites scaffolds endowed with antibacterial properties aimed to be used as bone grafts. Alginate/HAp composite scaffolds were produced by internal gelation followed by a freeze-drying process in order to a porous structure be obtained. Subsequently, silver nanoparticles (AgNPs) were mixed with a lactose modified-chitosan solution that was further adsorbed on the scaffolds through electrostatic interaction. The attained results showed that AgNPs were able to provide good antimicrobial properties to composite scaffolds for a time window compatible with a short-term protection from early-infections associated to temporary bone implants. Furthermore, silver ions and nanoparticles release did not affect osteoblasts viability (211).

Bioactive molecules like growth factors, peptides, genes or drugs have been widely described to promote the bone regeneration process by triggering cell adhesion/proliferation, providing antibacterial activity and by decreasing the host inflammatory response. Lee and collaborators reported new collagen hybrid scaffolds composed of nanofibers containing amphiphilic peptide, heparan sulfate, and low doses of BMP-2 for BTE applications. Their results showed that large volumes of bone were regenerated in bone critical size defect using low doses of BMP-2. Thus, they concluded that by mimicking the heparin binding sites found at the native ECM, the regeneration capacity of growth factors was increased (212). In a different study, Cui et al. investigated an injectable borate bioactive glass cement containing vancomycin aimed to be used to treat osteomyelitis in a rabbit tibial model. The vancomycin-loaded cement was able to cure 87% of the osteomyelitis cases and also promoted bone regeneration (213).

In the following topic, different strategies used to avoid scaffolds contaminations by bacteria strains is presented.

1.2.6.8. Strategies used for enhancing 3D scaffolds antibacterial activity

One of the most common strategies used for preventing scaffolds bacterial colonization, relies on the functionalization of scaffolds with antimicrobials such as antibiotics, quaternary ammonium compounds, heavy metal compounds (e.g. silver, tributyltin and mercury) and halogens (e.g. iodine) (214, 215). Despite being able to prevent scaffold implantation-related infections, these systems still present some handicaps such as trigger microbial resistance and environmental contamination issues (204).

Recently a new approach described as contact-active antimicrobial surface coatings have been used to enhance biomaterials performance against microorganisms. Therapeutic drugs can be incorporated in these coatings by using different methods such as depositing (166), layer by layer (216) or surface grafting (217). On Table 1.3 are presented the main antibacterial compounds that have been used so far as surface coatings to promote scaffolds' bactericidal activity. The impregnation of titanium dioxide onto polydimethylsiloxane surface by liquid phase deposition, avoided surface's bacteria contamination (218). In another study, a layer-by-layer technique was used to embedded chromogranin A on the surface of PMMA structures. This system revealed to be successful to avoid the growth of *Candida albicans* (219). Gabriel *et al.* reported the grafting of a Peptide LL-37 onto a titanium surface that conferred antimicrobial activity to these implants (220). In a study performed by Shi and co-workers, Ti alloy substrate surfaces were functionalized by covalently grafting carboxymethyl chitosan and BMP-2. Their results showed that the modified Ti alloy substrates were able to reduce bacterial adhesion while promoting implant integration in the bone tissue (221).

Adams and his team developed thin films loaded with vancomycin to avoid implant associated infections of Ti rods (222). They were able not only to reduce the bacterial adhesion

but also to prevent the development of osteomyelitis. In another work performed by Feng *et al.*, it was described the incorporation of PLGA nanospheres loaded with doxycycline into PLLA nanofiber scaffolds aimed for promoting an extended therapeutic action during bone infections (223). It was demonstrated that these structures were able to provide the inhibition of common bacterial growth for a long period. The bactericidal effect of rifampin has also been reported for PCL scaffolds by Ruckh and collaborators (224). PCL scaffolds allowed the sustained release of rifampin for 8 hours that was able to avoid *Staphylococcus epidermis* and *Pseudomonas aeruginosa* scaffolds contaminations. Shi *et al.* produced new PLGA/lecithin scaffolds containing different biomolecules, namely gentamycin and bovine serum albumin, for bone applications (225). The addition of lecithin allowed an improved encapsulation of the biomolecules used in this study, which contributed not only to support bone regeneration but also to prevent *E. coli* contamination.

Another solution that has been used to prevent microbial contamination consists on the incorporation of silver on scaffolds. As previously reported in literature, silver is mainly incorporated in scaffolds in the form of nanoparticles (226-228). Saravanan and collaborators have reported the production of a bio-composite scaffolds containing chitosan/nano-hydroxyapatite/nano-silver for BTE (226). Their results showed that the scaffolds have the potential to prevent bacterial infection during reconstructive surgery of bone. Furthermore, Prokopovich *et al.* described that oleic acid capped silver nanoparticles encapsulated in PMMA-based bone cement prevents bone infections (229), caused by *Methicillin Resistant Staphylococcus aureus*, *S. aureus, Staphylococcus epidermidis* and *Acinetobacter baumannii* (229).

Alternatively, to silver and antibiotics, antimicrobial peptides (AMPs) have arisen to boost the therapeutic approaches against infections. In BTE, these peptides have also been incorporated in scaffolds. Wang *et al.* reported the production of a PCL-chitosan nanofiber scaffolds with enhanced resistance to bacterial colonization. To achieve that, PEG/acrylic acid microgels were used to coat the surface of PCL-chitosan scaffolds and, subsequently, they were immersed on a solution of cationic oligopeptide (L5) (230). Their study revealed that these scaffolds were able to prevent *S. epidermidis* colonization while promoting osteoblast adhesion, spreading, and proliferation on scaffolds' surface. Recently, Nie *et al.* evaluated the effect of the functionalization of the Ti surface with of K-12 AMP for reducing bacterial contamination and enhance osteogenesis (231). The results showed that the K-12 peptide enhanced the biological properties of bioinert Ti, by conferring it antibacterial activity and enhanced osteogenic differentiation of hBMSCs.

Table 1.3 Different antibacterial agents used to confer scaffolds bactericidal activity

Therapeutic agent	Type	Targets	Refs
Gentamicin	Antibiotics	*Escherichia. coli*	(225)
Doxycycline	Antibiotics	*Escherichia coli* *Staphylococcus. aureus*	(223)
Rifampin	Antibiotics	*Pseudomonas aeruginosa* *Staphylococcus epidermis*	(224)
Vancomycin	Antibiotics	*Staphylococcus aureus*	(232)
L5	AMP	*Staphylococcus epidermidis*	(230)
K-12	AMP	*Methicillin Resistant Staphylococcus epidermidis* *Staphylococcus epidermidis*	(231)
Silver	Metal	*Acinetobacter baumannii* *Bacillus subtilis* *Methicillin Resistant Staphylococcus aureus* *Staphylococcus aureus* *Staphylococcus epidermidis*	(226, 229)
Chitosan	Polysaccharide	*Staphylococcus aureus*	(233)

1.3. Vascular Tissue Engineering

1.3.1. Vascular diseases

According to the data from 2016 of the World Health statistics, cardiovascular diseases (CVD) are the leading cause of death in humans (234). Between them, coronary heart disease (CHD) is responsible for 19% of deaths in men and 20% of deaths in women (23). Although there is no cure for this disease, CHD symptoms can be attenuated through medication, coronary angioplasty or coronary artery bypass grafting (CABG) surgery. CABG redirects the blood of the collapsed arteries by using grafts obtained from other blood vessels of the body. Usually, it includes the internal mammary artery, radial artery and saphenous vein (SV).

1.3.2. Vascular grafts

Among the available autografts used to treat small diameter vessel diseases, the SV is the preferred choice due to its easy surgical access and harvesting (235). Moreover, since it is an autologous graft, it presents several benefits like availability, biocompatibility, diminished immune response and does not require certificate of approval from regulatory agencies. However, these type of veins do not present adequate mechanical properties when they are used to replace high pressure arterial vessels. Such mismatch may cause excessive dilatation (aneurysm), intimal hyperplasia and accelerated atherosclerosis (236). Consequently, several surgical procedures are required to avoid those injuries, where the number of interventions are limited by the amount of SV tissue available in the host to perform the implant. It is known that one third of the patients that suffer from peripheral arterial disease have inadequate grafts (237). Such fact highlights the need for alternative solutions, that can fulfil such demand. Thus, new grafts are currently being developed using synthetic materials, namely, polyethylene terephthalate (Dacron), expanded polytetrafluoroethylene (Teflon) and polyurethane. Dacron and Teflon have been reported as viable grafts to replace vessels with larger diameters (>6mm internal diameter). Nevertheless, when the blood vessel diameter is inferior to 6mm, these alternatives are rejected by body's immune system. Such fact is explained by the occlusion of the vessel that can lead to thrombosis, aneurysm and intimal hyperplasia (238). Thus, TE arises as an alternative to develop new vascular grafts.

1.3.3. Vascular grafts aimed for Tissue Engineering applications

One of the biggest innovations that was attained in the cardiovascular tissue engineering area involved the successful implantation of small-diameter tissue-engineered vascular grafts (TEVGs) (239, 240). However, the traditional methods, that are used for the production of these structures, require the use of bioreactors, that have high costs and long manufacture periods associated. Moreover, thrombosis and stenosis remain significant drawbacks presented by the traditional grafts that can result in low patency rates (238).

Ideally, TEVG must fulfil a set of properties that comprise bactericidal activity, low immunogenicity, adequate mechanical strength, promotion of tissue remodelling, stimuli responsiveness, low thrombogenicity, suitable porosity, long term patency, cost effective and be ready to be used (24, 241). To address such challenges, vascular tissue engineering (VTE) is currently focused on using different approaches to produce grafts that comprise molecular self-assembly, solvent casting–particulate leaching technique, thermally induced phase separation and electrospinning process. From these techniques, electrospinning has been the focus of different studies due to its ability to produce micro and nanofibers, that closely resemble the microenvironment found on natural ECM. The capacity to mimic the natural ECM is considered a key factor for the production of tissue engineered vascular grafts (242). The versatility of electrospinning technique allows the use of a wide range of materials, that include natural and synthetic polymers or even composite mixtures of ECM components (159, 243, 244). In addition, the capacity of producing fibrous meshes with nano/micron-sized pores and a large surface area, makes this method the preferred choice in several areas of research, like biotechnology (245, 246), regenerative medicine (159, 243, 244, 247, 248) and electronics (249, 250). Moreover, the ability to produce aligned nanofibers is fundamental for cells to acquire a similar alignment to that observed in blood vessels.

So far, polyurethane (PU), gelatin, collagen type I, PCL, polyethylene oxide (PEO), PGA, elastin, silk fibroin, PLGA polymers and blends produced with these materials were used to produce TEVGs (22). Zhu *et al.* described that aligned PCL fibers coated with fibrin were able to support smooth muscle cells survival and function (251). In another study, chitosan-collagen-thermoplastic polyurethane (TPU) nanofibrous scaffolds showed adequate properties to support Schwann and endothelial cells functionality while providing suitable mechanical properties (252). Merkle and collaborators produced electrospun nanofibers with poly vinyl alcohol and gelatin for vascular tissue applications. Their results demonstrated that this system could support cell growth, while minimizing platelet deposition (253). Moreover, a similar study performed by Fang *et al.*, showed that nanofibrous scaffolds functionalized with heparin and containing endothelial progenitor cells were able to reduce the platelet deposition and increased cell recruitment, thus highlighting their potential for small diameter vascular regeneration (254). However, only few studies reported the characterization of such materials in *in vivo* assays (255, 256), which emphasizes the early development stage of these grafts, that

need further optimization and evaluation in clinical assays. Still, some drawbacks like the poor surface properties and small pore sizes can avoid cell penetration and also contribute for reducing cell viability. To surpass those limitations, biodegradable polymers have been investigated in order to produce new vascular grafts.

1.3.3.1. Synthetic polymers

Poly ε-caprolactone

In TE, PCL has been widely used for scaffolds production due to its rheological and viscoelastic properties. Despite its slow degradation profile, PCL is a cheap synthetic material that has already been approved by FDA for producing devices aimed for drug delivery. Moreover, PCL has been used in different approaches for bone, skin, tendon, cartilage, blood vessel and cardiovascular tissue engineering (257-261).

In VTE area, the traditional vascular grafts display two major drawbacks, namely, the risk of thrombogenicity and low durability. To overcome these handicaps, PCL arises as a viable solution due to its properties like elasticity, mechanical strength and biocompatibility. Also its easy processing into micro and nanofibers by using electrospinning technique makes PCL a potential candidate for vascular graft applications (262). Zhang and co-workers incorporated natural lecithin into cholesterol-PCL to improve its performance as a vascular graft (21). The preliminary results showed that these scaffolds had their hemocompatibility and cytocompatibility enhanced and that their combination with the MSCs and endothelial cells (ECs) is a promising approach for producing TEVGs. A recent study performed by Ducan *et al.* described the production of a tubular vascular tissue engineered scaffold composed of PCL and collagen with core–shell structured fibers (263). It was demonstrated that the scaffold was able to support vascular cells, ECs and SMCs attachment, growth and proliferation. In addition, it also allowed SMCs migration to its interior.

Poly (glycolic acid)

Poly glycolic acid (PGA) presents a simple chemical structure, with a high degree of crystallinity, a high melting temperature and low solubility in organic solvents (264). Moreover, it also displays a very high strength and Young Modulus, suitable degradation profile and natural by-products that allow its application in several biomedical areas such as BTE and VTE (265, 266). In VTE area, PGA has been used to produce nanofibrous meshes that are aimed to be used as TEVGs. Boland *et al.* have reported the production of electrospun PGA scaffolds that were treated with hydrochloric acid in order to improve the soft-tissue biocompatibility (267). Their results demonstrated that the acidic treatment performed on PGA scaffolds was able to improve their biocompatibility, which was proven by high rates of cell proliferation. Hajiali and co-

workers used different ratios of gelatin and PGA to produce TEVGs and the obtained results revealed that the incorporation of gelatin allowed the improvement of the biological and mechanical properties of PGA scaffolds (268).

Poly (lactic acid)

Poly (lactic acid) (PLA) is an aliphatic polyester that presents three isomeric forms d(-), l(+) and racemic (d, l), where the commonly used isomer is the (l), since it can be metabolized in the body via Krebs cycle (269). Its degradation by-products are eliminated from the body in the form of carbon dioxide and water, an important feature that allowed its approval by FDA (270). PLA can be obtained by the polymerization of lactic acid (LA) through a direct condensation process or by ring opening polymerization (271). Its monomeric unit, LA, is normally produced by converting sugar or starch (obtained from corn, wheat or rice, through bacterial fermentation or a petrochemical method). This biomaterial is also endowed of a high tensile strength, elongation, and Young Modulus, that makes it suitable for being used in a wide range of biomedical applications including sutures, clips, orthopaedic devices and drug delivery systems production (272, 273). However, this biopolymer has also some limitations such as poor toughness, slow degradation rate, hydrophobicity and lack of reactive groups (274). To overcome these disadvantages, PLA has been combined with other biomaterials.

In VTE area, PLA nanofibrous meshes have arisen as a potential therapeutic approach due to features like biocompatibility, degradability and mechanically stability (275-277). In order to recreate the structure of a blood vessel, Wang and co-workers produced a bilayer electrospun scaffold composed of PLA in the outer layer and silk fibroin/gelatin in the inner layer (278). These 3D structures showed to be able to support the growth and proliferation of different cell types, specifically 3T3 mouse fibroblasts that grew on the outer PLA layer and the ECs that grew on silk fibroin/gelatin inner layer. Although a minimal inflammatory response was observed during implantation, the formation of a connective vascular network was also noticed at a rate that was compatible with implant degradation (278). In a recent study, Weijie *et al.* reported the production of cistanche polysaccharide (CDPS)/PLA scaffolds using coaxial electrospinning. The outer layer was made of PLA while the inner layer was composed of CDPS. These CDPS/PLA coaxial scaffolds were hemocompatible and also provide appropriated biomechanical properties (273).

Poly(lactic-co-glycolic) acid

Poly(lactic-co-glycolic) acid (PLGA) is a linear copolymer that can have different ratios of its monomer units, LA and glycolic acid (GA) (Figure 1.11d). It is available as d-, l-, and d,l-isomers. The PLGA arrangement is based on the ratio of lactide to glycolide used in the

polymerization reaction. Compared to pure PLA and PGA, PLGA possess high solubility in chlorinated solvents, tetrahydrofuran, acetone or ethyl acetate (279). Moreover, this polymer can assume any shape and size and encapsulate biomolecules of any size. Its physical properties are controlled by several features such as molecular weight of the monomers, the exposure time to water and the storage temperature (280). PLGA is also approved by FDA for drug delivery due to its biodegradability, biocompatibility, mechanical properties and easy processing (281-283). It has been used for the production of grafts, sutures, implants and prosthetic devices (281). In VTE, PLGA has been applied in order to reproduce the biological and mechanical features found in native vascular tissues (284). Lui et al. produced electrospun PLGA loaded with vancomycin prosthetic grafts in order to prevent infections. These grafts were able to provide local and sustained delivery of high concentrations of vancomycin (285).

In a recent study, Hen and collaborators evaluated the performance of double-layered electrospun membranes loaded with vascular endothelial growth factor (VEGF) and platelet-derived growth factor-bb (PDGF). The multi-layered system composed of PCL/gelatin in the outer layer, PLGA loaded with VEGF/gelatin in the middle layer and poly(ethylene glycol)-b-poly(L-lactideco-caprolactone (PELCL) loaded with PDGF/gelatin in the inner layer, showed a high effectiveness in the replacing of rabbit carotid artery for 8 weeks. During this period this system performed a sustained release of the bioactive molecules, VEGF and PDGF, that promoted the revascularization of the blood vessel (286).

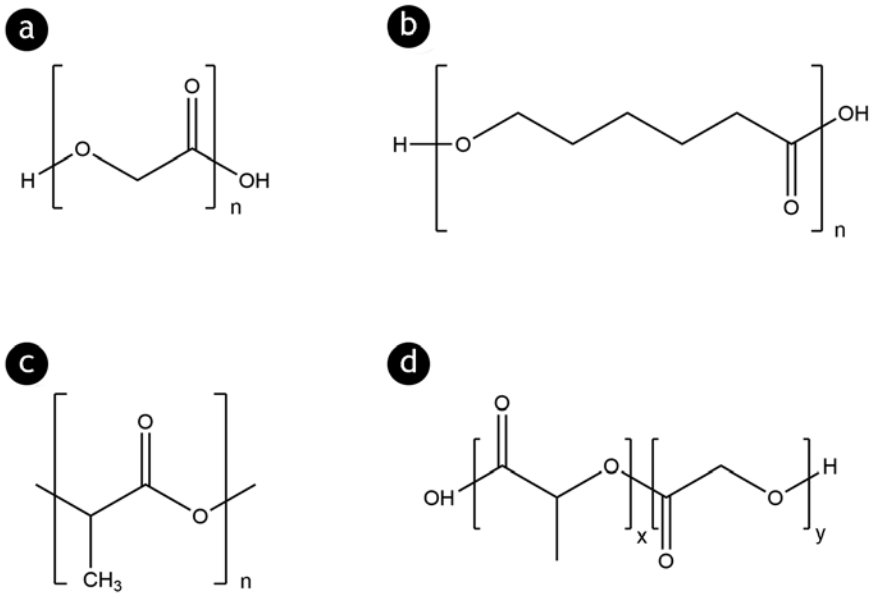

Figure 1.11 Chemical structure of the synthetic polymers: a) PGA, b) PCL, c) PLA, d) PLGA. x refers to LA units and y to GA units.

1.3.4. Clinical Trials of tissue engineered vascular grafts

Despite the amount of studies performed in the area of vascular tissue, only a few percentage of the TEVGs developed so far are currently being tested in clinical trials. In Table 1.4 are presented the TEVGs that have been evaluated or under evaluation in clinical trials.

Table 1.4 Different TEVGs that have been evaluated in clinical trials.

Device	Composition	Limitations	Application	Refs
Venous TEVG	PLCL* reinforced with PGA and seeded with BM-MNCs*	Graft stenosis	Extra cardiac total cavo-pulmonary connections	(287)
Cytograft™	Autologous Fibroblasts and ECs	Endogenous immune response	Vascular access to Haemodialysis	(240, 288)
Decellularized donor iliac vein	Host stem cells	Risk of immune rejection by inappropriate decellularization	Bypass conduit for extrahepatic portal venous obstruction	(20)
Humacyte™	Cadaveric smooth muscle cells seeded on a PGA scaffold	Risk of immune rejection by inappropriate decellularization	Large and small diameter grafts	(289)
Lifeline™	Fibroblasts, EC	Stenosis Stenosis	Brachioaxillary arteriovenous graft	(290, 291)

* BM-MNCs - autologous bone marrow mononuclear cells; PLCL – L-lactive and ε-caprolactone.

In 2001, a cardiac total cavo-pulmonary connection was performed using a TEVG. The implant composition comprised a 50:50 mixture of L-lactide and ε-caprolactone (PLCL) reinforced with PGA, that was loaded with autologous bone marrow mononuclear cells (BM-MNCs). The obtained results showed that this TEVG was clinically viable for long-term applications since cases of graft-related mortality or evidence of graft rupture, aneurysm, infection, or ectopic calcification were not observed. However, around 24% of patients still had graft stenosis, an issue that was overcomed by performing percutaneous angioplasties (287).

Cytograft™ was one of the first TEVGs to be tested in clinical assays and was based on a cell sheet method that did not require the use of biodegradable polymer scaffolds. In this system, fibroblasts were cultured in a culture flask containing a higher amount of sodium ascorbate to promote the formation of an ECM. After that, the cell sheet is matured and wrapped around a Teflon-coated, stainless-steel temporary support tube and kept for at least 10 weeks. Cytograft™ was then tested in 10 patients with failing dialysis access. The results showed that 3 out of the 10 grafts tested were not successful due to structural failure (240, 288). However, the production time can exceed 36 weeks, which avoids the availability of these grafts to be ready to use. Furthermore, despite showing suitable properties, such as adequate

flow, this TEVG was not allowed to be tested in brachioaxillary arteriovenous graft intervention as it mismatch the compliance of the coronary artery (290). Further studies revealed that improvements of the manufacturing process of this TEGV allowed their storage for a long time period. The application of this last generation of grafts were not successfully, where 2 patients required interventions for stenosis and 1 died from infectious causes (291).

Humacyte™ was another approach based on the *in vitro* growing of vascular smooth muscle cells on a biodegradable PGA scaffold. This production protocol allows the reproduction of the structure of the native blood vessel. At the end, the PGA cultured vessel has to be decellularized to avoid immunological reactions. However, the risk of incomplete removal of all the cell-based material and the long term of production are concerns that limit the use of this type of grafts. Not withstand, the *in vivo* application of these grafts have demonstrated satisfactory results when applied as artery bypass models, which are currently under clinical evaluation to be used as a HD access with 60 grafts implanted at 6 centres worldwide (289).

Recently, Olausson and collaborators produced a decellularized iliac vein containing host stem cells to be used as a bypass vessel to relieve extrahepatic portal venous obstruction in a child. The obtained results showed that the child was able to recover the hepatic function without any signs of obstruction in the post-surgical period (20).

In this thesis, PCL and acrylate gelatine materials were chosen to produce a new TEVG since they present properties such as mechanical strength, biocompatibility, cell binding domains as well as thrombogenic and haemolytic compatible with that of the native tissue.

1.4. References

1. Nations U. World population ageing: 1950-2050. New York: Department of Economic and Social Affairs. 2002.

2. Lanza R, Langer R, Vacanti JP. Principles of tissue engineering: Academic press; 2011.

3. Santos CFL, Silva AP, Lopes L, Pires I, Correia IJ. Design and production of sintered ß-tricalcium phosphate 3D scaffolds for bone tissue regeneration. Materials Science and Engineering: C. 2012;32(5):1293-8.

4. Torres AL, Gaspar VM, Serra IR, Diogo GS, Fradique R, Silva AP, et al. Bioactive polymeric–ceramic hybrid 3D scaffold for application in bone tissue regeneration. Materials Science and Engineering: C. 2013;33(7):4460-9.

5. Sowjanya J, Singh J, Mohita T, Sarvanan S, Moorthi A, Srinivasan N, et al. Biocomposite scaffolds containing chitosan/alginate/nano-silica for bone tissue engineering. Colloids and Surfaces B: Biointerfaces. 2013;109:294-300.

6. Lode A, Meissner K, Luo Y, Sonntag F, Glorius S, Nies B, et al. Fabrication of porous scaffolds by three-dimensional plotting of a pasty calcium phosphate bone cement under mild conditions. Journal of Tissue Engineering and Regenerative Medicine. 2014;8(9):682-93.

7. Shrivats AR, McDermott MC, Hollinger JO. Bone tissue engineering: state of the union. Drug Discovery Today. 2014;19(6):781-6.

8. Chen Q, Thouas GA. Metallic implant biomaterials. Materials Science and Engineering: R: Reports. 2015;87:1-57.

9. Kim J, McBride S, Tellis B, Alvarez-Urena P, Song Y-H, Dean DD, et al. Rapid-prototyped PLGA/ß-TCP/hydroxyapatite nanocomposite scaffolds in a rabbit femoral defect model. Biofabrication. 2012;4(2):025003.

10. Ji C, Annabi N, Hosseinkhani M, Sivaloganathan S, Dehghani F. Fabrication of poly-DL-lactide/polyethylene glycol scaffolds using the gas foaming technique. Acta Biomaterialia. 2012;8(2):570-8.

11. Park SA, Lee SH, Kim WD. Fabrication of porous polycaprolactone/hydroxyapatite (PCL/HA) blend scaffolds using a 3D plotting system for bone tissue engineering. Bioprocess and biosystems engineering. 2011;34(4):505-13.

12. Liu X, Smith LA, Hu J, Ma PX. Biomimetic nanofibrous gelatin/apatite composite scaffolds for bone tissue engineering. Biomaterials. 2009;30(12):2252-8.

13. Alvarez K, Nakajima H. Metallic Scaffolds for Bone Regeneration. Materials. 2009;2(3):790-832.

14. Weinand C, Pomerantseva I, Neville CM, Gupta R, Weinberg E, Madisch I, et al. Hydrogel-β-TCP scaffolds and stem cells for tissue engineering bone. Bone. 2006;38(4):555-63.

15. Deville S, Saiz E, Tomsia AP. Freeze casting of hydroxyapatite scaffolds for bone tissue engineering. Biomaterials. 2006;27(32):5480-9.

16. Daculsi G, Fellah B, Miramond T, Durand M. Osteoconduction, Osteogenicity, Osteoinduction, what are the fundamental properties for a smart bone substitutes. IRBM. 2013;34(4):346-8.

17. Kim HN, Jiao A, Hwang NS, Kim MS, Kim D-H, Suh K-Y. Nanotopography-guided tissue engineering and regenerative medicine. Advanced Drug Delivery Reviews. 2013;65(4):536-58.

18. Opie LH. Heart physiology: from cell to circulation: Lippincott Williams & Wilkins; 2004.

19. Lu D, Kassab GS. Role of shear stress and stretch in vascular mechanobiology. Journal of the Royal Society Interface. 2011;8(63):1379-85.

20. Olausson M, Patil PB, Kuna VK, Chougule P, Hernandez N, Methe K, et al. Transplantation of an allogeneic vein bioengineered with autologous stem cells: a proof-of-concept study. The Lancet. 2012;380(9838):230-7.

21. Zhang M, Wang K, Wang Z, Xing B, Zhao Q, Kong D. Small-diameter tissue engineered vascular graft made of electrospun PCL/lecithin blend. Journal of Materials Science: Materials in Medicine. 2012;23(11):2639-48.

22. Hasan A, Memic A, Annabi N, Hossain M, Paul A, Dokmeci MR, et al. Electrospun scaffolds for tissue engineering of vascular grafts. Acta biomaterialia. 2014;10(1):11-25.

23. Townsend N, Nichols M, Scarborough P, Rayner M. Cardiovascular disease in Europe—epidemiological update 2015. European Heart Journal. 2015:ehv428.

24. Seifu DG, Purnama A, Mequanint K, Mantovani D. Small-diameter vascular tissue engineering. Nature Reviews Cardiology. 2013;10(7):410-21.

25. O'Brien FJ. Biomaterials & scaffolds for tissue engineering. Materials Today. 2011;14(3):88-95.

26. Hench L. Biomaterials. Science. 1980;208(4446):826-31.

27. Navarro M, Michiardi A, Castano O, Planell J. Biomaterials in orthopaedics. Journal of the Royal Society Interface. 2008;5(27):1137-58.

28. Shastri VP, Altankov G, Lendlein A. Advances in Regenerative Medicine: Role of Nanotechnology, and Engineering Principles: Springer; 2010.

29. Narayan RJ. The next generation of biomaterial development. Philosophical Transactions of the Royal Society of London A: Mathematical, Physical and Engineering Sciences. 2010;368(1917):1831-7.

30. Jandt KD. Evolutions, Revolutions and Trends in Biomaterials Science – A Perspective. Advanced Engineering Materials. 2007;9(12):1035-50.

31. Hench LL, Polak JM. Third-generation biomedical materials. Science. 2002;295(5557):1014-7.

32. Hench LL, Polak JM. Third-generation biomedical materials. Science. 2002;295(5557):1014-7.

33. Holzapfel BM, Reichert JC, Schantz J-T, Gbureck U, Rackwitz L, Nöth U, et al. How smart do biomaterials need to be? A translational science and clinical point of view. Advanced Drug Delivery Reviews. 2013;65(4):581-603.

34. Hutmacher DW, Schantz JT, Lam CXF, Tan KC, Lim TC. State of the art and future directions of scaffold-based bone engineering from a biomaterials perspective. Journal of Tissue Engineering and Regenerative Medicine. 2007;1(4):245-60.

35. Das A, Botchwey E. Evaluation of angiogenesis and osteogenesis. Tissue Engineering Part B: Reviews. 2011;17(6):403-14.

36. Karageorgiou V, Kaplan D. Porosity of 3D biomaterial scaffolds and osteogenesis. Biomaterials. 2005;26(27):5474-91.

37. Bueno EM, Glowacki J. Biologic foundations for skeletal tissue engineering. Synthesis Lectures on Tissue Engineering. 2011;3(1):1-220.

38. Daley WP, Peters SB, Larsen M. Extracellular matrix dynamics in development and regenerative medicine. Journal of Cell Science. 2008;121(3):255-64.

39. Mouw JK, Ou G, Weaver VM. Extracellular matrix assembly: a multiscale deconstruction. Nature reviews Molecular cell biology. 2014;15(12):771-85.

40. Yue B. Biology of the extracellular matrix: an overview. Journal of Glaucoma. 2014:S20.

41. Korkusuz F. Musculoskeletal Research and Basic Science: Springer; 2016.

42. Colman RW. Hemostasis and thrombosis: basic principles and clinical practice: Lippincott Williams & Wilkins; 2006.

43. Kini U, Nandeesh B. Physiology of bone formation, remodeling, and metabolism. Radionuclide and hybrid bone imaging: Springer; 2012. p. 29-57.

44. Sykaras N, Opperman LA. Bone morphogenetic proteins (BMPs): how do they function and what can they offer the clinician? Journal of Oral Science. 2003;45(2):57-73.

45. Abe E. Function of BMPs and BMP antagonists in adult bone. Annals of the New York Academy of Sciences. 2006;1068(1):41-53.

46. Feeley BT, Gamradt SC, Hsu WK, Liu N, Krenek L, Robbins P, et al. Influence of BMPs on the formation of osteoblastic lesions in metastatic prostate cancer. Journal of Bone and Mineral Research. 2005;20(12):2189-99.

47. Wu S, Liu X, Yeung KW, Liu C, Yang X. Biomimetic porous scaffolds for bone tissue engineering. Materials Science and Engineering: R: Reports. 2014;80:1-36.

48. Jang J-H, Castano O, Kim H-W. Electrospun materials as potential platforms for bone tissue engineering. Advanced Drug Delivery Reviews. 2009;61(12):1065-83.

49. Marks SC, Popoff SN. Bone cell biology: the regulation of development, structure, and function in the skeleton. American Journal of Anatomy. 1988;183(1):1-44.

50. Brydone A, Meek D, Maclaine S. Bone grafting, orthopaedic biomaterials, and the clinical need for bone engineering. Proceedings of the Institution of Mechanical Engineers, Part H: Journal of Engineering in Medicine. 2010;224(12):1329-43.

51. Mellon S, Tanner K. Bone and its adaptation to mechanical loading: a review. International Materials Reviews. 2012;57(5):235-55.

52. Standring S. Grays Anatomy 40thEdition. Anatomical Basis Of Clinical Practice, Churchill Livingstone, London. 2008;40:415.

53. You L, Temiyasathit S, Lee P, Kim CH, Tummala P, Yao W, et al. Osteocytes as mechanosensors in the inhibition of bone resorption due to mechanical loading. Bone. 2008;42(1):172-9.

54. Kular J, Tickner J, Chim SM, Xu J. An overview of the regulation of bone remodelling at the cellular level. Clinical biochemistry. 2012;45(12):863-73.

55. Anderson HC. Matrix vesicles and calcification. Current rheumatology reports. 2003;5(3):222-6.

56. Eriksen EF. Cellular mechanisms of bone remodeling. Reviews in Endocrine and Metabolic Disorders. 2010;11(4):219-27.

57. Frost HM. Tetracycline-based histological analysis of bone remodeling. Calcified Tissue International. 1969;3(1):211-37.

58. Matsuzaki M, Pant R, Kulkarni B, Kinra S. Comparison of Bone Mineral Density between Urban and Rural Areas: Systematic Review and Meta-Analysis. PloS one. 2015;10(7):e0132239.

59. Willson T, Nelson SD, Newbold J, Nelson RE, LaFleur J. The clinical epidemiology of male osteoporosis: a review of the recent literature. Clinical epidemiology. 2015;7:65.

60. Yamaguchi M. Nutritional factors and bone homeostasis: synergistic effect with zinc and genistein in osteogenesis. Molecular and Cellular Biochemistry. 2012;366(1-2):201-21.

61. Del Valle HB, Yaktine AL, Taylor CL, Ross AC. Dietary reference intakes for calcium and vitamin D: National Academies Press; 2011.

62. Yamaguchi M. Isoflavone and Bone Metabolism: Its Cellular Mechanism and Preventive Role in Bone Loss. Journal of Health Science. 2002;48(3):209-22.

63. Yamaguchi M. Role of zinc in bone metabolism and preventive effect on bone disorder. Biomedical Research on Trace Elements. 2007;18(4):346-66.

64. Orriss IR, MacRae VE. Editorial overview: Musculoskeletal: Where are we with treating musculoskeletal disorders? Current Opinion in Pharmacology. 2016;28:iv-vi.

65. Masi L. Epidemiology of osteoporosis. Clinical Cases in Mineral and Bone Metabolism. 2008;5(1):11.

66. Bliuc D, Alarkawi D, Nguyen TV, Eisman JA, Center JR. Risk of subsequent fractures and mortality in elderly women and men with fragility fractures with and without osteoporotic bone density: the Dubbo Osteoporosis Epidemiology Study. Journal of Bone and Mineral Research. 2015;30(4):637-46.

67. Cauley JA. Risk factors: Diabetes, fractures and mortality [mdash] statin therapy. Nature Reviews Endocrinology. 2015;11(7):387-9.

68. Teng GG, Curtis eR, Saag KG. Mortality and osteoporotic fractures: is the link causal, and is it modifiable? Clinical and experimental rheumatology. 2008;26(5 0 51):S125-S37.

69. Meunier PJ, Roux C, Seeman E, Ortolani S, Badurski JE, Spector TD, et al. The Effects of Strontium Ranelate on the Risk of Vertebral Fracture in Women with Postmenopausal Osteoporosis. New England Journal of Medicine. 2004;350(5):459-68.

70. Paget J. On a form of chronic inflammation of bones (osteitis deformans). Medico-chirurgical transactions. 1877;60:37.

71. Corral-Gudino L, Borao-Cengotita-Bengoa M, Del Pino-Montes J, Ralston S. Epidemiology of Paget's disease of bone: a systematic review and meta-analysis of secular changes. Bone. 2013;55(2):347-52.

72. Vallet M, Ralston SH. Biology and Treatment of Paget's Disease of Bone. Journal of cellular biochemistry. 2016;117(2):289-99.

73. Sabharwal R, Gupta S, Sepolia S, Panigrahi R, Mohanty S, Subudhi SK, et al. An Insight in to Paget's Disease of Bone. Nigerian Journal of Surgery : Official Publication of the Nigerian Surgical Research Society. 2014;20(1):9-15.

74. Woolf AD, Pfleger B. Burden of major musculoskeletal conditions. Bulletin of the World Health Organization. 2003;81(9):646-56.

75. Loeser RF, Goldring SR, Scanzello CR, Goldring MB. Osteoarthritis: a disease of the joint as an organ. Arthritis & Rheumatism. 2012;64(6):1697-707.

76. Silverwood V, Blagojevic-Bucknall M, Jinks C, Jordan J, Protheroe J, Jordan K. Current evidence on risk factors for knee osteoarthritis in older adults: a systematic review and meta-analysis. Osteoarthritis and Cartilage. 2015;23(4):507-15.

77. Johnson VL, Hunter DJ. The epidemiology of osteoarthritis. Best practice & research Clinical rheumatology. 2014;28(1):5-15.

78. Dimitriou R, Mataliotakis GI, Angoules AG, Kanakaris NK, Giannoudis PV. Complications following autologous bone graft harvesting from the iliac crest and using the RIA: a systematic review. Injury. 2011;42:S3-S15.

79. Griffin KS, Davis KM, McKinley TO, Anglen JO, Chu T-MG, Boerckel JD, et al. Evolution of Bone Grafting: Bone Grafts and Tissue Engineering Strategies for Vascularized Bone Regeneration. Clinical Reviews in Bone and Mineral Metabolism. 2015:1-13.

80. Drosos G, Babourda E, Magnissalis E, Giatromanolaki A, Kazakos K, Verettas D. Mechanical characterization of bone graft substitute ceramic cements. Injury. 2012;43(3):266-71.

81. Seiler 3rd J, Johnson J. Iliac crest autogenous bone grafting: donor site complications. Journal of the Southern Orthopaedic Association. 1999;9(2):91-7.

82. Yazar S, Lin C-H, Wei F-C. One-stage reconstruction of composite bone and soft-tissue defects in traumatic lower extremities. Plastic and Reconstructive Surgery. 2004;114(6):1457-66.

83. Grabowski G, Cornett CA. Bone graft and bone graft substitutes in spine surgery: current concepts and controversies. Journal of the American Academy of Orthopaedic Surgeons. 2013;21(1):51-60.

84. Gebhardt MC, Flugstad DI, Springfield DS, Mankin HJ. The use of bone allografts for limb salvage in high-grade extremity osteosarcoma. Clinical orthopaedics and related research. 1991(270):181-96.

85. Eastlund T. Bacterial infection transmitted by human tissue allograft transplantation. Cell and Tissue Banking. 2006;7(3):147-66.

86. Delloye C, Cornu O, Druez V, Barbier O. Bone allografts. Bone & Joint Journal. 2007;89(5):574-80.

87. Yang Y-G, Sykes M. Xenotransplantation: current status and a perspective on the future. Nature Reviews Immunology. 2007;07(07):519-31.

88. Geetha M, Singh A, Asokamani R, Gogia A. Ti based biomaterials, the ultimate choice for orthopaedic implants–a review. Progress in Materials Science. 2009;54(3):397-425.

89. Le Guéhennec L, Soueidan A, Layrolle P, Amouriq Y. Surface treatments of titanium dental implants for rapid osseointegration. Dental Materials.23(7):844-54.

90. Hollister SJ. Porous scaffold design for tissue engineering. Nature Materials. 2005;4(7):518-24.

91. Collins MN, Birkinshaw C. Hyaluronic acid based scaffolds for tissue engineering—A review. Carbohydrate Polymers. 2013;92(2):1262-79.

92. Williams D. Summary and definitions. Progress in biomedical engineering: definition in biomaterials (4) Amsterdam: Elsevier Science Publisher BV. 1987:66-71.

93. Le X, Poinern GEJ, Ali N, Berry CM, Fawcett D. Engineering a biocompatible scaffold with either micrometre or nanometre scale surface topography for promoting protein adsorption and cellular response. International Journal of Biomaterials. 2013;2013.

94. Williams DF. On the mechanisms of biocompatibility. Biomaterials. 2008;29(20):2941-53.

95. Smith BD, Grande DA. The current state of scaffolds for musculoskeletal regenerative applications. Nature Reviews Rheumatology. 2015;11(4):213-22.

96. Wise DL, Trantolo DJ, Lewandrowski K-U, Gresser JD, Cattaneo MV, Yaszemski MJ. Biomaterials engineering and devices: human applications: Springer; 2000.

97. Bose S, Roy M, Bandyopadhyay A. Recent advances in bone tissue engineering scaffolds. Trends in Biotechnology. 2012;30(10):546-54.

98. Olszta MJ, Cheng X, Jee SS, Kumar R, Kim Y-Y, Kaufman MJ, et al. Bone structure and formation: a new perspective. Materials Science and Engineering: R: Reports. 2007;58(3):77-116.

99. Hollister SJ. Porous scaffold design for tissue engineering. Nat Mater. 2005;4(7):518-24.

100. Liu Y, Lim J, Teoh S-H. Review: development of clinically relevant scaffolds for vascularised bone tissue engineering. Biotechnology Advances. 2013;31(5):688-705.

101. Balla VK, Bodhak S, Bose S, Bandyopadhyay A. Porous tantalum structures for bone implants: fabrication, mechanical and in vitro biological properties. Acta Biomaterialia. 2010;6(8):3349-59.

102. Parithimarkalaignan S, Padmanabhan TV. Osseointegration: An Update. The Journal of the Indian Prosthodontic Society. 2013;13(1):2-6.

103. Rezwan K, Chen QZ, Blaker JJ, Boccaccini AR. Biodegradable and bioactive porous polymer/inorganic composite scaffolds for bone tissue engineering. Biomaterials. 2006;27(18):3413-31.

104. Rogero SO, Malmonge SM, Lugão AB, Ikeda TI, Miyamaru L, Cruz ÁS. Biocompatibility study of polymeric biomaterials. Artificial Organs. 2003;27(5):424-7.

105. Lee MH, Arcidiacono JA, Bilek AM, Wille JJ, Hamill CA, Wonnacott KM, et al. Considerations for tissue-engineered and regenerative medicine product development prior to clinical trials in the United States. Tissue Engineering Part B: Reviews. 2009;16(1):41-54.

106. Venkatesan J, Bhatnagar I, Manivasagan P, Kang K-H, Kim S-K. Alginate composites for bone tissue engineering: A review. International Journal of Biological Macromolecules. 2015;72:269-81.

107. Valente JFA, Valente TAM, Alves P, Ferreira P, Silva A, Correia IJ. Alginate based scaffolds for bone tissue engineering. Materials Science and Engineering: C. 2012;32(8):2596-603.

108. Chandika P, Ko S-C, Oh G-W, Heo S-Y, Nguyen V-T, Jeon Y-J, et al. Fish collagen/alginate/chitooligosaccharides integrated scaffold for skin tissue regeneration application. International Journal of Biological Macromolecules. 2015;81:504-13.

109. Wang C-C, Yang K-C, Lin K-H, Liu H-C, Lin F-H. A highly organized three-dimensional alginate scaffold for cartilage tissue engineering prepared by microfluidic technology. Biomaterials. 2011;32(29):7118-26.

110. Diogo GS, Gaspar VM, Serra IR, Fradique R, Correia IJ. Manufacture of β-TCP/alginate scaffolds through a Fab@home model for application in bone tissue engineering. Biofabrication. 2014;6(2):025001.

111. Shteyer E, Ya'acov AB, Zolotaryova L, Sinai A, Lichtenstein Y, Pappo O, et al. Reduced liver cell death using an alginate scaffold bandage: A novel approach for liver reconstruction after extended partial hepatectomy. Acta Biomaterialia. 2014;10(7):3209-16.

112. Sapir Y, Kryukov O, Cohen S. Integration of multiple cell-matrix interactions into alginate scaffolds for promoting cardiac tissue regeneration. Biomaterials. 2011;32(7):1838-47.

113. Lee KY, Jeong L, Kang YO, Lee SJ, Park WH. Electrospinning of polysaccharides for regenerative medicine. Advanced Drug Delivery Reviews. 2009;61(12):1020-32.

114. Castilho M, Rodrigues J, Pires I, Gouveia B, Pereira M, Moseke C, et al. Fabrication of individual alginate-TCP scaffolds for bone tissue engineering by means of powder printing. Biofabrication. 2015;7(1):015004.

115. Quinlan E, López-Noriega A, Thompson E, Kelly HM, Cryan SA, O'Brien FJ. Development of collagen–hydroxyapatite scaffolds incorporating PLGA and alginate microparticles for the controlled delivery of rhBMP-2 for bone tissue engineering. Journal of Controlled Release. 2015;198:71-9.

116. Moshaverinia A, Ansari S, Chen C, Xu X, Akiyama K, Snead ML, et al. Co-encapsulation of anti-BMP2 monoclonal antibody and mesenchymal stem cells in alginate microspheres for bone tissue engineering. Biomaterials. 2013;34(28):6572-9.

117. Levengood SKL, Zhang M. Chitosan-based scaffolds for bone tissue engineering. Journal of Materials Chemistry B. 2014;2(21):3161-84.

118. Pillai CKS, Paul W, Sharma CP. Chitin and chitosan polymers: Chemistry, solubility and fiber formation. Progress in Polymer Science. 2009;34(7):641-78.

119. Kiang T, Wen J, Lim HW, Leong KW. The effect of the degree of chitosan deacetylation on the efficiency of gene transfection. Biomaterials. 2004;25(22):5293-301.

120. Malafaya PB, Silva GA, Reis RL. Natural-origin polymers as carriers and scaffolds for biomolecules and cell delivery in tissue engineering applications. Advanced Drug Delivery Reviews. 2007;59(4-5):207-33.

121. Beringer LT, Kiechel MA, Komiya Y, Donius AE, Habas R, Wegst UGK, et al. Osteoblast biocompatibility of novel chitosan crosslinker, hexamethylene-1,6-diaminocarboxysulfonate. Journal of Biomedical Materials Research Part A. 2015;103(9):3026-33.

122. Ignjatović N, Wu V, Ajduković Z, Mihajilov-Krstev T, Uskoković V, Uskoković D. Chitosan-PLGA polymer blends as coatings for hydroxyapatite nanoparticles and their effect on antimicrobial properties, osteoconductivity and regeneration of osseous tissues. Materials Science and Engineering: C.

123. Muzzarelli R, Mattioli-Belmonte M, Tietz C, Biagini R, Ferioli G, Brunelli M, et al. Stimulatory effect on bone formation exerted by a modified chitosan. Biomaterials. 1994;15(13):1075-81.

124. Jin H-H, Kim D-H, Kim T-W, Shin K-K, Jung JS, Park H-C, et al. In vivo evaluation of porous hydroxyapatite/chitosan–alginate composite scaffolds for bone tissue engineering. International Journal of Biological Macromolecules. 2012;51(5):1079-85.

125. Fan J, Park H, Lee MK, Bezouglaia O, Fartash A, Kim J, et al. Adipose-derived stem cells and BMP-2 delivery in chitosan-based 3D constructs to enhance bone regeneration in a rat mandibular defect model. Tissue Engineering Part A. 2014;20(15-16):2169-79.

126. Serra I, Fradique R, Vallejo M, Correia T, Miguel S, Correia I. Production and characterization of Chitosan/Gelatin/ß-TCP scaffolds for improved bone tissue regeneration. Materials Science and Engineering: C. 2015.

127. Zhou Z, Chen J, Peng C, Huang T, Zhou H, Ou B, et al. Fabrication and physical properties of gelatin/sodium alginate/hyaluronic acid composite wound dressing hydrogel. Journal of Macromolecular Science, Part A. 2014;51(4):318-25.

128. Su K, Wang C. Recent advances in the use of gelatin in biomedical research. Biotechnology letters. 2015;37(11):2139-45.

129. Elzoghby AO, Samy WM, Elgindy NA. Protein-based nanocarriers as promising drug and gene delivery systems. Journal of Controlled Release. 2012;161(1):38-49.

130. Xia Y, Mei F, Duan Y, Gao Y, Xiong Z, Zhang T, et al. Bone tissue engineering using bone marrow stromal cells and an injectable sodium alginate/gelatin scaffold. Journal of Biomedical Materials Research Part A. 2012;100(4):1044-50.

131. Arafat MT, Lam CXF, Ekaputra AK, Wong SY, Li X, Gibson I. Biomimetic composite coating on rapid prototyped scaffolds for bone tissue engineering. Acta Biomaterialia. 2011;7(2):809-20.

132. Yamamoto M, Hokugo A, Takahashi Y, Nakano T, Hiraoka M, Tabata Y. Combination of BMP-2-releasing gelatin/ß-TCP sponges with autologous bone marrow for bone regeneration of X-ray-irradiated rabbit ulnar defects. Biomaterials. 2015;56:18-25.

133. Bae MS, Yang DH, Lee JB, Heo DN, Kwon Y-D, Youn IC, et al. Photo-cured hyaluronic acid-based hydrogels containing simvastatin as a bone tissue regeneration scaffold. Biomaterials. 2011;32(32):8161-71.

134. Oommen OP, Wang S, Kisiel M, Sloff M, Hilborn J, Varghese OP. Smart design of stable extracellular matrix mimetic hydrogel: synthesis, characterization, and in vitro and in vivo evaluation for tissue engineering. Adv Funct Mater. 2013;23(10):1273-80.

135. Burdick JA, Prestwich GD. Hyaluronic acid hydrogels for biomedical applications. Advanced Materials. 2011;23(12).

136. Kim J, Kim IS, Cho TH, Lee KB, Hwang SJ, Tae G, et al. Bone regeneration using hyaluronic acid-based hydrogel with bone morphogenic protein-2 and human mesenchymal stem cells. Biomaterials. 2007;28(10):1830-7.

137. Jhan H-J, Liu J-J, Chen Y-C, Liu D-Z, Sheu M-T, Ho H-O. Novel injectable thermosensitive hydrogels for delivering hyaluronic acid-doxorubicin nanocomplexes to locally treat tumors. Nanomedicine. 2015;10(8):1263-74.

138. Campoccia D, Doherty P, Radice M, Brun P, Abatangelo G, Williams DF. Semisynthetic resorbable materials from hyaluronan esterification. Biomaterials. 1998;19(23):2101-27.

139. Cui N, Qian J, Liu T, Zhao N, Wang H. Hyaluronic acid hydrogel scaffolds with a triple degradation behavior for bone tissue engineering. Carbohydrate Polymers. 2015;126:192-8.

140. Ginebra MP, Espanol M, Montufar EB, Perez RA, Mestres G. New processing approaches in calcium phosphate cements and their applications in regenerative medicine. Acta Biomaterialia. 2010;6(8):2863-73.

141. Kuang GM, Yau W, Wu J, Yeung KW, Pan H, Lam W, et al. Strontium exerts dual effects on calcium phosphate cement: Accelerating the degradation and enhancing the osteoconductivity both in vitro and in vivo. Journal of Biomedical Materials Research Part A. 2015;103(5):1613-21.

142. Woodard JR, Hilldore AJ, Lan SK, Park C, Morgan AW, Eurell JAC, et al. The mechanical properties and osteoconductivity of hydroxyapatite bone scaffolds with multi-scale porosity. Biomaterials. 2007;28(1):45-54.

143. Apelt D, Theiss F, El-Warrak AO, Zlinszky K, Bettschart-Wolfisberger R, Bohner M, et al. In vivo behavior of three different injectable hydraulic calcium phosphate cements. Biomaterials. 2004;25(7–8):1439-51.

144. Song G, Habibovic P, Bao C, Hu J, van Blitterswijk CA, Yuan H, et al. The homing of bone marrow MSCs to non-osseous sites for ectopic bone formation induced by osteoinductive calcium phosphate. Biomaterials. 2013;34(9):2167-76.

145. Samavedi S, Whittington AR, Goldstein AS. Calcium phosphate ceramics in bone tissue engineering: a review of properties and their influence on cell behavior. Acta Biomaterialia. 2013;9(9):8037-45.

146. Alves Cardoso D, Jansen J, G Leeuwenburgh S. Synthesis and application of nanostructured calcium phosphate ceramics for bone regeneration. Journal of Biomedical Materials Research Part B: Applied Biomaterials. 2012;100(8):2316-26.

147. Choi AH, Ben-Nissan B, Conway RC, Macha IJ. Advances in calcium phosphate nanocoatings and nanocomposites. Advances in Calcium Phosphate Biomaterials: Springer; 2014. p. 485-509.

148. Valiense H, Barreto M, Resende RF, Alves AT, Rossi AM, Mavropoulos E, et al. In vitro and in vivo evaluation of strontium-containing nanostructured carbonated hydroxyapatite/sodium alginate for sinus lift in rabbits. Journal of Biomedical Materials Research Part B: Applied Biomaterials. 2016;104(2):274-82.

149. Asa'ad F, Pagni G, Pilipchuk SP, Giannì AB, Giannobile WV, Rasperini G. 3D-Printed Scaffolds and Biomaterials: Review of Alveolar Bone Augmentation and Periodontal Regeneration Applications. International Journal of Dentistry. 2016;2016.

150. Karadzic I, Vucic V, Jokanovic V, Debeljak-Martacic J, Markovic D, Petrovic S, et al. Effects of novel hydroxyapatite-based 3D biomaterials on proliferation and osteoblastic differentiation of mesenchymal stem cells. Journal of Biomedical Materials Research Part A. 2015;103(1):350-7.

151. Zhou Y, Xu L, Zhang X, Zhao Y, Wei S, Zhai M. Radiation synthesis of gelatin/CM-chitosan/ß-tricalcium phosphate composite scaffold for bone tissue engineering. Materials Science and Engineering: C. 2012;32(4):994-1000.

152. Gaalen Sv, Kruyt M, Meijer G, Mistry A, Mikos A, Beucken Jvd, et al. Chapter 19 - Tissue engineering of bone. In: Blitterswijk Cv, Thomsen P, Lindahl A, Hubbell J, Williams DF, Cancedda R, et al., editors. Tissue engineering. Burlington: Academic Press; 2008. p. 559-610.

153. Santos CF, Silva AP, Lopes L, Pires I, Correia IJ. Design and production of sintered ß-tricalcium phosphate 3D scaffolds for bone tissue regeneration. Materials Science and Engineering: C. 2012;32(5):1293-8.

154. Arahira T, Todo M. Effects of Proliferation and Differentiation of Mesenchymal Stem Cells on Compressive Mechanical Behavior of Collagen/ß-TCP Composite Scaffold. Journal of the Mechanical Behavior of Biomedical Materials. 2014;39:218-30.

155. Wei X, He K, Yu S, Zhao W, Xing G, Liu Y, et al. RGD Peptide-Modified Poly(lactide-co-glycolide)/β-Tricalcium Phosphate Scaffolds Increase Bone Formation After Transplantation in a Rabbit Model. Journal of Biomaterials and Tissue Engineering. 2015;5(5):378-86.

156. Pilipchuk SP, Plonka AB, Monje A, Taut AD, Lanis A, Kang B, et al. Tissue engineering for bone regeneration and osseointegration in the oral cavity. Dental Materials. 2015;31(4):317-38.

157. Rahaman MN, Day DE, Sonny Bal B, Fu Q, Jung SB, Bonewald LF, et al. Bioactive glass in tissue engineering. Acta Biomaterialia. 2011;7(6):2355-73.

158. Jones JR. Review of bioactive glass: From Hench to hybrids. Acta Biomaterialia. 2013;9(1):4457-86.

159. Jung S, Day D, Day T, Stoecker W, Taylor P, editors. Treatment of non-healing diabetic venous stasis ulcers with bioactive glass nanofibers. Wound Repair and Regeneration; 2011: Wiley.

160. Neel EAA, Chrzanowski W, Knowles JC. Biological performance of titania containing phosphate-based glasses for bone tissue engineering applications. Materials Science and Engineering: C. 2014;35:307-13.

161. El-Meliegy E, Farag M, Knowles J. Dissolution and drug release profiles of phosphate glasses doped with high valency oxides. Journal of Materials Science: Materials in Medicine. 2016;27(6):1-10.

162. Wu C, Chang J. A review of bioactive silicate ceramics. Biomedical Materials. 2013;8(3):032001.

163. Shalumon K, Sowmya S, Sathish D, Chennazhi K, Nair SV, Jayakumar R. Effect of incorporation of nanoscale bioactive glass and hydroxyapatite in PCL/chitosan nanofibers for bone and periodontal tissue engineering. Journal of Biomedical Nanotechnology. 2013;9(3):430-40.

164. Rezabeigi E, Wood-Adams PM, Drew RA. Surface Modification of Sol-Gel-Derived 45S5 Bioglass® for Incorporation in Polylactic Acid (PLA). Advances in Bioceramics and Porous Ceramics VI (eds R Narayan, P Colombo, S Kirihara and S Widjaja), John Wiley & Sons, Inc. 2013.

165. Luo Y, Wu C, Lode A, Gelinsky M. Hierarchical mesoporous bioactive glass/alginate composite scaffolds fabricated by three-dimensional plotting for bone tissue engineering. Biofabrication. 2013;5(1):015005.

166. Pishbin F, Mouriño V, Gilchrist J, McComb D, Kreppel S, Salih V, et al. Single-step electrochemical deposition of antimicrobial orthopaedic coatings based on a bioactive glass/chitosan/nano-silver composite system. Acta Biomaterialia. 2013;9(7):7469-79.

167. Nguyen DT, Burg KJ. Bone tissue engineering and regenerative medicine: Targeting pathological fractures. Journal of Biomedical Materials Research Part A. 2015;103(1):420-9.

168. Loh QL, Choong C. Three-dimensional scaffolds for tissue engineering applications: Role of porosity and pore size. Tissue Engineering Part B: Reviews. 2013;19(6):485-502.

169. Hoque ME, Chuan YL, Pashby I. Extrusion based rapid prototyping technique: an advanced platform for tissue engineering scaffold fabrication. Biopolymers. 2012;97(2):83-93.

170. Nandakumar A, Barradas A, de Boer J, Moroni L, van Blitterswijk C, Habibovic P. Combining technologies to create bioactive hybrid scaffolds for bone tissue engineering. Biomatter. 2013;3(2):e23705.

171. Kim H, Kim HW, Suh H. Sustained release of ascorbate-2-phosphate and dexamethasone from porous PLGA scaffolds for bone tissue engineering using mesenchymal stem cells. Biomaterials. 2003;24(25):4671-9.

172. Mozafari M, Moztarzadeh F, Rabiee M, Azami M, Maleknia S, Tahriri M, et al. Development of macroporous nanocomposite scaffolds of gelatin/bioactive glass prepared through layer solvent casting combined with lamination technique for bone tissue engineering. Ceramics International. 2010;36(8):2431-9.

173. Cao H, Kuboyama N. A biodegradable porous composite scaffold of PGA/β-TCP for bone tissue engineering. Bone. 2010;46(2):386-95.

174. Zhu N, Chen X. Biofabrication of tissue scaffolds: INTECH Open Access Publisher; 2013.

175. Yoon JJ, Park TG. Degradation behaviors of biodegradable macroporous scaffolds prepared by gas foaming of effervescent salts. Journal of biomedical materials research. 2001;55(3):401-8.

176. Kim TK, Yoon JJ, Lee DS, Park TG. Gas foamed open porous biodegradable polymeric microspheres. Biomaterials. 2006;27(2):152-9.

177. Di Maio E, Salerno A, Iannace S. Scaffolds with tubular/isotropic bi-modal pore structures by gas foaming and fiber templating. Materials Letters. 2013;93:157-60.

178. Sachlos E, Czernuszka J. Making tissue engineering scaffolds work. Review: the application of solid freeform fabrication technology to the production of tissue engineering scaffolds. European cells & materials. 2003;5(29):39-40.

179. Janik H, Marzec M. A review: Fabrication of porous polyurethane scaffolds. Materials Science and Engineering: C. 2015;48:586-91.

180. Almirall A, Larrecq G, Delgado JA, Martı▫nez S, Planell JA, Ginebra MP. Fabrication of low temperature macroporous hydroxyapatite scaffolds by foaming and hydrolysis of an α-TCP paste. Biomaterials. 2004;25(17):3671-80.

181. Rowlands A, Lim SA, Martin D, Cooper-White JJ. Polyurethane/poly (lactic-co-glycolic) acid composite scaffolds fabricated by thermally induced phase separation. Biomaterials. 2007;28(12):2109-21.

182. Mao J, Duan S, Song A, Cai Q, Deng X, Yang X. Macroporous and nanofibrous poly(lactide-co-glycolide)(50/50) scaffolds via phase separation combined with particle-leaching. Materials Science and Engineering: C. 2012;32(6):1407-14.

183. Heijkants R, van Calck R, van Tienen T, de Groot J, Pennings A, Buma P, et al. Polyurethane scaffold formation via a combination of salt leaching and thermally induced phase separation. Journal of Biomedical Materials Research Part A. 2008;87(4):921-32.

184. Sultana N, Wang M. PHBV/PLLA-based composite scaffolds fabricated using an emulsion freezing/freeze-drying technique for bone tissue engineering: surface modification and in vitro biological evaluation. Biofabrication. 2012;4(1):015003.

185. Zhu Y, Wan Y, Zhang J, Yin D, Cheng W. Manufacture of layered collagen/chitosan-polycaprolactone scaffolds with biomimetic microarchitecture. Colloids and Surfaces B: Biointerfaces. 2014;113:352-60.

186. Bhardwaj N, Sow WT, Devi D, Ng KW, Mandal BB, Cho N-J. Correction: Silk fibroin–keratin based 3D scaffolds as a dermal substitute for skin tissue engineering. Integrative Biology. 2014;7(1):142-.

187. Seol Y-J, Kang T-Y, Cho D-W. Solid freeform fabrication technology applied to tissue engineering with various biomaterials. Soft Matter. 2012;8(6):1730-5.

188. Gauvin R, Chen Y-C, Lee JW, Soman P, Zorlutuna P, Nichol JW, et al. Microfabrication of complex porous tissue engineering scaffolds using 3D projection stereolithography. Biomaterials. 2012;33(15):3824-34.

189. Chen M, Le DQ, Baatrup A, Nygaard JV, Hein S, Bjerre L, et al. Self-assembled composite matrix in a hierarchical 3-D scaffold for bone tissue engineering. Acta Biomaterialia. 2011;7(5):2244-55.

190. Yao Q, Wei B, Liu N, Li C, Guo Y, Shamie AN, et al. Chondrogenic Regeneration Using Bone Marrow Clots and a Porous Polycaprolactone-Hydroxyapatite Scaffold by Three-Dimensional Printing. Tissue Engineering Part A. 2015;21(7-8):1388-97.

191. Melocchi A, Parietti F, Loreti G, Maroni A, Gazzaniga A, Zema L. 3D printing by fused deposition modeling (FDM) of a swellable/erodible capsular device for oral pulsatile release of drugs. Journal of Drug Delivery Science and Technology. 2015; 30:360-7.

192. Colosi C, Costantini M, Latini R, Ciccarelli S, Stampella A, Barbetta A, et al. Rapid prototyping of chitosan-coated alginate scaffolds through the use of a 3D fiber deposition technique. Journal of Materials Chemistry B. 2014;2(39):6779-91.

193. Shor L, Güçeri S, Chang R, Gordon J, Kang Q, Hartsock L, et al. Precision extruding deposition (PED) fabrication of polycaprolactone (PCL) scaffolds for bone tissue engineering. Biofabrication. 2009;1(1):015003.

194. Xiong Z, Yan Y, Zhang R, Sun L. Fabrication of porous poly (L-lactic acid) scaffolds for bone tissue engineering via precise extrusion. Scripta Materialia. 2001;45(7):773-9.

195. Mota C, Puppi D, Chiellini F, Chiellini E. Additive manufacturing techniques for the production of tissue engineering constructs. Journal of Tissue Engineering and Regenerative Medicine. 2015;9(3):174-90.

196. Yilgor P, Yilmaz G, Onal M, Solmaz I, Gundogdu S, Keskil S, et al. An in vivo study on the effect of scaffold geometry and growth factor release on the healing of bone defects. Journal of Tissue Engineering and Regenerative Medicine. 2013;7(9):687-96.

197. Shuai C, Mao Z, Lu H, Nie Y, Hu H, Peng S. Fabrication of porous polyvinyl alcohol scaffold for bone tissue engineering via selective laser sintering. Biofabrication. 2013;5(1):015014.

198. Eshraghi S, Das S. Micromechanical finite-element modeling and experimental characterization of the compressive mechanical properties of polycaprolactone–hydroxyapatite composite scaffolds prepared by selective laser sintering for bone tissue engineering. Acta Biomaterialia. 2012;8(8):3138-43.

199. Kolan KC, Leu MC, Hilmas GE, Brown RF, Velez M. Fabrication of 13-93 bioactive glass scaffolds for bone tissue engineering using indirect selective laser sintering. Biofabrication. 2011;3(2):025004.

200. Mazzoli A. Selective laser sintering in biomedical engineering. Medical & Biological Engineering & Computing. 2013;51(3):245-56.

201. Oliveira A, Costa S, Sousa R, Reis R. Nucleation and growth of biomimetic apatite layers on 3D plotted biodegradable polymeric scaffolds: effect of static and dynamic coating conditions. Acta Biomaterialia. 2009;5(5):1626-38.

202. Inzana JA, Olvera D, Fuller SM, Kelly JP, Graeve OA, Schwarz EM, et al. 3D printing of composite calcium phosphate and collagen scaffolds for bone regeneration. Biomaterials. 2014;35(13):4026-34.

203. Luo Y, Lode A, Sonntag F, Nies B, Gelinsky M. Well-ordered biphasic calcium phosphate–alginate scaffolds fabricated by multi-channel 3D plotting under mild conditions. Journal of Materials Chemistry B. 2013;1(33):4088-98.

204. Guo B, Lei B, Li P, Ma PX. Functionalized scaffolds to enhance tissue regeneration. Regenerative Biomaterials. 2015;2(1):47-57.

205. Chitnis AS, Edwards JR, Ricks PM, Sievert DM, Fridkin SK, Gould CV. Device-Associated Infection Rates, Device Utilization, and Antimicrobial Resistance in Long-Term Acute Care

Hospitals Reporting to the National Healthcare Safely Network, 2010. Infection Control. 2012;33(10):993-1000.

206. Muszanska AK, Rochford ET, Gruszka A, Bastian AA, Busscher HJ, Norde W, et al. Antiadhesive polymer brush coating functionalized with antimicrobial and rgd peptides to reduce biofilm formation and enhance tissue integration. Biomacromolecules. 2014;15(6):2019-26.

207. Thien DVH, Hsiao SW, Ho MH, Li CH, Shih JL. Electrospun chitosan/hydroxyapatite nanofibers for bone tissue engineering. J Mater Sci. 2013;48(4):1640-5.

208. Cardoso GBC, Maniglio D, Volpato FZ, Tondon A, Migliaresi C, Kaunas RR, et al. Oleic acid surfactant in polycaprolactone/hydroxyapatite-composites for bone tissue engineering. Journal of Biomedical Materials Research Part B: Applied Biomaterials. 2016;104(6):1076-82.

209. Saravanan S, Sameera DK, Moorthi A, Selvamurugan N. Chitosan scaffolds containing chicken feather keratin nanoparticles for bone tissue engineering. International Journal of Biological Macromolecules. 2013;62:481-6.

210. Hickey DJ, Ercan B, Sun L, Webster TJ. Adding MgO nanoparticles to hydroxyapatite–PLLA nanocomposites for improved bone tissue engineering applications. Acta Biomaterialia. 2015;14:175-84.

211. Marsich E, Bellomo F, Turco G, Travan A, Donati I, Paoletti S. Nano-composite scaffolds for bone tissue engineering containing silver nanoparticles: preparation, characterization and biological properties. Journal of Materials Science: Materials in Medicine. 2013;24(7):1799-807.

212. Lee SS, Huang BJ, Kaltz SR, Sur S, Newcomb CJ, Stock SR, et al. Bone regeneration with low dose BMP-2 amplified by biomimetic supramolecular nanofibers within collagen scaffolds. Biomaterials. 2013;34(2):452-9.

213. Cui X, Zhao C, Gu Y, Li L, Wang H, Huang W, et al. A novel injectable borate bioactive glass cement for local delivery of vancomycin to cure osteomyelitis and regenerate bone. Journal of Materials Science: Materials in Medicine. 2014;25(3):733-45.

214. Kristinsson K, Jansen B, Treitz U, Schumacher-Perdreau F, Peters G, Pulverer G. Antimicrobial activity of polymers coated with iodine-complexed polyvinylpyrrolidone. Journal of biomaterials applications. 1991;5(3):173-84.

215. Kumar A, Vemula PK, Ajayan PM, John G. Silver-nanoparticle-embedded antimicrobial paints based on vegetable oil. Nature Materials. 2008;7(3):236-41.

216. Zhang T, Zhou P, Zhan Y, Shi X, Lin J, Du Y, et al. Pectin/lysozyme bilayers layer-by-layer deposited cellulose nanofibrous mats for antibacterial application. Carbohydrate Polymers. 2015;117:687-93.

217. Saini S, Belgacem N, Mendes J, Elegir G, Bras J. Contact Antimicrobial Surface Obtained by Chemical Grafting of Microfibrillated Cellulose in Aqueous Solution Limiting Antibiotic Release. ACS Applied Materials & Interfaces. 2015;7(32):18076-85.

218. Girshevitz O, Nitzan Y, Sukenik CN. Solution-deposited amorphous titanium dioxide on silicone rubber: a conformal, crack-free antibacterial coating. Chemistry of Materials. 2008;20(4):1390-6.

219. Etienne O, Gasnier C, Taddei C, Voegel J-C, Aunis D, Schaaf P, et al. Antifungal coating by biofunctionalized polyelectrolyte multilayered films. Biomaterials. 2005;26(33):6704-12.

220. Gabriel M, Nazmi K, Veerman EC, Nieuw Amerongen AV, Zentner A. Preparation of LL-37-grafted titanium surfaces with bactericidal activity. Bioconjugate Chemistry. 2006;17(2):548-50.

221. Shi Z, Neoh KG, Kang ET, Poh CK, Wang W. Surface Functionalization of Titanium with Carboxymethyl Chitosan and Immobilized Bone Morphogenetic Protein-2 for Enhanced Osseointegration. Biomacromolecules. 2009;10(6):1603-11.

222. Adams CS, Antoci V, Harrison G, Patal P, Freeman TA, Shapiro IM, et al. Controlled release of vancomycin from thin sol-gel films on implant surfaces successfully controls osteomyelitis. Journal of Orthopaedic Research. 2009;27(6):701-9.

223. Feng K, Sun H, Bradley MA, Dupler EJ, Giannobile WV, Ma PX. Novel Antibacterial Nanofibrous PLLA Scaffolds. Journal of controlled release : official journal of the Controlled Release Society. 2010;146(3):363-9.

224. Ruckh TT, Oldinski RA, Carroll DA, Mikhova K, Bryers JD, Popat KC. Antimicrobial effects of nanofiber poly (caprolactone) tissue scaffolds releasing rifampicin. Journal of Materials Science: Materials in Medicine. 2012;23(6):1411-20.

225. Shi X, Wang Y, Ren L, Huang W, Wang D-A. A protein/antibiotic releasing poly (lactic-co-glycolic acid)/lecithin scaffold for bone repair applications. International Journal of Pharmaceutics. 2009;373(1):85-92.

226. Saravanan S, Nethala S, Pattnaik S, Tripathi A, Moorthi A, Selvamurugan N. Preparation, characterization and antimicrobial activity of a bio-composite scaffold containing chitosan/nano-hydroxyapatite/nano-silver for bone tissue engineering. International Journal of Biological Macromolecules. 2011;49(2):188-93.

227. Sivolella S, Stellini E, Brunello G, Gardin C, Ferroni L, Bressan E, et al. Silver nanoparticles in alveolar bone surgery devices. Journal of Nanomaterials. 2012;2012:15.

228. Nirmala R, Kang H-S, Park H-M, Navamathavan R, Jeong IS, Kim HY. Silver-Loaded Biomimetic Hydroxyapatite Grafted Poly (ε-caprolactone) Composite Nanofibers: A Cytotoxicity Study. Journal of Biomedical Nanotechnology. 2012;8(1):125-32.

229. Prokopovich P, Köbrick M, Brousseau E, Perni S. Potent antimicrobial activity of bone cement encapsulating silver nanoparticles capped with oleic acid. Journal of Biomedical Materials Research Part B: Applied Biomaterials. 2015;103(2):273-81.

230. Wang Q, Yu X, Libera M. Reducing Bacterial Colonization of 3-D Nanofiber Cell Scaffolds by Hierarchical Assembly of Microgels and an Antimicrobial Peptide. Advanced Healthcare Materials. 2013;2(5):687-91.

231. Ao H, Chen C, Xie K, Zhou J, Long T, Tang T, et al. Covalent immobilization of KR-12 peptide onto a titanium surface for decreasing infection and promoting osteogenic differentiation. RSC Advances. 2016;6(52):46733-43.

232. Ma T, Shang B-C, Tang H, Zhou T-H, Xu G-L, Li H-L, et al. Nano-hydroxyapatite/chitosan/konjac glucomannan scaffolds loaded with cationic liposomal vancomycin: preparation, in vitro release and activity against Staphylococcus aureus biofilms. Journal of Biomaterials Science, Polymer Edition. 2011;22(12):1669-81.

233. Miguel SP, Ribeiro MP, Brancal H, Coutinho P, Correia IJ. Thermoresponsive chitosan–agarose hydrogel for skin regeneration. Carbohydrate Polymers. 2014;111:366-73.

234. Carlberg C, Ulven SM, Molnár F. Nutrition and Common Diseases. Nutrigenomics: Springer; 2016. p. 3-23.

235. Desai ND, Cohen EA, Naylor CD, Fremes SE. A randomized comparison of radial-artery and saphenous-vein coronary bypass grafts. New England Journal of Medicine. 2004;351(22):2302-9.

236. Davies MG, Hagen P-O. Pathophysiology of vein graft failure: a review. European Journal of Vascular and Endovascular Surgery. 1995;9(1):7-18.

237. Roll S, Müller-Nordhorn J, Keil T, Scholz H, Eidt D, Greiner W, et al. Dacron® vs. PTFE as bypass materials in peripheral vascular surgery–systematic review and meta-analysis. BMC Surgery. 2008;8(1):1.

238. Tan A, Gundogan B, Farhatnia Y, Nayyer L, Mahdibeiraghdar S, Rajadas J, et al. Tissue engineering vascular grafts a fortiori: looking back and going forward. Expert Opinion on Biological Therapy. 2015;15(2):231-44.

239. L'Heureux N, Dusserre N, Konig G, Victor B, Keire P, Wight TN, et al. Human tissue-engineered blood vessels for adult arterial revascularization. Nature Medicine. 2006;12(3):361-5.

240. L'Heureux N, McAllister TN, de la Fuente LM. Tissue-engineered blood vessel for adult arterial revascularization. New England Journal of Medicine. 2007;357(14):1451-3.

241. Benrashid E, McCoy CC, Youngwirth LM, Kim J, Manson RJ, Otto JC, et al. Tissue engineered vascular grafts: Origins, development, and current strategies for clinical application. Methods. 2015;99:13-9.

242. Barnes CP, Sell SA, Boland ED, Simpson DG, Bowlin GL. Nanofiber technology: designing the next generation of tissue engineering scaffolds. Advanced Drug Delivery Reviews. 2007;59(14):1413-33.

243. Nagiah N, Johnson R, Anderson R, Elliott W, Tan W. Highly Compliant Vascular Grafts with Gelatin-Sheathed Coaxially Structured Nanofibers. Langmuir. 2015;31(47):12993-3002.

244. Lee H, Yeo M, Ahn S, Kang DO, Jang CH, Lee H, et al. Designed hybrid scaffolds consisting of polycaprolactone microstrands and electrospun collagen-nanofibers for bone tissue regeneration. Journal of Biomedical Materials Research Part B: Applied Biomaterials. 2011;97(2):263-70.

245. Wu H, Kong J, Yao X, Zhao C, Dong Y, Lu X. Polydopamine-assisted attachment of ß-cyclodextrin on porous electrospun fibers for water purification under highly basic condition. Chemical Engineering Journal. 2015;270:101-9.

246. Correia TR, Antunes BP, Castilho PH, Nunes JC, de Amorim MTP, Escobar IC, et al. A bi-layer electrospun nanofiber membrane for plasmid DNA recovery from fermentation broths. Separation and Purification Technology. 2013;112:20-5.

247. Xu H, Li HY, Chang J. Controlled drug release from a polymer matrix by patterned electrospun nanofibers with controllable hydrophobicity. Journal of Materials Chemistry B. 2013;1(33):4182-8.

248. Bonino CA, Krebs MD, Saquing CD, Jeong SI, Shearer KL, Alsberg E, et al. Electrospinning alginate-based nanofibers: From blends to crosslinked low molecular weight alginate-only systems. Carbohydrate Polymers. 2011;85(1):111-9.

249. Gheibi A, Latifi M, Merati AA, Bagherzadeh R. Piezoelectric electrospun nanofibrous materials for self-powering wearable electronic textiles applications. Journal of Polymer Research. 2014;21(7):1-7.

250. Saetia K, Schnorr JM, Mannarino MM, Kim SY, Rutledge GC, Swager TM, et al. Spray-Layer-by-Layer Carbon Nanotube/Electrospun Fiber Electrodes for Flexible Chemiresistive Sensor Applications. Adv Funct Mater. 2014;24(4):492-502.

251. Zhu Y, Cao Y, Pan J, Liu Y. Macro-alignment of electrospun fibers for vascular tissue engineering. Journal of Biomedical Materials Research Part B: Applied Biomaterials. 2010;92(2):508-16.

252. Huang C, Chen R, Ke Q, Morsi Y, Zhang K, Mo X. Electrospun collagen–chitosan–TPU nanofibrous scaffolds for tissue engineered tubular grafts. Colloids and Surfaces B: Biointerfaces. 2011;82(2):307-15.

253. Merkle VM, Martin D, Hutchinson M, Tran PL, Behrens A, Hossainy S, et al. Hemocompatibility of Poly(vinyl alcohol)–Gelatin Core–Shell Electrospun Nanofibers: A Scaffold for

Modulating Platelet Deposition and Activation. ACS Applied Materials & Interfaces. 2015;7(15):8302-12.

254. Fang J, Zhang J, Du J, Pan Y, Shi J, Peng Y, et al. Orthogonally Functionalizable Polyurethane with Subsequent Modification with Heparin and Endothelium-Inducing Peptide Aiming for Vascular Reconstruction. ACS Applied Materials & Interfaces. 2016.

255. Wise SG, Byrom MJ, Waterhouse A, Bannon PG, Ng MK, Weiss AS. A multilayered synthetic human elastin/polycaprolactone hybrid vascular graft with tailored mechanical properties. Acta Biomaterialia. 2011;7(1):295-303.

256. Soletti L, Nieponice A, Hong Y, Ye SH, Stankus JJ, Wagner WR, et al. In vivo performance of a phospholipid-coated bioerodable elastomeric graft for small-diameter vascular applications. Journal of Biomedical Materials Research Part A. 2011;96(2):436-48.

257. Fu S, Ni P, Wang B, Chu B, Zheng L, Luo F, et al. Injectable and thermo-sensitive PEG-PCL-PEG copolymer/collagen/n-HA hydrogel composite for guided bone regeneration. Biomaterials. 2012;33(19):4801-9.

258. Franco RA, Nguyen TH, Lee B-T. Preparation and characterization of electrospun PCL/PLGA membranes and chitosan/gelatin hydrogels for skin bioengineering applications. Journal of Materials Science: Materials in Medicine. 2011;22(10):2207-18.

259. Bosworth L, Clegg P, Downes S. Electrospun nanofibres of polycaprolactone, and their use for tendon regeneration. International Journal of Nano and Biomaterials. 2008;1(3):263-79.

260. Alves da Silva M, Martins A, Costa-Pinto A, Costa P, Faria S, Gomes M, et al. Cartilage tissue engineering using electrospun PCL nanofiber meshes and MSCs. Biomacromolecules. 2010;11(12):3228-36.

261. Nottelet B, Pektok E, Mandracchia D, Tille JC, Walpoth B, Gurny R, et al. Factorial design optimization and in vivo feasibility of poly (ε-caprolactone)-micro-and nanofiber-based small diameter vascular grafts. Journal of Biomedical Materials Research Part A. 2009;89(4):865-75.

262. de Valence S, Tille J-C, Mugnai D, Mrowczynski W, Gurny R, Möller M, et al. Long term performance of polycaprolactone vascular grafts in a rat abdominal aorta replacement model. Biomaterials. 2012;33(1):38-47.

263. Nannan D, Xue G, Lin Y, Aiying Z, Zengguo F, Lianrui G, et al. A vascular tissue engineering scaffold with core–shell structured nano-fibers formed by coaxial electrospinning and its biocompatibility evaluation. Biomedical Materials. 2016;11(3):035007.

264. Carletti E, Motta A, Migliaresi C. Scaffolds for tissue engineering and 3D cell culture. 3D Cell Culture: Methods and Protocols. 2011:17-39.

265. Chen G, Ushida T, Tateishi T. Scaffold design for tissue engineering. Macromolecular Bioscience. 2002;2(2):67-77.

266. Sabir MI, Xu X, Li L. A review on biodegradable polymeric materials for bone tissue engineering applications. J Mater Sci. 2009;44(21):5713-24.

267. Boland ED, Telemeco TA, Simpson DG, Wnek GE, Bowlin GL. Utilizing acid pretreatment and electrospinning to improve biocompatibility of poly (glycolic acid) for tissue engineering. Journal of Biomedical Materials Research Part B: Applied Biomaterials. 2004;71(1):144-52.

268. Hajiali H, Shahgasempour S, Naimi-Jamal MR, Peirovi H. Electrospun PGA/gelatin nanofibrous scaffolds and their potential application in vascular tissue engineering. International Journal of Nanomedicine. 2011;6:2133-41.

269. Bazile DV, Ropert C, Huve P, Verrecchia T, Marlard M, Frydman A, et al. Body distribution of fully biodegradable [14C]-poly(lactic acid) nanoparticles coated with albumin after parenteral administration to rats. Biomaterials. 1992;13(15):1093-102.

270. Marin E, Briceño MI, Caballero-George C. Critical evaluation of biodegradable polymers used in nanodrugs. International Journal of Nanomedicine. 2013;8:3071-91.

271. Santoro M, Shah SR, Walker JL, Mikos AG. Poly (lactic acid) nanofibrous scaffolds for tissue engineering. Advanced Drug Delivery Reviews. 2016.

272. Yao L, Song Q, Bai W, Zhang J, Miao D, Jiang M, et al. Facilitated brain delivery of poly (ethylene glycol)–poly (lactic acid) nanoparticles by microbubble-enhanced unfocused ultrasound. Biomaterials. 2014;35(10):3384-95.

273. Weijie Z, Zhuo C, Sujuan M, Yonggang W, Fei Z, Keyi W, et al. Cistanche polysaccharide (CDPS)/polylactic acid (PLA) scaffolds based coaxial electrospinning for vascular tissue engineering. International Journal of Polymeric Materials and Polymeric Biomaterials. 2016;65(1):38-46.

274. Rasal RM, Janorkar AV, Hirt DE. Poly(lactic acid) modifications. Progress in Polymer Science. 2010;35(3):338-56.

275. Gugutkov D, Gustavsson J, Cantini M, Salmeron-Sanchez M, Altankov G. Electrospun fibrinogen-PLA nanofibres for vascular tissue engineering. J Tissue Eng Regen Med. 2016.

276. Chen C, Lv G, Pan C, Song M, Wu C, Guo D, et al. Poly(lactic acid) (PLA) based nanocomposites--a novel way of drug-releasing. Biomedical materials (Bristol, England). 2007;2(4):L1-4.

277. Llorens E, Calderon S, del Valle LJ, Puiggali J. Polybiguanide (PHMB) loaded in PLA scaffolds displaying high hydrophobic, biocompatibility and antibacterial properties. Materials science & engineering C, Materials for biological applications. 2015;50:74-84.

278. Wang S, Zhang Y, Wang H, Yin G, Dong Z. Fabrication and properties of the electrospun polylactide/silk fibroin-gelatin composite tubular scaffold. Biomacromolecules. 2009;10(8):2240-4.

279. Makadia HK, Siegel SJ. Poly lactic-co-glycolic acid (PLGA) as biodegradable controlled drug delivery carrier. Polymers. 2011;3(3):1377-97.

280. Houchin M, Topp E. Physical properties of PLGA films during polymer degradation. Journal of Applied Polymer Science. 2009;114(5):2848-54.

281. Jain RA. The manufacturing techniques of various drug loaded biodegradable poly (lactide-co-glycolide)(PLGA) devices. Biomaterials. 2000;21(23):2475-90.

282. Jain R, Shah NH, Malick AW, Rhodes CT. Controlled drug delivery by biodegradable poly (ester) devices: different preparative approaches. Drug Development and Industrial Pharmacy. 1998;24(8):703-27.

283. Prasad S, Cody V, Hanlon D, Edelson R, Saltzman M, Sasaki C, et al. Biopolymer nanoparticles as antigen delivery vehicles for immunotherapy of head and neck squamous cell carcinoma (HNSCC). Clinical Otolaryngology. 2008;33(3):304-.

284. Vorp DA, Maul T, Nieponice A. Molecular aspects of vascular tissue engineering. Frontiers in Bioscience. 2005;10:768-89.

285. Liu K-S, Lee C-H, Wang Y-C, Liu S-J. Sustained release of vancomycin from novel biodegradable nanofiber-loaded vascular prosthetic grafts: in vitro and in vivo study. International Journal of Nanomedicine. 2015;10:885-91.

286. Zhang H, Jia X, Han F, Zhao J, Zhao Y, Fan Y, et al. Dual-delivery of VEGF and PDGF by double-layered electrospun membranes for blood vessel regeneration. Biomaterials. 2013;34(9):2202-12.

287. Hibino N, McGillicuddy E, Matsumura G, Ichihara Y, Naito Y, Breuer C, et al. Late-term results of tissue-engineered vascular grafts in humans. The Journal of Thoracic and Cardiovascular Surgery. 2010;139(2):431-6. e2.

288. McAllister TN, Maruszewski M, Garrido SA, Wystrychowski W, Dusserre N, Marini A, et al. Effectiveness of haemodialysis access with an autologous tissue-engineered vascular graft: a multicentre cohort study. The Lancet. 2009;373(9673):1440-6.

289. Dahl SL, Kypson AP, Lawson JH, Blum JL, Strader JT, Li Y, et al. Readily available tissue-engineered vascular grafts. Science Translational Medicine. 2011;3(68):68ra9-ra9.

290. Wystrychowski W, Cierpka L, Zagalski K, Garrido S, Dusserre N, Radochonski S, et al. Case study: first implantation of a frozen, devitalized tissue-engineered vascular graft for urgent hemodialysis access. The Journal of Vascular Access. 2010;12(1):67-70.

291. Wystrychowski W, McAllister TN, Zagalski K, Dusserre N, Cierpka L, L'Heureux N. First human use of an allogeneic tissue-engineered vascular graft for hemodialysis access. Journal of Vascular Surgery. 2014;60(5):1353-7.

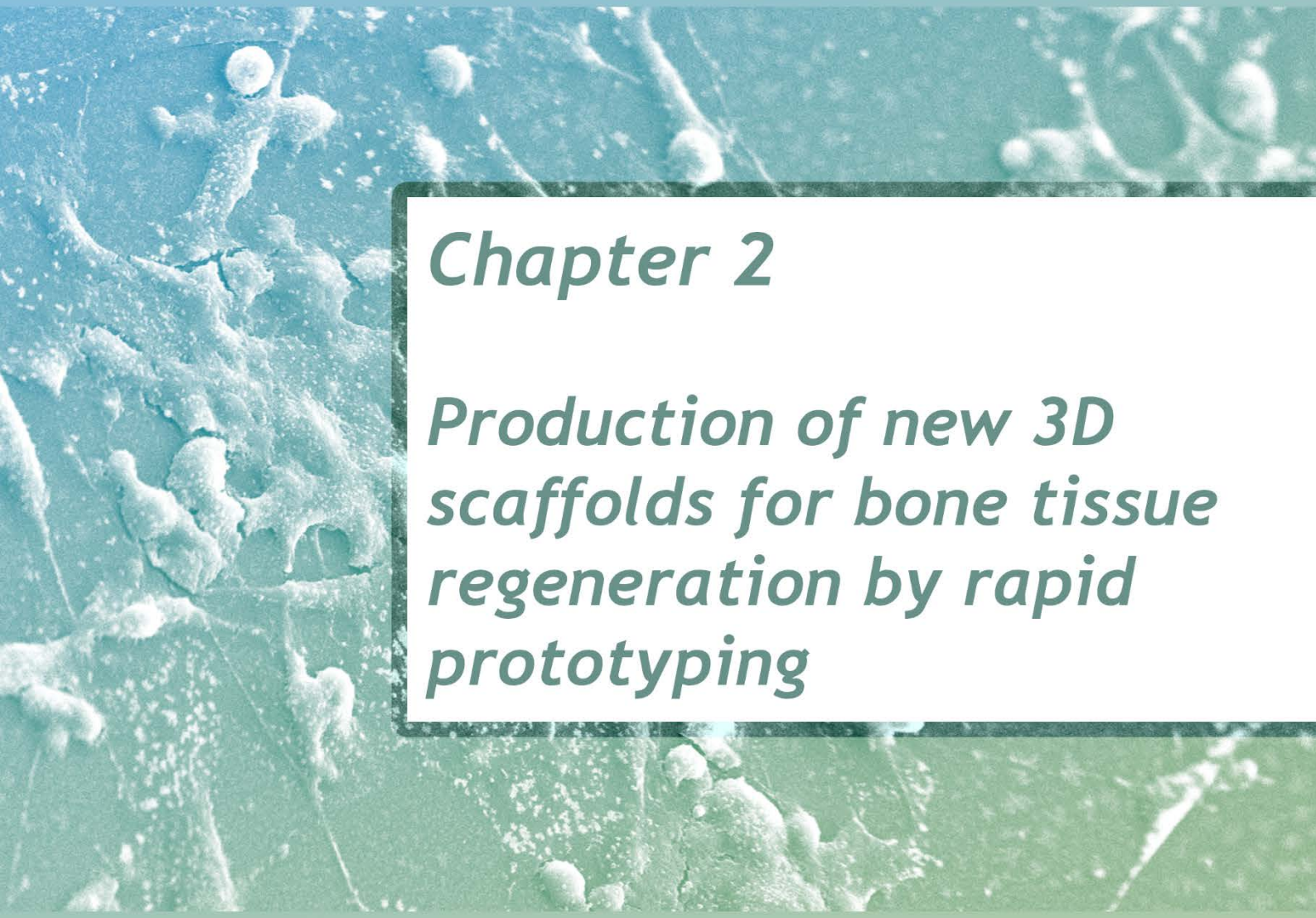

Chapter 2

Production of new 3D scaffolds for bone tissue regeneration by rapid prototyping

Correia, T.R

2. Production of new 3D scaffolds for bone tissue regeneration by rapid prototyping

R. Fradique,[a] T. R. Correia,[a] S. P. Miguel,[a] K.D. de Sá,[a] D.R. Figueira,[a] A.G. Mendonça,[b] and I. J. Correia[a†]

[a]CICS-UBI – Health Sciences Research Centre, University of Beira Interior, Av. Infante D. Henrique, 6200-506 Covilhã, Portugal

[b]Department of Chemistry, University of Beira Interior, R. Marquês d'Ávila e Bolama, 6201-001 Covilhã, Portugal

†Corresponding author; Address: Av. Infante D. Henrique 6200-506 Covilhã, Portugal. Tel. +351 275 329 002/3; Fax: +351 275 329 099. E-mail: icorreia@ubi.pt (Ilídio Correia)

Abstract

The incidence of bone disorders, whether due to trauma or pathology, has been trending upward with the ageing of the worldwide population. The currently available treatments for bone injuries are rather limited, involving mainly bone grafts and implants. A particularly promising approach for bone regeneration uses rapid prototyping (RP) technologies to produce 3D scaffolds with highly controlled structure and orientation, based on computer-aided design models or medical data. Herein, tricalcium phosphate (TCP)/alginate scaffolds were produced using RP and subsequently their physicochemical, mechanical and biological properties were characterized. The results showed that 60/40 of TCP and alginate formulation was able to match the compression and present a similar Young modulus to that of trabecular bone while presenting an adequate biocompatibility. Moreover, the biomineralization ability, roughness and macro and microporosity of scaffolds allowed cell anchoring and proliferation at their surface, as well as cell migration to its interior, processes that are fundamental for osteointegration and bone regeneration.

2.1. Introduction

Apart from traumatic events, the ageing of the worldwide population has led to an increased prevalence of bone tissue diseases, with up to 2.2 million people needing surgery every year.(1) The currently available treatments for bone defects involve the use of bone grafts, particularly autografts, which present serious restrictions such as limited availability, induction of chronic pain and the inability to promote the complete recovery of the patient. To overcome this healthcare problem, a huge effort has been made on the topic of bone tissue engineering in order to create new therapeutic approaches.(2) Artificial bone implants produced from metals, ceramics, polymers and composites have been widely used in bone reconstruction and regeneration.(3-10) Three dimensional (3D) structures, known as scaffolds, constitute one example of these artificial implants and have been produced with materials such as hydroxyapatite (HAp), tricalcium phosphate (TCP), poly(lactic-co-glycolic acid) (PLGA) or sodium alginate. Furthermore, scaffolds surfaces can be modified (surface coating, chemical treatment and polymerization) to improve bone healing(11), with some types of scaffolds being used for cell and growth factor delivery to the damaged tissues, while providing mechanical support during the tissue regeneration process.(12)

Nowadays, the development of a bone substitute involves the optimization of several parameters, such as biocompatibility, manufacturing simplicity, mechanical requirements, osteoconductivity, osteoinductivity and, depending on the type of implant to be produced (permanent or temporary), its degradation rate, that in some cases must be synchronized with the rate of tissue regeneration.(2, 12-17)

Several techniques have been described in literature as being suitable for producing bone replacements. Fiber bonding(18, 19), freeze drying(20, 21), melting(22, 23), phase inversion(24, 25) and solvent casting(26, 27) are the most employed techniques for scaffolds production. However, some of them present several disadvantages, such as the use of toxic solvents, inability to create large structures with appropriate mechanical properties, absence of pore size control and a limited number of usable materials.(28)

The latest advances in the area of computer technology allowed the development of rapid prototyping (RP) techniques that recently started to be used in the design of new 3D constructs aimed to be applied in the area of tissue engineering.(29, 30) So far, computer assisted design (CAD) models supported the manufacturing of highly reproducible 3D scaffolds.(31) To accomplish that, the 3D CAD models are replicated in a layer-by-layer routine, allowing scaffolds to be printed with different conformations and geometries, that may contribute for a significant improvement of scaffold's mechanical properties according to the demands of the damaged bone.(32) As an alternative, other researchers adapted a different strategy based on data collected from

routine medical examinations, where the produced scaffolds were specifically tailored, i.e. produced with high anatomic accuracy, to fulfil the particular demands of the injured bone tissue.(33-35) Santos *et al.* used a 3D printer (Zprinter 310 Plus) to produce scaffolds that replicated the computer tomography data of a human hand.(35)

Recently, our group used a Fab@Home plotter to produce TCP/Alginate scaffolds with high accuracy, that were previously designed with CAD software.(36) This procedure was adopted taking into account the plotter's cost, versatility and capacity to replicate CAD models with control and reproducibility, in a short period of time.(36, 37)

In this study, alginate and TCP were selected to reproduce the organic and inorganic components of the native bone matrix. TCP was used to mimic the mineral phase of the bone, due to its composition, high biocompatibility, bioactivity, great compressive strength, osteoconductivity(2, 38, 39), and also by presenting an *in vivo* bio-resorption rate that fulfils bone regeneration demands.(14, 38, 40) However, as other ceramics, it possesses a brittle behavior. To overcome this bottleneck, two strategies were selected to improve the mechanical properties of the scaffolds: various ratios of TCP/alginate were used and scaffolds with different geometries were designed using CAD software.

Alginate is a natural polysaccharide derived from brown seaweeds composed of 1,4-linked D-mannuronic acid (M) and α-L-guluronic acid (G) residues(41-43), and is known by its ability to form stable hydrogels when ionically crosslinked with divalent cations (e.g. Ca^{2+},$Sr^{2+}$and Ba^{2+}).(41, 44) In previous studies it has already been described the successful application of alginate in bone regeneration, either alone or in combination with other polymers and ceramics.(36, 45-48)

2.2. Materials and methods

2.2.1. Materials

Amphotericin B, bovine serum albumin (BSA), cacodylate buffer (MW=214.03g/mol), calcein, calcium chloride, Dulbecco's modified Eagle medium: nutrient mixture F12 (DMEM-F12), ethylenediaminetetraacetic acid (EDTA), gentamicin, glutaraldehyde 25% (v/v), L-glutamine, sodium alginate (MW=120kDa to 190kDa), trypan blue and trypsin were purchased from Sigma-Aldrich (Sintra, Portugal). Tricalcium phosphate (TCP) powder (MW=310.20g/mol) was obtained from Panreac® (Barcelona, Spain). 3-(4,5-dimethylthiazol-2-yl)-5-(3-carboxymethoxyphenyl)-2-(4-sulfophenyl)-2H tetrazolium reagent, inner salt (MTS) was bought from Promega (Madison, USA). Fetal bovine serum (FBS) was purchased from Biochrom AG (Berlin, Germany). Human osteoblast cells (406-05f) were obtained from Cell Applications, Inc. (San Diego, CA). 24 and 96-well plates were acquired from Orange Scientific (Braine L'Alleud, Belgium). Tris Base was obtained from Fischer Scientific (Lisbon, Portugal). Hoechst 33342® was acquired from Invitrogen (Carlsbad, CA).

2.2.2. Production of TCP/alginate composite scaffolds by RP

The 3D scaffolds were produced by RP using a Fab@Home plotter, as previously described.(36) TCP/alginate scaffolds were produced using prepared solutions of each compound in a proportion of 60/40 % (w/w), 70/30 % (w/w) and 80/20 % (w/w). Briefly, a 15% (w/v) alginate solution was prepared by dissolving the polymer in double deionized and filtered water (obtained using a Milli-Q Advantage A10 ultrapure Water Purification System; resistivity=18.2MΩ/cm at 25°C), with overnight agitation. The solution was then homogenized using an X10/25 Ultra-turrax (Ystral, Germany) for 30min. Finally, TCP powder was added to the alginate solutions to obtain the specific ratios described above, and subsequently the samples were homogenized. Then, a 5% $CaCl_2$ solution was added to the composite sample, (in a 0.14:1 volume ratio of $CaCl_2$ to alginate), and alginate polymer chains got crosslinked leading to an increase of the solution's viscosity that is fundamental for scaffolds production.(36) The used 3D model was designed using CAD/CAM software (OpenSCAD version 2014.3, ©2009-2014 Marius Kintel and Clifford Wolf). The developed 3D model was composed of several layers angled at 45° with the underlying layer (0°—45°—90°—135°), as shown in Figure 2.1. Briefly, the file containing the scaffold model was converted and exported to STL format. Following, a syringe (10cc Luer Lock) was filled with the composite solution for posterior extrusion. After the extrusion process, the scaffolds were maintained in a 5% $CaCl_2$ bath for 24h to achieve

a complete crosslinking. Afterwards, the scaffolds were air-dried at RT and subsequently freeze-dried for 24h.

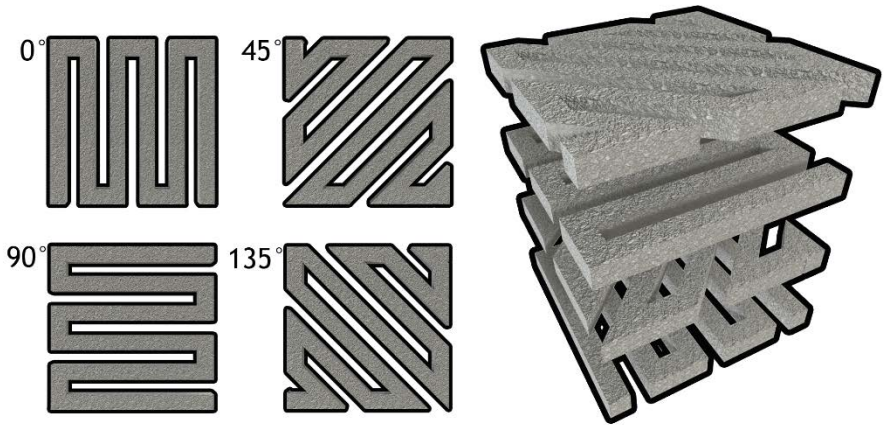

Figure 2.1 Schematic overview of the layered structure of the model.

2.2.3. Scanning Electron Microscopy analysis

Scanning Electron Microscopy (SEM) analysis of the scaffolds was performed in order to characterize the morphology, porosity and surface of the scaffolds. Samples were mounted onto aluminum stubs with Araldite glue and sputter-coated with gold using a Quorum Q150R ES sputter coater (Quorum Technologies, UK). The SEM images were then captured with different magnifications, at an acceleration voltage of 20kV, using a Hitachi S-3400N Scanning Electron Microscope (Hitachi, Japan).

2.2.4. Attenuated Total Reflectance - Fourier Transform Infrared Spectroscopy analysis

To characterize the chemical composition of the scaffolds, Attenuated Total Reflectance-Fourier Transform Infrared Spectroscopy (ATR-FTIR) was used. The spectra obtained for the samples represent the average of 128 scans, between 400 and 4000 cm^{-1}, with a spectral resolution of 4 cm^{-1}. All the samples were crushed to a powder, mounted on a diamond window, and the spectra were recorded with a Nicolet iS10 FTIR spectrophotometer (Thermo Scientific, Waltham, MA, USA). All the components used for scaffold production were also analyzed in pure state for a comparison to be made with the prepared samples (49).

2.2.5. Energy Dispersive Spectroscopic analysis

Energy Dispersive Spectroscopy (EDS) was used for the elemental composition analysis of the various scaffolds. The samples were placed on aluminum stubs, air-dried at RT and examined in an XFlash Detector 5010 (Bruker Nano, Germany).

2.2.6. Mechanical characterization of the scaffolds

Compression assays were performed in order to evaluate the mechanical behavior of the scaffolds. The scaffold's dimensions were noted and introduced into a Zwick® 1435 Material Prüfung (Ulm, Germany). The assays were performed using a crosshead speed of 3mm/min and a load cell of 5kN. Five specimens of each sample were used for each assay.

The compressive strength (C_s) of each scaffold was calculated according to Equation (1).(50)

$$Cs = \frac{F}{w \times l} \qquad (1)$$

Where *F* is the load at the time of fracture, and *w* and *l* represent the width and length of the scaffold, respectively.

The Young Modulus (YM) of each scaffold was calculated from the stress-strain relation, calculated by applying Equation (2).

$$YM = \frac{C_s}{H_d} \qquad (2)$$

Where H_d stands for the height deformation at maximum load and C_s is the scaffold compressive strength. Average values and standard deviations (S.D.) were determined for each sample.

2.2.7. Swelling studies

The swelling capacity of the scaffolds was determined following a method adapted from previously published work.(44) In brief, samples were immersed in Tris buffer (1M, pH=7.4), at 37°C, for 2 days (n=3). After absorbing the excess of Tris with filter paper, scaffolds were removed from the solution at predetermined intervals and weighed.

Following this process, the samples were re-immersed in the swelling solution. The swelling ratio of the scaffolds was evaluated using Equation (3).

Where W_t is the final weight of the scaffolds and W_0 their initial weight.

$$Swelling\ ratio\ (\%) = \frac{W_t - W_0}{W_0} \times 100 \quad (3)$$

2.2.8. Contact Angle Measurements

Contact angle measurements were performed using a OCAH 200 Contact Angle System (DataPhysics Instruments, Germany), operated in static mode at RT. This assay was performed using water as reference fluid.(36) For each sample, water drops were placed at various locations of the surface of the scaffold. The reported contact angles are the average of at least three measurements.

2.2.9. Evaluation of the porosity of the scaffolds

To determine the microporosity of the different scaffolds a liquid displacement method was used, according to the procedure previously reported.(50) In brief, scaffolds were weighed, immersed in absolute ethanol (EtOH) for 48h, and weighed again. EtOH was chosen for its ability to penetrate throughout the scaffolds without causing shrinking or swelling of the matrix(51). The porosity was then calculated by determining the amount of EtOH absorbed, through Equation (4):

$$Porosity\,(\%) = \frac{W_w - W_d}{D_{ethanol} \times V_{scaffold}} \times 100 \quad (4)$$

Where W_w and W_d are the wet and dry weights of the scaffolds, respectively, $D_{ethanol}$ represents the density of EtOH at RT and $V_{scaffold}$ the volume of the wet scaffold. Five replicates of each scaffold were used, and the data represents the average values obtained.

2.2.10. Characterization of the degradation profile of the scaffolds

The degradation profile of the composite scaffolds was investigated through a method previously published. (52, 53) In brief, scaffolds were placed in 24-well plates,

fully immersed in DMEM-F12 at 37°C. At predetermined intervals, samples were removed, completely dried and weighted. The degradation percentage at each point was calculated through equation (5):

$$Weight\ loss\,(\%) = (1 - \frac{W_i - W_t}{W_i}) \times 100 \quad (5)$$

Where *Wi* corresponds to the initial weight of the sample and *Wt* to the weight of the sample at time t.

2.2.11. *In vitro* Biomineralization Assay

The *in vitro* bioactivity of each scaffold was evaluated by submerging them in standard simulated body fluid (SBF), followed by incubation at 37°C for 7, 14, and 21 days, according to a method previously described in literature.(54) The SBF solution had a similar ionic concentration to that found in human blood plasma (142.0 mM Na^+, 5 mM K^+, 1.5 mM Mg^{2+}, 2.5 mM Ca^{2+}, 147.8 mM Cl^-, 4.2 mM HCO_3^-, 1.0 mM HPO_4^{2-}, and 0.5 mM SO_4^{2-}), and a pH of 7.4 at 37°C.(55) Three scaffolds of equal weight and shape were used. After the designated time, the scaffolds were removed and rinsed three times with deionised water to remove soluble inorganic ions. The deposition of calcium and phosphate ions on the composite surface was characterized by EDS.

2.2.12. Characterization of the biological properties of the scaffolds

2.2.12.1. Evaluation of cell viability and proliferation in the presence of the scaffolds

Human osteoblasts cells (hOB) were cultured in DMEM-F12, supplemented with 10% heat inactivated FBS, amphotericin B (100µg/mL) and gentamicin (100µg/mL) in 75 cm^2 T-flasks. Cells were maintained in a humidified environment at 37°C, with 5% CO_2, until confluence was attained. Subsequently, cells were trypsinized with 0.18% trypsin (1:250) and 5mM EDTA, and centrifuged for 5min. Prior to cell seeding, scaffolds were cut into pieces with appropriate sizes and placed into 96-well plates to be sterilized by UV irradiation for 30min. Following, cells were seeded at a density of $10x10^3$ cells per well, in order to evaluate cell viability and proliferation. The culture medium was replaced every two days until the end of the assay.

To evaluate the cytotoxic character of the 3D scaffolds, an MTS assay was performed at day 4 and 7.(36) The metabolic activity of the cells was assessed by quantifying the metabolic conversion of MTS to formazan. Briefly, the medium in each well was replaced with a mixture of 100µL of fresh culture medium and 20µL of MTS/phenazine methosulfate (PMS) reagent solution, and then the plate was incubated for 4h at 37°C. Following the incubation period, the supernatant was transferred into a 96-well microplate and the fluorescence intensity measured at 492nm, using a microplate reader (Anthos 2020, Biochrom, UK). Five replicates of each sample were used for each experimental condition. Cells cultured without materials were used as negative control (K^-) and cells cultured with EtOH (70%) were used as positive control (K^+).

2.2.12.2. Scanning Electron Microscopy analysis

In order to evaluate the cellular behavior in the presence of the scaffolds, SEM analysis was performed according to the method previously described by Lee and Chow.(56) Briefly, the samples were washed at RT with sodium cacodylate buffer solution (0.1M, pH = 7.4), and then fixed for 30min in a 2.5% (v/v) glutaraldehyde in 0.1M sodium cacodylate solution. Subsequently, samples were frozen in liquid nitrogen for 2min and then freeze-dried for 2h. SEM analysis was performed as described in section 2.3.

2.2.12.3. Confocal Laser Scanning Microscopy analysis

Confocal laser scanning microscopy (CLSM) was used to characterize the cell distribution within the 60/40 scaffold. This formulation was selected based on the results obtained herein. hOB nucleus were labelled with Hoescht 33342 (5µg/mL) and seeded in the presence of the scaffolds ($10x10^3$ cells/scaffold), in µ-Slide 8-well Ibidi imaging plates (Ibidi GmbH, Germany). After 24h, the scaffold was labelled with calcein (20µg/mL) and confocal images were acquired. Imaging experiments were performed in a Zeiss LSM 710 laser scanning confocal microscope (Carl Zeiss AG, Germany), where consecutive z-stacks were acquired. The 3D reconstruction and image analysis were performed using Zeiss Zen 2010 software.(36)

2.2.12.4. Statistical Analysis

One-way analysis of variance (ANOVA), with the Newman-Keuls post hoc test was used for comparison of the different test groups. A *p* value lower than 0.05 ($p<0.05$) was considered statistically significant. Data analysis was performed in GraphPad Prism v.6.0 software (Trial version, GraphPadSoftware, CA, USA).

2.3. Results and Discussion

2.3.2. Morphological characterization of the produced scaffolds

Different approaches have been used in the area of regenerative medicine to answer the limitations of the currently available therapeutics. Among them, RP technologies have proven to be a precious tool in every stage of development, greatly improving the design decision process and the scaffold's mechanical properties.

In this work, composite scaffolds composed of TCP and alginate were produced by RP, to mimic the natural bone matrix properties (20-30% organic, 70-80% inorganic).(14, 17) To do so, an optimization of the scaffold's production parameters was done. Figure 2.2 presents the CAD model used, as well as one of the scaffolds printed by RP. The designed model is a 13mm x 13mm x 13mm cube, with a porous structure. As described, it is composed by layers rotated 45° in relation to the underlying layer (0°—45°—90°—135°), in order to increase its mechanical resistance.

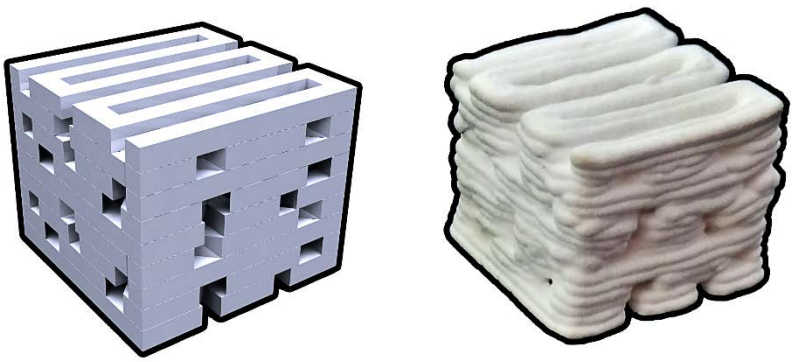

Figure 2.2 Images of the CAD model used (left) and of the final printed model (right).

Alginate was selected for scaffolds production due to its capacity to act as temporary extracellular matrix (ECM) for bone cells. In addition, the possibility of controlling the degradation rate of this polymer is of great importance for tailoring the properties of the scaffold.(41, 42) On the other hand, TCP was chosen due to its resemblance with the natural ceramic component of bone tissue, increased

biocompatibility, low cost, osteoconductivity and enhanced mechanical resistance.(2, 38, 39) Furthermore, the combination of these materials has already been shown to improve cell adhesion and proliferation, with the potential to allow cell growth and differentiation before implantation.(36, 57) Macroscopic images of the produced scaffolds are presented in Figure 2.3.

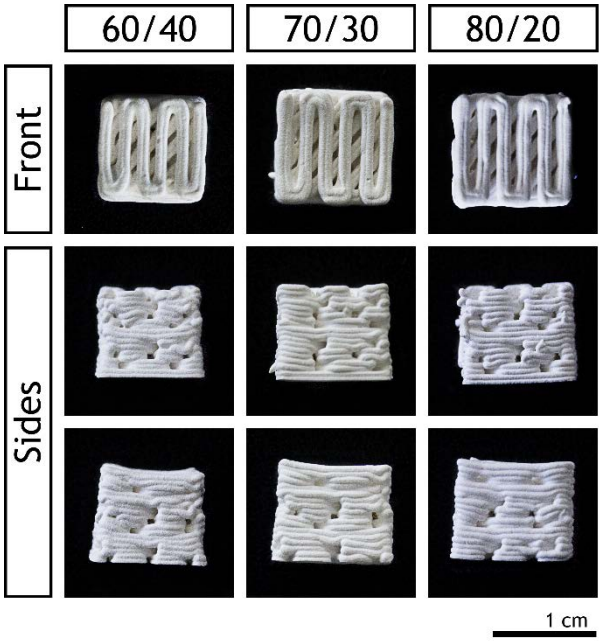

Figure 2.3 Representative macroscopic images of the different produced scaffolds.

Through the analysis of the images shown in Figure 2.3 it is possible to observe that the TCP content had a direct effect on the scaffold's structure, namely on the scaffold's dimensions, decreasing the shrinking endured. It was previously described that alginate gels and scaffolds suffer shrinkage during the drying process.(58) Other researchers have also reported that the presence of solid fillers, such as ceramic particles, in an alginate solution has a direct effect on the volume loss during the drying process.(59) It was noticed that the compression of the polymeric matrix leads to the compression of the TCP particles against each other. Herein, it was verified that the scaffolds containing the highest percentage of TCP suffered less shrinkage, since the amount of incompressible ceramic particles limits the shrinking that scaffolds can suffer. This is important, since an excess shrinking can greatly affect the scaffold's porosity and its mechanical properties.

Furthermore, the scaffolds surface morphology has a great effect on cell adhesion and, consequently, on the successful material implantation. Figure 2.4 shows SEM images acquired to characterize the surface morphology of the produced scaffolds.

Through the analysis of Figure 2.4 it is possible to verify that all the scaffolds presented similar surface characteristics, with high roughness and irregularities. It has

been previously described that the surface roughness of a scaffold has a great effect on protein adsorption and cell adhesion, upon scaffold implantation.(60, 61) On irregular surfaces, human osteoblasts present increased metabolism and ECM production, due to an increased contact surface available for promoting adhesion contact points.(6)

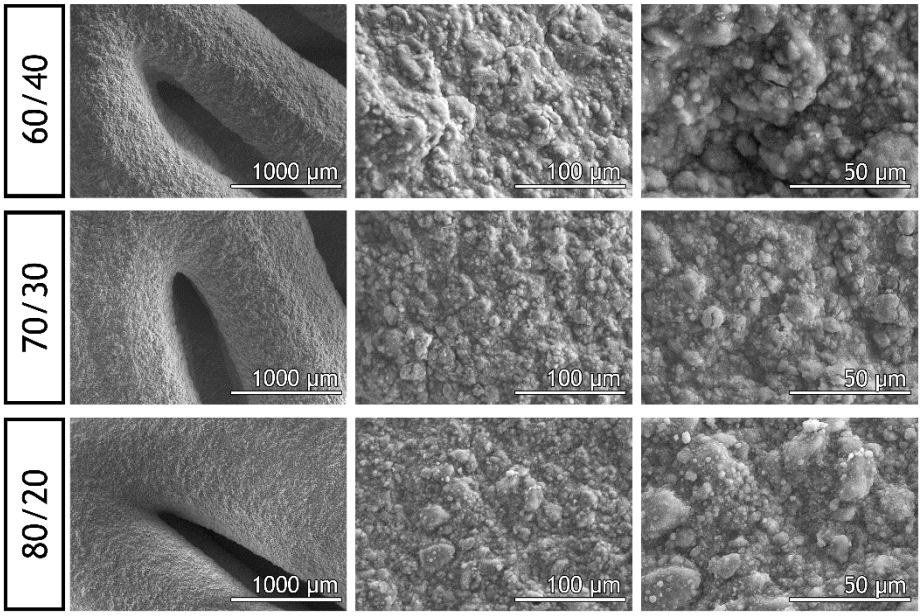

Figure 2.4. SEM images showing the morphology of the different produced scaffolds at different magnifications.

2.3.3. Characterization of the physicochemical properties of the scaffolds

2.3.3.1. ATR-FTIR analysis

An ATR-FTIR analysis was performed to evaluate the chemical composition of the scaffolds. The ATR-FTIR spectra of the raw materials and of the produced scaffolds are presented in Figure 2.5.

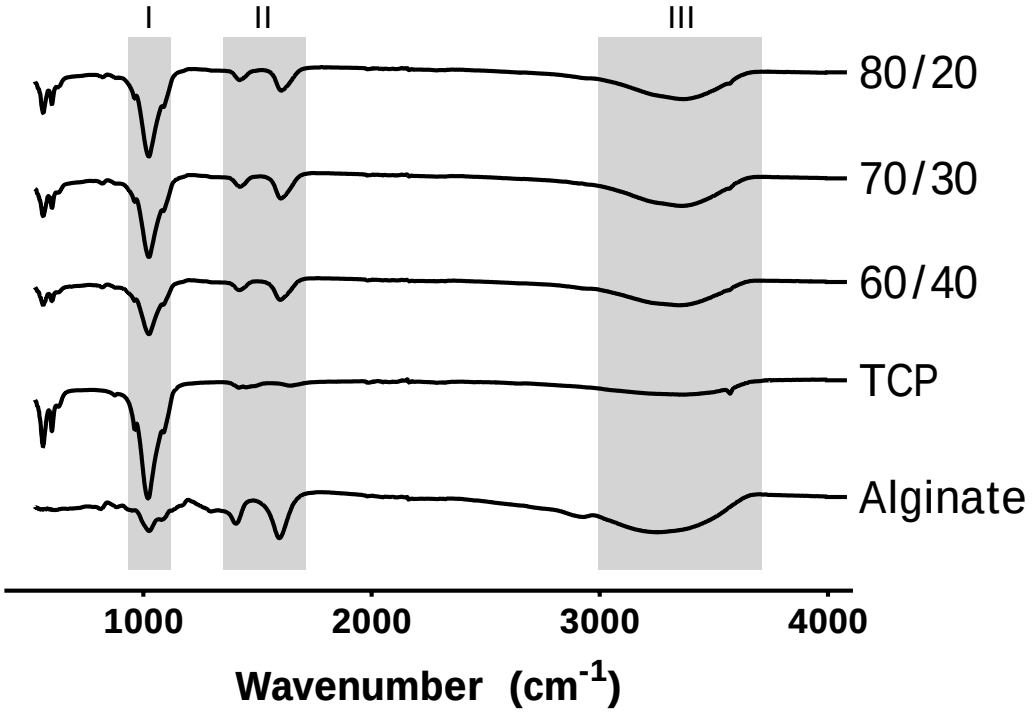

Figure 2.5 ATR-FTIR analysis of the alginate, TCP and TCP/alginate scaffolds (80/20, 70/30, and 60/40).

The ATR-FTIR spectrum of TCP presents a peak at 1020 cm^{-1} (I), that is characteristic of a P=O stretch vibration, thus revealing the presence of the inorganic phosphate components of TCP.(35) This peak is also present on the spectra of the produced scaffolds, with an intensity that is proportional to the ceramic content present in each sample. The ATR-FTIR spectrum of sodium alginate powder presented two peaks at 1400 and 1600 cm^{-1} (II), corresponding to the C=O stretching of the carboxylate group.(62) In addition, a stretching vibration correspondent to the O-H bonds of alginate appeared in the range 3000-3600 cm^{-1} (III).(63) These peaks were also present in the spectra of the different scaffolds, without perceptible variations among them.

2.3.3.2. Energy Dispersive Spectroscopy analysis

The elemental composition of the scaffolds was also characterized through EDS analysis, to elucidate the chemical composition of the scaffolds. Table 2.1 shows that samples with a higher amount of ceramic component have a greater percentage of phosphate and calcium. Such results are in agreement with the expectations, since these are the main components of TCP. In addition, the Ca/P ratios of the produced scaffolds are within the range described for native trabecular bone (2.33 ± 0.34).(64)

Table 2.1 EDS analysis of the produced TCP/alginate scaffolds (60/40, 70/30 and 80/20) and the Ca/P ratios determined for the produced scaffolds.

Elements / Sample	P (*at. %)	Ca (at. %)	Ca/P Ratio
60/40	2.89	8.48	2.93
70/30	4.35	9.42	2.17
80/20	4.71	10.28	2.18

*at.%- Atomic percentage.

2.3.3.3. Characterization of the mechanical properties of the scaffolds

A scaffold to be used in bone tissue regeneration must present adequate resistance and flexibility. The mechanical behavior of the produced scaffolds was analyzed by determining the resistance to compression and the Young's modulus (Figure 2.6).

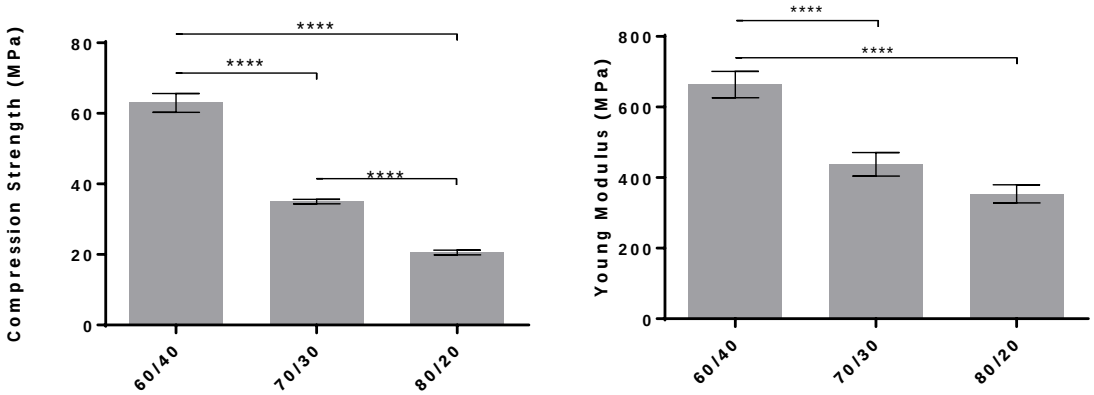

Figure 2.6 Characterization of the compressive strength (left) and young modulus (right) of the scaffolds. Statistical analysis of the results was performed using one-way ANOVA with Newman-Keuls post hoc test (**** $p \leq 0.0001$).

Previous studies described that 3D constructs with an increased ceramic content have an increased brittleness and, consequently, a lower mechanical resistance.(65, 66) The high TCP content of the 70/30 and 80/20 scaffolds produced here led to an increased brittleness and fragility, characteristic of pure ceramic scaffolds.(66) Furthermore, in a biphasic solution, the polymeric component (alginate in this case) creates a bone like structure by trapping the ceramic particles.(67) The comparison of the results obtained

here with those of bone demonstrated that the produced scaffolds have a compressive strength higher than that of trabecular bone (0.5 – 15 MPa). The 60/40 sample showed a compressive strength of 60 MPa and the 80/20 a value of 20 MPa. Furthermore, the 60/40 scaffolds showed a value for this property that is half of that displayed by the cortical bone (100—200 MPa). Such results show that this type of scaffolds have the required mechanical properties to be applied in non-load bearing sites. A large mismatch of the elastic modulus of the implant and that of the native bone tissue can cause stress shielding, and consequently, limited scaffold osteointegration.(68) In this context, the Young Modulus of the three specimens was also investigated, showing that the scaffolds with lowest ceramic content presented the highest modulus (663 MPa) , although all of them had a Young Modulus superior to that of cancellous bone (100—200 MPa(15)).

Therefore, taking into account these results the 60/40 scaffolds are the best candidates to be applied in bone regeneration, since they closely reproduce the native bone matrix composition, mimicking the fine balance of strength and elasticity present in trabecular bone tissue.

2.3.3.4. Swelling studies

The swelling capacity of a scaffold can have a deep impact on its biocompatibility and biologic performance. In fact, scaffolds with an increased capacity to absorb water promote protein adsorption and cell adhesion, leading to a reduced immune response from the host.(69) The swelling profiles obtained for the produced scaffolds are presented in Figure 2.7a. All scaffolds presented a rapid swelling in the first minutes and then stabilized after about 10h of immersion in Tris buffer (1M, pH = 7.4).

Valente *et al*. have already reported that a polymeric network composed of alginate is capable of absorbing large quantities of water by filling its void regions.(44) This effect was also confirmed in this study, where the scaffolds containing higher amounts of alginate presented a higher swelling ratio.

2.3.3.5. Contact angle analysis

In order to evaluate the hydrophilic character of the scaffolds, the contact angles were determined, as represented in Figure 2.7b. It is possible to observe that all the scaffolds presented a hydrophilic character, with contact angles below 70°. The 60/40 scaffolds showed a moderated hydrophilic character (≈50°) while the 70/30 and 80/20 presented an almost superhydrophilic character (≈20°). Hu et al. previously reported a direct correlation between the increase in the TCP content of the scaffolds and its hydrophilic character.(70) Scaffolds with moderate wettability improve cell attachment

and growth, since their surfaces have preferential adsorption of cell-adhesive proteins.(70, 71)

2.3.3.6. Scaffolds porosity evaluation

The microporosity of the scaffolds was determined by a liquid displacement method, using ethanol as displacement fluid. Figure 2.7c shows that the scaffolds with highest TCP content presented the highest porosity values (> 10% porosity). During the drying process the scaffolds suffer shrinking, which is responsible for the compression of the polymeric matrix. In this stage, the scaffolds with high ceramic content present more incompressible particles, thus limiting the amount of shrinkage that they can suffer, and consequently displaying an increased porosity.(35, 36)

These results corroborate the mechanical resistance data obtained. Porosity and density are inversely proportional, and are closely related to the mechanical resistance of a scaffold.(72) Therefore, the most resistant scaffolds are the denser, as can be observed in Figure 2.7c.

The porosity values obtained for the produced scaffolds are more similar to that of compact bone (3%), than those displayed by trabecular bone (80%).(73) However, this lack of microporosity is balanced by a regular and sufficient macroporosity, as can be observed in Figure 2.4. This macroporosity allows tissue ingrowth and osteointegration, and also facilitates the exchange of nutrients and metabolites from the interior of the s11caffolds.

2.3.3.7. Characterization of the degradation profile of the scaffolds

The degradation rate of the scaffolds should be compatible with the duration of new bone formation, in order for the scaffold to be replaced during the regeneration process without affecting the mechanical stability of the tissue at the injured site.(74)

The degradation profile of the produced scaffolds is presented in Figure 2.7d. The results obtained showed that the scaffolds present a degradation profile dependent on its relative alginate content, with those containing a higher percentage of the polymer enduring a greater loss of mass. Under *in vivo* conditions, alginate depolymerizes by spontaneous alkaline elimination of its glycosidic linkages. Moreover, this polymer can also suffer disintegration by gradual exchange of calcium ions with sodium, reversing the gelling process.(41) On the other hand, TCP can suffer cell-mediated degradation when implanted *in vivo,* being solubilized while new tissue formation occurs.(75)

Nonetheless, none of the scaffolds produced here lost more than 60% of its mass, and all of them stabilized after 4 days, which is compatible with their application in bone tissue regeneration.

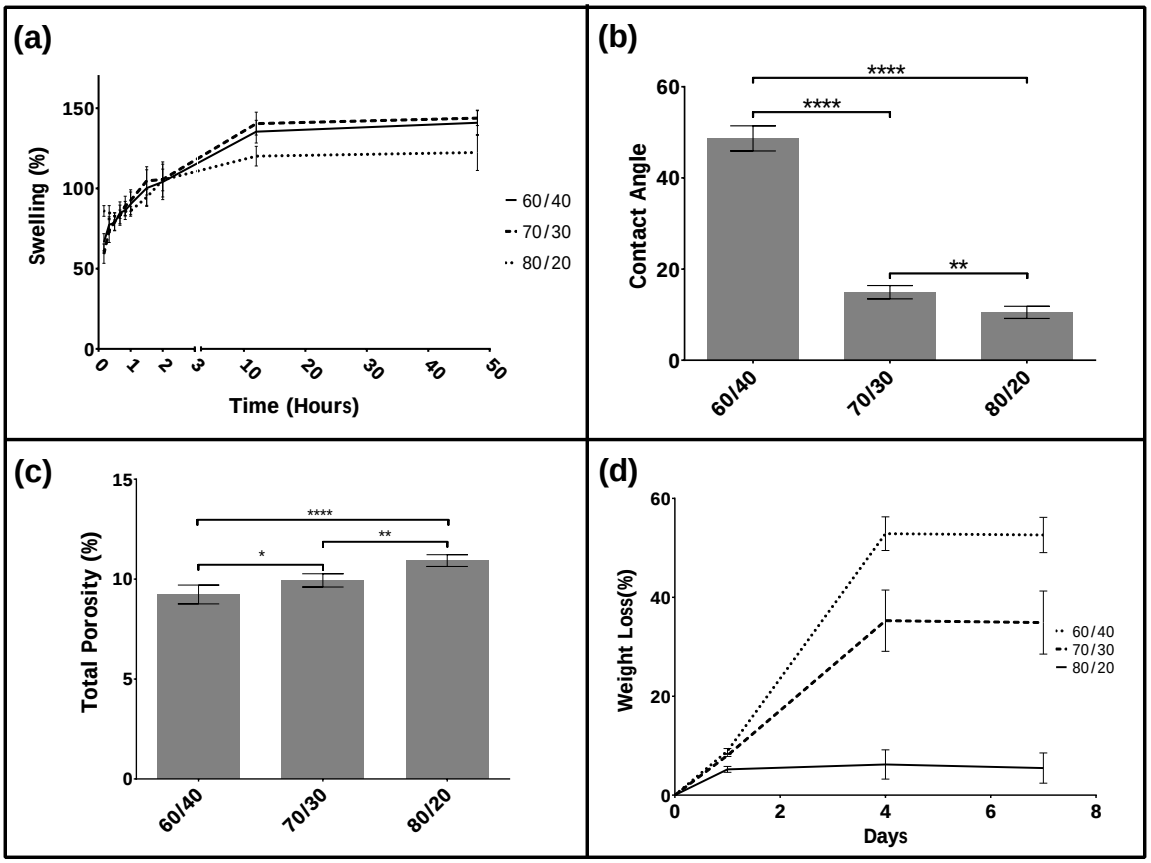

Figure 2.7 Characterization of the swelling profile of the scaffolds (a); Contact angle of the different produced scaffolds (b); Statistical analysis of the results was performed using one-way ANOVA with a Newman–Keuls test (** p≤ 0.01, **** p ≤ 0.0001); Scaffold's microporosity (c); Statistical analysis of the data was performed using one-way ANOVA with a Newman–Keuls test (∗ p≤ 0.05, ** p≤ 0.01, **** p≤ 0.0001, n = 5); and degradation profile of the scaffolds (d).

2.3.4. In vitro Biomineralization Assay

The *in vitro* mineralization ability of the composite scaffolds was studied using an SBF assay (Figure 2.8). The obtained results revealed that calcium and phosphate content of the scaffolds increased along time. In addition, this increase was more pronounced for the formulations with higher TCP content. As previously described, TCP is a bioactive ceramic capable of inducing mineralization at the surface of the scaffolds, increasing their biointegration(54, 76), and consequently the bone regeneration process.(76)

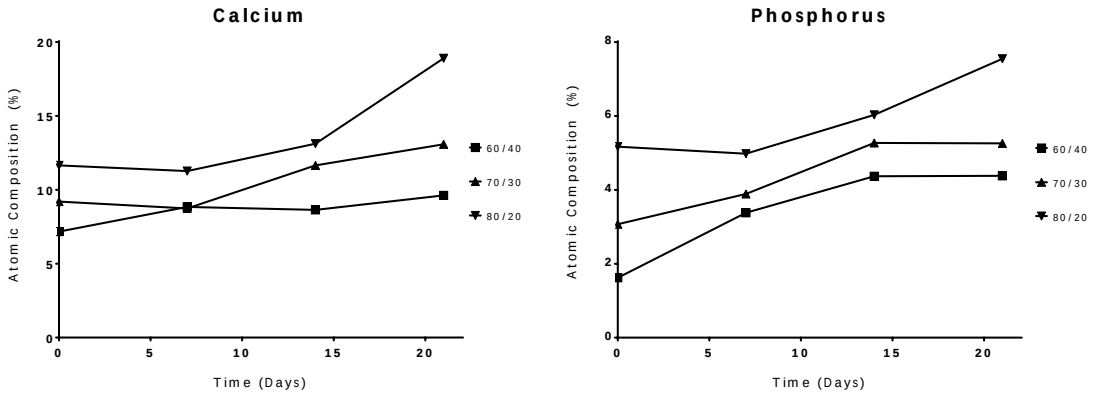

Figure 2.8 EDS analysis of the different scaffolds after 7, 14 and 21 days in SBF.

2.3.5. Characterization of the biological properties of the scaffolds

In vitro studies were performed to study the cytotoxic profile of the scaffolds. Human osteoblast cells were cultured in contact with the scaffolds for up to 7 days, and their viability assessed at days 4 and 7. The optical images acquired at the mentioned time points demonstrated that cells were able to proliferate in the presence of the composite scaffolds (please see Figure 2.9 for further details) and in the negative control. In the positive control, dead cells with their characteristic spherical shape were observed. To further characterize the cellular adhesion on the surface of the scaffolds, SEM images were also acquired (Figure 2.10a).

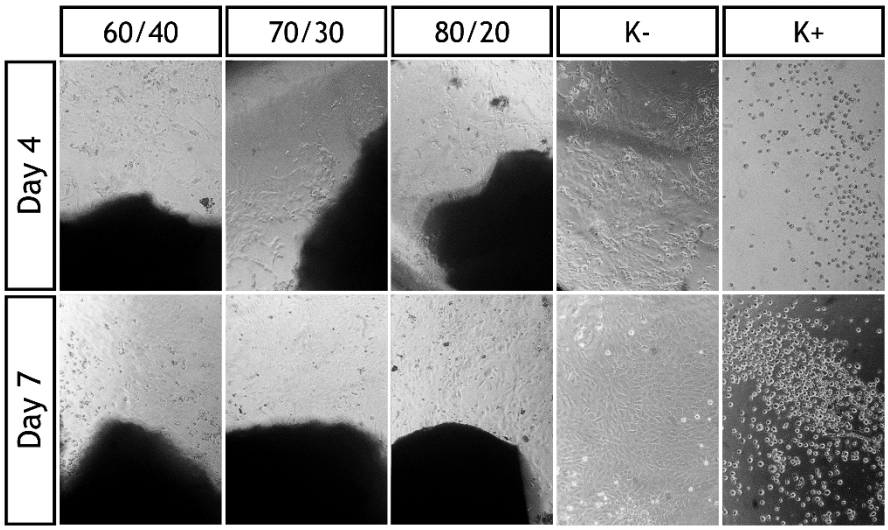

Figure 2.9 Optical images of human osteoblast cells seeded in the presence of the different materials after 4 and 7 days of incubation at a magnification of 100×.

As previously demonstrated, scaffolds showed a surface with high roughness, irregularities and a hydrophilic character that allowed cell adhesion. In fact, it is possible to observe that the cells were able to adhere to the surface of the material after 24h of being seeded. Moreover, after 7 days, most cells had spread throughout the entire surface of the scaffold, and a cell layer was observed, demonstrating that all the scaffolds presented a suitable surface for cell adhesion and proliferation.

The biocompatibility of the scaffolds was further evaluated through an MTS assay (Figure 2.10b). The results obtained in the MTS assay show that the cells remained viable after 4 and 7 days in the presence of all the produced scaffolds, indicating that all scaffolds provide an appropriate environment for cell adhesion and proliferation. The 60/40 formulation presented the highest cellular viability, which may be explained by their increased alginate content.(44, 47) Moreover, this formulation is the one that better reproduce the bone native constitution, further enhancing cell proliferation. These results can also be attributed to the osteogenic potential of TCP, which creates a layer that is similar to apatite on the surface of the material, due to its interaction with the surrounding medium.(77)

CLSM analysis was performed 24h after osteoblasts being seeded in contact with the 60/40 scaffold (Figure 2.10c). This formulation was selected based on the previously achieved results. A 3D reconstruction image is presented in Figures 2.10c_1 and c_2, showing that the osteoblasts were able to adhere and proliferate in the tested formulation. Such highlights its biocompatibility and suitable physicochemical properties. Moreover, the analysis of the orthogonal slices (Figure 2.10c_3) and colour coded depth analysis (Figure 2.10c_4) of 60/40 scaffold showed that osteoblasts migrate to the interior of the scaffold, with some cells being observed between 5 and 20µm within the structure of the scaffold. This cellular colonization of the structure will eventually allow the filling of the bone defect with new bone matrix, while the scaffold is biodegraded, thus leading to the restoring of the structure and functions of the native tissue.

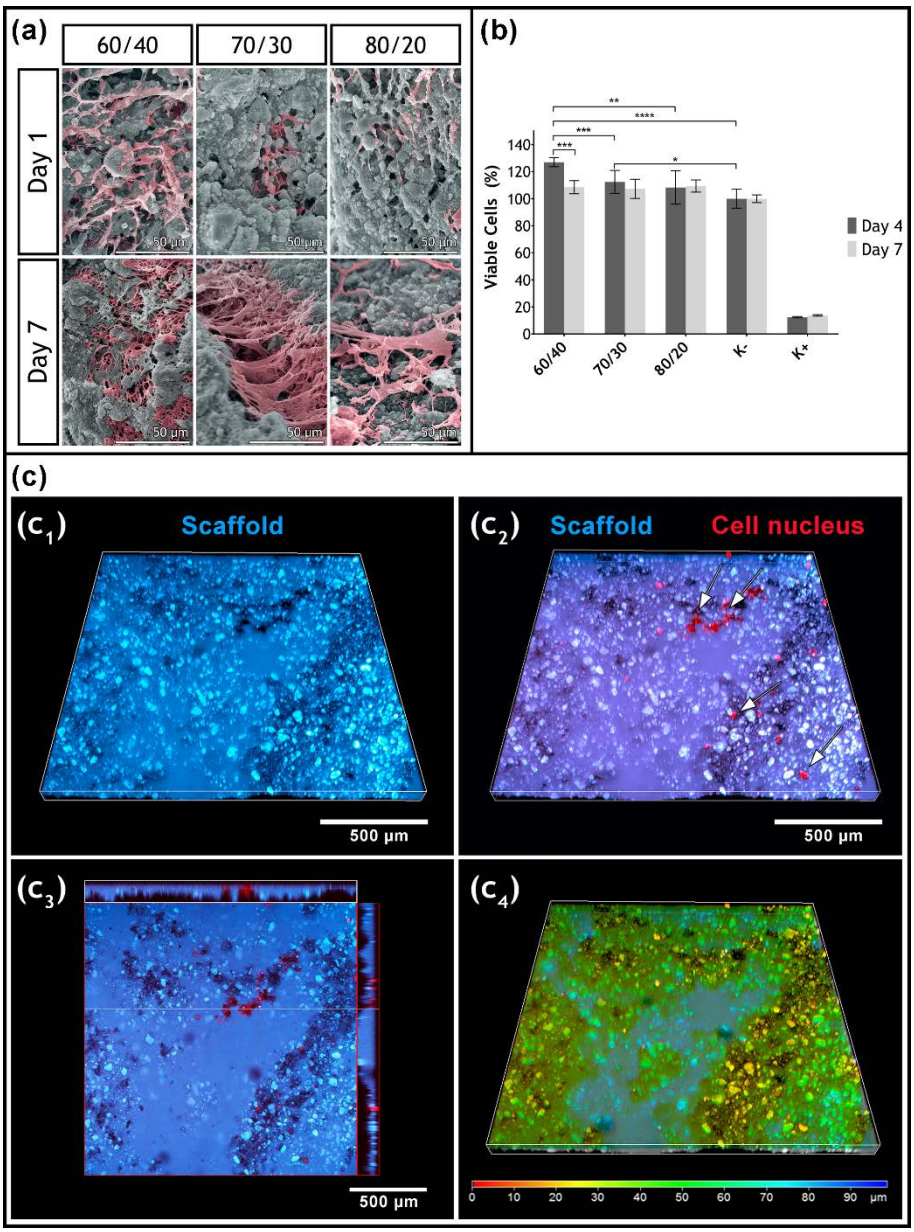

Figure 2.10. Characterization of the biological properties of the scaffolds. (a) SEM images of hOB in the presence of the scaffolds; (b) Evaluation of hOB viability when cultured in contact with the different scaffolds after 4 and 7 days; live cells (K-); dead cells (K+). Each result is the mean ± standard deviation of the mean of at least three independent experiments. Statistical analysis was performed using one-way ANOVA with Newman-Keuls post hoc test (* $p<0.05$, ** $p\leq 0.01$, *** $p\leq 0.001$, **** $p\leq 0.0001$); (c) 3D reconstruction images (c1 and c2), orthogonal projections (c3), and colour coded depth analysis (c4) of cells in contact with the 60/40 TCP/alginate scaffold (red= 0 µm, blue=90µm). Arrows show the presence of cells.

2.4. Conclusion

The huge demand of new therapeutic approaches for bone regeneration triggered the development of different studies. Herein, scaffolds with different ratios of TCP and alginate were successfully produced using a Fab@Home. Besides optimizing the ratios of TCP/alginate for scaffolds manufacture, authors also used CAD software to further improve the mechanical characteristics of the 3D constructs. The compression and young modulus of the different produced scaffolds were characterized and those with 60/40 of TCP and alginate were selected as the best formulation. The results obtained revealed that the properties of these scaffolds surpassed the standard values for compression and young modulus of the trabecular bone. In addition, the hydrophilic character of the produced scaffolds was also investigated. The 60/40 formulation showed a moderately hydrophilic character (≈50°) while the others presented a superhydrophilic character (≈20°). The moderately hydrophilic behaviour presented by the 60/40 structures allows protein adhesion at the surface of the materials, which is essential for cell adhesion and proliferation. Moreover, the biomineralization ability, roughness and macro and microporosity of scaffolds also contributed for cell anchoring and proliferation at their surface, as well as cell migration to its interior. These processes are fundamental for osteointegration and bone regeneration. Furthermore, the application of RP technologies for the production of the scaffolds can provide a great contribution to personalized therapy, since CAD tools can be used to design 3D structures that fulfil patient requirements and contribute to decrease the healing time. Encapsulation of cells and bioactive molecules in the produced scaffolds can also be hypothesized in a future of work, since no hazard agent is used during the scaffolds manufacture.

2.5. References

1. Giannoudis PV, Dinopoulos H, Tsiridis E. Bone substitutes: an update. Injury. 2005;36 Suppl 3:S20-7.

2. O'Brien FJ. Biomaterials & scaffolds for tissue engineering. Materials Today. 2011;14(3):88-95.

3. Bobe K, Willbold E, Morgenthal I, Andersen O, Studnitzky T, Nellesen J, et al. In vitro and in vivo evaluation of biodegradable, open-porous scaffolds made of sintered magnesium W4 short fibres. Acta Biomaterialia. 2013;9(10):8611-23.

4. Rai R, Keshavarz T, Roether JA, Boccaccini AR, Roy I. Medium chain length polyhydroxyalkanoates, promising new biomedical materials for the future. Materials Science and Engineering R: Reports. 2011;72(3):29-47.

5. He J, Huang T, Gan L, Zhou Z, Jiang B, Wu Y, et al. Collagen-infiltrated porous hydroxyapatite coating and its osteogenic properties: In vitro and in vivo study. Journal of Biomedical Materials Research - Part A. 2012;100 A(7):1706-15.

6. Chiara G, Letizia F, Lorenzo F, Edoardo S, Diego S, Stefano S, et al. Nanostructured Biomaterials for Tissue Engineered Bone Tissue Reconstruction. International Journal of Molecular Sciences. 2012;13(1):737-57.

7. Xie M, Olderøy MO, Zhang Z, Andreassen JP, Strand BL, Sikorski P. Biocomposites prepared by alkaline phosphatase mediated mineralization of alginate microbeads. RSC Advances. 2012;2(4):1457-65.

8. Wu S, Liu X, Yeung KWK, Hu T, Xu Z, Chung JCY, et al. Hydrogen release from titanium hydride in foaming of orthopedic NiTi scaffolds. Acta Biomaterialia. 2011;7(3):1387-97.

9. Alvarez K, Nakajima H. Metallic Scaffolds for Bone Regeneration. Materials. 2009;2(3):790-832.

10. Li Z, Gu X, Lou S, Zheng Y. The development of binary Mg-Ca alloys for use as biodegradable materials within bone. Biomaterials. 2008;29(10):1329-44.

11. Wu S, Liu X, Yeung KW, Liu C, Yang X. Biomimetic porous scaffolds for bone tissue engineering. Materials Science and Engineering: R: Reports. 2014;80:1-36.

12. Malda J, Visser J, Melchels FP, Jüngst T, Hennink WE, Dhert WJA, et al. 25th Anniversary Article: Engineering Hydrogels for Biofabrication. Advanced Materials. 2013;25(36):5011-28.

13. Frohlich M, Grayson W, Wan L, Marolt D, Drobnic M, Vunjak- Novakovic G. Tissue Engineered Bone Grafts: Biological Requirements, Tissue Culture and Clinical Relevance. Current Stem Cell Research & Therapy. 2008;3(4):254-64.

14. Gaalen Sv, Kruyt M, Meijer G, Mistry A, Mikos A, Beucken Jvd, et al. Chapter 19 - Tissue engineering of bone. In: Blitterswijk Cv, Thomsen P, Lindahl A, Hubbell J, Williams DF, Cancedda R, et al., editors. Tissue engineering. Burlington: Academic Press; 2008. p. 559-610.

15. Bose S, Roy M, Bandyopadhyay A. Recent advances in bone tissue engineering scaffolds. Trends in Biotechnology. 2012;30(10):546-54.

16. Ma PX. Biomimetic materials for tissue engineering. Advanced Drug Delivery Reviews. 2008;60(2):184-98.

17. Kneser U, Schaefer DJ, Polykandriotis E, Horch RE. Tissue engineering of bone: the reconstructive surgeon's point of view. Journal of Cellular and Molecular Medicine. 2006;10(1):7-19.

18. Mikos AG, Bao Y, Cima LG, Ingber DE, Vacanti JP, Langer R. Preparation of poly(glycolic acid) bonded fiber structures for cell attachment and transplantation. Journal of Biomedical Materials Research. 1993;27(2):183-9.

19. Tuzlakoglu K, Bolgen N, Salgado AJ, Gomes ME, Piskin E, Reis RL. Nano- and micro-fiber combined scaffolds: a new architecture for bone tissue engineering. Journal of materials science Materials in medicine. 2005;16(12):1099-104.

20. Deville S, Saiz E, Tomsia AP. Freeze casting of hydroxyapatite scaffolds for bone tissue engineering. Biomaterials. 2006;27(32):5480-9.

21. Kim H-W, Knowles JC, Kim H-E. Hydroxyapatite and gelatin composite foams processed via novel freeze-drying and crosslinking for use as temporary hard tissue scaffolds. Journal of Biomedical Materials Research Part A. 2005;72A(2):136-45.

22. Gomes ME, Ribeiro AS, Malafaya PB, Reis RL, Cunha AM. A new approach based on injection moulding to produce biodegradable starch-based polymeric scaffolds: morphology, mechanical and degradation behaviour. Biomaterials. 2001;22(9):883-9.

23. Mondrinos MJ, Dembzynski R, Lu L, Byrapogu VKC, Wootton DM, Lelkes PI, et al. Porogen-based solid freeform fabrication of polycaprolactone–calcium phosphate scaffolds for tissue engineering. Biomaterials. 2006;27(25):4399-408.

24. Duarte ARC, Mano JF, Reis RL. Dexamethasone-loaded scaffolds prepared by supercritical-assisted phase inversion. Acta Biomaterialia. 2009;5(6):2054-62.

25. Tsivintzelis I, Pavlidou E, Panayiotou C. Porous scaffolds prepared by phase inversion using supercritical CO2 as antisolvent: I. Poly(l-lactic acid). The Journal of Supercritical Fluids. 2007;40(2):317-22.

26. Suh SW, Shin JY, Kim J, Kim J, Beak CH, Kim DI, et al. Effect of different particles on cell proliferation in polymer scaffolds using a solvent-casting and particulate leaching technique. ASAIO journal (American Society for Artificial Internal Organs : 1992). 2002;48(5):460-4.

27. Sin D, Miao X, Liu G, Wei F, Chadwick G, Yan C, et al. Polyurethane (PU) scaffolds prepared by solvent casting/particulate leaching (SCPL) combined with centrifugation. Materials Science and Engineering: C. 2010;30(1):78-85.

28. Salgado AJ, Coutinho OP, Reis RL. Bone Tissue Engineering: State of the Art and Future Trends. Macromolecular Bioscience. 2004;4(8):743-65.

29. Daniel LC, Jeffrey IL, Lawrence JB, Hod L. Additive manufacturing for in situ repair of osteochondral defects. Biofabrication. 2010;2(3):035004.

30. Malone E, Lipson H. Fab@Home: the personal desktop fabricator kit. Rapid Prototyping Journal. 2007;13(4):245-55.

31. Fedorovich NE, Schuurman W, Wijnberg HM, Prins H-J, van Weeren PR, Malda J, et al. Biofabrication of Osteochondral Tissue Equivalents by Printing Topologically Defined, Cell-Laden Hydrogel Scaffolds. Tissue Engineering Part C: Methods. 2011;18(1):33-44.

32. Shaffer S, Yang K, Vargas J, Di Prima MA, Voit W. On reducing anisotropy in 3D printed polymers via ionizing radiation. Polymer. 2014;55(23):5969–79.

33. Martínez-Vázquez FJ, Perera FH, Miranda P, Pajares A, Guiberteau F. Improving the compressive strength of bioceramic robocast scaffolds by polymer infiltration. Acta Biomaterialia. 2010;6(11):4361-8.

34. Hockaday LA, Kang KH, Colangelo NW, Cheung PYC, Duan B, Malone E, et al. Rapid 3D printing of anatomically accurate and mechanically heterogeneous aortic valve hydrogel scaffolds. Biofabrication. 2012;4(3):035005.

35. Santos CFL, Silva AP, Lopes L, Pires I, Correia IJ. Design and production of sintered ß-tricalcium phosphate 3D scaffolds for bone tissue regeneration. Materials Science and Engineering: C. 2012;32(5):1293-8.

36. Diogo GS, Gaspar VM, Serra IR, Fradique R, Correia IJ. Manufacture of ß-TCP/alginate scaffolds through a Fab@home model for application in bone tissue engineering. Biofabrication. 2014;6(2):025001.

37. Kang KH, Hockaday LA, Butcher JT. Quantitative optimization of solid freeform deposition of aqueous hydrogels. Biofabrication. 2013;5(3):035001.

38. Rezwan K, Chen QZ, Blaker JJ, Boccaccini AR. Biodegradable and bioactive porous polymer/inorganic composite scaffolds for bone tissue engineering. Biomaterials. 2006;27(18):3413-31.

39. Schieker M, Seitz H, Drosse I, Seitz S, Mutschler W. Biomaterials as Scaffold for Bone Tissue Engineering. European Journal of Trauma. 2006;32(2):114-24.

40. Choi D, Kumta PN. Mechano-chemical synthesis and characterization of nanostructured ß-TCP powder. Materials Science and Engineering: C. 2007;27(3):377-81.

41. Andersen T, Strand BL, Formo K, Alsberg E, Christensen BE. Chapter 9 Alginates as biomaterials in tissue engineering. Carbohydrate Chemistry: Volume 37. 37: The Royal Society of Chemistry; 2012. p. 227-58.

42. Augst AD, Kong HJ, Mooney DJ. Alginate Hydrogels as Biomaterials. Macromolecular Bioscience. 2006;6(8):623-33.

43. Bonino CA, Krebs MD, Saquing CD, Jeong SI, Shearer KL, Alsberg E, et al. Electrospinning alginate-based nanofibers: From blends to crosslinked low molecular weight alginate-only systems. Carbohydrate Polymers. 2011;85(1):111-9.

44. Valente JFA, Valente TAM, Alves P, Ferreira P, Silva A, Correia IJ. Alginate based scaffolds for bone tissue engineering. Materials Science and Engineering: C. 2012;32(8):2596-603.

45. Lima AC, Batista P, Valente TA, Silva AS, Correia IJ, Mano JF. Novel methodology based on biomimetic superhydrophobic substrates to immobilize cells and proteins in hydrogel spheres for applications in bone regeneration. Tissue Engineering Part A. 2013;19(9-10):1175-87.

46. Valente J, Valente T, Alves P, Ferreira P, Silva A, Correia I. Alginate based scaffolds for bone tissue engineering. Materials Science and Engineering: C. 2012;32(8):2596-603.

47. Li Z, Ramay HR, Hauch KD, Xiao D, Zhang M. Chitosan–alginate hybrid scaffolds for bone tissue engineering. Biomaterials. 2005;26(18):3919-28.

48. Lin H-R, Yeh Y-J. Porous alginate/hydroxyapatite composite scaffolds for bone tissue engineering: Preparation, characterization, and in vitro studies. Journal of Biomedical Materials Research Part B: Applied Biomaterials. 2004;71B(1):52-65.

49. Yang F, Xia S, Tan C, Zhang X. Preparation and evaluation of chitosan-calcium-gellan gum beads for controlled release of protein. European Food Research and Technology. 2013;237(4):467-79.

50. Torres AL, Gaspar VM, Serra IR, Diogo GS, Fradique R, Silva AP, et al. Bioactive polymeric–ceramic hybrid 3D scaffold for application in bone tissue regeneration. Materials Science and Engineering: C. 2013;33(7):4460-9.

51. Jiankang H, Dichen L, Yaxiong L, Bo Y, Bingheng L, Qin L. Fabrication and characterization of chitosan/gelatin porous scaffolds with predefined internal microstructures. Polymer. 2007;48(15):4578-88.

52. Jeong SI, Jeon O, Krebs MD, Hill MC, Alsberg E. Biodegradable photo-crosslinked alginate nanofibre scaffolds with tuneable physical properties, cell adhesivity and growth factor release. European cells & materials. 2012;24:331-43.

53. Freed LE, Vunjak-Novakovic G, Biron RJ, Eagles DB, Lesnoy DC, Barlow SK, et al. Biodegradable Polymer Scaffolds for Tissue Engineering. Nature Biotechnology. 1994;12(7):689-93.

54. Kokubo T, Takadama H. How useful is SBF in predicting in vivo bone bioactivity? Biomaterials. 2006;27(15):2907-15.

55. Jalota S, Bhaduri SB, Tas AC. Using a synthetic body fluid (SBF) solution of 27 mM HCO3− to make bone substitutes more osteointegrative. Materials Science and Engineering: C. 2008;28(1):129-40.

56. Lee JTY, Chow KL. SEM sample preparation for cells on 3D scaffolds by freeze-drying and HMDS. Scanning. 2012;34(1):12-25.

57. Lawson MA, Barralet JE, Wang L, Shelton RM, Triffitt JT. Adhesion and growth of bone marrow stromal cells on modified alginate hydrogels. Tissue engineering. 2004;10(9-10):1480-91.

58. Dittrich R, Tomandl G, Despang F, Bernhardt A, Hanke T, Pompe W, et al. Scaffolds for Hard Tissue Engineering by Ionotropic Gelation of Alginate–Influence of Selected Preparation Parameters. Journal of the American Ceramic Society. 2007;90(6):1703-8.

59. Rassis DK, Saguy IS, Nussinovitch A. Collapse, shrinkage and structural changes in dried alginate gels containing fillers. Food Hydrocolloids. 2002;16(2):139-51.

60. Deligianni DD, Katsala ND, Koutsoukos PG, Missirlis YF. Effect of surface roughness of hydroxyapatite on human bone marrow cell adhesion, proliferation, differentiation and detachment strength. Biomaterials. 2000;22(1):87-96.

61. Rechendorff K, Hovgaard MB, Foss M, Zhdanov VP, Besenbacher F. Enhancement of Protein Adsorption Induced by Surface Roughness. Langmuir. 2006;22(26):10885-8.

62. Lawrie G, Keen I, Drew B, Chandler-Temple A, Rintoul L, Fredericks P, et al. Interactions between Alginate and Chitosan Biopolymers Characterized Using FTIR and XPS. Biomacromolecules. 2007;8(8):2533-41.

63. Daemi H, Barikani M. Synthesis and characterization of calcium alginate nanoparticles, sodium homopolymannuronate salt and its calcium nanoparticles. Scientia Iranica. 2012;19(6):2023-8.

64. Tzaphlidou M, Zaichick V. Calcium, Phosphorus, calcium-phosphorus ratio in rib bone of healthy humans. Biological Trace Element Research. 2003;93(1-3):63-74.

65. Mansur HS, Costa HS. Nanostructured poly(vinyl alcohol)/bioactive glass and poly(vinyl alcohol)/chitosan/bioactive glass hybrid scaffolds for biomedical applications. Chemical Engineering Journal. 2008;137(1):72-83.

66. Wei G, Ma PX. Structure and properties of nano-hydroxyapatite/polymer composite scaffolds for bone tissue engineering. Biomaterials. 2004;25(19):4749-57.

67. Román J, Cabañas MV, Peña J, Doadrio JC, Vallet-Regí M. An optimized ß-tricalcium phosphate and agarose scaffold fabrication technique. Journal of Biomedical Materials Research Part A. 2008;84A(1):99-107.

68. Shi L, Shi L, Wang L, Duan Y, Lei W, Wang Z, et al. The Improved Biological Performance of a Novel Low Elastic Modulus Implant. PLoS ONE. 2013;8(2):e55015.

69. Tam SK, Dusseault J, Bilodeau S, Langlois G, Hallé J-P, Yahia LH. Factors influencing alginate gel biocompatibility. Journal of Biomedical Materials Research Part A. 2011;98A(1):40-52.

70. Hu Y, Wang J, Xing W, Cao L, Liu C. Surface-modified pliable PDLLA/PCL/ß-TCP scaffolds as a promising delivery system for bone regeneration. Journal of Applied Polymer Science. 2014;131(20):n/a-n/a.

71. Dowling DP, Miller IS, Ardhaoui M, Gallagher WM. Effect of surface wettability and topography on the adhesion of osteosarcoma cells on plasma-modified polystyrene. Journal of biomaterials applications. 2011;26(3):327-47.

72. Karageorgiou V, Kaplan D. Porosity of 3D biomaterial scaffolds and osteogenesis. Biomaterials. 2005;26(27):5474-91.

73. Renders GAP, Mulder L, Van Ruijven LJ, Van Eijden TMGJ. Porosity of human mandibular condylar bone. Journal of Anatomy. 2007;210(3):239-48.

74. Dumas JE, Prieto EM, Zienkiewicz KJ, Guda T, Wenke JC, Bible J, et al. Balancing the rates of new bone formation and polymer degradation enhances healing of weight-bearing allograft/polyurethane composites in rabbit femoral defects. Tissue Engineering Part A. 2014;20(1-2):115-29.

75. Kamitakahara M, Ohtsuki C, Miyazaki T. Review paper: behavior of ceramic biomaterials derived from tricalcium phosphate in physiological condition. Journal of biomaterials applications. 2008;23(3):197-212.

76. Franco J, Hunger P, Launey ME, Tomsia AP, Saiz E. Direct write assembly of calcium phosphate scaffolds using a water-based hydrogel. Acta Biomaterialia. 2010;6(1):218-28.

77. Yin Y, Ye F, Cui J, Zhang F, Li X, Yao K. Preparation and characterization of macroporous chitosan–gelatin/ß-tricalcium phosphate composite scaffolds for bone tissue engineering. Journal of Biomedical Materials Research Part A. 2003;67A(3):844-55.

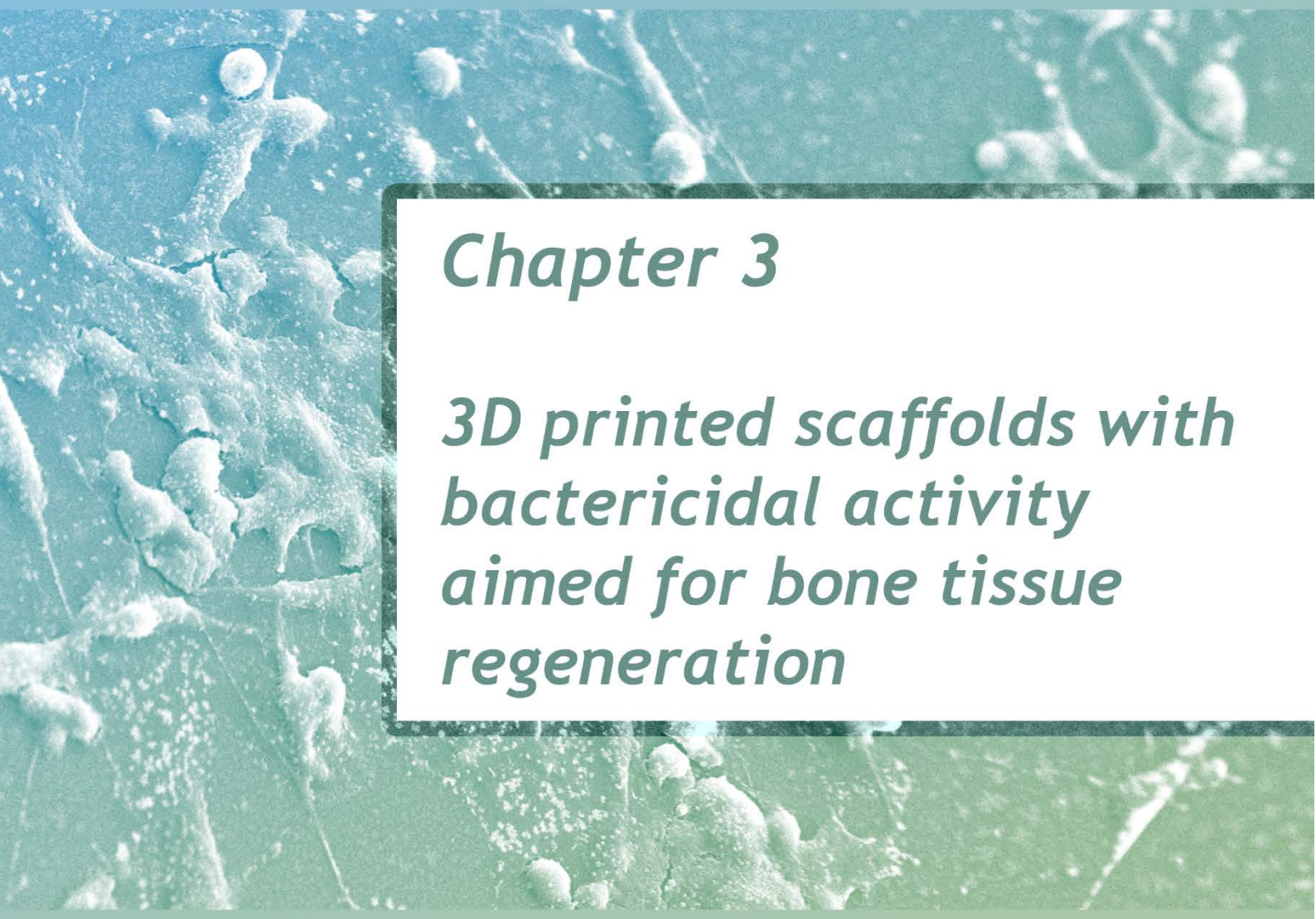

Chapter 3

3D printed scaffolds with bactericidal activity aimed for bone tissue regeneration

Correia, T.R

3. 3D printed scaffolds with bactericidal activity aimed for bone tissue regeneration

Tiago R. Correia[1], Daniela R. Figueira[1], Kevin D. de Sá[1], Sónia P. Miguel[1], Ricardo G. Fradique[1], António G. Mendonça[1,2] and Ilídio J. Correia[1,*]

[1] CICS-UBI – Centro de Investigação em Ciências da Saúde, Universidade da Beira Interior, Av. Infante D. Henrique, 6200-506 Covilhã, Portugal

[2] Departamento de Química, Universidade da Beira Interior, R. Marquês d'Ávila e Bolama, 6201-001 Covilhã, Portugal

* Corresponding author: icorreia@ubi.pt; Tel.: +351 275 329 002/3; Fax: +351 275 329 099

Abstract

Nowadays, the incidence of bone disorders has steeply ascended and it is expected to double in the next decade, especially due to the ageing of the worldwide population. Bone defects and fractures lead to reduced patient's quality of life. Autografts, allografts and xenografts have been used to overcome different types of bone injuries, although limited availability, immune rejection or implant failure demand the development of new bone replacements. Moreover, the bacterial colonization of bone substitutes is the main cause of implant rejection. To vanquish these drawbacks, researchers from tissue engineering area are currently using computer-aided design models or medical data to produce 3D scaffolds by Rapid Prototyping (RP). Herein, Tricalcium phosphate (TCP)/ Sodium Alginate (SA) scaffolds were produced using RP and subsequently functionalized with silver nanoparticles (AgNPs) through two different incorporation methods. The obtained results revealed that the composite scaffolds produced by direct incorporation of AgNPs are the most suitable for being used in bone tissue regeneration since they present appropriate mechanical properties, biocompatibility and bactericidal activity.

3.1. Introduction

Every year, fractures and bone diseases affect millions of people worldwide, especially the elderly population (1). To treat such illnesses, clinicians mainly use auto- and allografts to repair/restore bone critical defects (2). However, such procedures are unable to surpass limitations like donor site morbidity (in the case of autografts) or the risk of immunological rejection when allografts are used (3). In order to overcome such issues, synthetic scaffolds emerge as viable alternative in the field of tissue engineering.

Nowadays, new composite systems combining advantages of natural and synthetic biomaterials arise as viable options to fulfil the demand of new implants in the area of bone regeneration. Collagen nanofibers combined with polycaprolactone (PCL) microstrands is one example of such type of scaffolds. They assure good cell adhesion (through the aminoacid sequences available on collagen), and mechanical support, conferred principally by PCL (4). Similarly, the blending of chitosan, gelatin and ß-tricalcium phosphate was previously performed to produce 3D structures with appropriate mechanical properties, porosity and bioactivity, that are able to allow cell ingrowth and new bone tissue formation (5).

In the last years, several techniques and technologies, such as electrospinning, gas foaming or self-assembly have been used for scaffolds production. Electrospinning technique is used to reproduce the composition and structural features of natural bone extracellular matrix. Nanofibrous hydroxyapatite/chitosan scaffolds were seeded with bone mesenchymal stem cells (6). Gas foaming technique, which involves the application of gases like carbon dioxide, was used in the production of porous polyethylene glycol-based scaffolds (7). Self-assembly technique has been used in the production of silk/PCL scaffolds (8). All of these three types of scaffolds revealed promising properties for bone regeneration.

However, these fabrication methods present limitations such as low porosity, some degree of toxicity associated with use of organic solvents and reproducibility issues (9). Recently, 3D scaffolds printed using RP technologies arose as a feasible and cheap alternative to the current used methods, presenting accuracy and reproducibility in scaffolds production (10). Furthermore, RP techniques were able to precisely fabricate 3D scaffolds with defined shape, size, porosity and pore size distribution (11). Such is fundamental for the production of personalized implants that, until now, could not be produced through conventional methods (12). So far, different materials have been used for scaffolds production through RP (9, 13, 14). However, the obtained results showed that despite scaffolds present suitable mechanical properties, none of them is fully capable of avoiding the occurrence of local infections during bone healing process.

With the increasing concerns involving materials contaminated with pathogen bacteria, there is a huge demand for developing new and powerful antibacterial agents. In particular, current advances in the field of nanobiotechnology led to the development of new antibacterial nanoparticles produced with copper, zinc and/or silver (15, 16). Silver nanoparticles (AgNPs) due to their potential to prevent implant-based infections have been widely studied (17). Its

antimicrobial activity has been attributed mainly to its oxidized form (Ag+), which is able to anchor to the bacterial cell wall and to penetrate through it, thereby causing the disruption of cell membrane. The AgNPs can also interact with the thiol groups of many vital enzymes and, subsequently, inactivate them. Moreover, silver ions act on the phosphorus components of DNA which leads to inhibition of DNA replication (18). Due to their high surface area to volume ratio, AgNPs present enhanced reactivity against a range of different bacterial strains with clinical relevance (19). In fact, systems containing AgNPs are currently used in a variety of biomedical devices, like wound dressings, surgical devices and healthcare products (20).

Recently, our group produced 3D scaffolds of Tricalcium phosphate (TCP) and sodium alginate (SA) using RP technique (9). TCP [$Ca_3(PO_4)_2$] is a very popular form of calcium phosphate bioceramics due to its excellent biocompatibility, high bioactivity and thermodynamic stability. It can directly bind to natural bone, be gradually absorbed and replaced by natural bone (21). In turn, SA is a hydrophilic, biocompatible and biodegradable polymer which is also widely used in tissue engineering (22). The goal of the present study was to incorporate AgNPs in the TCP/SA 3D scaffolds produced by RP technique, using a Fab@home printer, in order to confer to the 3D bone substitute antibacterial activity. AgNPs were added to the 3D scaffolds through two methods: in the first one the AgNPs solution were directly incorporated in the composite mixture of TCP/SA before the printing step and in the second one AgNPs were added to the scaffolds through a physical adsorption process, already described in literature (19). The two methods were chosen in order to investigate which procedure confers better antimicrobial properties without compromising the biocompatibility of the scaffolds aimed for tissue engineering.

3.2. Materials and Methods

3.2.1. Materials

3-(4,5-dimethylthiazol-2-yl)-2,5-diphenyltetrazolium bromide (MTT) was purchased from Alfa Aesar (Ward Hill, USA). Acetic acid was bought from Pronolab (Barcelona, Spain). Ammonium hydroxide (NH_4OH) was purchased from Acros Organics (New Jersey, USA). Amphotericin B, Alizarin Red S, Calcium Chloride ($CaCl_2$), Dulbecco's modified Eagle's medium (DMEM-F12), Ethylenediaminetetraacetic acid (EDTA), Kanamycin, LB Broth, Phosphate-buffered saline solution (PBS), Resazurin sodium salt (7-hydroxy-3H-phenoxazin-3-one-10-oxide sodium salt), Sodium alginate (SA), Sodium borohydride ($NaBH_4$) and Trypsin were purchased from Sigma-Aldrich (Sintra, Portugal). Dimethyl sulfoxide (DMSO) was obtained from Thermo Fisher Scientific (Rockford, IL,USA). Fetal bovine serum (FBS) (free from any antibiotic) was acquired from Biochrom AG (Berlin, Germany). Normal human osteoblast (hOB) (406-05f) cryopreserved cells were purchased from Cell Applications, Inc. (San Diego, USA). Paraformaldehyde (PFA) was obtained from Merck, SA (Algés, Portugal). Polyvinylpyrrolidone (PVP) (molecular weight 44,000 g mol^{-1}) was acquired from BDH Chemicals Ltd (Poole, UK). Silver nitrate ($AgNO_3$), Sodium hydrogen carbonate ($NaHCO_3$) and Tricalcium phosphate (TCP) were obtained from Panreac (Barcelona, Spain). Tris Base was obtained from Fisher Scientific (Portugal).

3.2.2. Methods

3.2.2.1. Production of AgNPs

The AgNPs were produced through the chemical reduction of silver, as previously described elsewhere (17). Briefly, the AgNPs were synthesized using $AgNO_3$ and $NaBH_4$ (as metal precursor and reducing agent, respectively), at the required stoichiometric ratios. First, 5 mL of $AgNO_3$ solution (2 mM) were added dropwise to 30 mL of $NaBH_4$ solution (2 mM), under constant stirring and at room temperature (RT), until an $AgNO_3$:$NaBH_4$ molar ratio of 1:5 was achieved. AgNPs production was confirmed by the change in the solution color, from colorless to yellow, and afterward samples were stirred during 30 min. Then, for producing PVP-coated AgNPs (AgNP:PVP), 5 mL of 0.1 % solution of PVP (stabilizer agent) were added to the AgNPs solution, under constant stirring for 30min. Afterwards, PVP-coated AgNPs were recovered by centrifugation at 1700 rpm and washed with double deionized and filtered water, obtained using a Milli-Q Advantage A10 ultrapure Water Purification System (resistivity=18.2MΩ/cm, at 25°C), at the end of the process. All procedures were performed in the dark to prevent the photodecomposition of $AgNO_3$. To characterize the morphology of AgNPs produced in this study, transmission electron microscopy (TEM) images were acquired with a Hitachi–HT7700

microscope using an accelerating voltage of 80 kV. Moreover, the AgNPs size distribution was determined by dynamic light scattering (DLS) analysis.

3.2.2.2. Preparation of TCP/SA based scaffolds

The 3D scaffolds were produced using in a proportion of 50/50 (w/w) of TCP/SA, as previously described by Diogo and colleagues (9), using a Fab@Home printer to create well defined and highly reproducible structures (23). Initially, a 15% (w/v) sodium alginate solution was prepared by dissolving the polymer in double deionized and filtered water, obtained using a Milli-Q Advantage A10 ultrapure Water Purification System (resistivity=18.2MΩ/cm, at 25°C), using overnight agitation. The solution was then homogenized using an X10/25 Ultra-turrax® (Ystral, Germany) for 30 min. Finally, TCP powder was added to various samples according to the ratio of 50/50 of each component, and subsequently they were homogenized. After the dissolution of all components, a 5% (w/w) $CaCl_2$ solution was added to the composite mixture to attain a volume ratio of 1:2 for $CaCl_2$:alginate. $CaCl_2$ crosslinks the alginate polymer chains, increasing the viscosity and thus allowing a better control of the extrusion process for scaffold production. Lastly, a syringe (10 cc Luer Lock) was filled with the $CaCl_2$:alginate solution for posterior extrusion. After scaffolds printing, they were immersed in a 5% (w/w) $CaCl_2$ solution and incubated for 24h at RT. The crosslinked scaffolds were then frozen at -20°C and subsequently freeze-dried for 24h.

3.2.2.3. Functionalization of scaffolds with AgNPs

As presented in Figure 3.1, AgNPs were incorporated in scaffolds through two methods. The first one involved the direct incorporation (DI) of 20 mL of AgNPs solution (2 mM) in the composite mixture of 50/50 TCP/SA, followed by its homogenization using the turrax at RT. After the dissolution of all the components previously described, the mixture was used for printing the 3D scaffolds, as can be observed in Figure 3.1A. Once printed, the scaffolds containing AgNPs were then crosslinked and freeze-dried as previously described in section 2.2.2. Furthermore, the other 3D scaffolds were functionalized by AgNPs adsorption to their surface. To do so, each lyophilized scaffold was immersed in a 6-well plate with 1.5 mL AgNPs solution and left overnight at RT (Figure 3.1B), using an adaptation of the method described by Marsich and collaborators (19). Then, TCP/SA/AgNPs scaffolds were freeze-dried for 24h.

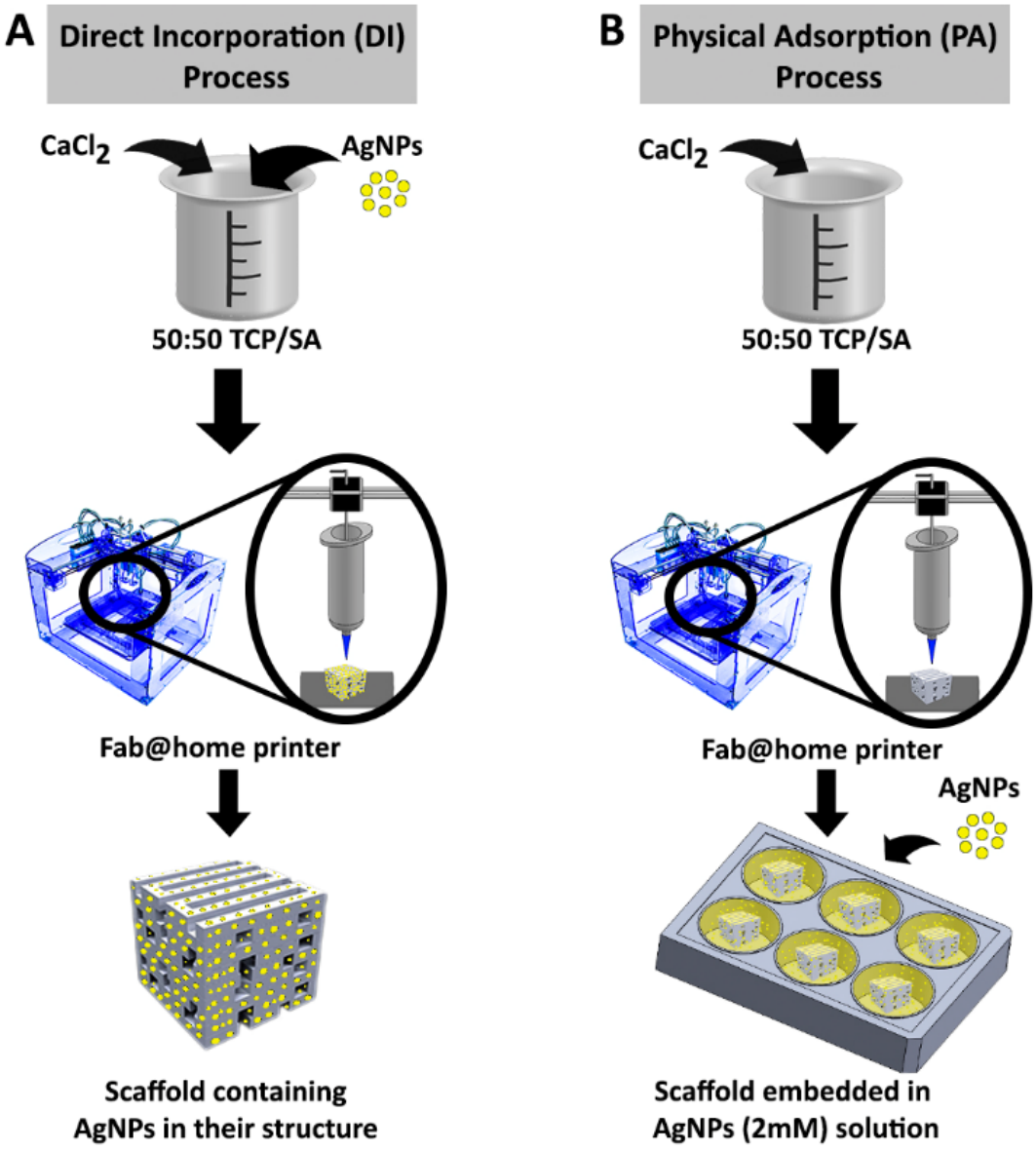

Figure 3.1 Schematic representation of scaffolds production using the direct incorporation (A) and physical adsorption (B) process.

3.2.2.4. Attenuated Total Reflectance-Fourier Transform Infrared Spectroscopy analysis

The physicochemical properties of the scaffolds were assessed by Attenuated Total Reflectance-Fourier Transform Infrared Spectroscopy (ATR-FTIR). The spectra obtained for the samples are the average of 128 scans, between 400 and 4000cm^{-1}, with a spectral resolution of 4cm^{-1} (5). All the samples were crushed to powder, mounted on a diamond window, and the spectra recorded with a Nicolet iS10 FTIR spectrophotometer (Thermo Scientific, Waltham, MA,

USA). All the scaffold components were also analyzed in their pure state, in order for a comparison with the samples spectra can be made. Furthermore, the presence of silver ions in both types of scaffolds was also checked.

3.2.2.5. Energy dispersive spectroscopic analysis

Energy Dispersive Spectroscopy (EDS) was used to perform the elemental characterization of the materials and also to evaluate the presence of silver ions on scaffolds. The samples were placed on aluminum stubs, air-dried at RT, sputter-coated with gold and analyzed in a XFlash Detector 5010 (Bruker Nano, Germany).

3.2.2.6. Characterization of the mechanical properties of the scaffolds

The mechanical behavior of the scaffolds was evaluated through compression assays as previously described by Torres (24). All the measurements were performed at RT using Zwick® 1435 Material Püfung (Ulm, Germany). The assays were performed using a crosshead speed of 2mm/min and a load cell of 5kN. Five specimens of each sample were used in each assay.

The compressive strength (Cs) of the scaffolds was calculated according to equation (1).

$$Cs = \frac{F}{w \times l} \qquad (1)$$

Where F corresponds to the load at the time of fracture, and w and l represent the width and length of the scaffold, respectively.

The Young Modulus (YM) was calculated through equation (2).

$$YM = \frac{C_s}{H_d} \qquad (2)$$

Where H_d stands for the height deformation at maximum load, and C_s is the scaffold compressive strength obtained from equation 1. Average values and standard deviations (s.d.) were determined for each sample as previously described in the literature (25).

3.2.2.7. Characterization of the swelling profile of the scaffolds

The swelling capacity of the scaffolds was evaluated through a method previously described in literature (26). Samples from each scaffold, with a known dry weight, were placed in Eppendorf tubes containing 2mL of Tris buffer (1M, pH=7.4), at 37°C. Then, scaffolds were retrieved from the solution at predetermined intervals (30, 60, 90, 120, 150, 180 and 210 min), and their weight was determined after removing the excess of Tris with a filter paper. Subsequently, samples were re-immersed in the buffer solution. Equation (3) was used to evaluate the swelling ratio of the samples.

$$Swelling\ ratio\ (\%) = \frac{W_t - W_0}{W_0} \times 100 \qquad (3)$$

Where W_0 represents the initial dry weight of the scaffolds and W_t is the final weight of scaffolds.

3.2.2.8. *In vitro* analysis of the biodegradation of the samples

Three samples of each scaffold formulation were weighed (W_i), placed in 6-well plates and fully immersed in DMEM-F12 at 37°C, accordingly to the method previously used by Jeong and colleagues (27). The DMEM-F12 was changed every 3 days and the weight of the samples was determined after 4, 7 and 14 days of incubation. To do so, scaffolds were washed in deionised water in order to remove ions adsorbed on scaffold's surface and then were lyophilized. The degradation of the scaffold was calculated using equation (4):

$$Weight\ loss\ (\%) = \frac{W_t}{W_i} \times 100 \qquad (4)$$

Where W_i corresponds to the initial weight of the sample and W_t to the weight of the sample at time t.

3.2.2.9. Scaffold's porosity analysis

The microporosity of the different scaffolds (1 × 1 × 1 cm) was determined using a liquid displacement method, adapted from Torres and collaborators (24). Briefly, scaffolds (n=3) were weighed, immersed in absolute ethanol (EtOH) for 48h in a closed vessel and then, weighed again. The porosity was calculated by the amount of EtOH absorbed, through equation (5):

$$Porosity\,(\%) = \frac{W_w - W_d}{D_{ethanol} \times V_{scaffold}} \times 100 \qquad (5)$$

Where W_w and W_d are the wet and dry weights of the scaffolds, respectively, $D_{ethanol}$ represents the density of EtOH at RT and $V_{scaffold}$ the volume of the wet scaffold.

The pore size of the different structures was also assessed by mercury intrusion porosimetry using an AutoPore IV 9500 equipment (Micromeritics Instrument Corporation, USA).

3.2.2.10. Characterization of scaffold biomineralization activity *in vitro*

In vitro formation of apatite layer on scaffold's surface can be reproduced in a protein-free and acellular simulated body fluid (SBF), whenever a similar ionic concentration close to that found in human blood plasma is used (28). This assay involved the immersion of scaffolds (n=5) of equal weight and shape in SBF (500 µL/well), prepared as previously described by Wang and collaborators (10), followed by samples incubation at 37°C for 1, 7 and 14 days. After each specific period, the scaffolds were removed and rinsed three times with deionized water. The biomineralization, i.e., deposition and formation of apatite layers on the surface of the scaffolds was characterized by Scanning Electron Microscopy (SEM) and EDS.

3.2.2.11. Characterization of the cytotoxic profile of the scaffolds

The cytotoxic profile of the scaffolds was evaluated in vitro following the International Standard Organization 10993-5 (29). In the cytotoxic assays, hOB were used as model cells and they were seeded ($10x10^3$ cells/well) in the presence of the materials in 96-well plates. Prior to cell seeding, scaffolds were cut into small pieces, placed into 96-well plates and then sterilized by UV irradiation for 30min. Then, 100 µL of culture medium was added to each well and the plate was incubated at 37°C, in a 5% CO_2 humidified atmosphere, for 24h. Subsequently, the culture medium was replaced every two days until the end of the assay. An MTT assay was performed at 1 and 7 days to characterize scaffolds biocompatibility. The metabolic conversion of MTT to formazan crystals is proportional to the number of viable cells. Briefly, 50µL of MTT (5mg/mL PBS) was added to each sample, followed by their incubation for 4h, at 37°C, in a 5% CO_2 atmosphere. The medium was then removed and cells were treated with 150 µL of DMSO (0.04N) for 30 min. A microplate reader (Biorad xMark microplate spectrophotometer) was used to determine the absorbance of each well at 570 nm. Five replicates of each sample were used. Cells cultured without materials were used as negative control (K^-), whereas cells cultured with EtOH (96%) were used as positive control (K^+).

3.2.2.12. Scanning Electron Microscopy analysis

Scanning Electron Microscopy (SEM) analysis was performed in order to characterize the morphology, pore size and cellular attachment on scaffold's surface. First, to evaluate morphology and porosity, samples of each scaffold formulation were mounted onto aluminium stubs with Araldite glue and sputter-coated with gold using a Quorum Q150R ES sputter coater. Subsequently, scaffold samples that were previously in contact with hOB were also prepared to assess cellular attachment on their surface. To do so, samples were washed with PBS at RT and fixed overnight with 2.5% (v/v) glutaraldehyde. After, samples were washed three times with PBS and dehydrated with growing concentrations of EtOH (50, 60, 70, 80, 90 and 99.9%). Subsequently, scaffolds were frozen using liquid nitrogen, freeze-dried for 3h. and finally mounted onto aluminium stubs with Araldite glue and sputter-coated with gold using a Quorum Q150R ES sputter coater. SEM images of the different scaffolds with/without cells were then captured with different magnifications, at an acceleration voltage of 20kV, using a Hitachi S-3400N Scanning Electron Microscope (30).

3.2.2.13. Alizarin red S staining

To evaluate calcium deposition on scaffolds, an Alizarin Red S (ARS) staining assay was performed according to a method previously described in literature (5). ARS forms reddish complexes in contact with calcium. To perform the ARS assay, cells were seeded ($10x10^3$ cells/well) in the presence of the materials, in 96-well plates. After being in contact with cells for 1 and 7 days, the scaffolds were rinsed five times in sterile PBS, and fixed with 2.5% PFA for 15min. Following, the samples were washed with distilled water and stained with 200 µL of ARS solution (2g/100 mL, pH=4.1-4.3), for 5min. Then, the excess of dye was removed with distilled water and optical microscopic images were acquired.

3.2.2.14. Determination of minimum inhibitory concentration of AgNPs

Minimum inhibitory concentration (MIC) of AgNPs was determined as previously described (31). Briefly, *Staphylococcus aureus* (1×10^6 colony-forming units (CFU) mL^{-1}) was inoculated in culture medium (LB Broth). Subsequently, different concentrations of AgNPs (33.125–265 µg/mL) were prepared and placed in contact with the bacterium in a 96-well plate. A negative control (suspension of *S. aureus*) and a positive control (containing Kanamycin antibiotic (30 mg/mL)) were also prepared. After that, the 96-well plate was incubated for 24 h, at 37 °C. In order to assess the bacterial growth, 10 µL of resazurin (1mg/mL) was added and, after 24 h, the fluorescence was measured using a fluorescence plate reader (Spectramax Gemini XS,

Molecular Devices LLC, USA) at an excitation/emission wavelength of 560/590 nm, respectively (31, 32).

3.2.2.15. Evaluation of the antimicrobial activity of the scaffolds

S.aureus, a gram-positive bacterium, was used as model to evaluate the bactericidal activity of the scaffolds. For this purpose, an agar diffusion method was used, where *s.aureus* (1×10^8 CFU mL^{-1}) was grown in sterilized LB broth and incubated for 4h at 37°C. 200 µL of the *s.aureus* suspension was placed on the LB agar growth plates and spread uniformly using a sterile cotton swab. The different formulations of scaffolds were placed on the top of the inoculated agar plates and incubated overnight at 37°C. Macroscopic images of the samples were acquired and the inhibition halos for each material were measured using *ImageJ* software. Moreover, in order to determine the appropriate amount of AgNPs that must be loaded within scaffolds, different 3D constructs containing different concentrations of AgNPs were produced and placed in contacted with *S. aureus* (1×10^8 CFU mL^{-1}) for 5 days. SEM images were acquired to monitor the bacterial growth at the surface of the different samples.

3.2.2.16. Confocal microscopic analysis

The analysis of cellular distribution within the TCP/SA/AgNPs DI scaffolds was performed by confocal laser scanning microscopy (CLSM). To do so, hOB were labelled with Hoescht 33342 (5µg/mL) and seeded in the presence of the scaffolds ($10x10^3$cells/scaffold) in µ-Slide 8-well Ibidi imaging plates (Ibidi GmbH, Germany). After 24h, the scaffold was labelled with calcein (20µg/mL) and confocal images were acquired. Imaging experiments were performed in a Zeiss LSM 710 laser scanning confocal microscope (Carl Zeiss AG., Germany), where consecutive z-stacks were acquired. The 3D reconstruction and image analysis were performed using *Zeiss Zen 2010* software.

3.2.2.17. Statistical Analysis

The statistical analysis of the obtained results was performed by using one-way analysis of variance (ANOVA), with the Newman-Keuls post hoc test. A p value lower than 0.05 ($p<0.05$) and 0.01 ($p<0.001$) was considered statistically significant.

3.3. Results and Discussion

3.3.1. Morphological characterization of the scaffolds

Morphological analysis of the scaffolds was performed to characterize their architectural features, which is a crucial parameter for their application in tissue engineering (Figure 3.2). To allow bone regeneration and to provide an interaction with the host bone, these 3D structures should fulfil requirements like biocompatibility, suitable mechanical properties, pore size and porosity, among others (33). During their air drying, scaffolds shrunk due to the presence of solid fillers in alginate solution, as already described by Rassis and collaborators (34). The presence of silver in the constructs was confirmed by their yellow color when compared with the white color presented by the control scaffold (19). It can also be stated that the scaffolds containing AgNPs produced through the DI process presents the most consistent and well defined structure.

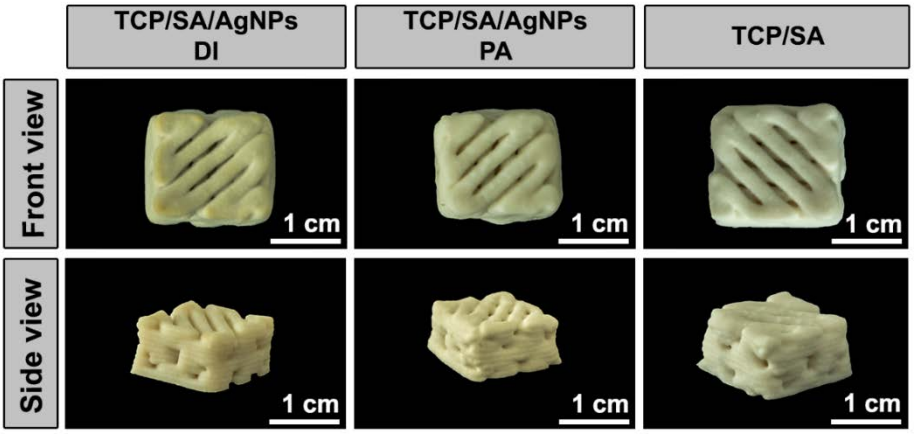

Figure 3.2. Macroscopic images of the scaffolds produced by DI, PA and without AgNPs (TCP/SA) (front and side view).

Moreover, scaffolds surface morphology and pore size were also characterized by SEM images (Figure 3.3A). The properties of scaffold's surface greatly influence cellular behavior (35). Herein, TCP is responsible for scaffold's heterogeneous structure and rough surface. In particular, it is known that human osteoblast cells show an increased adhesion, metabolism and extracellular matrix production when in contact with rough surfaces (36, 37). Furthermore, rough surfaces are also able to promote the differentiation of osteoblasts and trigger bone mineralization process (38). A porous microstructure is another important feature of bone scaffolds since it promotes bone ingrowth due to its high surface area that promotes protein adsorption, providing anchorage points for osteoblasts and increasing ionic solubility.

In addition, it has also been shown that pore interconnectivity has a positive influence on bone deposition rate and cell depth infiltration both in vitro and in vivo (39).

The SEM analysis revealed that scaffolds possess a macroporous interconnected homogenous structure that is compatible with cell penetration, adhesion and spreading. Furthermore, it is also compatible with nutrients diffusion, protein adsorption and neovascularization (40). Moreover, Figure 3.5D shows that scaffolds containing AgNPs have a higher porosity, as already described in literature. In fact, previous studies have reported a relationship between the incorporation of nanoparticles and the increase of the total porosity of polymeric and ceramic composite constructs (41, 42). Specifically, the scaffolds produced through DI are the most porous (≃60%) and presented a percentage of porosity within the range of that displayed by the trabecular bone, which is around 50-90% (14, 43, 44). In addition, the results obtained in the mercury intrusion porosimetry (MIP) assays have also shown that the pore structure of different scaffolds present similar values for the characteristic length: TCP/SA/AgNPs DI (53.5370 µm), TCP/SA/AgNPs PA (33.5881 µm), TCP/SA (52.0205 µm). Therefore, the RP scaffolds containing silver nanoparticles present an adequate porosity for improving cell migration, adhesion, proliferation and also enhance the transport of oxygen and nutrients. Furthermore, the morphology and size of silver nanoparticles were also characterized by TEM and DLS. In Figure 3.3B, it is possible to observe that silver nanoparticles show a spherical shape and a size distribution of 28.04 nm.

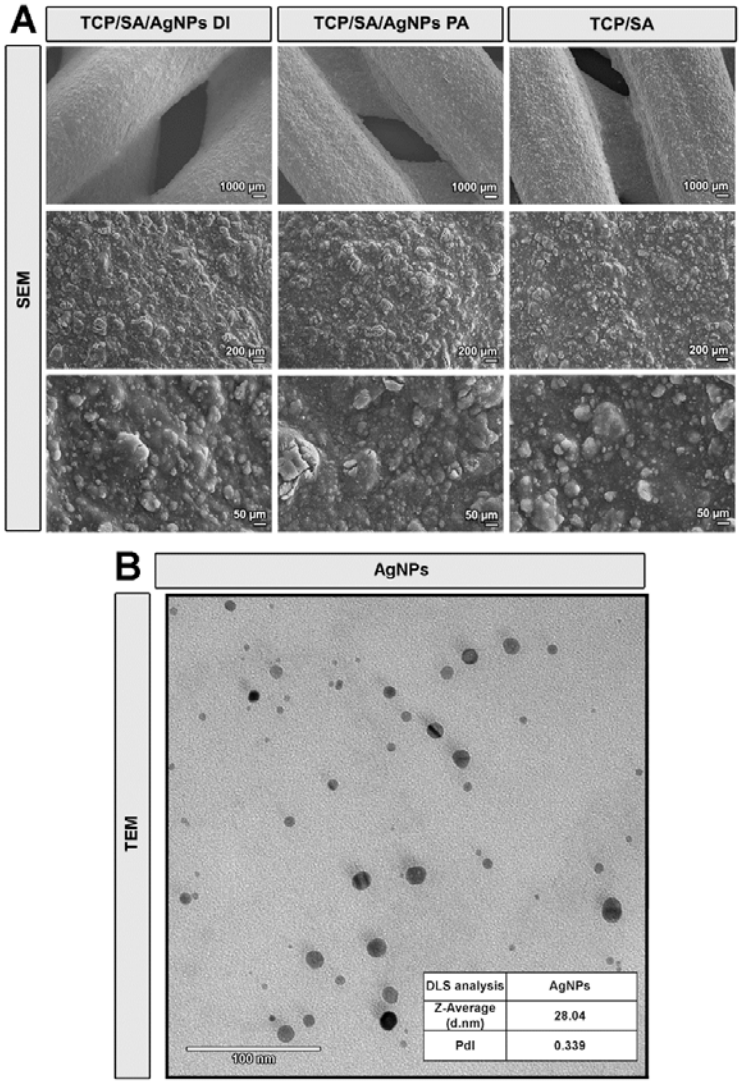

Figure 3.3. SEM images displaying the morphology of the scaffolds produced by DI, PA and without AgNPs (TCP/SA) at different magnifications (A); TEM characterization of the AgNPs morphology used on scaffolds production and respective DLS analysis (B).

3.3.2. Characterization of the physicochemical properties of the scaffolds

3.3.2.1. ATR-FTIR analysis

To evaluate the physicochemical properties of the different scaffolds produced by RP, ATR- FTIR analysis was performed. The ATR-FTIR spectra of raw materials and of the different produced scaffolds are presented in Figure 3.4. The TCP spectrum presents a main peak at 1020 cm^{-1}, which is characteristic of a P=O stretch vibration, revealing the presence of the inorganic phosphate components of TCP (45). This peak is also present on the spectra of the produced scaffolds showing a similar intensity to

that of the raw material. The FTIR spectrum of sodium alginate powder presented two main peaks at 1400 and 1600 cm^{-1}, that belong to the C=O stretching of the carboxylate group. In addition, a stretching vibration corresponding to the O-H bonds of alginate appeared in the range 3000 – 3600 cm^{-1} (46). These peaks were also observed in the spectra of different scaffolds, without perceptible variation among the different formulations. The $AgNO_3$ spectrum display a major peak at 1277 cm^{-1}, which is characteristic of the NO_3^- ion in its free form (17). The change in the electronic environment of the anion, due to the separation of the Ag^+ ion, caused this displacement. Furthermore, the characteristic peaks of $AgNO_3$ are not observed in the other spectra, which may result from the low concentrations of $AgNO_3$ used for scaffolds production.

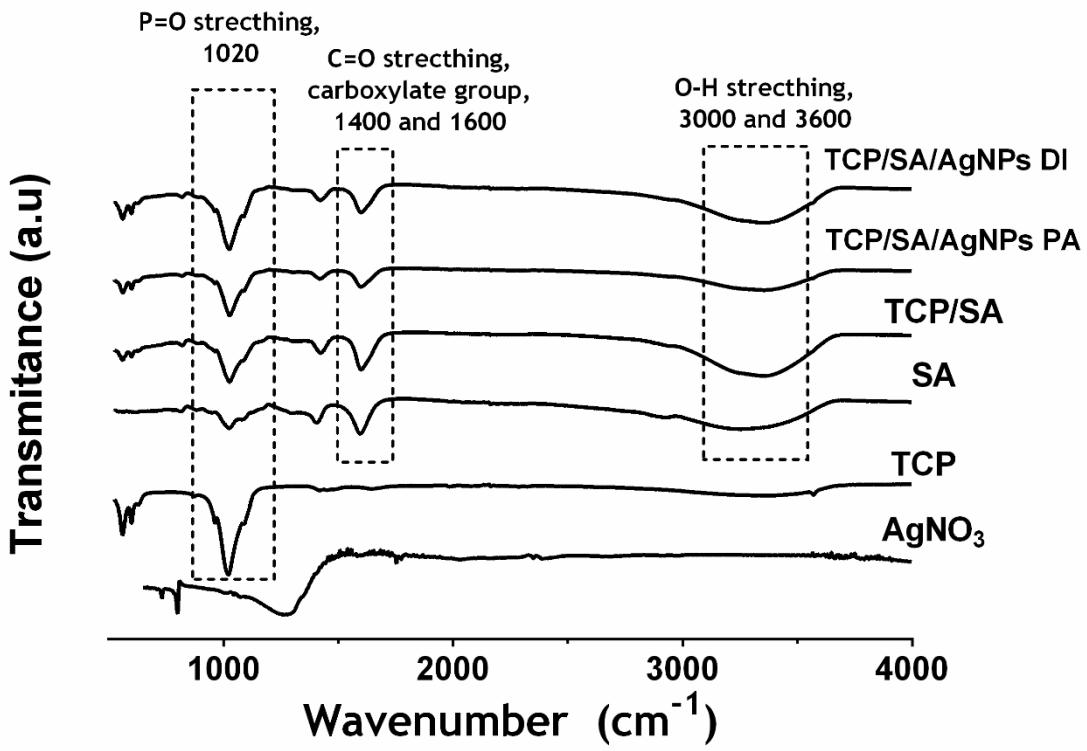

Figure 3.4. ATR-FTIR spectra for the different scaffolds produced and of the raw materials.

3.3.2.2. Energy dispersive spectroscopy analysis (EDS)

The EDS analysis was performed to characterize the chemical composition of the materials used for scaffolds production. The results obtained (Table 3.1) revealed that all scaffolds have high percentage of carbon and oxygen, which is explained by alginate presence. The phosphate and calcium ions characteristic of TCP, in turn, are present in similar amounts in the produced formulations. In the EDS assay, the Ag^+

ions are only detected at the surface of scaffolds produced by PA process. Such result can be explained by the fact that these scaffolds were placed in AgNPs bath and due to that the Ag ions adsorbed essentially to the scaffold's surface. Contrariwise, Ag^+ is not present at the surface of the scaffolds produced by DI process, since nanoparticles were internalized in the scaffold instead of being deposited on scaffold's surface (19).

Table 3.1 Data obtained in the EDS analysis of the produced 3D scaffolds: TCP/SA/AgNPs scaffold produced through DI process (A); TCP/SA/AgNPs scaffold produced through PA process (B) and TCP/SA scaffold (C).

Elements / Sample	C (*at. %)	O (at. %)	N (at. %)	P (at. %)	Cl (at. %)	Ca (at. %)	Ag (at. %)
TCP/SA/AgNPs DI	33.97	54.24	0.10	1.72	3.24	6.72	0.00
TCP/SA/AgNPs PA	36.19	58.53	0.10	1.41	0.36	3.29	0.12
TCP/SA	47.10	50.78	0.64	1.40	1.45	3.94	0.00

*at. % - Atomic percentage.

3.3.3. Characterization of the mechanical properties of the scaffolds

For being used in bone tissue engineering, scaffolds must be flexible and resistant to compression. The mechanical behavior of the 3D scaffolds produced in this study was characterized by testing their resistance to compression and by determining their Young Modulus (YM). Through the analysis of figure 3.5A, it is possible to conclude that the YM and Cs are higher for scaffolds without AgNPs. In fact, the addition of AgNPs decreased the compressive strength and YM of the scaffolds. However, the scaffolds containing AgNPs showed a compressive strength almost three times higher than that of the trabecular bone, which is approximately 20 MPa, and almost half of the resistance of cortical bone (≃150 MPa) (47).

Furthermore, it is important to emphasize that the mechanical properties of the scaffolds are also dependent on materials rate of biodegradation (48), since their integrity, stability and mechanical performance is dependent on this property. Moreover, it is highly desired that scaffolds biodegradation occurs at a rate that is compatible with the new bone formation. Ideally scaffold must be completely degraded when bone structure is fully reestablished. The biodegradation profile of the scaffolds at 4, 7 and 14 days is presented in the figure 3.5C. All the different scaffolds did not lose more than 45% of its mass. Weinand and collaborators have previously reported that cells can disperse throughout the structure of scaffolds and deposit new bone tissue after 7 days (49). The scaffold modified by physical

adsorption of the AgNPs showed a faster mass loss, which may be explained by the physical stress of the additional freeze-drying step in the method used for its production. Xu and colleagues have also showed that metallic nanoparticles induce a thermal conductivity in the nanocomposites that enhances their degradation rate (50). Furthermore, the scaffold modified by direct incorporation of the AgNPs did not present a significant mass loss when compared with the control (TCP/SA scaffold). Such result, may indicate that the internalization of the AgNPs induce a low thermal conductivity in the scaffold thus leading to a lower degradation rate.

The different scaffolds did not show any significant variations in the YM and all of them surpassed largely the YM of trabecular bone, which value is between 100 and 200 MPa (51). Therefore, all scaffolds tested are capable of reproducing the strength and elasticity of the trabecular bone tissue.

3.3.4. Evaluation of swelling profile of the scaffolds

An important parameter that influences the applicability of a scaffold to be used in tissue engineering is its swelling profile (52). The water uptake leads to an increase on scaffold's pore diameters that can have influence on cells, nutrients, bioactive molecules migration and waste products diffusion through their 3D structure. All this processes are all fundamental for bone regeneration (53). Scaffolds swelling profile obtained during 200 min of incubation in Tris buffer is presented in Figure 3.5B. It is possible to notice that all scaffolds presented a similar water uptake ability, with a rapid swelling behaviour in the first minutes, followed by a stabilization after 150 min of immersion.

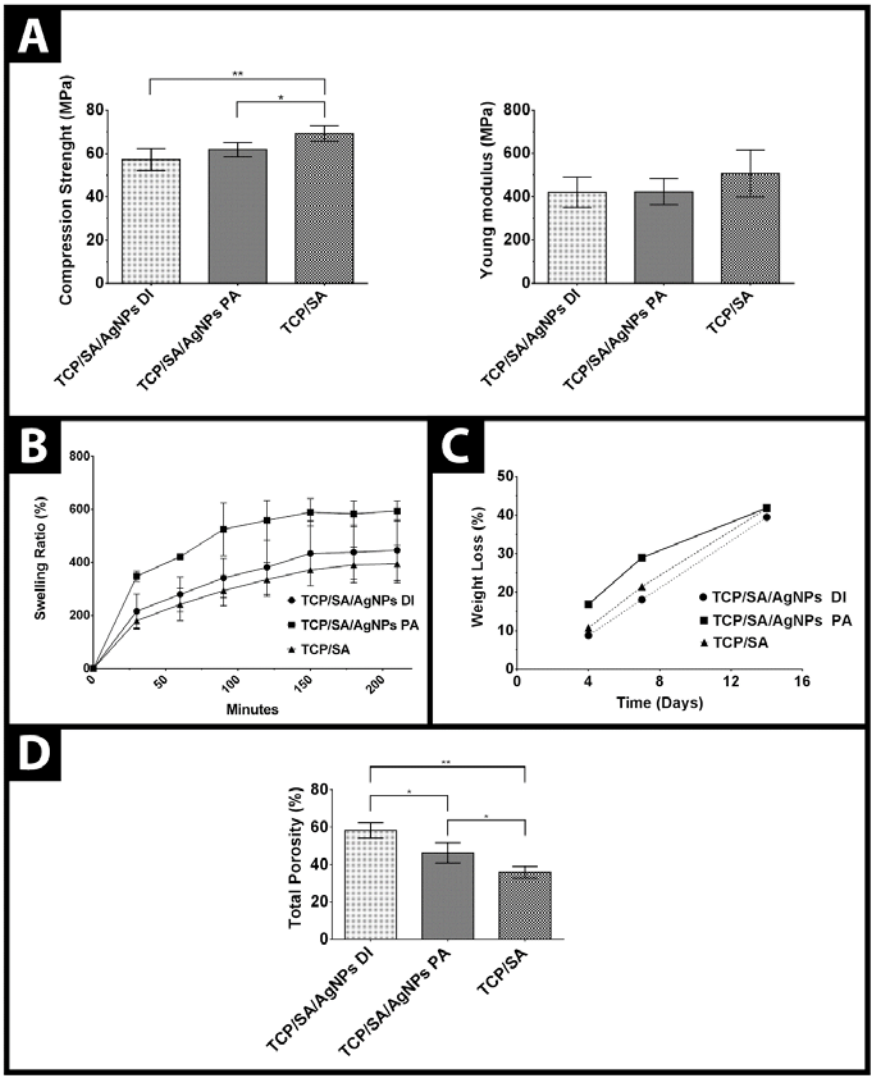

Figure 3.5. Evaluation of the physicochemical properties of the scaffolds (n=5). (A) Characterization of the compressive strength and Young Modulus of the produced scaffolds. (B) Swelling profile of the produced scaffolds; (C) Degradation profile of the scaffolds; (D) Determination of total porosity of the different scaffolds using the EtOH displacement method. Statistical analysis was performed using one-way ANOVA with Newman-Keuls tests (*p<0.05) (**p<0.001).

3.3.5. Biomineralization studies

The biomineralization studies showed that the scaffolds degree of mineralization increased after 7, 21 and 28 days, when scaffolds were in contact with a standard SBF solution, at physiological pH and at body temperature (Figure 3.6). No significant biomineralization variations have been noticed between the scaffolds with silver and those used as control. The incorporation of AgNPs did not affect the capacity of mineral deposition.

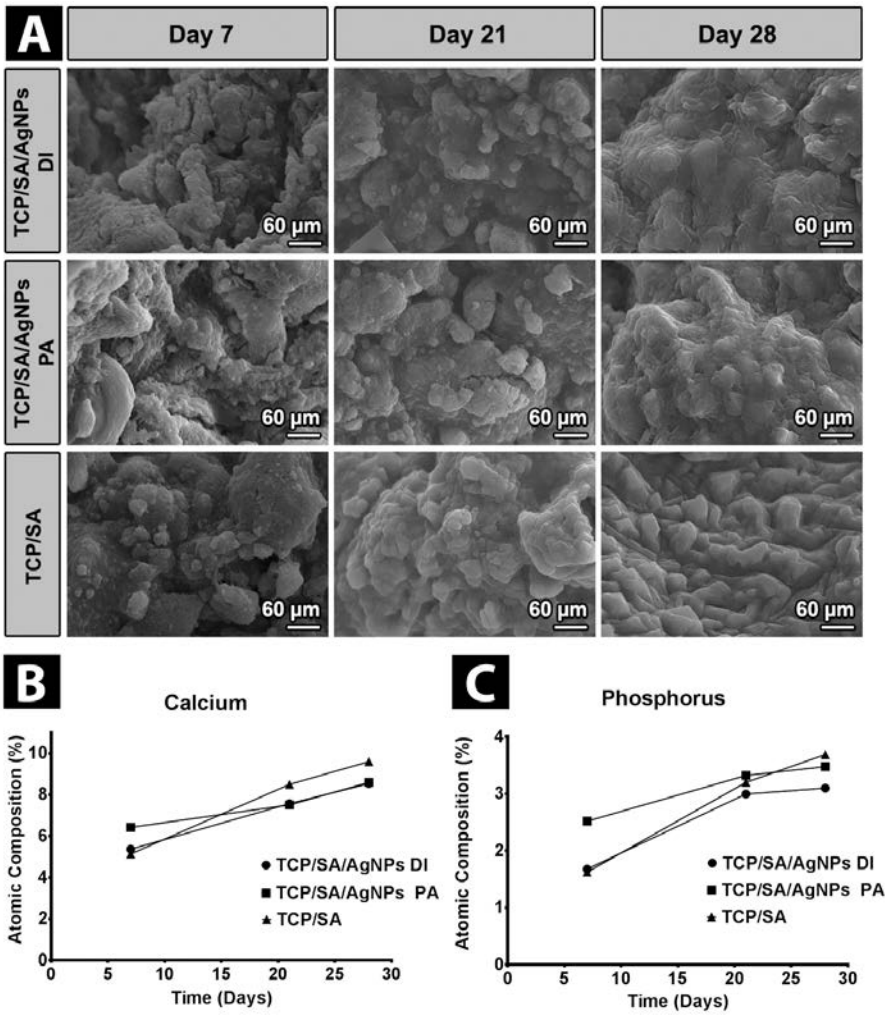

Figure 3.6. Scaffolds biomineralization: SEM images showing the mineralization of the composite scaffolds in SBF after 7, 21 and 28 days (A); Evaluation of scaffolds atomic composition of calcium (B) and phosphorus (C) after 7, 21 and 28 days.

3.3.6. Evaluation of the scaffolds cytotoxic profile

Scaffolds for being used in bone regeneration cannot trigger any adverse effect in the host. Herein, to evaluate scaffolds cytotoxicity an MTT assay was used. The metabolic conversion of MTT to formazan crystals is proportional to the number of viable cells present in each well. Osteoblast cells were chosen to perform this assay due to their important role in bone regeneration, specifically in bone matrix deposition and mineralization process (54). The results obtained in the MTT assay are presented in Figure 3.7A and it can be concluded that the cell proliferation in contact with the two distinct formulations of scaffolds containing AgNPs is comparable to that observed for control scaffolds, thus indicating that the incorporation of AgNPs in the

scaffolds did not impair cell proliferation. The degradation rate between the first and seventh day may be the cause for the decrease of cell viability in the scaffolds produced through DI. As the scaffold degradates, the nanoparticles became available and able to interact with cells. However, the percentage of cell viability verified for any of the produced scaffolds evidence their biocompatibility. Such is very important, since in literature there are studies that reported AgNPs toxicity for human cells (55-57).

Silver nanoparticles can be internalized by cells through endocytosis and become accumulated in several organelles, leading to damages in cell machinery or even cell death. The cytotoxic profile presented by scaffolds may be explained by the low concentration of AgNPs incorporated in the 3D structure of scaffolds (19). Generally, it is described that concentrations above of 5µg/mL exerts toxic biological effects (58).

3.3.7. Scanning Electron Microscopy analysis

SEM images of the cells in contact with scaffolds were also acquired (Figure 3.7B) and showed that cells adhered and grew in the presence of all the different 3D constructs. To characterize osteoblasts proliferation along time, SEM images were also acquired after 1 and 7 days. The images show that cells adhered and spread on scaffold's surface.

3.3.8. Alizarin Red S staining

The mineralization degree of 3D scaffolds performed by hOB was analyzed using an ARS staining assay. Optical microscope images of the mineralized matrix upon osteogenic stimulation at 1 and 7 days are shown in Figure 3.7C. The obtained results revealed an increase of scaffolds calcium content after 7 days, which indicates that all the formulations promoted osteoblast activity.

3.3.9. Confocal laser scanning microscopy analysis

To further characterize the biological performance of the scaffolds, an CLSM analysis was also performed 24h after hOB being seeded in contact with the TCP/SA/AgNPs DI scaffold (Figure 7D). This scaffold formulation was selected taking into account the results obtained in the MTT assay (section 3.3.6.) and antimicrobial evaluation (section 3.3.11.).

The scaffold structure was characterized by CLSM analysis as seen in Figure 3.7(D1). Moreover, the 3D reconstructions presented in figures 3.7(D2) and (D3) show that osteoblasts were able to adhere and proliferate in contact with the tested formulation, highlighting its biocompatibility and suitable physicochemical properties. Furthermore, the analysis of the orthogonal slices (Figure 3.7(D3)) and colour coded depth analysis (Figure 3.7(D4) of TCP/SA/AgNPs scaffold) showed that osteoblasts migrate into the interior of the scaffold, with some cells being observed at 20µm within the structure of the scaffold. The obtained results are in agreement with the data reported in literature for first day of culture (59). The cellular internalization in the scaffold structure is responsible for the filling of the bone defect with new bone matrix, while scaffold is biodegraded at a rate that is compatible with the restoring of the structure and functions of native tissue.

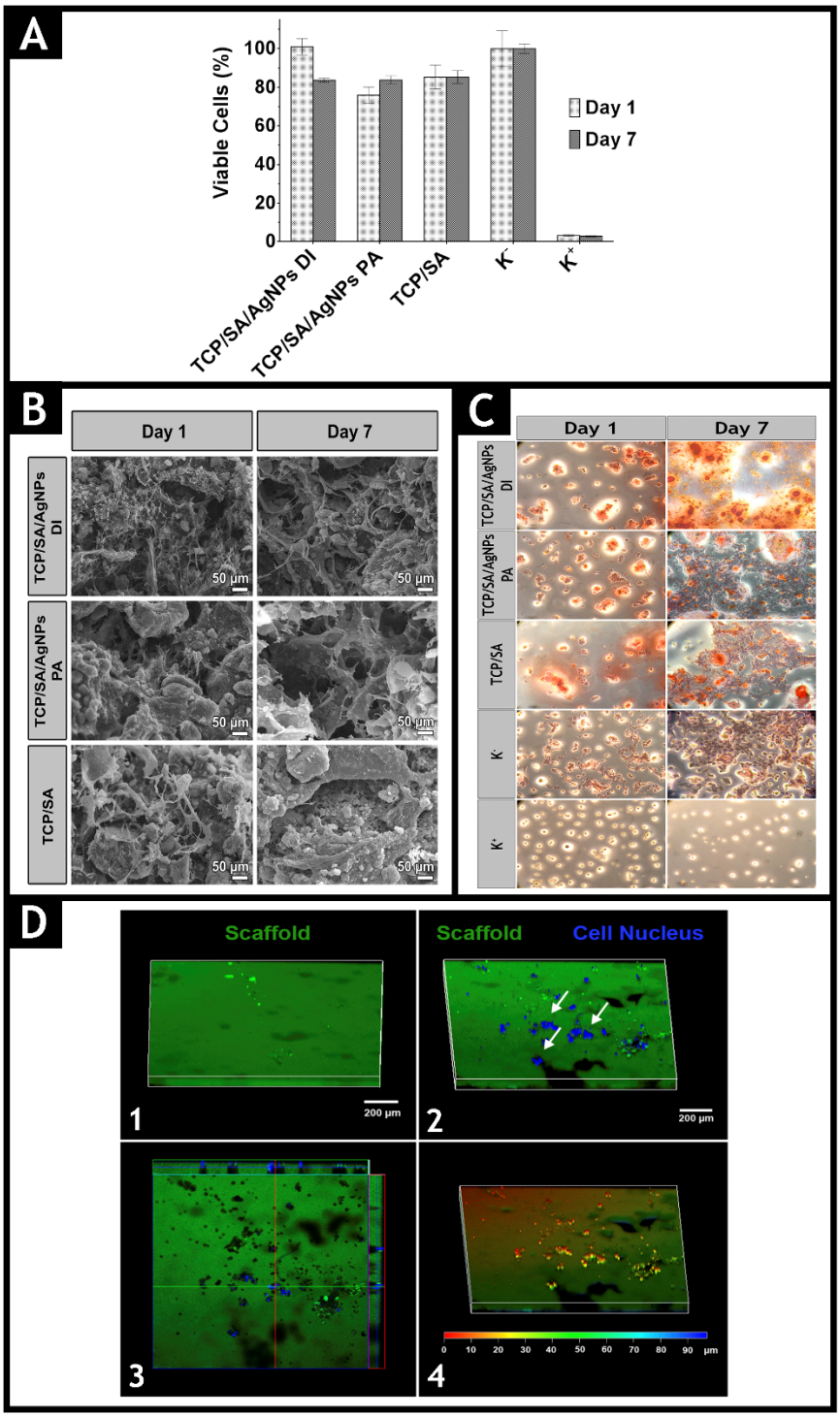

Figure 3.7. Characterization of the biological performance of the produced scaffolds. (A) Evaluation of cell viability when cells were seeded in contact with the different scaffolds formulations; (B) SEM images of osteoblast morphology in the presence of the scaffolds; (C) Qualitative evaluation of mineralization on the 3D scaffolds by hOB through alizarin red staining; (D) 3D reconstruction images (D1 and D2), orthogonal projections (D3) and colour coded depth analysis (D4) of the TCP/SA/AgNPs DI scaffold (red= 0 µm, blue= 90 µm). Arrows indicate the presence of cells.

3.3.10. Characterization of the minimum inhibitory concentration of the produced AgNPs

In this study silver nanoparticles were used to confer antibacterial properties to the scaffolds produced herein. Thus, S. aureus (1×10^6 CFU/mL) was incubated with different concentrations of AgNPs (ranging from 33 to 265 µg/mL), during 24h at 37°C. Subsequently, the MIC values were determined (Figure 3.8B) by performing a resazurin assay, as previously described (31, 60). The obtained results revealed that scaffolds loaded with AgNPs concentrations higher than 66.25 µg/mL showed the capacity to avoid bacterial growth (Figure 3.8A).

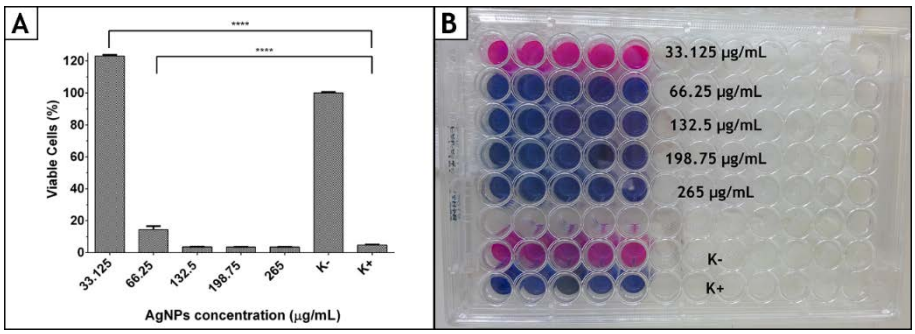

Figure 3.8. Characterization of antibacterial properties of the produced AgNPs: (A) MIC values obtained for AgNPs after 24h in contact with s. aureus (K^-(live bacteria); K^+(death bacteria)). Each result is the mean ± standard error of the mean of at least five independent experiments. Statistical analysis was performed using one-way ANOVA with Dunnet's post hoc test (****$p < 0.0001$); (B) Determination of MIC using a resazurin assay. Blue color corresponds to the death bacteria and pink to the live bacteria.

3.3.11. Characterization of the antimicrobial properties of the scaffolds

The bactericidal activity of the produced scaffolds was tested using S. aureus strain as model. This strain was chosen based on its wide presence in biomaterial-related infections, especially on orthopedic implants (61).

The growth profile of *s.aureus* in the presence of different scaffolds is depicted in Figure 3.9A, where the inhibitory halo was only observed for TCP/SA/AgNPs DI scaffold after 24h. Therefore, it can be concluded that AgNPs internalized in the scaffolds have the capacity to inhibit bacterial growth. In Figure 3.9A1, the diameter of the inhibitory halo was 0.820 cm. Such result can be explained by the involvement of AgNPs in the disruption of the bacterial membrane, inhibition of bacterial enzymatic activity and ATP production, thus avoiding bacteria growth. The obtained results are in agreement with previous studies, where *s.aureus* growth was inhibited in the presence of AgNPs (62).

However, the scaffold containing silver nanoparticles produced by PA process did not displayed an inhibitory activity (Figure 3.9A2). This has probably to do with the concentration of AgNPs adsorbed at scaffold's surface that may not be enough to trigger on inhibitory effect on *s.aureus*. On the other hand, the Scaffolds obtained by DI process may achieve a higher amount of AgNPs because AgNPs solution was mixed with the composite solution used to print the 3D structures, thus providing a higher entrapment of AgNPs during the layer-by-layer printing process.

Figure 3.9A3 shows the results obtained for the control scaffolds (TCP/SA) that had no AgNPs in their composition. As expected, no inhibitory halo was observed, which is due to the absence of silver in the scaffolds. These results are in agreement with those obtained in the SEM analysis during 5 days (Figure 3.9B). Furthermore, to verify the AgNPs properties used in this study, scaffolds with different concentrations of AgNPs were also produced in order to characterize their capacity to avoid bacterial growth during 5 days (Figure 3.10 and 3.11). Thus, it can be concluded that the best formulation to avoid biofilm formation at the surface is the TCP/SA/AgNPs DI (265 µg/mL).

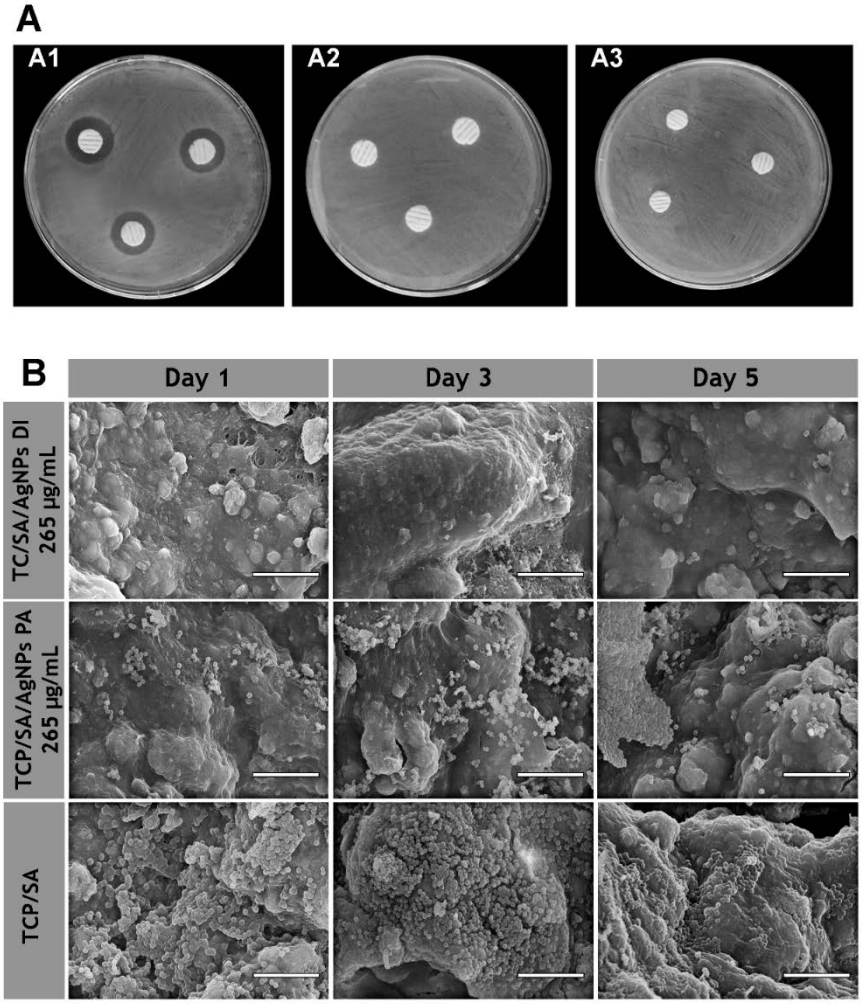

Figure 3.9. Characterization of the bactericidal activity of the produced scaffolds. (A) Macroscopic images of TCP/SA/AgNPs scaffold produced through DI process (A1), TCP/SA/AgNPs scaffold produced through PA process (A2) and TCP/SA scaffold (A3) in the presence of *s.aureus*. (B) SEM images of S. aureus in contact with scaffolds produced after 5 days (TCP/SA/AgNPs DI 265 µg/mL; TCP/SA/AgNPs PA 265 µg/mL and TCP/SA). Scale bars indicate 10 µm.

Actually, there are some commercially available composite scaffolds for bone regeneration containing TCP, like Mastergraft®, Chronos® and Mozaik®. Although these scaffolds present similar physicochemical and biological properties to the one used on this study, none of them is capable of preventing implant-based infections. This limitation in the commercially available bone scaffolds requires further research studies, like the one presented here, and investment in order to improve patient safety and reduce the incidence of healthcare associated infections. Lastly, the development of simple, cost-effective and fast technique, like the one used here, is fundamental for improving the rate of bone regeneration while avoiding infections at the implantation site.

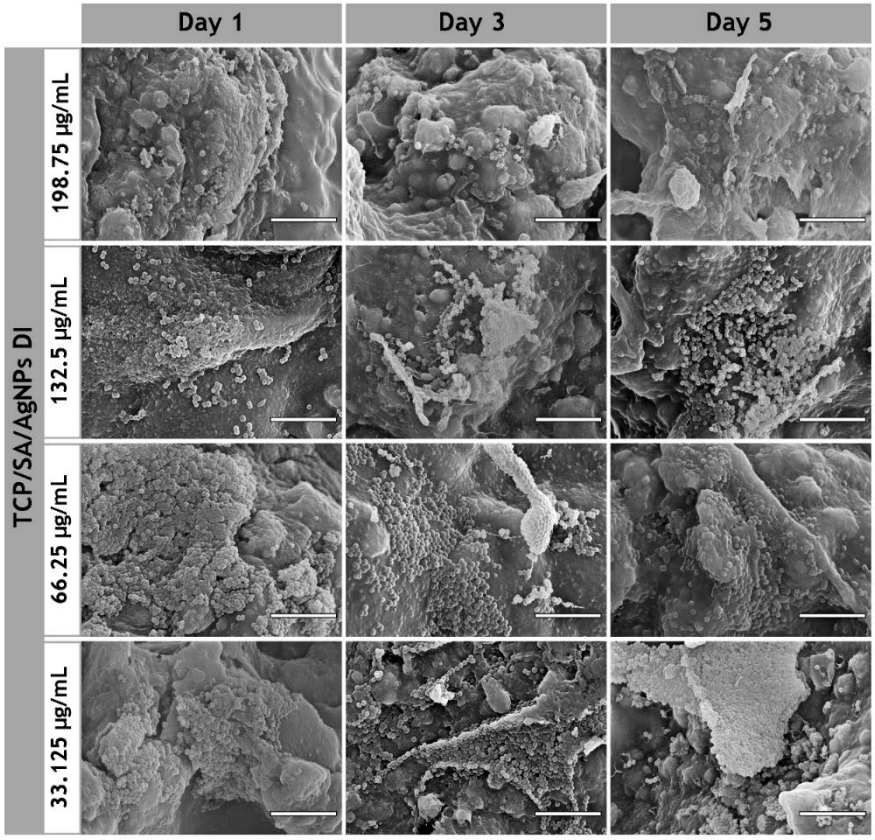

Figure 3.10 Characterization of the antibacterial activity of TCP/SA/AgNPs DI scaffold loaded with different concentration of AgNPs along 5 days. Scale bars indicate 10 µm.

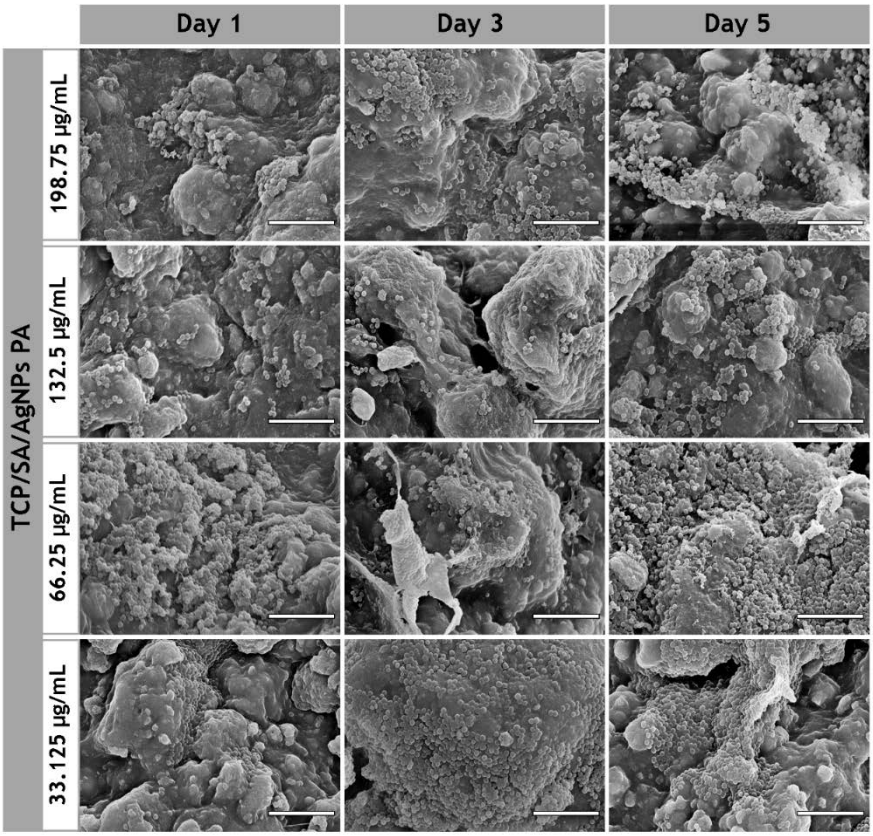

Figure 3.11. Characterization of the antibacterial activity of TCP/SA/AgNPs PA scaffold loaded with different concentration of AgNPs along 5 days. Scale bars indicate 10 µm.

3.4. Conclusions

The increasing incidence of bone disorders and fractures remains a challenging issue for today's society. Herein a simple and effective RP technique was used to produce scaffolds aimed for bone tissue regeneration. The 3D constructs were loaded with AgNPs to circumvent one of the major limitations associated with implants, i.e. bacterial contamination. The presence of silver on scaffolds would provide an additional measure to minimize the risk of infection and also prevent implant failure. Moreover, the produced scaffolds displayed a well-defined morphology and mechanical properties compatible with bone application. Moreover, scaffolds produced by DI allowed cell adhesion and internalization, which are crucial events for bone regeneration process.

In a near future in vivo studies must be performed in order to confirm the suitability of this scaffolds for bone regeneration and also to avoid bacterial contamination. In addition, the encapsulation of cells and bioactive molecules as growth factors and cytokines may also be tested in order to improve the bone healing process.

Acknowledgements

This work was supported by QREN (Programa Mais Centro) (CENTRO-07-0224-FEDER-002014). The authors would like to thank Professor João Castro Gomes and Jorge Bento for their technical support in mercury intrusion porosity analysis.

3.5. References

1. Yu X, Tang X, Gohil SV, Laurencin CT. Biomaterials for Bone Regenerative Engineering. Advanced Healthcare Materials. 2015;4:1268-5.

2. Inzana JA, Olvera D, Fuller SM, Kelly JP, Graeve OA, Schwarz EM, et al. 3D printing of composite calcium phosphate and collagen scaffolds for bone regeneration. Biomaterials. 2014;35(13):4026-34.

3. Dimitriou R, Jones E, McGonagle D, Giannoudis PV. Bone regeneration: current concepts and future directions. BMC medicine. 2011;9(1):66.

4. Lee H, Yeo M, Ahn S, Kang DO, Jang CH, Lee H, et al. Designed hybrid scaffolds consisting of polycaprolactone microstrands and electrospun collagen-nanofibers for bone tissue regeneration. Journal of Biomedical Materials Research Part B: Applied Biomaterials. 2011;97(2):263-70.

5. Serra I, Fradique R, Vallejo M, Correia T, Miguel S, Correia I. Production and characterization of Chitosan/Gelatin/ß-TCP scaffolds for improved bone tissue regeneration. Materials Science and Engineering: C. 2015;55:592-604.

6. Liu H, Peng H, Wu Y, Zhang C, Cai Y, Xu G, et al. The promotion of bone regeneration by nanofibrous hydroxyapatite/chitosan scaffolds by effects on integrin-BMP/Smad signaling pathway in BMSCs. Biomaterials. 2013;34(18):4404-17.

7. Ji C, Annabi N, Hosseinkhani M, Sivaloganathan S, Dehghani F. Fabrication of poly-DL-lactide/polyethylene glycol scaffolds using the gas foaming technique. Acta Biomaterialia. 2012;8(2):570-8.

8. Roohani-Esfahani S, Lu Z, Li J, Ellis-Behnke R, Kaplan D, Zreiqat H. Effect of self-assembled nanofibrous silk/polycaprolactone layer on the osteoconductivity and mechanical properties of biphasic calcium phosphate scaffolds. Acta Biomaterialia. 2012;8(1):302-12.

9. Diogo G, Gaspar V, Serra I, Fradique R, Correia I. Manufacture of ß-TCP/alginate scaffolds through a Fab@ home model for application in bone tissue engineering. Biofabrication. 2014;6(2):025001.

10. Wang MO, Vorwald CE, Dreher ML, Mott EJ, Cheng MH, Cinar A, et al. Evaluating 3D-Printed Biomaterials as Scaffolds for Vascularized Bone Tissue Engineering. Advanced Materials. 2015;27(1):138-44.

11. Liu Y, Lim J, Teoh S-H. Review: development of clinically relevant scaffolds for vascularised bone tissue engineering. Biotechnology Advances. 2013;31(5):688-705.

12. Shrivats AR, McDermott MC, Hollinger JO. Bone tissue engineering: state of the union. Drug Discovery Today. 2014;19(6):781-6.

13. Martínez-Vázquez F, Cabañas M, Paris J, Lozano D, Vallet-Regí M. Fabrication of novel Si-doped hydroxyapatite/gelatine scaffolds by rapid prototyping for drug delivery and bone regeneration. Acta Biomaterialia. 2015;15:200-9.

14. Kim J, McBride S, Tellis B, Alvarez-Urena P, Song Y-H, Dean DD, et al. Rapid-prototyped PLGA/ß-TCP/hydroxyapatite nanocomposite scaffolds in a rabbit femoral defect model. Biofabrication. 2012;4(2):025003.

15. Guzman M, Dille J, Godet S. Synthesis and antibacterial activity of silver nanoparticles against gram-positive and gram-negative bacteria. Nanomedicine: Nanotechnology, Biology and Medicine. 2012;8(1):37-45.

16. Azam A, Ahmed AS, Oves M, Khan MS, Habib SS, Memic A. Antimicrobial activity of metal oxide nanoparticles against Gram-positive and Gram-negative bacteria: a comparative study. International Journal of Nanomedicine. 2012;7:6003-9.

17. Silva E, Saraiva SM, Miguel SP, Correia IJ. PVP-coated silver nanoparticles showing antifungal improved activity against dermatophytes. Journal of Nanoparticle Research. 2014;16(11):1-13.

18. Chaloupka K, Malam Y, Seifalian AM. Nanosilver as a new generation of nanoproduct in biomedical applications. Trends in Biotechnology. 2010;28(11):580-8.

19. Marsich E, Bellomo F, Turco G, Travan A, Donati I, Paoletti S. Nano-composite scaffolds for bone tissue engineering containing silver nanoparticles: preparation, characterization and biological properties. Journal of Materials Science: Materials in Medicine. 2013;24(7):1799-807.

20. Prabhu S, Poulose EK. Silver nanoparticles: mechanism of antimicrobial action, synthesis, medical applications, and toxicity effects. International Nano Letters. 2012;2(1):1-10.

21. Samavedi S, Whittington AR, Goldstein AS. Calcium phosphate ceramics in bone tissue engineering: a review of properties and their influence on cell behavior. Acta Biomaterialia. 2013;9(9):8037-45.

22. Venkatesan J, Bhatnagar I, Manivasagan P, Kang K-H, Kim S-K. Alginate composites for bone tissue engineering: A review. International Journal of Biological Macromolecules. 2015;72:269-81.

23. Malone E, Lipson H. Fab@ Home: the personal desktop fabricator kit. Rapid Prototyping Journal. 2007;13(4):245-55.

24. Torres A, Gaspar V, Serra I, Diogo G, Fradique R, Silva A, et al. Bioactive polymeric–ceramic hybrid 3D scaffold for application in bone tissue regeneration. Materials Science and Engineering: C. 2013;33(7):4460-9.

25. Bland JM, Altman DG. Statistical methods for assessing agreement between two methods of clinical measurement. International Journal of Nursing Studies. 2010;47(8):931-6.

26. Coimbra P, Alves P, Valente T, Santos R, Correia I, Ferreira P. Sodium hyaluronate/chitosan polyelectrolyte complex scaffolds for dental pulp regeneration: synthesis and characterization. International Journal of Biological Macromolecules. 2011;49(4):573-9.

27. Jeong SI, Jeon O, Krebs MD, Hill MC, Alsberg E. Biodegradable photo-crosslinked alginate nanofibre scaffolds with tuneable physical properties, cell adhesivity and growth factor release. European Cells & Materials. 2012;24:331-43.

28. Rezwan K, Chen Q, Blaker J, Boccaccini AR. Biodegradable and bioactive porous polymer/inorganic composite scaffolds for bone tissue engineering. Biomaterials. 2006;27(18):3413-31.

29. ISO B. 10993-5: Biological evaluation of medical devices. Tests for in vitro cytotoxicity. 1999.

30. Ribeiro M, Morgado P, Miguel S, Coutinho P, Correia I. Dextran-based hydrogel containing chitosan microparticles loaded with growth factors to be used in wound healing. Materials Science and Engineering: C. 2013;33(5):2958-66.

31. Miguel SP, Ribeiro MP, Brancal H, Coutinho P, Correia IJ. Thermoresponsive chitosan–agarose hydrogel for skin regeneration. Carbohydrate Polymers. 2014;111:366-73.

32. Aziz MA, Cabral JD, Brooks HJ, Moratti SC, Hanton LR. Antimicrobial properties of a chitosan dextran-based hydrogel for surgical use. Antimicrobial agents and chemotherapy. 2012;56(1):280-7.

33. Cabañas M, Peña J, Román J, Ramírez-Santillán C, Matesanz M, Feito M, et al. Design of tunable protein-releasing nanoapatite/hydrogel scaffolds for hard tissue engineering. Materials Chemistry and Physics. 2014;144(3):409-17.

34. Rassis D, Saguy I, Nussinovitch A. Collapse, shrinkage and structural changes in dried alginate gels containing fillers. Food Hydrocolloids. 2002;16(2):139-51.

35. Burg KJ, Porter S, Kellam JF. Biomaterial developments for bone tissue engineering. Biomaterials. 2000;21(23):2347-59.

36. Serafim A, Mallet R, Pascaretti-Grizon F, Stancu I-C, Chappard D. Osteoblast-like cell behavior on porous scaffolds based on poly (styrene) fibers. BioMed Research International. 2014;2014.

37. Lange R, Lüthen F, Beck U, Rychly J, Baumann A, Nebe B. Cell-extracellular matrix interaction and physico-chemical characteristics of titanium surfaces depend on the roughness of the material. Biomolecular Engineering. 2002;19(2):255-61.

38. Dos Santos E, Farina M, Soares G, Anselme K. Chemical and topographical influence of hydroxyapatite and ß-tricalcium phosphate surfaces on human osteoblastic cell behavior. Journal of Biomedical Materials Research Part A. 2009;89(2):510-20.

39. Woodard JR, Hilldore AJ, Lan SK, Park C, Morgan AW, Eurell JAC, et al. The mechanical properties and osteoconductivity of hydroxyapatite bone scaffolds with multi-scale porosity. Biomaterials. 2007;28(1):45-54.

40. Yang S, Leong K-F, Du Z, Chua C-K. The design of scaffolds for use in tissue engineering. Part II. Rapid prototyping techniques. Tissue engineering. 2002;8(1):1-11.

41. Kim J, Van der Bruggen B. The use of nanoparticles in polymeric and ceramic membrane structures: review of manufacturing procedures and performance improvement for water treatment. Environmental Pollution. 2010;158(7):2335-49.

42. Tarabara VV. Multifunctional nanomaterial-enabled membranes for water treatment. Nanotechnology Applications for Clean Water. 2009;5:59-75.

43. Wilson C, van Blitterswijk C, Verbout A, Dhert W, de Bruijn J. Scaffolds with a standardized macro-architecture fabricated from several calcium phosphate ceramics using an indirect rapid prototyping technique. Journal of Materials Science: Materials in Medicine. 2011;22(1):97-105.

44. Murugan R, Ramakrishna S. Development of nanocomposites for bone grafting. Composites Science and Technology. 2005;65(15):2385-406.

45. Santos CF, Silva AP, Lopes L, Pires I, Correia IJ. Design and production of sintered ß-tricalcium phosphate 3D scaffolds for bone tissue regeneration. Materials Science and Engineering: C. 2012;32(5):1293-8.

46. Daemi H, Barikani M. Synthesis and characterization of calcium alginate nanoparticles, sodium homopolymannuronate salt and its calcium nanoparticles. Scientia Iranica. 2012;19(6):2023-8.

47. Bose S, Roy M, Bandyopadhyay A. Recent advances in bone tissue engineering scaffolds. Trends in Biotechnology. 2012;30(10):546-54.

48. Salgado AJ, Coutinho OP, Reis RL. Bone tissue engineering: state of the art and future trends. Macromolecular Bioscience. 2004;4(8):743-65.

49. Weinand C, Pomerantseva I, Neville CM, Gupta R, Weinberg E, Madisch I, et al. Hydrogel-ß-TCP scaffolds and stem cells for tissue engineering bone. Bone. 2006;38(4):555-63.

50. Xu X, Yang Q, Wang Y, Yu H, Chen X, Jing X. Biodegradable electrospun poly (L-lactide) fibers containing antibacterial silver nanoparticles. European Polymer Journal. 2006;42(9):2081-7.

51. Olszta MJ, Cheng X, Jee SS, Kumar R, Kim Y-Y, Kaufman MJ, et al. Bone structure and formation: a new perspective. Materials Science and Engineering: R: Reports. 2007;58(3):77-116.

52. Nair BP, Gangadharan D, Mohan N, Sumathi B, Nair PD. Hybrid scaffold bearing polymer-siloxane Schiff base linkage for bone tissue engineering. Materials Science and Engineering: C. 2015;52:333-42.

53. Valente J, Gaspar V, Antunes B, Countinho P, Correia I. Microencapsulated chitosan–dextran sulfate nanoparticles for controled delivery of bioactive molecules and cells in bone regeneration. Polymer. 2013;54(1):5-15.

54. Dempster DW, Raisz LG. Bone Physiology: Bone Cells, Modeling, and Remodeling. Nutrition and Bone Health2015. p. 37-56.

55. Kim S, Choi JE, Choi J, Chung K-H, Park K, Yi J, et al. Oxidative stress-dependent toxicity of silver nanoparticles in human hepatoma cells. Toxicology in Vitro. 2009;23(6):1076-84.

56. AshaRani P, Low Kah Mun G, Hande MP, Valiyaveettil S. Cytotoxicity and genotoxicity of silver nanoparticles in human cells. ACS Nano. 2008;3(2):279-90.

57. Arora S, Jain J, Rajwade J, Paknikar K. Cellular responses induced by silver nanoparticles: in vitro studies. Toxicology Letters. 2008;179(2):93-100.

58. Samberg ME, Loboa EG, Oldenburg SJ, Monteiro-Riviere NA. Silver nanoparticles do not influence stem cell differentiation but cause minimal toxicity. Nanomedicine. 2012;7(8):1197-209.

59. Liao S, Cui F, Zhu Y. Osteoblasts adherence and migration through three-dimensional porous mineralized collagen based composite: nHAC/PLA. Journal of Bioactive and Compatible polymers. 2004;19(2):117-30.

60. Gonzalez R, Tarloff J. Evaluation of hepatic subcellular fractions for Alamar blue and MTT reductase activity. Toxicology in vitro. 2001;15(3):257-9.

61. Arciola CR, Visai L, Testoni F, Arciola S, Campoccia D, Speziale P, et al. Concise survey of Staphylococcus aureus virulence factors that promote adhesion and damage to peri-implant tissues. The International Journal of Artificial Organs. 2011;34(9):771-80.

62. Kim JS, Kuk E, Yu KN, Kim J-H, Park SJ, Lee HJ, et al. Antimicrobial effects of silver nanoparticles. Nanomedicine: Nanotechnology, Biology and Medicine. 2007;3(1):95-101.

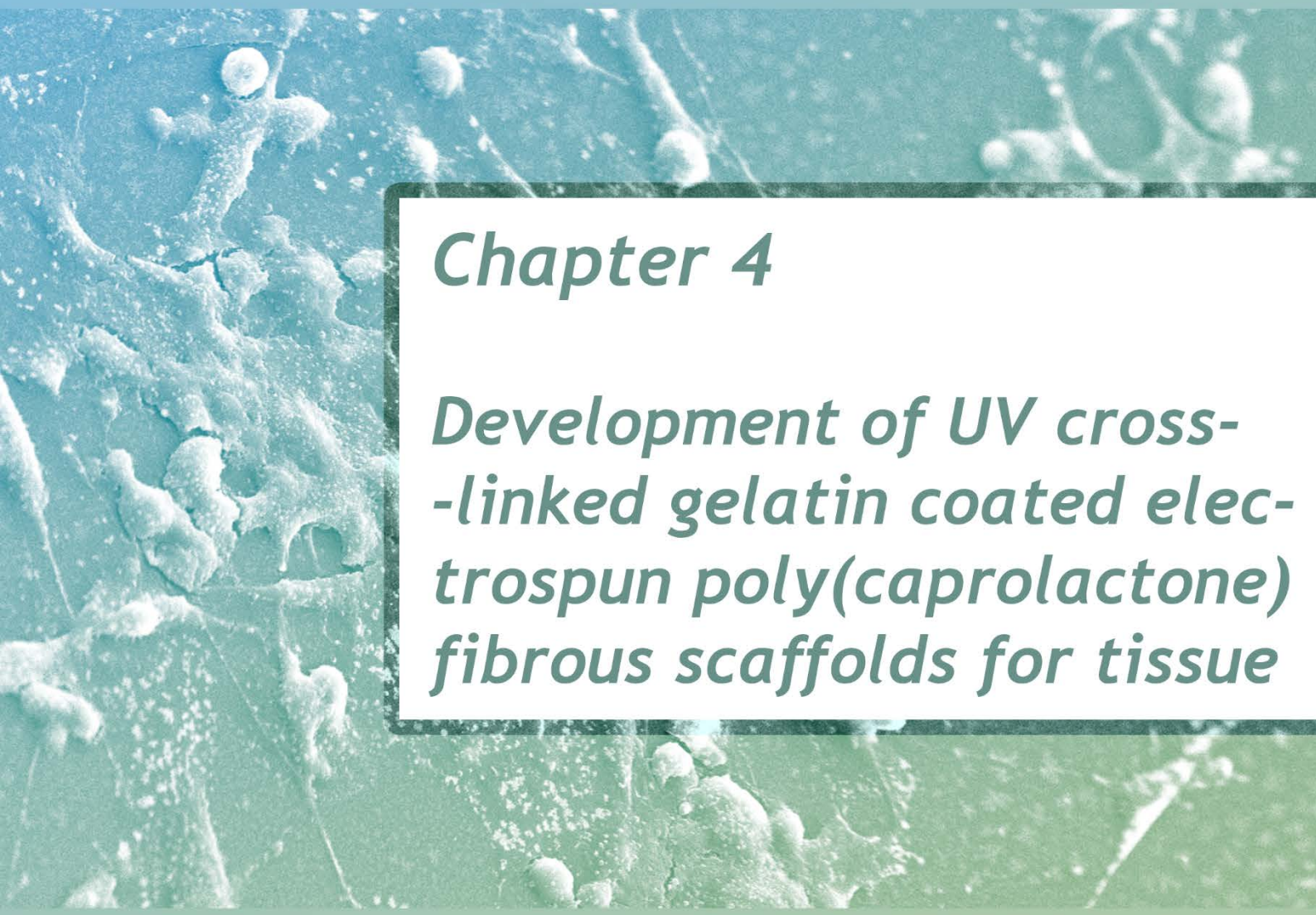

Chapter 4

Development of UV cross--linked gelatin coated electrospun poly(caprolactone) fibrous scaffolds for tissue

4. Development of UV cross-linked gelatin coated electrospun poly(caprolactone) fibrous scaffolds for tissue engineering

T. R. Correia[a], P. Ferreira[b,*], R. Vaz[b], P. Alves[b], M. M. Figueiredo[b], I. J. Correia[a,*], P. Coimbra[b]

[a] CICS-UBI, Health Sciences Research Center, University of Beira Interior, P-6200 506 Covilhã, Portugal

[b] CIEPQPF, Department of Chemical Engineering, University of Coimbra, P-3030 790 Coimbra, Portugal

Abstract

Cardiovascular disease is the leading cause of morbidity and mortality among industrialized countries. Vascular grafts are often required for the surgical treatments. Considering the limitations associated with the use of autografts and with the currently available synthetic materials, a growing demand in tissue engineered vascular grafts has been registered. During the work here described, electrospinning technique was used to prepared fibrous matrices to be applied as vascular implants. For that purpose, electrospun polycaprolactone (PCL) fibrous mats were produced and afterwards coated with different hydrogel formulations based in photocrosslinkable gelatin (GelMA) and the macromers poly(ethylene glycol) acrylate (PEGA) and poly(ethylene glycol) diacrylate (PEGDA). These were further photocrosslinked under UV irradiation using Irgacure® 2959 (by BASF) as the photoinitiator. The suitability of the coated scaffolds for the intended application, was evaluated by assessing their chemical/physical properties as well as their interaction with blood and endothelial cells.

4.1. Introduction

Heart and blood vessel diseases are generally addressed as cardiovascular disease. Such term includes numerous problems, many of which related to a medical condition called atherosclerosis in which a substance called plaque builds up in the walls of the arteries. The result is the thickening and hardening of those arteries as well as the eventual reduction or complete blockage of the blood flow (1). This blockage may be caused by the narrowing of the vessel, by the detachment of a piece of the plaque or by the formation of a clot on the surface of the plaque area. These situations compromise blood flow reducing oxygen supply to organs and other parts of the body and may result in strokes or heart attacks (2). Consequently, cardiovascular disease is the leading cause of death as well as disability among men and women worldwide (3). By the year of 2030, it is projected that cardiovascular disease will be responsible for 25 million deaths worldwide (4). Vascular grafts are generally used to treat such conditions and are mostly needed to bypass obstructed arteries (5), repair aneurisms (6) as well as repair congenital cardiovascular defects in children (7). The currently used vascular grafts fall into two categories: autologous grafts and grafts made from synthetic materials. Although autografts (such as saphenous/arm veins or mammalian/radial artery) remain the standard clinical procedure used for the replacement of small diameter blood vessels (< 6 mm), they present some limitations. These mainly involve the common unsuitability of the necessary vessels caused by previous pathological conditions like phlebitis, varicosities or hypoplasia (8). Also, surgical vessel harvest is generally accompanied by donor site morbidity (9). Synthetic vascular grafts made from expanded polytetrafluoroethylene (PTFE, Gore-Tex®) or polyethylene terephthalate (PET, Dacron®), have been successfully used to replace large diameter blood vessels (≥ 6 mm) in clinical studies. Despite their consistent mechanical properties, these materials lack biocompatibility having poor interaction with vascular cells (10). They also present a thrombogenic character since they generate foreign body reactions triggering local platelet aggregation and thrombosis. This effect prevents them from being used to replace small diameter (< 6 mm) vessels (11). In addition, the synthetic materials used in the clinic have been found to lack growth potential (12), which is critical for children, and often require a second surgery to replace the implants. Current research in tissue engineered grafts, namely for the ones with small diameter, has been focused on the development of optimised scaffolds in which endothelial cells (ECs) may be seeded onto the lumen of the grafts to allow the formation of a monolayer of ECs before implantation. This ECs monolayer mimics the conditions in natural blood vessels and therefore this approach allows the graft to be easily accepted and integrated in the organism circumventing some adverse effects like thrombogenicity (13). Several strategies may be used to optimize both adherence and growth of ECs to the surface of synthetic vascular grafts. One of the most promising ones is the modification of such surfaces with extracellular matrix (ECM) proteins and their derivatives (including collagen, fibronectin or gelatin) (14). Another approach relies on the use of electrospun structures, which possess nanofibrous morphology, a high number of

interconnected pores and high surface to volume ratio (15). These features mimic the ones formed in the ECM of natural tissues and have demonstrated to enable cell growth as well as efficient exchange of nutrients and metabolic wastes between scaffolds and their environment (11). Electrospinning has been used for the fabrication of scaffolds from several biodegradable polymers either synthetic or natural (16). Synthetic polymers include poly(ε-caprolactone) (PCL), poly(lactic acid) (PLA), poly(glycolic acid) (PGA) and the copolymer poly(lactide-co-glycolide) (PLGA). Amongst natural polymers, proteins have been the most used including collagen, elastin and gelatin (17-21). Previous studies showed that electrospun protein scaffolds successfully promoted cell adhesion, migration and proliferation. However, scaffolds prepared from natural components alone are still constrained by fast degradation, total dissolution, and weak mechanical properties (21). Due to these limitations, electrospun scaffolds have been prepared by combining synthetic and natural materials in order to allow the production of materials with optimized mechanical strength and biological interaction (11). In this work, PCL fibrous mats produced by electrospinning are aimed to be used as scaffolds for vascular regeneration. These scaffolds were further coated with different hydrogel formulations based on photocrosslinkable gelatin (GelMA, obtained by reacting gelatin with methacrylic anhydride) and the macromers poly(ethylene glycol) acrylate (PEGA) and poly(ethylene glycol) diacrylate (PEGDA). The macromers solutions were then photocrosslinked under UV irradiation, using Irgacure® 2959 (by BASF) as the photoinitiator. In order to evaluate the coated scaffolds suitability for the intended application, their chemical/physical properties as well as their interaction with biological components, like blood and endothelial cells were assessed.

4.2. Materials and Methods

4.2.1. Materials

CellTiter 96® Aqueous One Solution Reagent (MTS) was purchased from Promega (Madison, USA). Fetal bovine serum (FBS) was purchased from Biochrom AG (Berlin, Germany). Amphotericin B, Eagle's Minimum Essential Medium (MEM), gelatin type A (from porcine skin, 300 bloom), methacrylic anhydride (MAA), polycaprolactone (PCL, M_n ~80 kDa), poly(ethylene glycol) acrylate (PEGA, M_n ~375 Da) and poly(ethylene glycol) diacrylate (PEGDA, M_n ~575 Da), trypsin were purchased from Sigma–Aldrich (Sintra, Portugal). The photoinitiator 1-[4-(2-hydroxyethoxy)phenyl]-2-hydroxy-2-methyl-1-propan-1-one (Irgacure®2959) was kindly provided by Ciba Specialty Chemicals. Anticoagulated rabbit blood (ACD blood), used in the haemocompatibility tests, was bought from PROBIOLÓGICA (Biologic Products Company) (Lisbon, Portugal) and used in the same day it was received. All other chemicals used were of reagent grade and were used as received.

4.2.2. Synthesis of GelMA

The preparation of GelMA has been previously described in detail (22, 23). Briefly, 10 g of gelatin was dissolved in 100 mL of phosphate buffer saline (PBS, pH 7.4) at 50°C, 1 mL of MMA was added under vigorously magnetic stirring conditions, and the mixture was left to react for one hour at 50°C. The reaction mixture was then poured into dialysis bags and dialyzed for 4 days against distilled water at room temperature. After, the reaction products were frozen and freeze-dried during 3 days.

4.2.3. Preparation of PCL fibrous mats

The PCL fibrous mats were produced by electrospinning in a homemade set-up (24). The formulation and operational parameters used were selected based on the data available in literature and also in our own experience. First, a 15% (w/v) PCL solution was prepared by dissolving the polymer in 10 mL of a cosolvent mixture of chloroform (CLF) and dimethylformamide (DMF) (7:3 v/v). The solution was filled into a syringe, which was then placed in a syringe pump (NE-1000 Multiphaser, New Era Pump Systems) and connected with a stainless steel needle through a Teflon tube. The solution was fed into the needle at a constant flow rate of 2.5 mL/h and a positive high voltage (~ 17 kV) was applied, at the tip of the needle, using a high voltage power supply (SL 10W-300W, Spellman). The formed polymeric fibers were collected on a piece of aluminum foil covering an electrically grounded quadrangular copper

plate place about 15-20 cm placed under the needle. At the end, the formed fibrous mats were put in a vacuum oven overnight, in order to evaporate some residual solvent, and then stored in a desiccator until further use.

4.2.4. Coating of the PCL fibrous mats with the photocrosslinkable GelMA based hydrogels

The PCL fibrous mats were coated with six different hydrogel formulations based in GelMA and the macromers PEGA and PEGDA. The hydrogels precursor solutions were prepared in distilled water and divided in two groups: solutions containing a total content of solids (GelMA and macromer) of 1% (w/v) or 10% (w/v). For each group, three formulations were prepared: one containing only GelMA, other with 50% GelMA and 50% PEGA (in weight), and another, composed of 50% GelMA and 50% PEGDA. The photoinitiator Irgacure®2959 (0.015% (w/v)) was added to all formulations. The solutions were prepared at a temperature of 50ºC in a thermostat water bath, and used immediately after preparation. For the coating process, the PCL fibrous mats were cut into strips and submerged in the warm hydrogel precursor solution for about 3 minutes. The strips were then retrieved from the solution and the excess of solution was removed. The impregnated samples were then photocrosslinked using a Multiband UV UVGL-48 model from Mineral Light® Lamp (wavelengths of 254-354nm) during 10 minutes for each side of the sample. After photocrosslinking, the samples were put in a refrigerator at 4ºC overnight and in the next day dried in a vacuum oven at room temperature.

4.2.5. Surface characterization of the coated PCL fibrous mats

The surface morphologies of the uncoated and coated PCL fibrous mats were analyzed by scanning electron microscopy (SEM). The samples were placed on double-sided graphite tape, attached onto a metal surface, and sputter-coated with gold. SEM images were acquired at 10 kV with a JSM-5310 (JEOL, Japan) scanning electron microscope. The average fibers diameter and size distribution of the uncoated PCL fibrous mats were estimated from SEM images, using the image analysis software ImageJ (ImageJ 1.46r; 2012). Samples were also analyzed by Fourier transform infrared-attenuated total reflectance (FTIR-ATR) spectroscopy in order to obtain evidences of the presence of GelMA at the surface of the coated PCL fibrous mats. A JASCO FT-IR-4200 spectrometer equipped with a Golden Gate Single Reflection Diamond ATR accessory was used to acquire the spectra in the range of 500-4000 cm^{-1}, at 128 scans and with a resolution of 4 cm^{-1}. The water contact angles of the uncoated and hydrogel coated PCL mats were measured with a Dataphysics OCA-20 contact angle analyzer (DataPhysics Instruments, Filderstadt, Germany) using the sessile drop method. The samples were attached to a glass slide and placed in the sample stage. A droplet of deionized water (10 µL) was

automatically dispersed onto the sample surface and its evolution with time was recorded with a CCD video camera attached to the equipment. From the film frames, the water contact angles along time were automatically calculated by the equipment software.

4.2.6. Blood compatibility

Blood compatibility assays were performed *in vitro* according to the International Standard Organization (ISO) 10993-4 (25). For each prepared PCL fibrous mats (n=3), both haemolytic potential and thrombogenicity were evaluated. The haemolysis tests were performed as described in the American Society for Testing and Materials (ASTM) F 756-00 standard (26). Shortly, mats with 21 cm^2 were incubated at 37ºC, for 72 hours, in 7 mL of PBS (10 M, pH=7.4). Afterwards, the samples were removed and incubated with diluted anticoagulated rabbit blood (ACD blood) (10 mg/mL ± 1 mg/mL) at 37ºC, for 3 hours, and gently inverted twice every 30 minutes to maintain materials in contact with blood. Positive (+) (total haemolysis) and negative (-) controls were obtained by adding rabbit blood to distilled water and PBS solution, respectively. After centrifugation at 750×g (15 min), the haemoglobin released by haemolysis ([Hb]) was measured by optical density of the supernatants at 540 nm using a spectrophotometer UV-vis (Jasco V550) (25, 26). The percentage of haemolysis (HI) was determined according to equation 1.

$$HI = \frac{[Hb]_{test} - [Hb]_{negativecontrol}}{[Hb]_{positivecontrol} - [Hb]_{negativecontrol}} \times 100 \qquad (1)$$

According to the ASTM F 765-00 (26) materials are classified as non-haemolytic when 0 > HI > 2, slightly haemolytic when 2 > HI > 5 and haemolytic when HI > 5.

The evaluation of thrombus formation on the mats surface was carried out by gravimetric analysis, using an adaptation of the method described by Imai and Nose (27). The mats were first immersed in a PBS solution (pH 7.4) and incubated at 37ºC, for 48h. Then, PBS was removed and 250 µL of ACD blood was carefully placed on the surface of each mat. Blood clotting was initiated by adding 25 µL of 0.10 M $CaCl_2$. The samples were then incubated at 37ºC and after 40 minutes coagulation was interrupted, by addition of 5 mL of water. The resultant clots were fixed with 1 mL of 36% (w/w) formaldehyde solution and then dried at 37ºC, until a constant weight be attained. The percentage of thrombogenicity was determined by using equation 2.

$$\%thrombogenicity = \frac{m_{test} - m_{negativecontrol}}{m_{positivecontrol} - m_{negativecontrol}} \times 100 \qquad (2)$$

4.2.7. Proliferation of corneal endothelial cells in presence of PCL fibrous mats

Rabbit corneal endothelial cells (CEC) were isolated as previously described (28) and were seeded in 25 cm^2 T-flasks, using as culture medium MEM with heat-inactivated FBS (10% v/v) and growth factors (fibroblast growth factor (FGF), epidermal growth factor (EGF), nerve growth factor (NGF)). After cells attained confluence, they were trypsinized by a 3–5 min incubation in 0.18% trypsin (1:250) and 5 mM EDTA. Subsequently, cells were centrifuged, resuspended in culture medium and then seeded in T-flasks of 75 cm^2. Hereafter, cells were kept in a 5% CO_2 humidified atmosphere, at 37°C, inside an incubator (29, 30). To characterize cell behavior in the presence of the different materials, membranes were placed in a 96-well plates and sterilized by UV exposure for at least 30 minutes. Then CEC were cultured at a density of $2x10^4$ cells/well. Cell growth was monitored using an Olympus CX41 inverted light microscope (Tokyo, Japan) equipped with an Olympus SP-500 UZ digital camera for 24, 48 and 72 hours.

4.2.8. Characterization of the cytotoxicity profile of the PCL fibrous mats

In order to evaluate the cytotoxic profile of the PCL fibrous mats, CEC ($2x10^4$ cells/well) were seeded in the presence of the materials, in 96-well plates, with 100 µL of MEM. Then samples were incubated at 37ºC, in a 5% CO_2 humidified atmosphere. After different incubation periods (24, 48 and 72 hours), cell viability was assessed through a MTS assay. To do so, a mixture of 100 µL of fresh medium and 20 µL of MTS was added to each sample and then they were incubated for 4 hours, at 37°C, in a 5% CO_2 atmosphere. The absorbance of each well was determined at 492 nm using a microplate reader (Biorad xMark microplate spectrophotometer). Wells containing cells in the culture medium without materials were used as negative control (K^-). EtOH 96% was added to wells containing cells to be used as a positive control (K^+) (29, 30). Statistical analysis of the obtained results was performed using one-way ANOVA with the Newman-Keuls post hoc test.

4.2.9. Cell-PCL fibrous mats interaction analysis

Scanning Electron Microscopy (SEM) analysis was performed to characterize the cellular attachment on membranes surface. Herein, CEC ($2x10^4$ cells/well) were seeded onto the surface of the materials placed on 96-well plate. After each period of incubation (24, 48 and 72 hours), samples were washed with PBS at room temperature and fixed overnight with 2.5% (v/v) glutaraldehyde. Subsequently, membranes were frozen using liquid nitrogen, freeze-dried

for 3 hours, mounted on aluminum stubs with Araldite glue and finally sputter-coated with gold using a Quorum Q150R ES sputter coater. SEM images were then acquired with different magnifications, at an acceleration voltage of 20kV, using a Hitachi S-3400N Scanning Electron Microscope (29).

4.3. Results and Discussion

Gelatin methacrylamide (GelMA) is a gelatin derivative with pendent methacrylamide moieties susceptible of undergoing radical polymerization when exposed to UV irradiation in the presence of an appropriated photoinitiator (22, 23, 31). The synthesis of GelMA involves the reaction the ε-amino groups in gelatin with MAA (Fig. 4.1a). By employing different amounts of MMA it is possible to control the degree of substitution (DS) of the obtained GelMA derivatives (i.e. the percentage of ε-amino groups substituted by methacrylamide groups), and in this way to produce photocrosslinked GelMA hydrogels with different properties (22, 23, 31). In this work, GelMA was prepared according to the original procedure reported by Van den Bulcke et al (22), using a molar ratio of MAA to free NH_2 groups of 2:1, which according to our previous work originates a GelMA with a DS of about 75% (determined through a colorimetric method based on the reagent 2,4,6-trinitrobenzene sulfonic acid (TNBS)) (32). The photocrosslinking ability and the tunable physicochemical properties of GelMA, allied with its remarkable biological properties – that include excellent biocompatibility, non-immunogenicity and an outstanding capacity to promote cell adhesion and grow - make this gelatin derivative a very popular material for tissue engineering applications (31). Further, by combining GelMA with other photocrosslinkable synthetic components, such as the macromeres PEGA and PEGDA used in this work (Fig 4.1b), it is possible to improve the mechanical properties and slowdown the enzymatic degradation of the resultant material, which can be important in many tissue engineering applications (33).

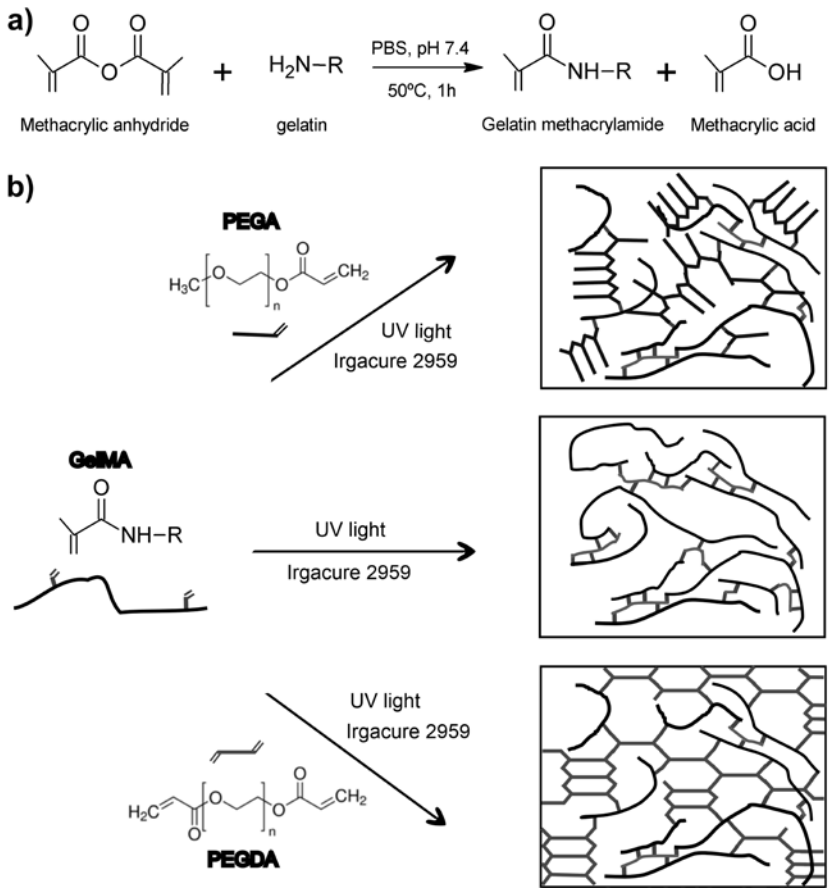

Figure 4.1 Schematic representation of gelatin functionalization reaction (a) and hydrogels network formation (b).

4.3.1. Surface characterization of the coated PCL fibrous mats

The surface morphology of the uncoated and hydrogel-coated PCL fibrous mats can be observed in Fig. 4.2. Neat PCL mats were formed by continuous fibers with an average diameter of around 1.8 µm, displaying smooth surfaces without visible pores (Fig. 4.2a). Figs. 4.2b, 4.2d and 4.2f show the morphology of the coated PCL mats prepared with 1% (w/v) hydrogel precursor solutions. Evidences of a hydrogel coating on the surface of the fibers can be observed not only by the appearance of roughness on the fibers surface but also by the irregularity of the fibers contours. It was also noticed that the hydrogel partially filled the spaces formed between the fibers, reducing the inter-fibers porosity. These same features can be perceived in a more noticeable way for the PCL-GelMA-PEGA-10 and PCL-GelMA-PEGDA-10 mats, coated with 10% (w/v) hydrogel precursor solutions (Fig. 4.2e and 4.2g). As for the PCL-GelMA-10 mats, coated with a 10% GelMA precursor solution (Fig. 4.2c), the coating treatment resulted in the total cover of the mat's surface by a relatively thick and dense GelMA film. This outcome is a consequence of the high viscosity of the 10% GelMA solution when compared to the viscosities

of the other precursor solutions. The relatively high viscosity restricted the infiltration of the solution throughout the inter-fiber pores and favored the quick setting of the solution at the surface of the mat –due to physical gelation- when the mat was removed from the harm GelMA precursor solution.

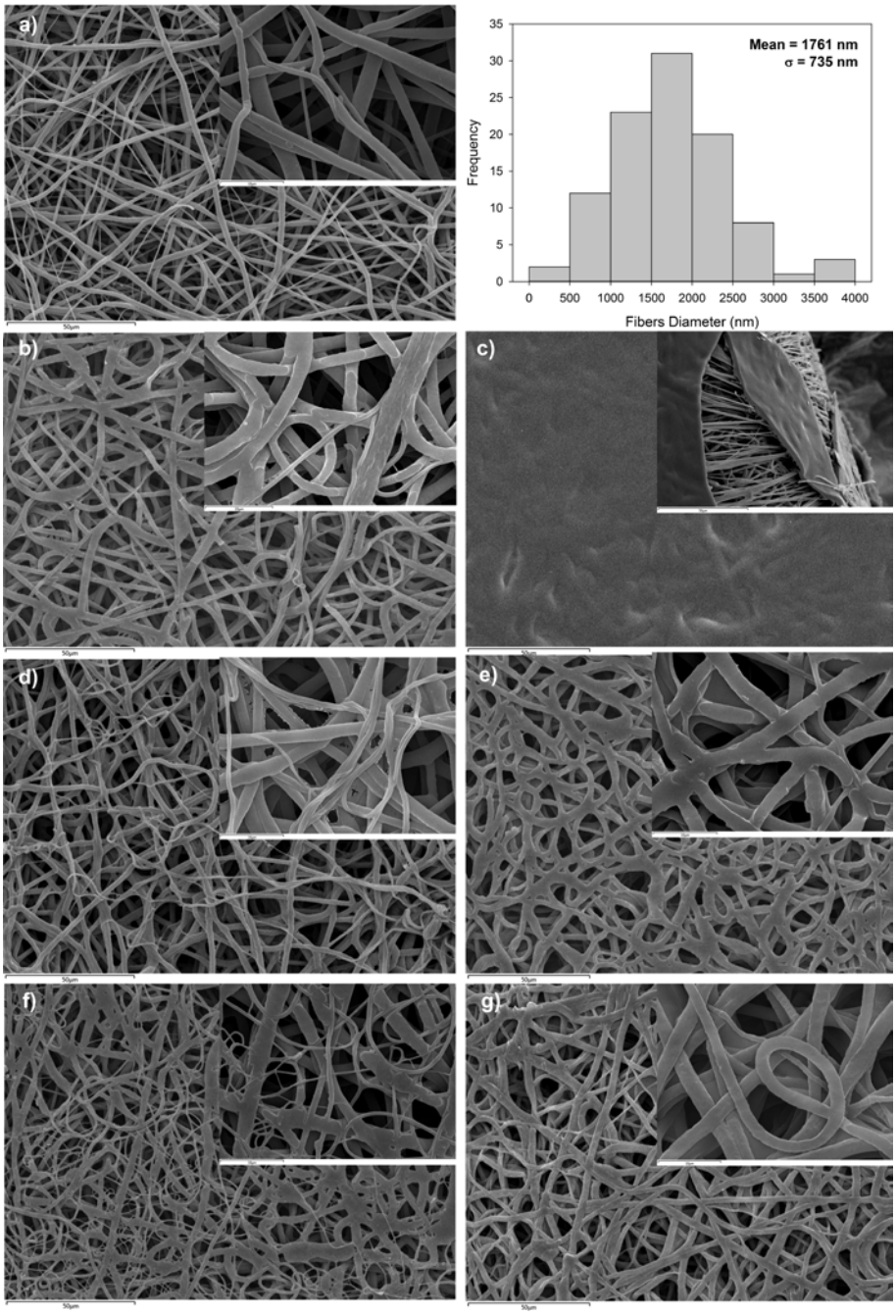

Figure 4.2. SEM images of the surface morphology of the uncoated PCL mats (a) and hydrogel-coated mats PCL-GelMA-1 (b), PCL-GelMA-10 (c), PCL-GelMA-PEGA-1 (d), PCL-GelMA-PEGA-10 (e), PCL-GelMA-PEGDA-1 (f), and PCL-GelMA-PEGDA-10 (g). Amplifications: 750× (main figures) and 3500× (inserted figures, except insert (c), that has an amplification of 1000×). Top right: fibers diameter distribution of the uncoated PCL mats.

ATR-FTIR spectra were acquired in order to confirm the presence of GelMA on the surface of the coated PCL mats. Fig. 4.3 shows the spectra of PCL, of GelMA (after photocrosslinking) and of the coated samples. The most informative region of these spectra is situated between 2000 and 1500 cm^{-1}, where the strongest vibrational bands of both PCL and GelMA appear. They are the carbonyl stretching band of PCL (C=O), situated around 1725 cm^{-1} (34), and the amide I (1700-1600 cm^{-1}) and amide II (1565 – 1520 cm^{-1}) bands of the amide bond in GelMA (35). The spectra of the PCL mats coated with 1% precursor hydrogel solutions (Fig. 4.3a) showed that the gelatin´s amide I and amide II bands appear with very weak intensities immediately after the C=O stretching vibration of PCL, which make them almost imperceptible. This is quite evident for the coatings PCL-GelMA-PEGDA-1 and PCL-GelMA-PEGA-1. In contrast, in the spectra of PCL-GelMA-PEGDA-10 and PCL-GelMA-PEGA-10, that were coated with 10% precursor solutions (Fig. 4.3b), the amide bands have stronger intensities, which indicates the presence of a higher amount of gelatin chains at the surface of the samples – i.e., a thicker coating, as was expected and as the SEM images indicated. As for the PCL-GelMA-10 coating, its spectrum is identical to the one of GelMA, without the possibility of attributing any visible bands to PCL. This indicates that the PCL mat was totally coated with a GelMA film, as can be observed in the SEM images.

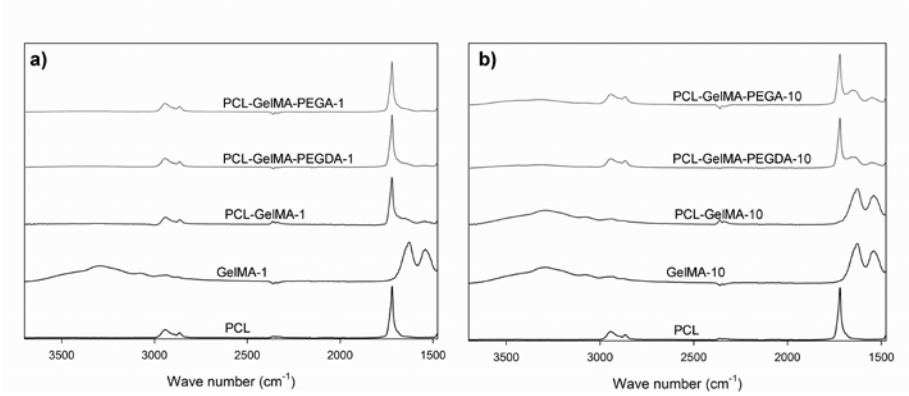

Figure 4.3 ATR-FTIR spectra of the coated PCL mats with 1% (w/v) hydrogel precursor solutions (a) and 10% (w/v) hydrogel precursor solutions (b).

The effect of the hydrogel coatings in the wettability characteristics of the PCL fibrous mats was accessed by time-dependent water contact angle measurements, presented in Fig. 4.4. The uncoated PCL mat displayed an initial water contact angle of 140º, that remained constant for all the recorded time (180s), attesting the elevated hydrophobicity and extremely poor water wettability of the PCL mats. These features are not only due to the hydrophobic nature of PCL but also to the topography of the mats surface. For example, electrospun mats usually display higher water contact angles than the angles observed in smooth surface films (36-38). In fact, the hydrophobicity and wetting characteristics of electrospun films are not only determined by the surface chemistry but are also extremely affected by fibers´ morphology and orientation and also by mats porosity (36-39). As can be seen in Fig. 4.4, and

as expected, the hydrogel coating clearly improved the wettability of the PCL mats. However, distinctive water contact angle profiles were obtained for the different hydrogel formulations. For the 10% hydrogel coatings, the water contact angles displayed a slowly and gradual decrease along time, while the water contact angles of the 1% hydrogel coatings, namely the PCL-GelMA-PEGA-1 and PCL-GelMA-PEGDA-1, decreased faster, reaching the 0º in 60 - 80 secs. The water contact angle profile of the sample PCL-GelMA-1 displayed somehow a distinctive behavior, exhibiting a rapid decrease in the first seconds before stabilizing and remaining almost constant for the rest of the recorded time. These different profiles result probably from the effects and interactions of two factors: the different hydrogels chemical compositions and the different extension in which each coating affects the inter-fibers porosity of the mats. As could be observed in the SEM images, the 10% hydrogel solutions based coatings substantially reduced the porosity of the mats, reducing in this way the contribution of the capillary effect for the water absorption (39), and probably explaining the smooth dynamic contact angle profiles registered for these coatings. In contrast, the porosity of the mats coated with the 1% hydrogel solutions was less affected by the coating process, implicating a higher contribution of the porosity – and the capillary effect associated with it – in the water absorption mechanism and, consequentially, in the dynamic water contact angles. On the other hand, the effect of the chemical composition of the hydrogels must also be considered. Compared to the PEG macromers, the GelMA was relatively more hydrophobic (40), which means that the hydrogel coatings that incorporate PEGA or PEGDA will be more hydrophilic than the ones constituted only by GelMA. This is supported by the initial contact angles (t = 0 s) obtained for the different hydrogel coatings (Fig. 4.4). For example, the initial contact angle of PCL-GelMA-10 was approximately 120º, while the initial contact angles of PCL-GelMA-PEGA-10 and PCL-GelMA-PEGDA-10 were around 80º. Similarly, the initial contact angle of PCL-GelMA-1 was approximately 100º, in contrast with the initial contact angles of GelMA-PEGA-1 and PCL-GelMA-PEGDA-1 that presented values close to 70º and 40º, respectively.

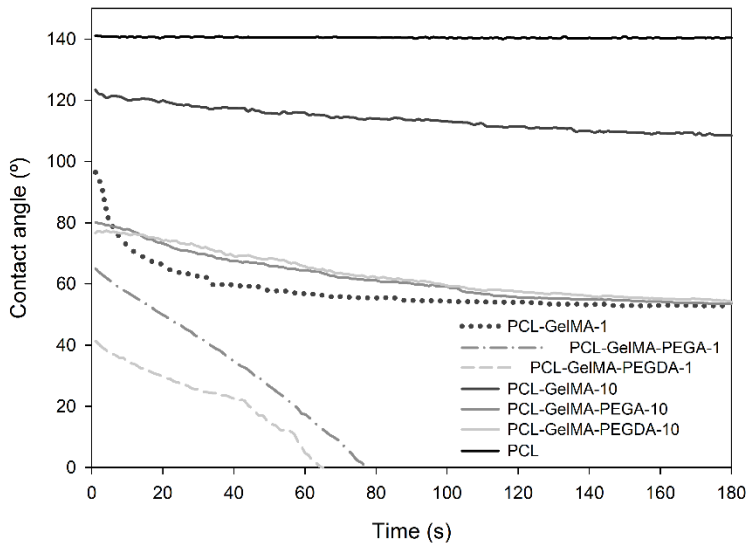

Figure 4.4. Water contact angles in function of time for the uncoated and hydrogel coated PCL mats.

4.3.2. Blood compatibility

The haemolysis index (HI) of the uncoated and hydrogel-coated PCL fibrous mats was evaluated according to ASTM F 756-00 (26) using the cyanmethemoglobin method. This method allows the quantification of minor levels of plasma hemoglobin that may not be measurable under *in vivo* conditions (41). Fig. 4.5 shows the results of the haemolysis test performed by direct and indirect contact between the mats and blood.

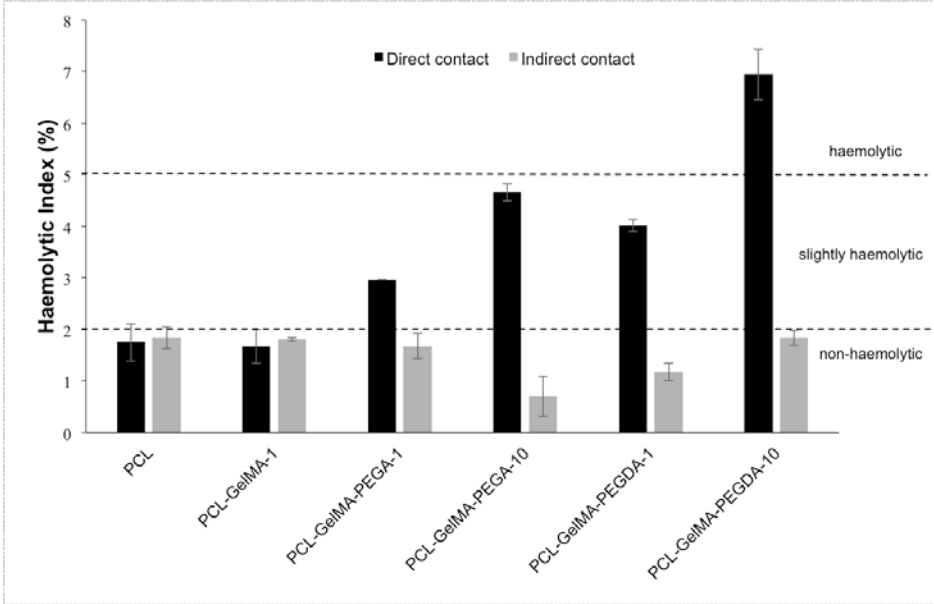

Figure 4.5. Values of % haemolysis (HI) of the samples in direct contact with ACD blood and of the samples after incubation in PBS (indirect contact). Data are expressed as mean±SME (n= 3).

A notable result was obtained for the PCL-GelMA-10 mat. It was impossible to measure the haemolytic index of this mat through direct and indirect contact, since the mat absorbed the blood and PBS, respectively, due to its total cover of the mat's surface by a relatively thick and dense GelMA film, observed in the SEM images in (Fig. 4.2c). Looking at the direct contact results presented in Fig. 4.5, the uncoated PCL mat and PCL-GelMA-1 mat were non-haemolytic, while the remaining samples showed to be slightly haemolytic, except the mat PCL-GelMA-PEGDA-10, which presented a haemolytic effect. However, it is important to notice that after the mats were incubated in PBS (indirect contact) the haemolysis results dropped to non-haemolytic values. This indicates that the disruption of the erythrocyte membranes and consequent Hb release was caused by components that were effectively washed away by the PBS. To evaluate the ability of thrombus formation on the surface of the produced mats, the percentage of thrombogenicity was calculated and expressed as mean ± standard error of the mean (Fig. 4.6). When materials are designed to be applied as vascular implants, no clots can be formed on their surface or otherwise an arterial embolism may occur. The obtained results showed that all mats have a tendency to form clots, and therefore have a slight thrombogenic character. From Fig. 4.6 it is evident that the samples with 10% have the higher tendency to induce clots formation, probably due to the presence of the GelMA layer which induced a lower surface energy. The thrombogenic capacity is related to the strong and irreversible adsorption of proteins to the surface of the films, improved by low values of surface energy (42). Low surface energy results are reported to be an important factor on the first stage of the coagulation cascade that ends in thrombus formation (43). Since all the mats show some ability to induce the thrombus formation, the incorporation of an antiplatelet drug should be envisioned in order to avoid platelet aggregation and thrombus formation.

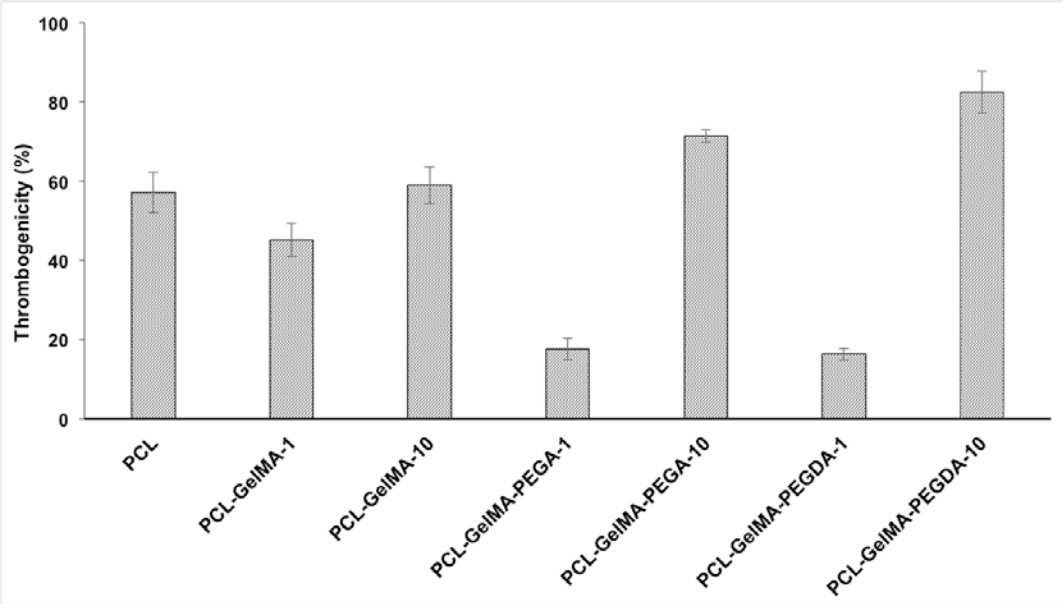

Figure 4.6 Values of % thrombogenicity obtained for each sample after 40 minutes of contact with blood. Thrombogenicity was calculated and expressed as mean ± standard error of the mean±SME (n= 3).

4.3.6. Characterization of the PCL fibrous mats biocompatibility

The PCL fibrous mats cytotoxic profile was assessed through *in vitro* studies. At each incubation time period (24, 48 and 72 hours), cell adhesion and proliferation was monitored using an inverted light microscope (Fig. 4.7 and Fig. 4.8). During the 72 hours, the cells in contact with PCL, PCL-GelMA-1, PCL-GelMA-10 mats were able to proliferate, like in the negative control (K^-). For the same time point, PCL-GelMA-PEGA-10, PCL-GelMA-PEGDA-1, PCL-GelMA-PEGDA-10 mats and positive control (K^+) displayed cells with spherical shape, *i.e.* dead cells.

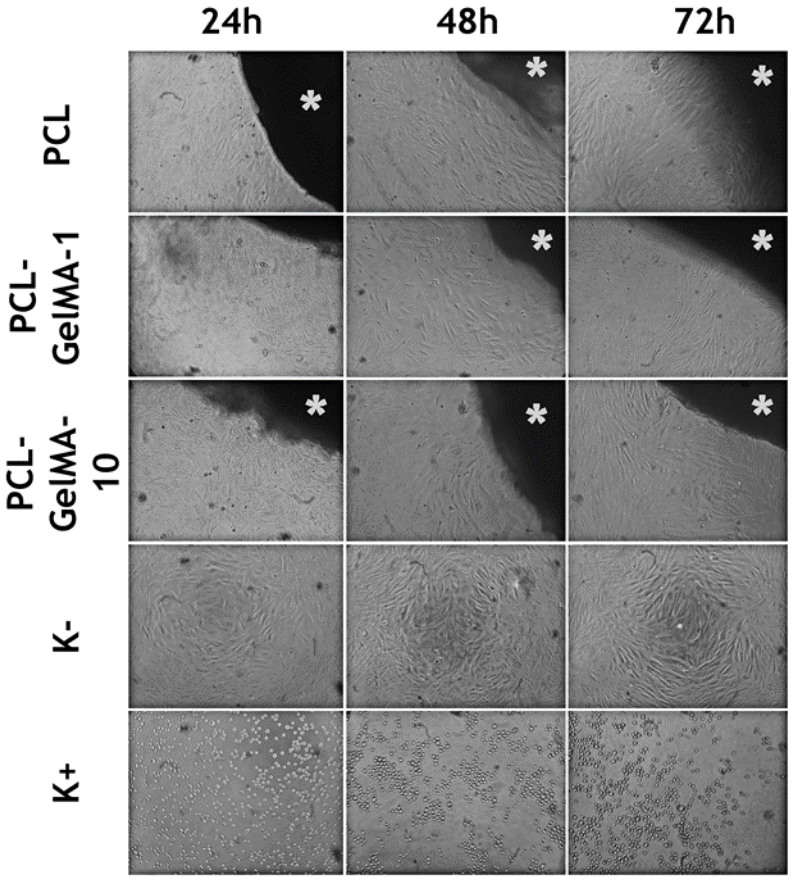

Figure 4.7. Microscopic images of CEC in contact with the PCL, PCL-GelMA-1 and PCL-GelMA-10 mats after 24, 48 and 72 hours of incubation at a magnification of 100×.

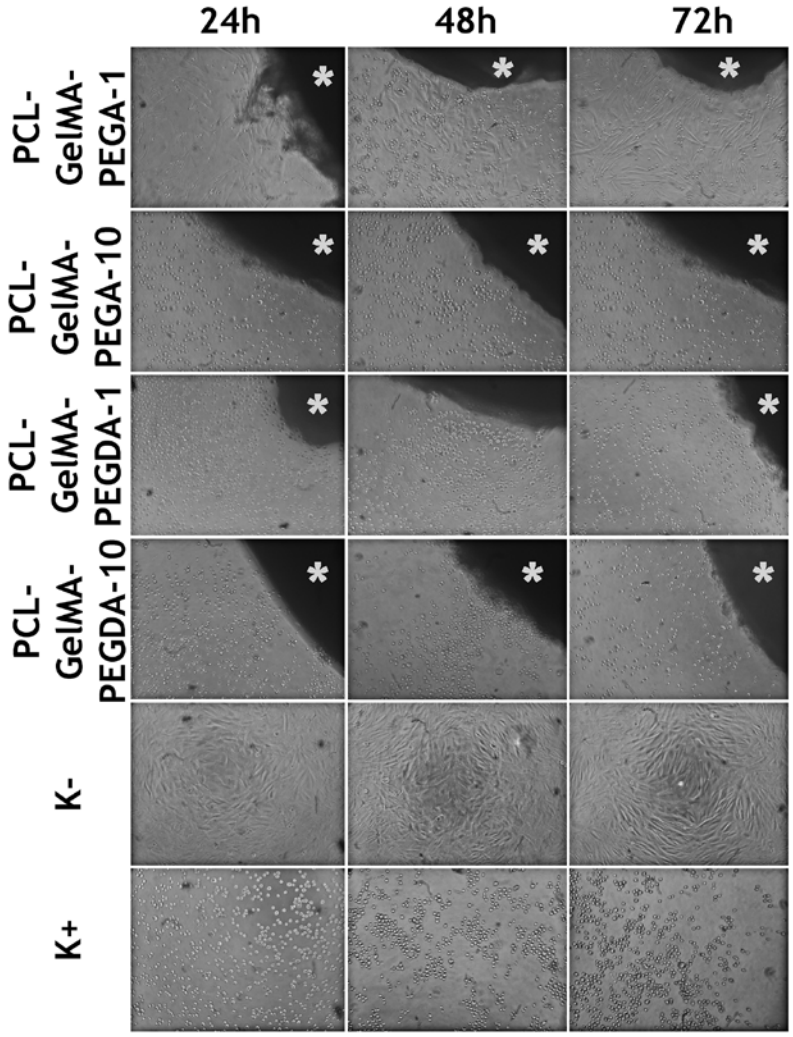

Figure 4.8 Microscopic images of CEC in contact with the PCL-GelMA-PEGA-1, PCL-GelMA-PEGA-10, PCL-GelMA-PEGDA-1 and PCL-GelMA-PEGDA-10 mats after 24, 48 and 72 hours of incubation at a magnification of 100×.

Furthermore, a MTS assay was also performed to characterize cell viability in the presence of mats (Fig. 4.9). The obtained results showed that after 72 hours of incubation, the PCL, PCL-GelMA-1, PCL-GelMA-10 mats in contact with CEC did not trigger any cytotoxic effect, whereas the materials PCL-GelMA-PEGA-1, PCL-GelMA-PEGA-10, PCL-GelMA-PEGDA-1 and PCL-GelMA-PEGDA-10 induced high levels of toxicity. Such results can be explained by the incorporation of PEGA and PEGDA macromers on mats coating. In literature it is described that a 4-arm PEGA, on its pure state, can induce cell cytotoxicity (44). In addition, Zhu et al. previously showed that cells displayed a higher adhesion and proliferation in contact with a PEGDA hydrogel than with PEGDA macromere counterpart (45). Moreover, in another study performed by Shin and collaborators it was reported that after 24 hours, cell viability is dependent on PEGDA concentration, i.e. higher concentrations of PEGDA were able to reduce cell viability (46).

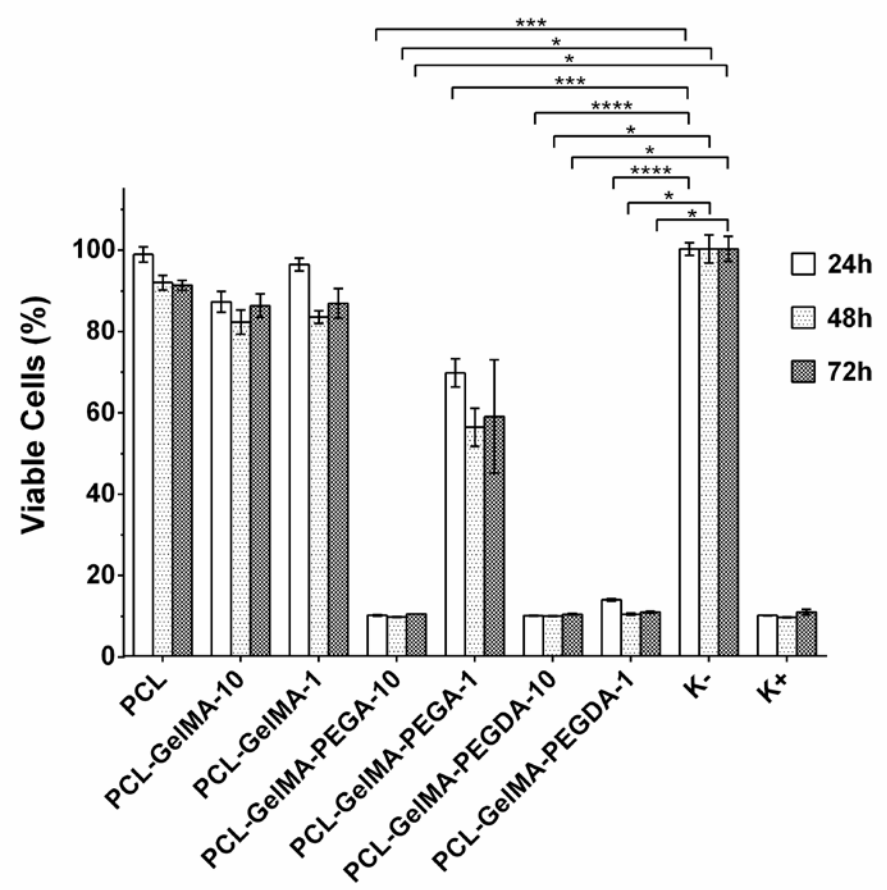

Figure 4.9. Characterization of cell viability when cultured in contact with the different PCL fibrous mats after 24, 48 and 72 hours; live cells (K-); dead cells (K+). Each result represents the mean ± standard deviation of the mean of at least three independent experiments. Statistical analysis was performed using one-way ANOVA with Newman-Keuls post hoc test (* $p<0.05$, *** $p\leq 0.001$, **** $p\leq 0.0001$).

4.3.7. Cell- PCL fibrous mats interaction analysis

Cell–PCL fibrous mats interaction were assessed *in vitro* by seeding CEC on the materials surface for 72 hours. As can be observed seen in Fig.4.10 and Fig. 4.11, cells were able to adhere at the surface of the materials after 24 hours of incubation. However, only PCL, PCL-GelMA-1, PCL-GelMA-10 mats allowed cell spreading and proliferation after 48 hours of incubation. At 72 hours, in accordance to the results previously obtained in the MTS, only PCL, PCL-GelMA-1, PCL-GelMA-10 mats allowed cell spreading on their surfaces.

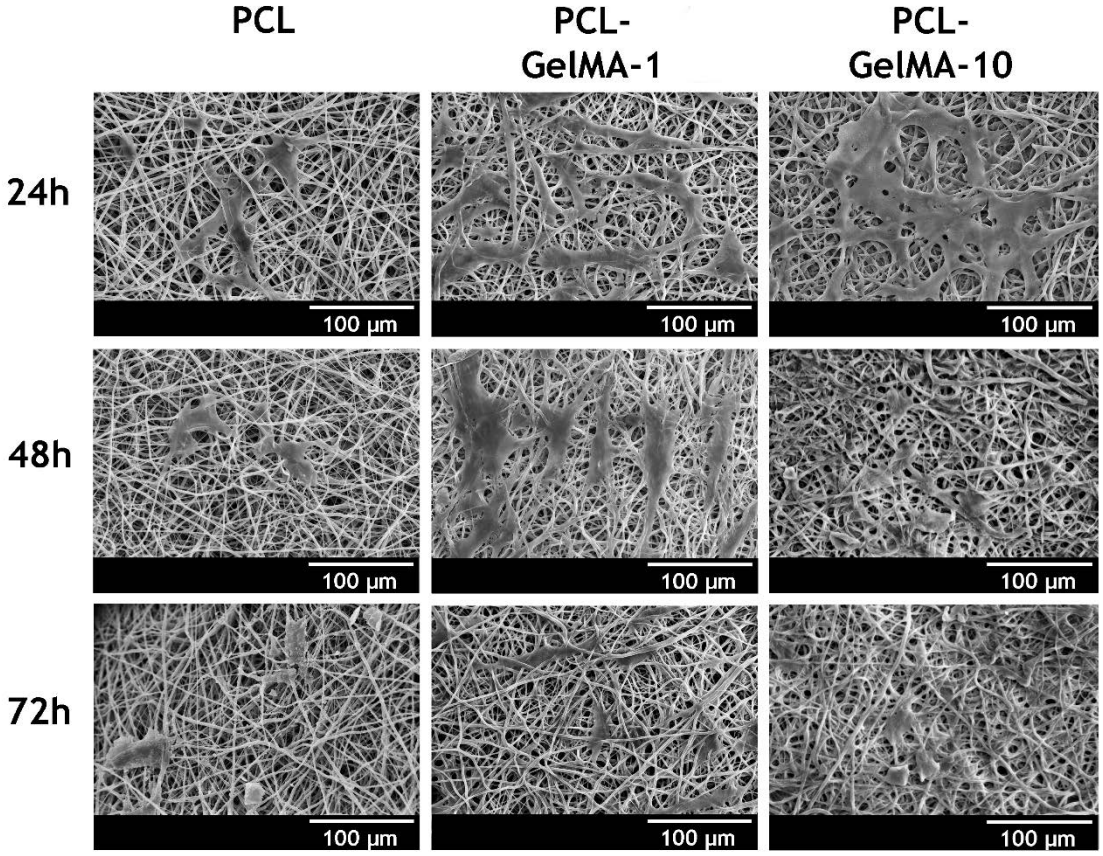

Figure 4.10 SEM images of cells interacting with PCL, PCL-GelMA-1 and PCL-GelMA-10 membranes surface after 24, 48 and 72 hours of incubation.

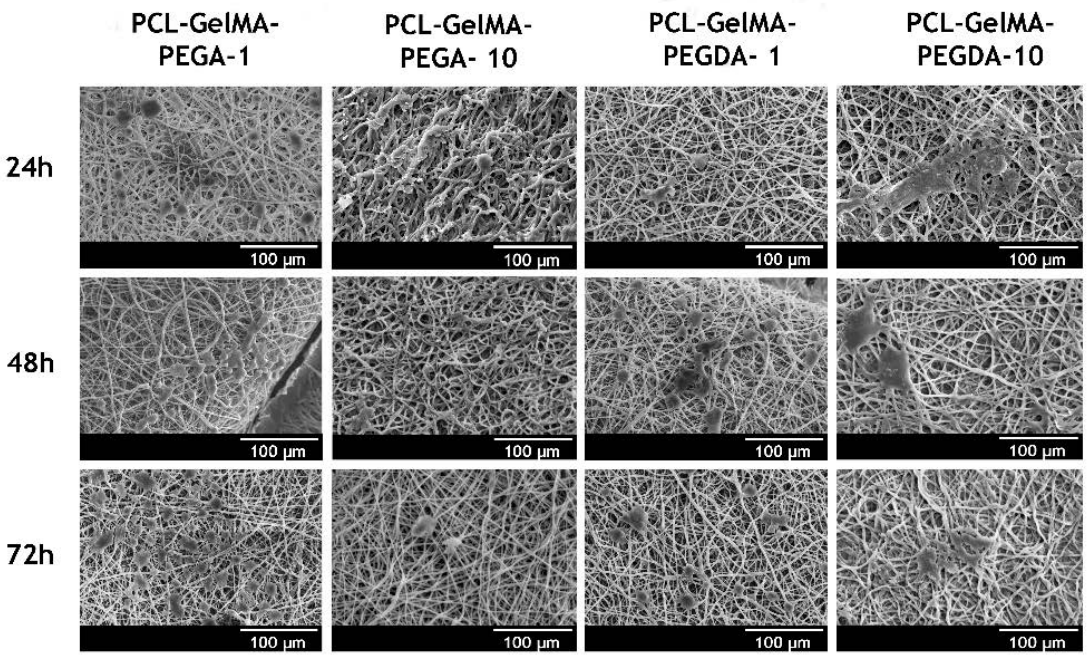

Figure 4.11 SEM images of cells interacting with PCL-GelMA-PEGA-1, PCL-GelMA-PEGA-10, PCL-GelMA-PEGDA-1 and PCL-GelMA-PEGDA-10 membranes surface after 24, 48 and 72 hours of incubation.

4.4. Conclusions

PCL fibrous mats were successfully coated with several hydrogel formulations constituted by GelMA, a photocrosslinkable gelatin derivative with favourable biological properties, and two PEG based photopolymerizable macromers. The presence of the coatings was confirmed by ATR-FTIR analysis and by SEM. The SEM images also revealed that the thickness of the coating could be controlled by manipulating the GelMA concentration in the hydrogel precursor solutions. The water contact angle analysis proved that the hydrophilicity and wettability of the PCL mats were drastically improved by the application of the coatings, especially for the hydrogel coatings incorporating the two photocrosslinked PEG macromers. Further, cells were able to adhere and proliferate at the surface of the PCL, PCL-GelMA-10 and PCL-GelMA-1 materials during the time frame of the study. Accordingly, in the blood compatibility evaluation tests, the mats showed to be non-haemolytic when previously incubated in PBS (indirect contact), although they present a slight thrombogenic character. To assess this performance limitation, the incorporation of an antiplatelet drug into the mats for avoiding platelet aggregation and also inhibit thrombus formation should now be considered for future application of fibrous mats as vascular implants.

Acknowledgments

Authors would like to acknowledge funding from FEDER (POCI-COMPETE 2020, project number 007491) and Portuguese Science Foundation (FCT) (UID/Multi/00709). Patrícia Coimbra (SFRH-BPD-73367-2010), Patrícia Alves (SFRH/BPD/69410/2010) and Paula Ferreira (SFRH/BPD/86338/2012) gratefully acknowledge FCT for the financial support.

4.5. References

1. Fortier A, Gullapalli V, Mirshams RA. Review of biomechanical studies of arteries and their effect on stent performance. IJC Heart & Vessels. 2014;4:12-8.

2. Jamkhande PG, Chandak PG, Dhawale SC, Barde SR, Tidke PS, Sakhare RS. Therapeutic approaches to drug targets in atherosclerosis. Saudi Pharmaceutical Journal. 2014;22(3):179-90.

3. Appelman Y, van Rijn BB, Monique E, Boersma E, Peters SA. Sex differences in cardiovascular risk factors and disease prevention. Atherosclerosis. 2015;241(1):211-8.

4. Okwuosa IS, Lewsey SC, Adesiyun T, Blumenthal RS, Yancy CW. Worldwide disparities in cardiovascular disease: Challenges and solutions. International journal of cardiology. 2016;202:433-40.

5. He W, Nieponice A, Soletti L, Hong Y, Gharaibeh B, Crisan M, et al. Pericyte-based human tissue engineered vascular grafts. Biomaterials. 2010;31(32):8235-44.

6. Rodrigues A, Figueiredo L, Bordado J. Abrasion behaviour of polymeric textiles for endovascular stent-grafts. Tribology International. 2013;63:265-74.

7. Patterson JT, Gilliland T, Maxfield MW, Church S, Naito Y, Shinoka T, et al. Tissue-engineered vascular grafts for use in the treatment of congenital heart disease: from the bench to the clinic and back again. Regenerative medicine. 2012;7(3):409-19.

8. Chlupac J, Filova E, Bacakova L. Blood vessel replacement: 50 years of development and tissue engineering paradigms in vascular surgery. Physiological Research. 2009;58:S119.

9. Catto V, Farè S, Freddi G, Tanzi MC. Vascular tissue engineering: Recent advances in small diameter blood vessel regeneration. ISRN Vascular Medicine. 2014;2014.

10. Wise SG, Waterhouse A, Michael P, Ng MK. Extracellular matrix molecules facilitating vascular biointegration. Journal of functional biomaterials. 2012;3(3):569-87.

11. Fu W, Liu Z, Feng B, Hu R, He X, Wang H, et al. Electrospun gelatin/PCL and collagen/PLCL scaffolds for vascular tissue engineering. Int J Nanomedicine. 2014;9:2335-44.

12. Hibino N, McGillicuddy E, Matsumura G, Ichihara Y, Naito Y, Breuer C, et al. Late-term results of tissue-engineered vascular grafts in humans. The Journal of Thoracic and Cardiovascular Surgery. 2010;139(2):431-6. e2.

13. Elsayed Y, Lekakou C, Labeed F, Tomlins P. Fabrication and characterisation of biomimetic, electrospun gelatin fibre scaffolds for tunica media-equivalent, tissue engineered vascular grafts. Materials Science and Engineering: C. 2016;61:473-83.

14. He W, Ma Z, Teo WE, Dong YX, Robless PA, Lim TC, et al. Tubular nanofiber scaffolds for tissue engineered small-diameter vascular grafts. Journal of biomedical materials research Part A. 2009;90(1):205-16.

15. Bagnasco DS, Ballarin FM, Cymberknop L, Balay G, Negreira C, Abraham G, et al. Elasticity assessment of electrospun nanofibrous vascular grafts: A comparison with femoral ovine arteries. Materials Science and Engineering: C. 2014;45:446-54.

16. Hasan A, Memic A, Annabi N, Hossain M, Paul A, Dokmeci MR, et al. Electrospun scaffolds for tissue engineering of vascular grafts. Acta biomaterialia. 2014;10(1):11-25.

17. Wong CS, Liu X, Xu Z, Lin T, Wang X. Elastin and collagen enhances electrospun aligned polyurethane as scaffolds for vascular graft. Journal of Materials Science: Materials in Medicine. 2013;24(8):1865-74.

18. Wu T, Jiang B, Wang Y, Yin A, Huang C, Wang S, et al. Electrospun poly (l-lactide-co-caprolactone)–collagen–chitosan vascular graft in a canine femoral artery model. Journal of Materials Chemistry B. 2015;3(28):5760-8.

19. Nagiah N, Johnson R, Anderson R, Elliott W, Tan W. Highly Compliant Vascular Grafts with Gelatin-Sheathed Coaxially Structured Nanofibers. Langmuir. 2015;31(47):12993-3002.

20. Yazdanpanah A, Tahmasbi M, Amoabediny G, Nourmohammadi J, Moztarzadeh F, Mozafari M. Fabrication and characterization of electrospun poly-L-lactide/gelatin graded tubular scaffolds: Toward a new design for performance enhancement in vascular tissue engineering. Progress in Natural Science: Materials International. 2015;25(5):405-13.

21. Zhan J, Lan P. The review on electrospun gelatin fiber scaffold. Journal of Research Updates in Polymer Science. 2012;1(2):59.

22. Van Den Bulcke AI, Bogdanov B, De Rooze N, Schacht EH, Cornelissen M, Berghmans H. Structural and rheological properties of methacrylamide modified gelatin hydrogels. Biomacromolecules. 2000;1(1):31-8.

23. Coimbra P, Gil M, Figueiredo M. Tailoring the properties of gelatin films for drug delivery applications: Influence of the chemical cross-linking method. International journal of biological macromolecules. 2014;70:10-9.

24. Natu MV, de Sousa HC, Gil M. Effects of drug solubility, state and loading on controlled release in bicomponent electrospun fibers. International journal of pharmaceutics. 2010;397(1):50-8.

25. ISO E. 10993-4: 2007–Biological evaluation of medical devices–Part 4: Selection of tests for interactions with blood. ISO; 2002.

26. F756-00 A. Standard Practice for Assessment of Hemolytic Properties of Materials. ASTM International West Conshohocken, PA, USA; 2000.

27. Imai Y, Nose Y. A new method for evalution of antithrombogenicity of materials. Journal of biomedical materials research. 1972;6(3):165-72.

28. Natu MV, Sardinha JP, Correia IJ, Gil M. Controlled release gelatin hydrogels and lyophilisates with potential application as ocular inserts. Biomedical Materials. 2007;2(4):241.

29. Ribeiro MP, Espiga A, Silva D, Baptista P, Henriques J, Ferreira C, et al. Development of a new chitosan hydrogel for wound dressing. Wound repair and regeneration. 2009;17(6):817-24.

30. Carreira A, Ferreira P, Ribeiro M, Correia T, Coutinho P, Correia I, et al. New drug-eluting lenses to be applied as bandages after keratoprosthesis implantation. International journal of pharmaceutics. 2014;477(1):218-26.

31. Yue K, Trujillo-de Santiago G, Alvarez MM, Tamayol A, Annabi N, Khademhosseini A. Synthesis, properties, and biomedical applications of gelatin methacryloyl (GelMA) hydrogels. Biomaterials. 2015;73:254-71.

32. Coimbra P, Gil MH, Figueiredo M. Tailoring the properties of gelatin films for drug delivery applications: Influence of the chemical cross-linking method. International Journal of Biological Macromolecules. 2014;70(0):10-9.

33. Pierce BF, Tronci G, Rößle M, Neffe AT, Jung F, Lendlein A. Photocrosslinked Co-Networks from Glycidylmethacrylated Gelatin and Poly(ethylene glycol) Methacrylates. Macromolecular Bioscience. 2012;12(4):484-93.

34. Elzein T, Nasser-Eddine M, Delaite C, Bistac S, Dumas P. FTIR study of polycaprolactone chain organization at interfaces. J Colloid Interface Sci. 2004;273(2):381-7.

35. Cebi N, Durak MZ, Toker OS, Sagdic O, Arici M. An evaluation of Fourier transforms infrared spectroscopy method for the classification and discrimination of bovine, porcine and fish gelatins. Food Chemistry. 2016;190:1109-15.

36. Zhu MF, Zuo WW, Yu H, Yang W, Chen YM. Superhydrophobic surface directly created by electrospinning based on hydrophilic material. J Mater Sci. 2006;41(12):3793-7.

37. Yohe ST, Freedman JD, Falde EJ, Colson YL, Grinstaff MW. A Mechanistic Study of Wetting Superhydrophobic Porous 3D Meshes. Adv Funct Mater. 2013;23(29):3628-37.

38. Xu H, Li HY, Chang J. Controlled drug release from a polymer matrix by patterned electrospun nanofibers with controllable hydrophobicity. Journal of Materials Chemistry B. 2013;1(33):4182-8.

39. Huang FL, Wang QQ, Wei QF, Gao WD, Shou HY, Jiang SD. Dynamic wettability and contact angles of poly(vinylidene fluoride) nanofiber membranes grafted with acrylic acid. Express Polymer Letters. 2010;4(9):551-8.

40. Wei D, Xiao W, Sun J, Zhong M, Guo L, Fan H, et al. A biocompatible hydrogel with improved stiffness and hydrophilicity for modular tissue engineering assembly. Journal of Materials Chemistry B. 2015;3(14):2753-63.

41. Ferreira P, Coelho J, Gil M. Development of a new photocrosslinkable biodegradable bioadhesive. International journal of pharmaceutics. 2008;352(1):172-81.

42. Zhao C, Liu X, Nomizu M, Nishi N. Blood compatible aspects of DNA-modified polysulfone membrane—protein adsorption and platelet adhesion. Biomaterials. 2003;24(21):3747-55.

43. Poussard L, Burel F, Couvercelle J-P, Lesouhaitier O, Merhi Y, Tabrizian M, et al. In vitro thrombogenicity investigation of new water-dispersible polyurethane anionomers bearing carboxylate groups. Journal of Biomaterials Science, Polymer Edition. 2005;16(3):335-51.

44. Geng X, Mo X, Fan L, Yin A, Fang J. Hierarchically designed injectable hydrogel from oxidized dextran, amino gelatin and 4-arm poly (ethylene glycol)-acrylate for tissue engineering application. Journal of Materials Chemistry. 2012;22(48):25130-9.

45. Zhu J, Tang C, Kottke-Marchant K, Marchant RE. Design and synthesis of biomimetic hydrogel scaffolds with controlled organization of cyclic RGD peptides. Bioconjugate chemistry. 2009;20(2):333-9.

46. Shin H, Temenoff JS, Mikos AG. In vitro cytotoxicity of unsaturated oligo [poly (ethylene glycol) fumarate] macromers and their cross-linked hydrogels. Biomacromolecules. 2003;4(3):552-60.

Chapter 5

Concluding remarks and future perspectives

Correia, T.R

5. Concluding remarks and future perspectives

The ageing of the worldwide population is associated with an increasing number of illnesses like degenerative bone diseases, fractures and cardiovascular diseases.

Fractures may occur as a consequence of a disease or accident and normally affect different bones. The current bone therapeutic solutions available in the market have limitations concerning porosity/mechanical strength balance, appropriate shape and bactericidal capacity. In this context, TE has been focused on the development of new therapeutic solutions that can be applied in personalized bone therapy.

On the other hand, cardiovascular diseases are responsible for more deaths than any other disease. The bad eating habits, the absence of daily exercise and ageing contribute for the development of pathologies like atherosclerosis, obesity and insulin resistance. The demand for a substitute vessel that is able to provide the required mechanical properties as well as the adequate biological environment is still a milestone. The currently available devices in the market have limited mechanical properties and lack of term patency's.

To overcome those handicaps, TE researchers have been studying different biomaterials in order to fulfil the demand for new bone and vascular grafts.

In this thesis, new 3D scaffolds with bactericidal activity and new electrospun meshes were produced. In chapter 2 it is described the successful design and production of new 3D composites scaffolds using a RP technique. Scaffolds with different ratios of TCP and alginate were successfully produced using a Fab@Home. The compression and young modulus of the different produced scaffolds were characterized and those with 60/40 of TCP and alginate were selected as the best formulation since they were able to surpass the standard values for compression and young modulus of the trabecular bone. In addition, the 60/40 formulation showed a moderately hydrophilic character that is crucial to allow protein adhesion at the surface of the materials and, consequently, cell adhesion and proliferation. Moreover, the biomineralization ability, roughness and macro and microporosity of scaffolds also revealed to be fundamental for osteointegration and bone regeneration. Furthermore, the application of RP technologies for the production of the scaffolds contributes for a personalized therapy, since CAD tools can be used to design 3D structures that fulfil patient requirements and reduce the healing time.

The microorganisms contamination during clinical intervention is a reality that is responsible for most of implant failure. To overcome such clinical handicap, new implants with antibacterial capacity are being currently developed. The 3D TCP/sodium alginate scaffolds previously reported in chapter 2 were functionalized with silver nanoparticles to address the microorganism's colonization issue. To accomplish that, different methods to load the silver nanoparticles (direct impregnation and physical adsorption) were studied and compared in chapter 3. Moreover, to assure the best balance between the cytotoxic profile of the system and the bactericidal activity,

different concentrations of silver nanoparticles were used. The results showed that the 3D TCP/sodium alginate scaffolds loaded with silver nanoparticles by direct impregnation were the ones with the best performance, displaying a bactericidal activity for up to 5 days. Thus, the functionalization of scaffolds with silver nanoparticles highlights the potential contribute of using this approach to prevent infections during implantation of the medical device.

The experimental work presented in chapter 4, reports the use of a simple and cost effective method to produce new TEVGs that are able to reproduce the native structure of blood vessels. So far, the electrospinning technique has been extensively described in the literature for the production of 3D meshes at micro and nanoscale range. Herein, PCL was chosen since it presents properties such as mechanical strength, elasticity and biocompatibility. Moreover, to enhance the biological performance of the final structure different formulations of gelatin (specific adhesion motifs) were used as a coating. The obtained results revealed that these 3D meshes had physicochemical and biological features compatible with cell adhesion and proliferation processes. In addition, they also presented a non-haemolytic character as well as a low thrombogenicity, features that contribute for avoiding thrombus formation. In conclusion, the TEVG developed in this study shows that it is possible to use cheap polymers to promote an improved vascular tissue regeneration.

In a near future, the different tissue engineering systems that were developed in this study can be further optimized in order to improve their performance in the pretended biomedical applications. The 3D scaffolds that incorporated with silver nanoparticles can be further functionalized with bioactive molecules (growth factors or ECM components) or with chemical groups for promoting an improved bone healing. Additionally, the enhancing of the antimicrobial properties of the 3D constructs might also be considered in order to extend the duration time of the protection against infectious agents. Alternatively, other production techniques, such as electrospinning, can also be combined with RP in order to improve the physical features of the scaffolds like pore size, surface area to volume ratio and hydrophilicity that will enhance cell migration, attachment and internalization.

The therapeutic approach developed for VTE applications was focused on the reproduction of the three layers that are commonly found on blood vessels. Recently, the electrospinning process involving the use of coaxial spinning of materials has been applied to promote adequate compliance and structural support to TEVG. Such innovation allows the production of hollow fibers that can be obtained to reproduce the anatomical structure of blood vessels in a simple, fast and cost-effective way. Yet, it is still necessary to translate these new TEVGs to clinical trials. On the other hand, the production of hollow fibers that better mimic the structure of a blood vessel might also be a promising approach to avoid the elasticity issues related to blood flow. Furthermore, the addition of anticoagulation agents for improving vascular graft thrombogenicity should be also considered as a new challenge in future work.